THE BELL SYSTEM TECHNICAL JOURNAL

Radio Propagation Fundamentals*

By KENNETH BULLINGTON

(Manuscript received June 21, 1956)

The engineering of radio systems requires an estimate of the power loss between the transmitter and the receiver. Such estimates are affected by many factors, including reflections, fading, refraction in the atmosphere, and diffraction over the earth's surface.

In this paper, radio transmission theory and experiment in all frequency bands of current interest are summarized. Ground wave and sky wave transmission are included, and both line of sight and beyond horizon transmission are considered. The principal emphasis is placed on quantitative charts that are useful for engineering purposes.

I. INTRODUCTION

The power radiated from a transmitting antenna is ordinarily spread over a relatively large area. As a result the power available at most receiving antennas is only a small fraction of the radiated power. This ratio of radiated power to received power is called the radio transmission loss and its magnitude in some cases may be as large as 10^{15} to 10^{20} (150 to 200 decibels).

The transmission loss between the transmitting and receiving antennas determines whether the received signal will be useful. Each radio

---

* This paper has been prepared for use in a proposed "Antenna Handbook" to be published by McGraw-Hill.

system has a maximum allowable transmission loss which, if exceeded, results in either poor quality or poor reliability. Reasonably accurate predictions of transmission loss can be made on paths that approximate the ideals of either free space or plane earth. On many paths of interest, however, the path geometry or atmospheric conditions differ so much from the basic assumptions that absolute accuracy cannot be expected; nevertheless, worthwhile results can be obtained by using two or more different methods of analysis to "box in" the answer.

The basic concept in estimating radio transmission loss is the loss expected in free space; that is, in a region free of all objects that might absorb or reflect radio energy. This concept is essentially the inverse square law in optics applied to radio transmission. For a one wavelength separation between nondirective (isotropic) antennas, the free space loss is 22 db and it increases by 6 db each time the distance is doubled. The free space transmission ratio at a distance d is given by:

$$\frac{P_r}{P_t} = \left(\frac{\lambda}{4\pi d}\right)^2 g_t g_r \qquad (1a)$$

where:

$$P_r = \text{received power}$$
$$P_t = \text{radiated power}$$ measured in same units

$$\lambda = \text{wavelength in same units as } d$$

$$g_t \text{ (or } g_r) = \text{power gain of transmitting (or receiving) antenna}$$

The power gain of an ideal isotropic antenna that radiates power uniformly in all directions is unity by definition. A small doublet whose over-all physical length is short compared with one-half wavelength has a gain of $g = 1.5$ (1.76 decibels) and a one-half wave dipole has a gain of 2.15 decibels in the direction of maximum radiation. A nomogram for the free space transmission loss between isotropic antennas is given in Fig. 1.

When antenna dimensions are large compared with the wavelength, a more convenient form of the free space ratio is[1]

$$\frac{P_r}{P_t} = \frac{A_t A_r}{(\lambda d)^2} \qquad (1b)$$

where $A_{t,r}$ = effective area of transmitting or receiving antennas.

Another form of expressing free space transmission is the concept of

the free space field intensity E_0 which is given by:

$$E_0 = \frac{\sqrt{30P_t g_t}}{d} \text{ volts per meter} \tag{2}$$

where d is in meters and P_t in watts.

The use of the field intensity concept is frequently more convenient than the transmission loss concept at frequencies below about 30 mc,
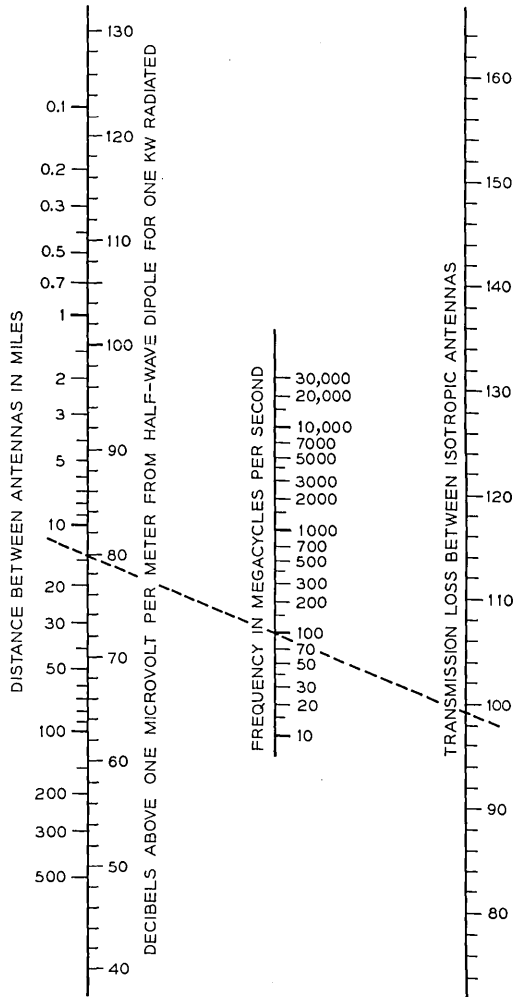

Fig. 1 — Free space transmission.

where external noise is generally controlling and where antenna dimensions and heights are comparable to or less than a wavelength. The free space field intensity is independent of frequency and its magnitude for one kilowatt radiated from a half-wave dipole is shown on the left hand scale on Fig. 1.

The concept of free space transmission assumes that the atmosphere is perfectly uniform and nonabsorbing and that the earth is either infinitely far away or its reflection coefficient is negligible. In practice, the modifying effects of the earth, the atmosphere and the ionosphere need to be considered. Both theoretical and experimental values for these effects are described in the following sections.

II. TRANSMISSION WITHIN LINE OF SIGHT

The presence of the ground modifies the generation and the propagation of radio waves so that the received power or field intensity is ordinarily less than would be expected in free space.[2] The effect of plane earth on the propagation of radio waves is given by

$$\underbrace{\frac{E}{E_0} = 1}_{\substack{\text{Direct} \\ \text{Wave}}} + \underbrace{Re^{j\Delta}}_{\substack{\text{Reflected} \\ \text{Wave}}} + \underbrace{(1 - R)Ae^{j\Delta}}_{\substack{\text{``Surface} \\ \text{Wave''}}} + \underbrace{\cdots}_{\substack{\text{Induction Field} \\ \text{and Secondary} \\ \text{Effects of the} \\ \text{Ground}}} \qquad (3)$$

where

R = reflection coefficient of the ground

A = "surface wave" attenuation factor

$\Delta = \dfrac{4\pi h_1 h_2}{\lambda d}$

$h_{1,2}$ = antenna heights measured in same units as the wavelength and distance

The parameters R and A vary with both polarization and the electrical constants of the ground. In addition, the term "surface wave" has led to considerable confusion since it has been used in the literature to stand for entirely different concepts. These factors are discussed more completely in Section IV. However, the important point to note in this section is that considerable simplification is possible in most practical cases, and that the variations with polarization and ground constants

and the confusion about the surface wave can often be neglected. For near grazing paths, R is approximately equal to -1 and the factor A can be neglected as long as both antennas are elevated more than a wavelength above the ground (or more than 5–10 wavelengths above sea water). Under these conditions the effect of the earth is independent of polarization and ground constants and (3) reduces to

$$\left| \frac{E}{E_0} \right| = \sqrt{\frac{P_r}{P_o}} = 2\sin\frac{\Delta}{2} = 2\sin\frac{2\pi h_1 h_2}{\lambda d} \tag{4}$$

where P_0 is the received power expected in free space.

The above expression is the sum of the direct and ground reflected rays and shows the lobe structure of the signal as it oscillates around the free space value. In most radio applications (except air to ground) the principal interest is in the lower part of the first lobe; that is, where $\Delta/2 < \pi/4$. In this case, $\sin\Delta/2 \approx \Delta/2$ and the transmission loss over plane earth is given by:

$$\begin{aligned} \frac{P_r}{P_t} &= \left(\frac{\lambda}{4\pi d}\right)^2 \left(\frac{4\pi h_1 h_2}{\lambda d}\right)^2 g_t g_r \\ &= \left(\frac{h_1 h_2}{d^2}\right)^2 g_t g_r \end{aligned} \tag{5}$$

It will be noted that this relation is independent of frequency and it is shown in decibels in Fig. 2 for isotropic antennas. Fig. 2 is not valid when the indicated transmission loss is less than the free space loss shown in Fig. 1, because this means that Δ is too large for this approximation.

Although the transmission loss shown in (5) and in Fig. 2 has been derived from optical concepts that are not strictly valid for antenna heights less than a few wavelengths, approximate results can be obtained for lower heights by using h_1 (or h_2) as the larger of either the actual antenna height or the minimum effective antenna height shown in Fig. 3. The concept of minimum effective antenna height is discussed further in Section IV. The error that can result from the use of this artifice does not exceed ± 3 db and occurs where the actual antenna height is approximately equal to the minimum effective antenna height.

The sine function in (4) shows that the received field intensity oscillates around the free space value as the antenna heights are increased. The first maximum occurs when the difference between the direct and ground reflected waves is a half wavelength. The signal maxima have a magnitude $1 + |R|$ and the signal minima have a magnitude of $1 - |R|$.

Frequently the amount of clearance (or obstruction) is described in terms of Fresnel zones. All points from which a wave could be reflected

with a path difference of one-half wavelength form the boundary of the first Fresnel zone; similarly, the boundary of the nth Fresnel zone consists of all points from which the path difference is $n/2$ wavelengths. The nth Fresnel zone clearance H_n at any distance d_1 is given by:

$$H_n = \sqrt{\frac{n\lambda d_1(d - d_1)}{d}} \qquad (6)$$

Although the reflection coefficient is very nearly equal to -1 for

FIG. 2 — Transmission loss over plane earth.

FIG. 3 — Minimum effective antenna height.

grazing angles over smooth surfaces, its magnitude may be less than unity when the terrain is rough. The classical Rayleigh criterion of roughness indicates that specular reflection occurs when the phase deviations are less than about $\pm(\pi/2)$ and that the reflection coefficient will be substantially less than unity when the phase deviations are greater than $\pm(\pi/2)$. In most cases this theoretical boundary between specular and diffuse reflection occurs when the variations in terrain exceed $\frac{1}{8}$ to $\frac{1}{4}$ of the first Fresnel zone clearance. Experimental results with microwave transmission have shown that most practical paths are "rough" and ordinarily have a reflection coefficient in the range of 0.2–0.4. In addition, experience has shown that the reflection coefficient is a statistical problem and cannot be predicted accurately from the path profile.[3]

Fading Phenomena

Variations in signal level with time are caused by changing atmospheric conditions. The severity of the fading usually increases as either the frequency or path length increases. Fading cannot be predicted accurately but it is important to distinguish between two general types: (1) inverse bending and (2) multipath effects. The latter includes the fading caused by interference between direct and ground reflected waves as well as interference between two or more separate paths in the atmosphere. Ordinarily, fading is a temporary diversion of energy to some other than the desired location; fading caused by absorption of energy is discussed in a later paragraph.

The path of a radio wave is not a straight line except for the ideal case of a uniform atmosphere. The transmission path may be bent up or down depending on atmospheric conditions. This bending may either increase or decrease the effective path clearance and inverse bending may have the effect of transforming a line of sight path into an obstructed one. This type of fading may last for several hours. The frequency of its occurrence and its depth can be reduced by increasing the path clearance, particularly in the middle of the path.
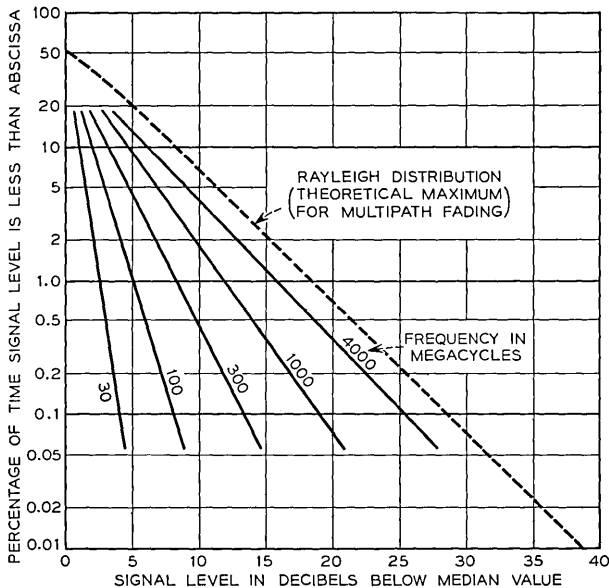

FIG. 4 — Typical fading characteristics in the worst month on 30 to 40 mile line-of-sight paths with 50 to 100 foot clearance.

Severe fading may occur over water or on other smooth paths because the phase difference between the direct and reflected rays varies with atmospheric conditions. The result is that the two rays sometimes add and sometimes tend to cancel. This type of fading can be minimized, if the terrain permits, by locating one end of the circuit high while the other end is very low. In this way the point of reflection is placed near the low antenna and the phase difference between direct and reflected rays is kept relatively steady.

Most of the fading that occurs on "rough" paths with adequate clearance is the result of interference between two or more rays traveling slightly different routes in the atmosphere. This multipath type of fading is relatively independent of path clearance and its extreme condition approaches the Rayleigh distribution. In the Rayleigh distribution, the probability that the instantaneous value of the field is greater than the value R is exp $[-(R/R_0)]$, where R_0 is the rms value.

Representative values of fading on a path with adequate clearance are shown on Fig. 4. After the multipath fading has reached the Rayleigh distribution, a further increase in either distance or frequency increases the number of fades of a given depth but decreases the duration so that the product is the constant indicated by the Rayleigh distribution.

Miscellaneous Effects

The remainder of this Section describes some miscellaneous effects of line of sight transmission that may be important at frequencies above about 1,000 mc. These effects include variation in angles of arrival, maximum useful antenna gain, useful bandwidth, the use of frequency or space diversity, and atmospheric absorption.

On line of sight paths with adequate clearance some components of the signal may arrive with variations in angle of arrival of as much as $\frac{1}{2}°$ to $\frac{3}{4}°$ in the vertical plane, but the variations in the horizontal plane are less than $0.1°$.[4, 5] Consequently, if antennas with beamwidths less than about $0.5°$ are used, there may occasionally be some loss in received signal because most of the incoming energy arrives outside the antenna beamwidth. Signal variations due to this effect are usually small compared with the multipath fading.

Multipath fading is selective fading and it limits both the maximum useful bandwidth and the frequency separation needed for adequate frequency diversity. For 40-db antennas on a 30-mile path the fading on frequencies separated by 100–200 mc is essentially uncorrelated regardless of the absolute frequency. With less directive antennas, uncorrelated fading can occur at frequencies separated by less than 100 mc.[6, 7]

Larger antennas (more narrow beamwidths) will decrease the fast multipath fading and widen the frequency separation between uncorrelated fading but at the risk of increasing the long term fading associated with the variations in the angle of arrival.

Optimum space diversity, when ground reflections are controlling, requires that the separation between antennas be sufficient to place one antenna on a field intensity maximum while the other is in a field intensity minimum. In practice, the best spacing is usually not known because the principal fading is caused by multipath variations in the atmosphere. However, adequate diversity can usually be achieved with a vertical separation of 100–200 wavelengths.

At frequencies above 5,000–10,000 mc, the presence of rain, snow, or fog introduces an absorption in the atmosphere which depends on the amount of moisture and on the frequency. During a rain of cloud burst proportions the attenuation at 10,000 mc may reach 5 db per mile and at 25,000 mc it may be in excess of 25 db per mile.[8] In addition to the effect of rainfall some selective absorption may result from the oxygen and water vapor in the atmosphere. The first absorption peak due to water vapor occurs at about 24,000 mc and the first absorption peak for oxygen occurs at about 60,000 mc.

III. TROPOSPHERIC TRANSMISSION BEYOND LINE OF SIGHT

A basic characteristic of electromagnetic waves is that the energy is propagated in a direction perpendicular to the surface of uniform phase. Radio waves travel in a straight line only as long as the phase front is plane and is infinite in extent.

Energy can be transmitted beyond the horizon by three principal methods: reflection, refraction and diffraction. Reflection and refraction are associated with either sudden or gradual changes in the direction of the phase front, while diffraction is an edge effect that occurs because the phase surface is not infinite. When the resulting phase front at the receiving antenna is irregular in either amplitude or position, the distinctions between reflection, refraction, and diffraction tend to break down. In this case the energy is said to be scattered. Scattering is frequently pictured as a result of irregular reflections although irregular refraction plus diffraction may be equally important.

The following paragraphs describe first the theories of refraction and of diffraction over a smooth sphere and a knife edge. This is followed by empirical data derived from experimental results on the transmission to points far beyond the horizon, on the effects of hills and trees, and on fading phenomena.

Refraction

The dielectric constant of the atmosphere normally decreases gradually with increasing altitude. The result is that the velocity of transmission increases with the height above the ground and, on the average, the radio energy is bent or refracted toward the earth. As long as the change in dielectric constant is linear with height, the net effect of refraction is the same as if the radio waves continued to travel in a straight line but over an earth whose modified radius is:

$$ka \; = \; \frac{a}{1 + \dfrac{a}{2}\dfrac{d\epsilon}{dh}} \tag{7}$$

where

a = true radius of earth

$\dfrac{d\epsilon}{dh}$ = rate of change of dielectric constant with height

Under certain atmospheric conditions the dielectric constant may increase $(0 < k < 1)$ over a reasonable height, thereby causing the radio waves in this region to bend away from the earth. This is the cause of the inverse bending type of fading mentioned in the preceding section. It is sometimes called substandard refraction. Since the earth's radius is about 2.1×10^7 feet, a decrease in dielectric constant of only 2.4×10^{-8} per foot of height results in a value of $k = \frac{4}{3}$, which is commonly assumed to be a good average value.[9] When the dielectric constant decreases about four times as rapidly (or by about 10^{-7} per foot of height), the value of $k = \infty$. Under such a condition, as far as radio propagation is concerned, the earth can then be considered flat, since any ray that starts parallel to the earth will remain parallel.

When the dielectric constant decreases more rapidly than 10^{-7} per foot of height, radio waves that are radiated parallel to, or at an angle above the earth's surface, may be bent downward sufficiently to be reflected from the earth. After reflection the ray is again bent toward the earth, and the path of a typical ray is similar to the path of a bouncing tennis ball. The radio energy appears to be trapped in a duct or waveguide between the earth and the maximum height of the radio path. This phenomenon is variously known as trapping, duct transmission, anomalous propagation, or guided propagation.[10, 11] It will be noted that in this case the path of a typical guided wave is similar in form to the path of sky waves, which are lower-frequency waves trapped between the

earth and the ionosphere. However, there is little or no similarity be-
tween the virtual heights, the critical frequencies, or the causes of re-
fraction in the two cases.

Duct transmission is important because it can cause long distance
interference with another station operating on the same frequency;
however, it does not occur often enough nor can its occurrence be pre-
dicted with enough accuracy to make it useful for radio services requir-
ing high reliability.

Diffraction Over a Smooth Spherical Earth and Ridges

Radio waves are also transmitted around the earth by the phenomenon
of diffraction. Diffraction is a fundamental property of wave motion,
and in optics it is the correction to apply to geometrical optics (ray
theory) to obtain the more accurate wave optics. In other words, all
shadows are somewhat "fuzzy" on the edges and the transition from
"light" to "dark" areas is gradual, rather than infinitely sharp. Our
common experience is that light travels in straight lines and that shad-
ows are sharp, but this is only because the diffraction effects for these
very short wavelengths are too small to be noticed without the aid of
special laboratory equipment. The order of magnitude of the diffraction
at radio frequencies may be obtained by recalling that a 1,000-mc radio
wave has about the same wavelength as a 1,000-cycle sound wave in
air, so that these two types of waves may be expected to bend around
absorbing obstacles with approximately equal facility.

The effect of diffraction around the earth's curvature is to make possi-
ble transmission beyond the line-of-sight. The magnitude of the loss
caused by the obstruction increases as either the distance or the fre-
quency is increased and it depends to some extent on the antenna
height.[12] The loss resulting from the curvature of the earth is indicated
by Fig. 5 as long as neither antenna is higher than the limiting value
shown at the top of the chart. This loss is in addition to the transmission
loss over plane earth obtained from Fig. 2.

When either antenna is as much as twice as high as the limiting value
shown on Fig. 5, this method of correcting for the curvature of the earth
indicates a loss that is too great by about 2 db, with the error increasing
as the antenna height increases. An alternate method of determining the
effect of the earth's curvature is given by Fig. 6. The latter method is
approximately correct for any antenna height, but it is theoretically
limited in distance to points at or beyond the line-of-sight, assuming
that the curved earth is the only obstruction. Fig. 6 gives the loss rela-
tive to free-space transmission (and hence is used with Fig. 1) as a func-

tion of three distances: d_1 is the distance to the horizon from the lower antenna, d_2 is the distance to the horizon from the higher antenna, and d_3 is the distance beyond the line-of-sight. In other words, the total distance between antennas, $d = d_1 + d_2 + d_3$. The distance to the horizon over smooth earth is given by:

$$d_{1,2} = \sqrt{2kah_{1,2}} \qquad (8)$$

where $h_{1,2}$ is the appropriate antenna height and ka is the effective earth's radius.

The preceding discussion assumes that the earth is a perfectly smooth sphere and the results are critically dependent on a smooth surface and a uniform atmosphere. The modification in these results caused by the

SCALE A
LIMITING ANTENNA HEIGHT IN FEET
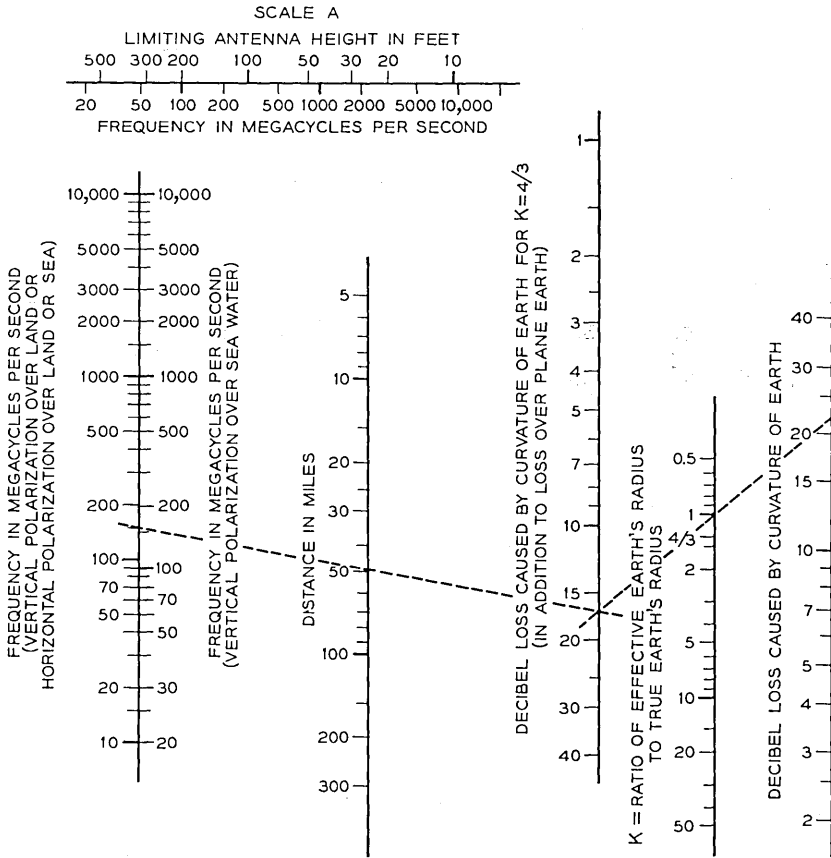
FIG. 5 — Diffraction loss around a perfect sphere.

presence of hills, trees, and buildings is difficult or impossible to compute, but the order of magnitude of these effects may be obtained from a consideration of the other extreme case, which is propagation over a perfectly absorbing knife edge.

The diffraction of plane waves over a knife edge or screen causes a shadow loss whose magnitude is shown on Fig. 7. The height of the obstruction H is measured from the line joining the two antennas to the top of the ridge. It will be noted that the shadow loss approaches 6 db
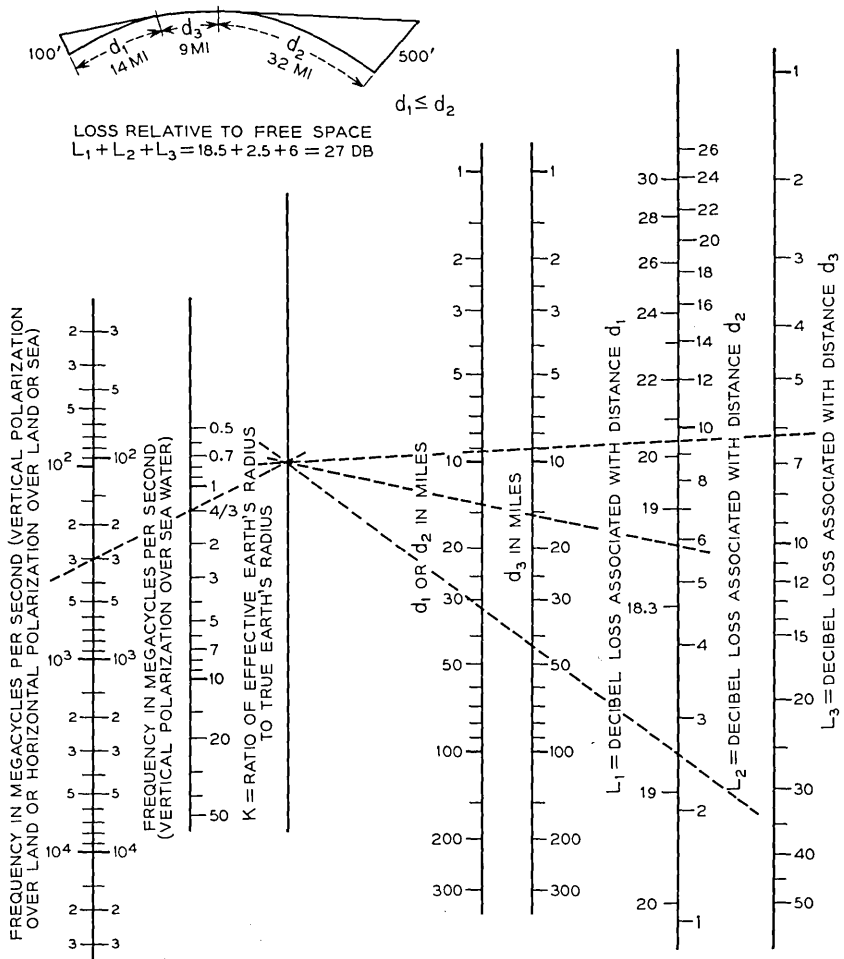
FIG. 6 — Diffraction loss relative to free space transmission at all locations beyond line-of-sight over a smooth sphere.

as H approaches 0 (grazing incidence), and that it increases with increasing positive values of H. When the direct ray clears the obstruction, H is negative, and the shadow loss approaches 0 db in an oscillatory manner as the clearance is increased. In other words, a substantial clearance is required over line-of-sight paths in order to obtain "free-space" transmission. The knife edge diffraction calculation is substantially independent of polarization as long as the distance from the edge is more than a few wavelengths.
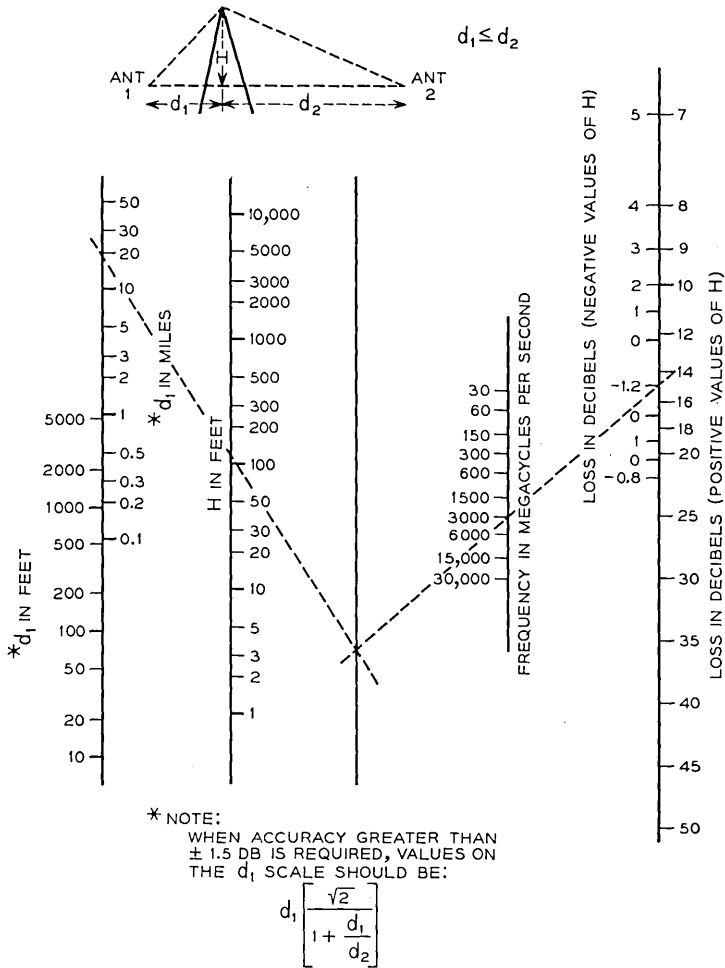
FIG. 7 — Knife-edge diffraction loss relative to free space.
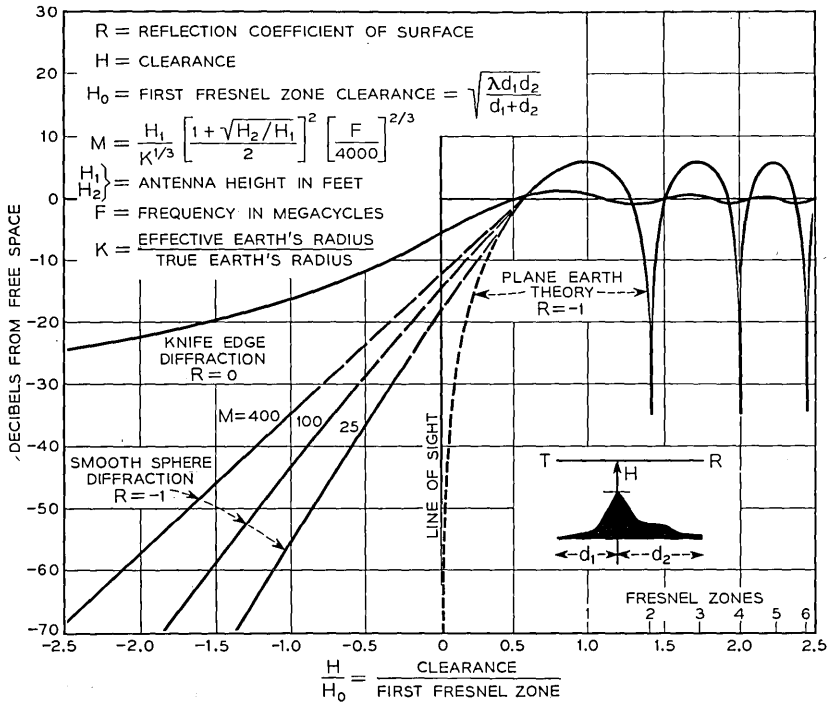
FIG. 8 — Transmission loss versus clearance.

At grazing incidence, the expected loss over a ridge is 6 db (Fig. 7) while over a smooth spherical earth Fig. 6 indicates a loss of about 20 db. More accurate results in the vicinity of the horizon can be obtained by expressing radio transmission in terms of path clearance measured in Fresnel zones as shown in Fig. 8. In this representation the plane earth theory and the ridge diffraction can be represented by single lines; but the smooth sphere theory requires a family of curves with a parameter M that depends primarily on antenna heights and frequency. The big difference in the losses predicted by diffraction around a perfect sphere and by diffraction over a knife edge indicates that diffraction losses depend critically on the assumed type of profile. A suitable solution for the intermediate problem of diffraction over a rough earth has not yet been obtained.

Experimental Data Far Beyond the Horizon

Most of the experimental data at points far beyond the horizon fall in between the theoretical curves for diffraction over a smooth sphere

and for diffraction over a knife edge obstruction. Various theories have been advanced to explain these effects but none has been reduced to a simple form for every day use.[13] The explanation most commonly accepted is that energy is reflected or scattered from turbulent air masses in the volume of air that is enclosed by the intersection of the beamwidths of the transmitting and receiving antennas.[14]

The variation in the long term median signals with distance has been derived from experimental results and is shown in Fig. 9 for two frequencies.[15] The ordinate is in db below the signal that would have been expected at the same distance in free space with the same power and the same antennas. The strongest signals are obtained by pointing the antennas at the horizon along the great circle route. The values shown on Fig. 9 are essentially annual averages taken from a large number of paths, and substantial variations are to be expected with terrain, climate, and season as well as from day to day fading.

Antenna sites with sufficient clearance so that the horizon is several miles away will, on the average, provide a higher median signal (less loss) than shown on Fig. 9. Conversely, sites for which the antenna must be pointed upward to clear the horizon will ordinarily result in appreciably more loss than shown on Fig. 9. In many cases the effects of path length and angles to the horizon can be combined by plotting the experimental results as a function of the angle between the lines drawn tangent to the horizon from the transmitting and receiving sites.[16]
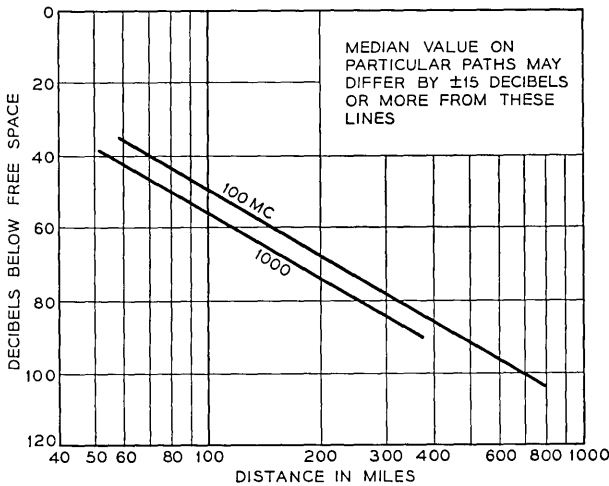

FIG. 9 — Beyond-horizon transmission — median signal level versus distance.

When the path profile consists of a single sharp obstruction that can be seen from both terminals, the signal level may approach the value predicted by the knife edge diffraction theory.[17] While several interesting and unusual cases have been recorded, the knife edge or "obstacle gain" theory is not applicable to the typical but only to the exceptional paths.

As in the case of line-of-sight transmission the fading of radio signals beyond the horizon can be divided into fast fading and slow fading. The fast fading is caused by multipath transmission in the atmosphere, and for a given size antenna, the rate of fading increases as either the frequency or the distance is increased. This type of fading is much faster than the maximum fast fading observed on line of sight paths, but the two are similar in principle. The magnitude of the fades is described by the Rayleigh distribution.

Slow fading means variations in average signal level over a period of hours or days and it is greater on beyond horizon paths than on line-of-sight paths. This type of fading is almost independent of frequency and seems to be associated with changes in the average refraction of the atmosphere. At distances of 150 to 200 miles the variations in hourly median value around the annual median seem to follow a normal probability law in db with a standard deviation of about 8 db. Typical fading distributions are shown on Fig. 10.

The median signal levels are higher in warm humid climates than in cold dry climates and seasonal variations of as much as ±10 db or more from the annual median have been observed.[18]

Since the scattered signals arrive with considerable phase irregularities in the plane of the receiving antenna, narrow-beamed (high gain) antennas do not yield power outputs proportional to their theoretical area gains. This effect has sometimes been called loss in antenna gain, but it is a propagation effect and not an antenna effect. On 150 to 200 miles this loss in received power may amount to one or two db for a 40 db gain antenna, and perhaps six to eight db for a 50 db antenna. These extra losses vary with time but the variations seem to be uncorrelated with the actual signal level.

The bandwidth that can be used on a single radio carrier is frequently limited by the selective fading caused by multipath or echo effects. Echoes are not troublesome as long as the echo time delays are very short compared with one cycle of the highest baseband frequency. The probability of long delayed echoes can be reduced (and the rate of fast fading can be decreased) by the use of narrow beam antennas both within and beyond the horizon.[19, 20] Useful bandwidths of several mega-

cycles appear to be feasible with the antennas that are needed to provide adequate signal-to-noise margins. Successful tests of television and of multichannel telephone transmission have been reported on a 188-mile path at 5,000 mc.[21]

The effects of fast fading can be reduced substantially by the use of either frequency or space diversity. The frequency or space separation required for diversity varies with time and with the degree of correlation that can be tolerated. A horizontal (or vertical) separation of about 100 wavelengths is ordinarily adequate for space diversity on 100- to 200-mile paths. The corresponding figure for the required frequency separation for adequate diversity seems likely to be more than 20 mc.
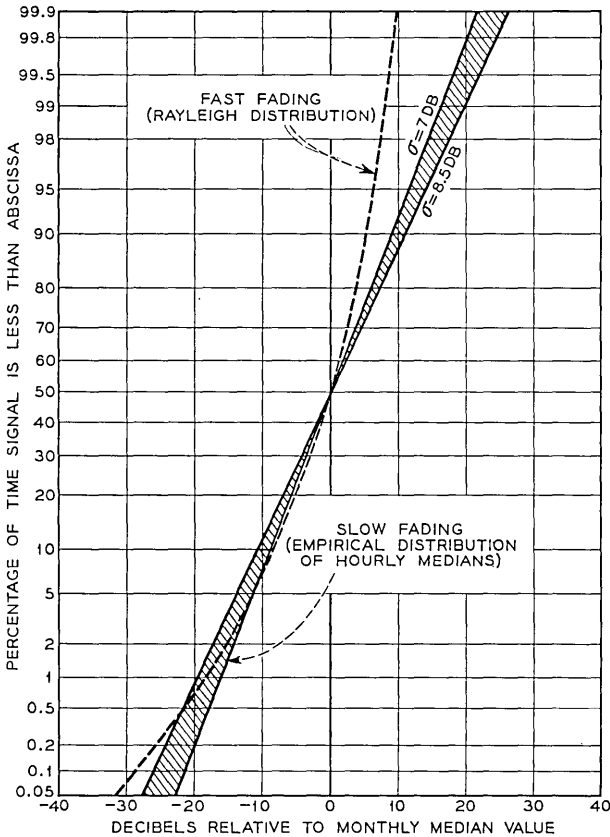
FIG. 10 — Typical fading characteristics at points far beyond the horizon.

Effects of Nearby Hills — Particularly on Short Paths

The experimental results on the effects of hills indicate that the shadow losses increase with the frequency and with the roughness of the terrain.[22]

An empirical summary of the available data is shown on Fig. 11. The roughness of the terrain is represented by the height H shown on the profile at the top of the chart. This height is the difference in elevation between the bottom of the valley and the elevation necessary to obtain line of sight from the transmitting antenna. The right hand scale in Fig. 11 indicates the additional loss above that expected over plane earth. Both the median loss and the difference between the median and the 10 per cent values are shown. For example, with variations in terrain of 500 feet, the estimated median shadow loss at 450 mc is about 20 db and the
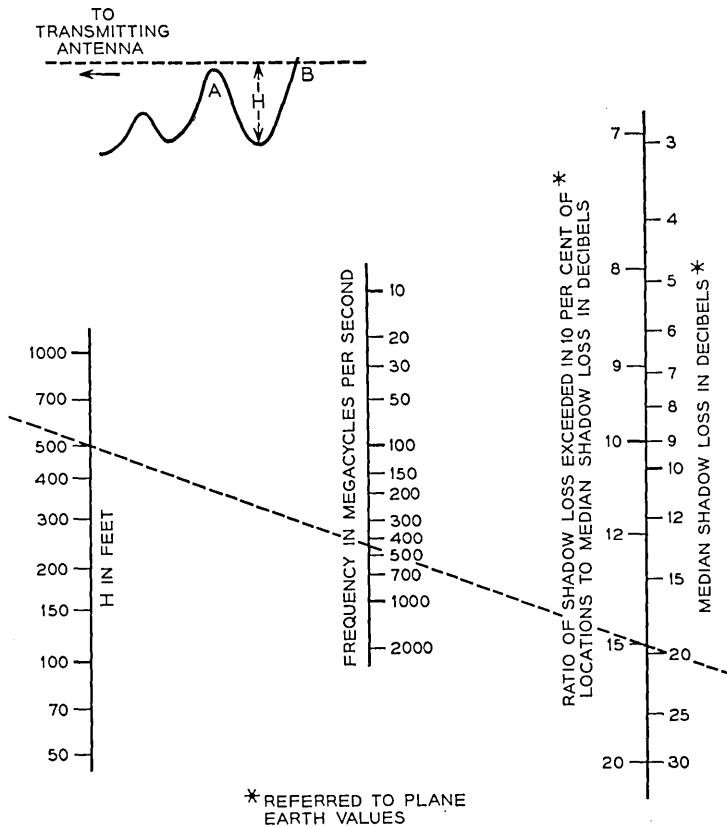
FIG. 11 — Estimated distribution of shadow losses.

shadow loss exceeded in only 10 per cent of the possible locations between points A and B is about $20 + 15 = 35$ db. It will be recognized that this analysis is based on large-scale variations in field intensity, and does not include the standing wave effects which sometimes cause the field intensity to vary considerably within a few feet.

Effects of Buildings and Trees

The shadow losses resulting from buildings and trees follow somewhat different laws from those caused by hills. Buildings may be more transparent to radio waves than the solid earth, and there is ordinarily much more back scatter in the city than in the open country. Both of these factors tend to reduce the shadow losses caused by the buildings but, on the other hand, the angles of diffraction over or around the buildings are usually greater than for natural terrain. In other words, the artificial canyons caused by buildings are considerably narrower than natural valleys, and this factor tends to increase the loss resulting from the presence of buildings. The available quantitative data on the effects of buildings are confined primarily to New York City. These data indicate that in the range of 40 to 450 mc there is no significant change with frequency, or at least the variation with frequency is somewhat less than that noted in the case of hills.[23] The median field intensity at street level for random locations in Manhattan (New York City) is about 25 db below the corresponding plane earth value. The corresponding values for the 10 per cent and 90 per cent points are about 15 and 35 db, respectively.

Typical values of attenuation through a brick wall, are from 2 to 5 db at 30 mc and 10 to 40 db at 3,000 mc, depending on whether the wall is dry or wet. Consequently most buildings are rather opaque at frequencies of the order of thousands of megacycles.

When an antenna is surrounded by moderately thick trees and below tree-top level, the average loss at 30 mc resulting from the trees is usually 2 or 3 db for vertical polarization and is negligible with horizontal polarization. However, large and rapid variations in the received field intensity may exist within a small area, resulting from the standing-wave pattern set up by reflections from trees located at a distance of several wavelengths from the antenna. Consequently, several near-by locations should be investigated for best results. At 100 mc the average loss from surrounding trees may be 5 to 10 db for vertical polarization and 2 or 3 db for horizontal polarization. The tree losses continue to increase as the frequency increases, and above 300 to 500 mc they tend to be independent of the type of polarization. Above 1,000 mc, trees that are thick

enough to block vision are roughly equivalent to a solid obstruction of the same over-all size.

IV. MEDIUM AND LOW FREQUENCY GROUND WAVE TRANSMISSION

Wherever the antenna heights are small compared with the wavelength, the received field intensity is ordinarily stronger with vertical polarization than with horizontal and is stronger over sea water than over poor soil. In these cases the "surface wave" term in (3) cannot be neglected. This use of the term "surface wave" follows Norton's usage and is not equivalent to the Sommerfeld or Zenneck "surface waves."

The parameter A is the plane earth attenuation factor for antennas at ground level. It depends upon the frequency, ground constants, and type of polarization. It is never greater than unity and decreases with increasing distance and frequency, as indicated by the following approximate equation: [24, 25]

$$A \approx \frac{-1}{1 + j \dfrac{2\pi d}{\lambda} (\sin \theta + z)^2} \qquad (9)$$

where

$z = \dfrac{\sqrt{\epsilon_0 - \cos^2 \theta}}{\epsilon_0}$ for vertical polarization

$z = \sqrt{\epsilon_0 - \cos^2 \theta}$ for horizontal polarization

$\varepsilon_0 = \epsilon - j60\sigma\lambda$

$\theta =$ angle between reflected ray and the ground

$\quad = 0$ for antennas at ground level

$\epsilon =$ dielectric constant of the ground relative to unity in free space

$\sigma =$ conductivity of the ground in mhos per meter

$\lambda =$ wavelength in meters

In terms of these same parameters the reflection coefficient of the ground is given by[26]

$$R = \frac{\sin \theta - z}{\sin \theta + z} \qquad (10)$$

When $\theta \ll |z|$ the reflection coefficient approaches -1; when $\theta \gg |z|$

(which can happen only with vertical polarization) the reflection coefficient approaches $+1$. The angle for which the reflection coefficient is a minimum is called the pseudo-Brewster angle and it occurs for $\sin \theta = |z|$.

For antennas approaching ground level the first two terms in (3) cancel each other (h_1 and h_2 approach zero and R approaches -1) and the magnitude of the third term becomes

$$| (1 - R)A | \approx \frac{2}{\frac{2\pi d}{\lambda} z^2} = \frac{4\pi h_0^2}{\lambda d} \tag{11}$$

where h_0 = minimum effective antenna height shown in Fig. 3

$$= \left| \frac{\lambda}{2\pi z} \right|$$

The surface wave term arises because the earth is not a perfect reflector. Some energy is transmitted into the ground and sets up ground currents, which are distorted relative to what would have been the case in an ideal perfectly reflecting surface. The surface wave is defined as the vertical electric field for vertical polarization, or the horizontal electric field for horizontal polarization, that is associated with the extra components of the ground currents caused by lack of perfect reflection. Another component of the electric field associated with the ground currents is in the direction of propagation. It accounts for the success of the wave antenna at lower frequencies, but it is always smaller in magnitude than the surface wave as defined above. The components of the electric vector in three mutually perpendicular co-ordinates are given by Norton.[27]

In addition to the effect of the earth on the propagation of radio waves, the presence of the ground may also affect the impedance of low antennas and thereby may have an effect on the generation and reception of radio waves.[28] As the antenna height varies, the impedance oscillates around the free space value, but the variations in impedance are usually unimportant as long as the center of the antenna is more than a quarter-wavelength above the ground. For vertical grounded antennas (such as are used in standard AM broadcasting) the impedance is doubled and the net effect is that the maximum field intensity is 3 db above the free space value instead of 6 db as indicated in (4) for elevated antennas.

Typical values of the field intensity to be expected from a grounded quarter-wave vertical antenna are shown in Fig. 12 for transmission over poor soil and in Fig. 13 for transmission over sea water. These charts in-
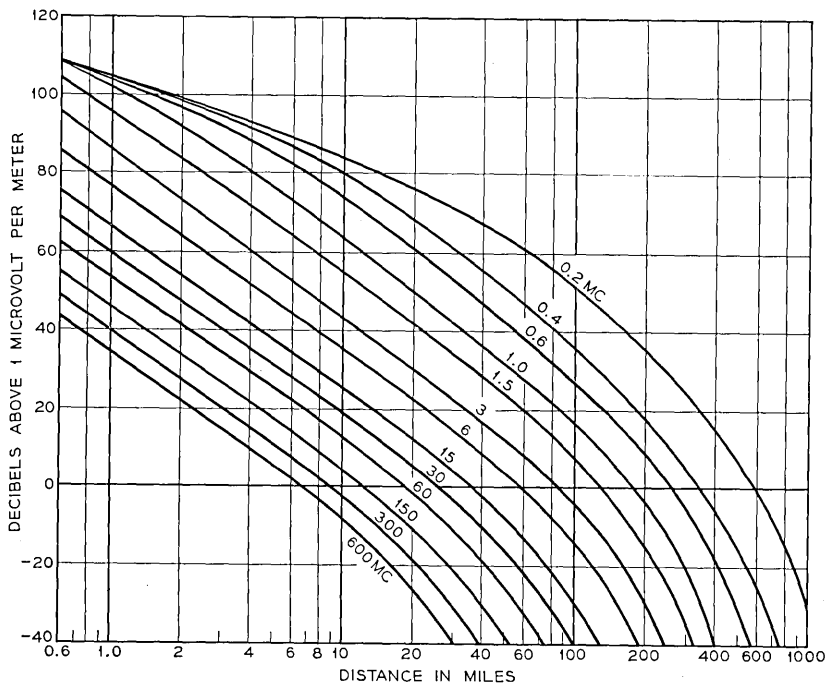
FIG. 12 — Field intensity for vertical polarization over poor soil for 1-kw radiated power from a grounded whip antenna.
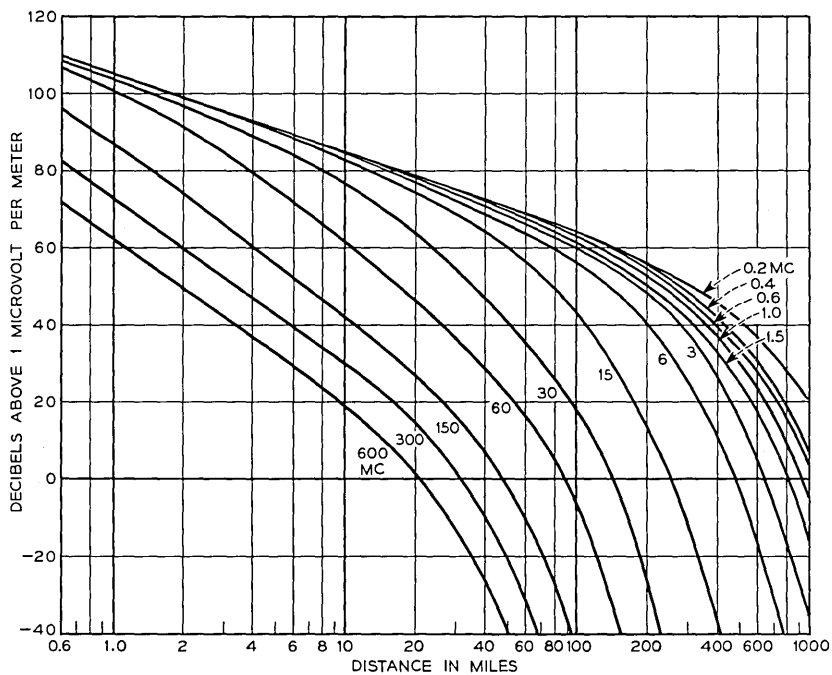
FIG. 13 — Field intensity for vertical polarization over sea water for 1-kw radiated power from a grounded whip antenna.

clude the effect of diffraction and average refraction around a smooth spherical earth as discussed in Section III, but do not include the ionospheric effects described in the next Section. The increase in signal obtained by raising either antenna height is shown in Fig. 14 for poor soil and Fig. 15 for sea water.
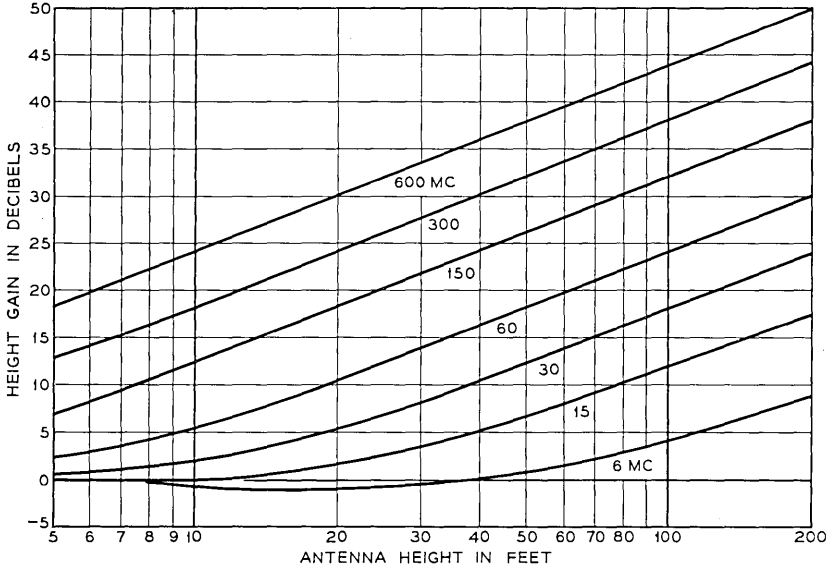
FIG. 14 — Antenna height gain factor for vertical polarization over poor soil.
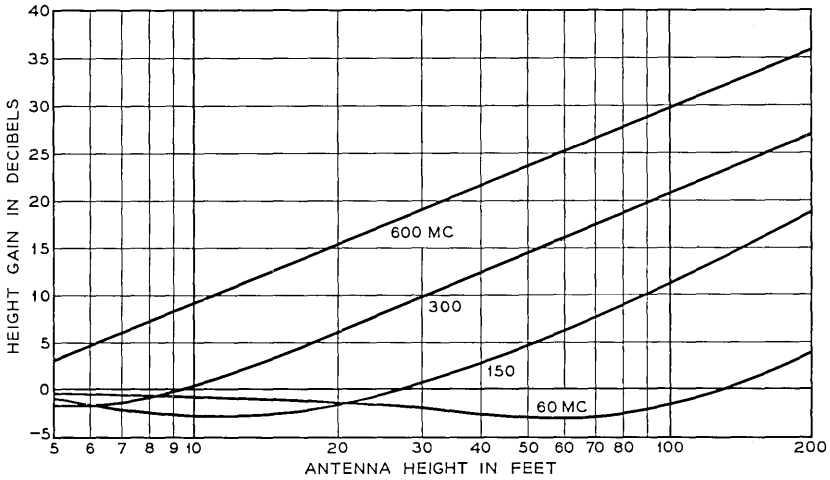
FIG. 15 — Antenna height gain factor for vertical polarization over sea water.

V. IONOSPHERIC TRANSMISSION

In addition to the tropospheric or ground wave transmission discussed in the preceding sections, useful radio energy at frequencies below about 25 to 100 mc may be returned to the earth by reflection from the ionosphere, which consists of several ionized layers located 50 to 200 miles above the earth. The relatively high density of ions and free electrons in this region provides an effective index of refraction of less than one, and the resulting transmission path is similar to that in the well known optical phenomenon of total internal reflection. The mechanism is generally spoken of as reflection from certain virtual heights.[29] Polarization is not maintained in ionospheric transmission and the choice depends on the antenna design that is most efficient at the desired elevation angles.

Regular Ionospheric Transmission

The ionosphere consists of three or more distinct layers. This does not mean that the space between layers is free of ionization but rather that the curve of ion density versus height has several distinct peaks. The E, $F1$, and $F2$ layers are present during the daytime but the F_1 and F_2 combine to form a single layer at night. A lower layer called the D layer is also present during the day, but its principal effect is to absorb rather than reflect.

Information about the nature of the inosphere has been obtained by transmitting pulsed radio signals directly overhead and by recording the signal intensity and the time delay of the echoes returned from these layers. At night all frequencies below the critical frequency f_c are returned to earth with an average signal intensity that is about 3 to 6 db below the free space signal that would be expected for the round trip distance. At frequencies higher than the critical frequency the signal intensity is very weak or undetectable. Typical values of the critical frequency for Washington, D. C., are shown in Fig. 16.

During the daytime, the critical frequency is increased 2 to 3 times over the corresponding nighttime value. This apparent increase in the useful frequency range for ionospheric transmission is largely offset by the heavy daytime absorption which reaches a maximum in the 1 to 2-mc range. This absorption is caused by interaction between the free electrons and the earth's magnetic field. The absence of appreciable absorption at night indicates that most of the free electrons disappear when the sun goes down. Charged particles traveling in a magnetic field have a resonant or gyromagnetic frequency, and for electrons in the earth's magnetic field, of about 0.5 gauss, this resonance occurs at about 1.4
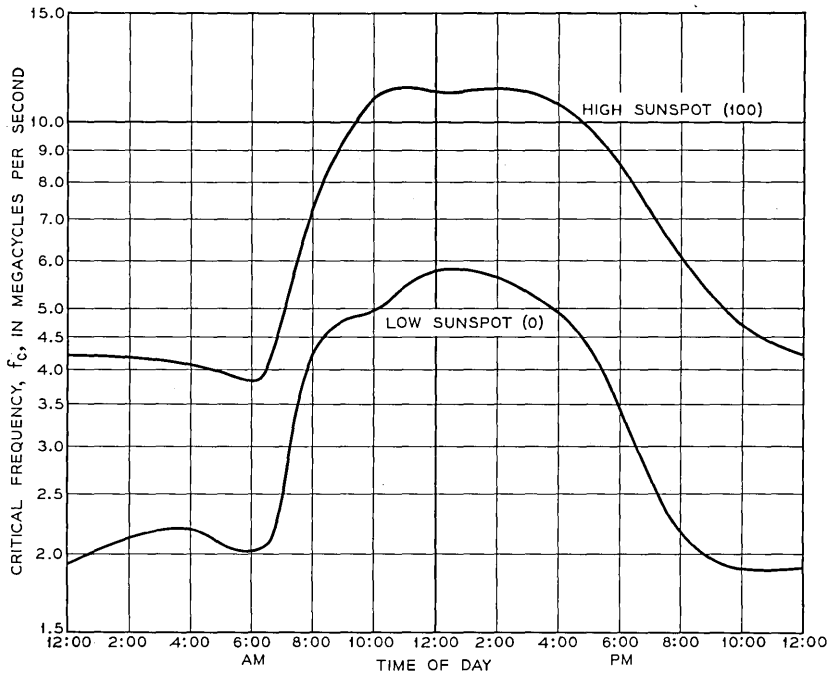
FIG. 16 — Typical diurnal variation of critical frequency for January at latitude 40 degrees.

mc. The magnitude of the absorption varies with the angle of the sun above the horizon and is a maximum about noon. The approximate midday absorption is shown on Fig. 17 in terms of db per 100 miles of path length. (On short paths this length is the actual path traveled, not the distance along the earth's surface.)

Long distance transmission requires that the signal be reflected from the ionosphere at a small angle instead of the perpendicular incidence used in obtaining the critical frequency. For angles other than directly overhead an assumption which seems to be borne out in practice is that the highest frequency for which essentially free space transmission is obtained is $f_c/\sin \alpha$, where α is the angle between the radio ray and ionospheric layer. This limiting frequency is greater than the critical frequency and is called the maximum usable frequency which is usually abbreviated muf. The curved geometry limits the distance that can be obtained with one-hop transmission to about 2,500 miles and the muf at the longer distances does not exceed 3 to 3.5 times the critical frequency.

The difference between day and night effects means that most sky-
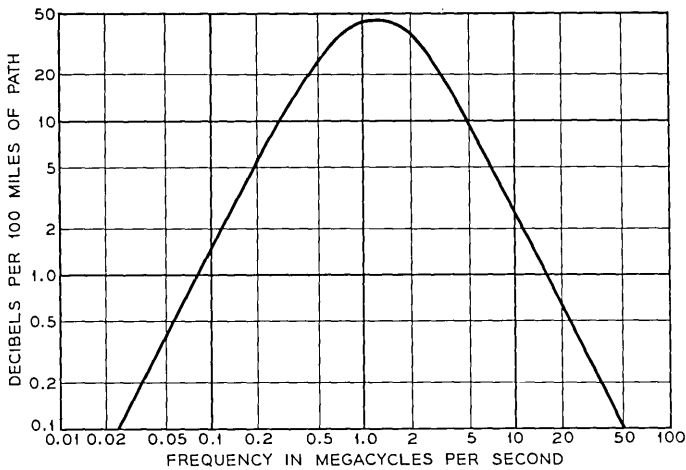
FIG. 17 — Typical values of midday ionospheric absorption.

wave paths require at least two frequencies. A relatively low frequency is needed to get under the nighttime muf and a higher frequency is needed that is below the daytime muf but above the region of high absorption. This lower limit depends on the available signal-to-noise margin and is commonly called the lowest useful high frequency.

Frequencies most suitable for transmission of 1000 miles or more will ordinarily not be reflected at the high angles needed for much shorter distances. As a result the range of skywave transmission ordinarily does not overlap the range of groundwave transmission, and the intermediate region is called the skip zone because the signal is too weak to be useful. At frequencies of a few megacycles the groundwave and skywave ranges may overlap with the result that severe fading occurs when the two signals are comparable in amplitude.

In addition to the diurnal variations in frequency and in absorption there are systematic changes with season, latitude, and with the nominally eleven-year sunspot cycle. Random changes in the critical frequency of about ±15 per cent from the monthly median value are also to be expected from day to day.

The F layer is the principal contributor to transmission beyond 1,000 to 1,500 miles and typical values of the maximum usable frequency can be summarized as follows: The median nighttime critical frequency for F layer transmission at the latitude at Washington, D. C., is about 2 mc in the month of June during a period of low sunspot activity. All frequencies below about 2 mc are strongly reflected to earth while the higher

frequencies are either greatly attenuated or are lost in outer space. The approximate maximum usable frequency for other conditions is greater than 2 mc by the ratios shown in Table I.

TABLE I

Variation With	Multiplying factor
(1) Time of Day	
Midnight	1 (Reference)
Early Afternoon—June	2
December	3
(2) Path Length	
Less than 200 Miles	1 (Reference)
Approx. 1000 Miles	2
More than 2500 Miles	3.5
(3) Sunspot Cycle	
Minimum	1 (Reference)
For one year in five—June	1.5
December	2
For one year in fifty—June	2
December	3

When all of the above variations add "in phase," transmission for distances of 2,500 miles or more is possible at frequencies up to 40 to 60 mc. For example, using the table, 2,500-mile transmission on an early December afternoon in one year out of five can be expected on a frequency of about 42 mc, which is $3 \times 3.5 \times 2 = 21$ times the reference critical frequency of 2 mc. Peaks of the sunspot cycle occurred in 1937 and in 1947–1948 so another peak is expected in 1958–1959.

The maximum usable frequency also varies with the geomagnetic latitude but, as a first approximation, the above values are typical of continental U. S. Forecasts of the muf to be expected throughout the world are issued monthly by the National Bureau of Standards.[30, 31] These estimates include the diurnal, seasonal, and sunspot effects.

Another type of absorption, over and above the usual daytime absorption, occurs both day and night on transmission paths that travel through the auroral zone. The auroral zones are centered on the north and south magnetic poles at about the same distance as the Arctic Circle is from the geographical north pole. During periods of magnetic storms these auroral zones expand over an area much larger than normal and thereby disrupt communication by introducing unexpected absorption. These conditions of poor transmission can last for hours and sometimes even for days. These periods of increased absorption are more common in the polar regions than in the temperate zones or the tropics because of the proximity of the auroral zone and are frequently called HF "blackouts." During a "blackout," the signal level is decreased considerably

but the signal does not drop out completely. It appears possible that the outage time normally associated with HF transmission could be greatly reduced by the use of transmitter power and antenna size comparable to that needed in the ionospheric scatter method described below.

In addition to the auroral zone absorption, there are shorter periods of severe absorption over the entire hemisphere facing the sun. These erratic and unpredictable effects which seem to be associated with eruptions on the sun are called sudden ionospheric disturbances (SID's) or the Dellinger effect.

The preceding information is based primarily on F layer transmission. The E layer is located closer to the earth than the F layer and the maximum transmission distance for a single reflection is about 1,200 miles.

Reflections from the E layer sometimes occur at frequencies above about 20 mc but are erratic in both time and space. This phenomenon has been explained by assuming that the E layer contains clouds of ionization that are variable in size, density, and location. The maximum frequency returned to earth may at times be as high as 70 or 80 mc.[32] The high values are more likely to occur during the summer, and during the minimum of the sunspot cycle.

Rapid multipath fading exists on ionospheric circuits and is superimposed on the longer term variations discussed above. The amplitude of the fast fading follows the Rayleigh distribution and echo delays up to several milliseconds are observed. These delays are 10^4 to 10^5 times as long as for tropospheric transmission. As a result of these relatively long delays uncorrelated selective fading can occur within a few hundred cycles. This produces the distortion on voice circuits that is characteristic of "short wave" transmission.

Ionospheric Scatter

The maximum usable frequency used in conventional skywave transmission is defined as the highest frequency returned to earth for which the average transmission is within a few db of free space. As the frequency increases above the muf the signal level decreases rapidly but does not drop out completely. Although the signal level is low, reliable transmission can be obtained at frequencies up to 50 mc or higher and to distances up to at least 1,200 to 1,500 miles.[33] In this case the signal is 80 to 100 db below the free space value and its satisfactory use requires much higher power and larger antennas than are ordinarily used in ionospheric transmission. The approximate variation in median signal level with frequency is shown in Fig. 18.

Ionospheric scatter is apparently the result of reflections from many
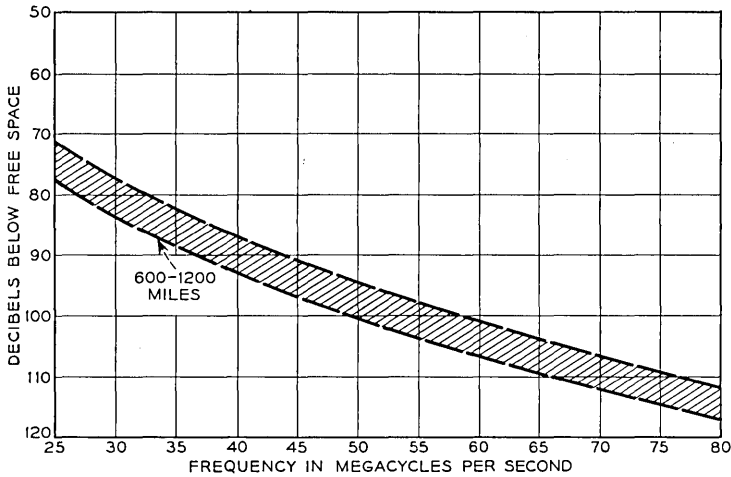
Fig. 18 — Median signal levels for ionospheric scatter transmission.

patches of ionization in the E layer. It is suspected that meteors are important in establishing and in maintaining this ionization but this has not been clearly determined.

In common with other types of transmission, the fast fading follows a Rayleigh distribution. The distribution of hourly median values relative to the long term median (after the high signals resulting from sporadic E transmission have been removed) is approximately a normal probability law with a standard deviation of about 6 to 8 db.

Ionospheric scatter transmission is suitable for several telegraph channels but the useful bandwidth is limited by the severe selective fading that is characteristic of all ionospheric transmission.

VI. NOISE LEVELS

The usefulness of a radio signal is limited by the "noise" in the receiver. This noise may be either unwanted external interference or the first circuit noise in the receiver itself.

Atmospheric static is ordinarily controlling at frequencies below a few megacycles while set noise is the primary limitation at frequencies above 200 to 500 mc. In the 10- to 200-mc band the controlling factor depends on the location, time of day, etc. and may be either atmospheric static, man made noise, cosmic noise, or set noise.

The theoretical minimum circuit noise caused by the thermal agitation of the electrons at usual atmospheric temperatures is 204 db below one

watt per cycle of bandwidth; that is, the thermal noise power, in dbw is −204 + 10 log (bandwidth). The first circuit or set noise is usually higher than the theoretical minimum by a factor known as the noise figure. For example, the set noise in a receiver with a 6-kc noise bandwidth and an 8-db noise figure is 158 db below 1 watt, which is equivalent to 0.12 microvolts across 100 ohms. Variations in thermal noise and set noise follow the Rayleigh distribution, but the quantitative reference is usually the rms value (63.2 per cent point), which is 1.6 db higher than the median value shown on Figs. 4 and 10. Momentary thermal noise peaks more than 10 to 12 db above the median value occur for a small percentage of the time.

Atmospheric static is caused by lightning and other natural electrical disturbances, and is propagated over the earth by ionospheric transmission. Static levels are generally stronger at night than in the daytime. Atmospheric static is more noticeable in the warm tropical areas where the storms are most frequent than it is in the colder northern regions which are far removed from the lightning storms.

Typical average values of noise in a 6-kc band are shown on Fig. 19. The atmospheric static data are rough yearly averages for a latitude of 40°. Typical summer averages are a few db higher than the value on Fig. 19 and the corresponding winter values are a few db lower. The average noise levels in the tropics may be as much as 15 db higher than
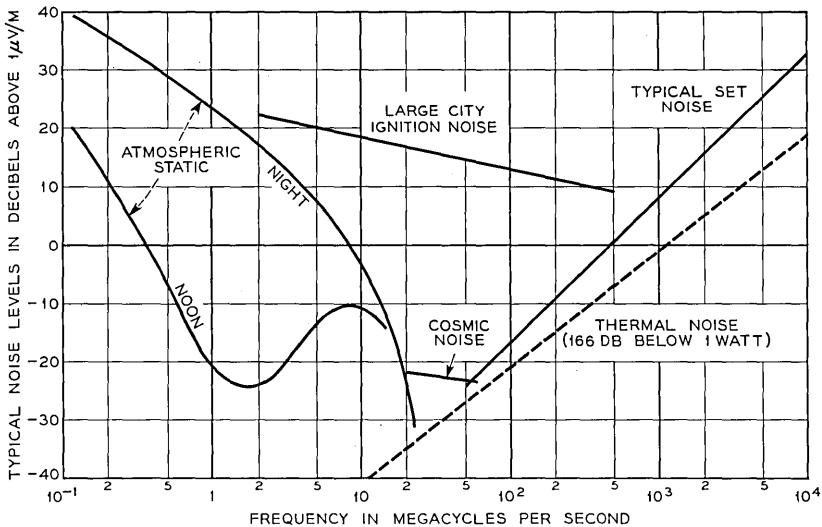

FIG. 19 — Typical average noise level in a 6-kc band.

for latitudes of 40° while in the Arctic region the noise may be 15 to 25 db lower. The corresponding values for other bandwidths can be obtained by adding 10 db for each 10-fold increase in bandwidth. More complete estimates of atmospheric noise on a world wide basis are given in the National Bureau of Standards Bulletin 462.[29] These noise data are based on measurements with a time constant of 100 to 200 milliseconds. Noise peaks, as measured on a cathode ray tube, may be considerably higher.

The man made noise shown on Fig. 19 is caused primarily by operation of electric switches, ignition noise, etc., and may be a controlling factor at frequencies below 200 to 400 mc. Since radio transmission in this frequency range is primarily tropospheric (ground wave), man made noise can be relatively unimportant beyond 10 to 20 miles from the source. In rural areas, the controlling factor can be either set noise or cosmic noise.

Cosmic and solar noise is a thermal type interference of extra-terrestial origin.[34] Its practical importance as a limitation on communication circuits seems to be in the 20- to 80-mc range. Cosmic noise has been found at much higher frequencies but its magnitude is not significantly above set noise. On the other hand, noise from the sun increases as the frequency increases and may become the controlling noise source when high gain antennas are used. The rapidly expanding science of radio astronomy is investigating the variations in both time and frequency of these extra-terrestial sources of radio energy.

REFERENCES

1. H. T. Friis, A Note on a Simple Transmission Formula Proc. I.R.E., **34,** pp. 254–256, May, 1946.
2. K. Bullington, Radio Propagation at Frequencies Above 30 Megacycles, Proc. I.R.E., **35,** pp. 1122–1136; Oct., 1947.
3. K. Bullington, Reflection Coefficients of Irregular Terrain, Proc. I.R.E., **42,** pp. 1258–1262; Aug., 1954.
4. W. M. Sharpless, Measurements of the Angle of Arrival of Microwaves, Proc. I.R.E., **34,** pp. 837–845, Nov., 1946.
5. A. B. Crawford and W. M. Sharpless, Further Observations of the Angle of Arrival of Microwaves, Proc. I.R.E., **34,** pp. 845–848, Nov., 1946.
6. A. B. Crawford and W. C. Jakes, Selective Fading of Microwaves, B.S.T.J., **31,** pp. 68–90; January, 1952.
7. R. L. Kaylor, A Statistical Study of Selective Fading of Super High Frequency Radio Signals, B.S.T.J., **32,** pp. 1187–1202, Sept., 1953.
8. H. E. Bussey, Microwave Attenuation Statistics Estimated from Rainfall and Water Vapor Statistics, Proc. I.R.E., **38,** pp. 781–785, July, 1950.
9. J. C. Schelleng, C. R. Burrows, E. B. Ferrell, Ultra-Short Wave Propagation, B.S.T.J., **12,** pp. 125–161, April, 1933.
10. MIT Radiation Laboratory Series, L. N. Ridenour, Editor-in-Chief, Volume 13, Propagation of Short Radio Waves, D. E. Kerr, Editor, 1951, McGraw-Hill.

11. Summary Technical Report of the Committee on Propagation, National Defense Research Committee. Volume 1, Historical and Technical survey. Volume 2, Wave Propagation Experiments. Volume 3, Propagation of Radio Waves. Stephen S. Attwood, editor, Washington, D.C., 1946.

12. C. W. Burrows and M. C. Gray, The Effect of the Earth's Curvature on Ground Wave Propagation, Proc. I.R.E., **29,** pp. 16–24, Jan., 1941.

13. K. Bullington Characteristics of Beyond-Horizon Radio Transmission, Proc. I.R.E., **43,** p. 1175; Oct., 1955.

14. W. E. Gordon, Radio Scattering in The Troposphere, Proc. I.R.E., **43,** p. 23, Jan., 1955.

15. K. Bullington, Radio Transmission Beyond the Horizon in the 40- to 4,000 MC Band, Proc. I.R.E., **41,** pp. 132–135, Jan., 1953.

16. K. A. Norton, P. L. Rice and L. E. Vogler, The Use of Angular Distance in Estimating Transmission Loss and Fading Range for Propagation Through a Turbulent Atmosphere Over Irregular Terrain, Proc. I.R.E., **43,** pp. 1488–1526, Oct., 1955.

17. F. H. Dickson, J. J. Egli, J. W. Herbstreit, and G. S. Wickizer, Large Reductions of VHF Transmission Loss and Fading by Presence of Mountain Obstacle in Beyond Line-Of-Sight Paths, Proc. I.R.E., **41,** pp. 967–9, Aug., 1953.

18. K. Bullington, W. J. Inkster and A. L. Durkee, Results of Propagation Tests at 505 MC and 4090 MC on Beyond-Horizon Paths, Proc. I.R.E., **43,** pp. 1306–1316, Oct., 1955.

19. Same as 13.

20. H. G. Booker and J. T. deBettencourt, Theory of Radio Transmission by Tropospheric Scattering Using Very Narrow Beams, Proc. I.R.E., **43,** pp. 281–290, March, 1955.

21. W. H. Tidd, Demonstration of Bandwidth Capabilities of Beyond-Horizon Tropospheric Radio Propagation, Proc. I.R.E., **43,** pp. 1297–1299, October, 1955.

22. K. Bullington, Radio Propagation Variations at VHF and UHF, Proc. I.R.E., **38,** pp. 27–32, Jan., 1950.

23. W. R. Young, Comparison of Mobile Radio Transmission at 150, 450, 900 and 3700 MC, B.S.T.J., **31,** pp. 1068–1085, Nov., 1952.

24. K. A. Norton, The Physical Reality of Space and Surface Waves in the Radiation Field of Radio Antennas, Proc. I.R.E., **25,** pp. 1192–1202, Sept., 1937.

25. Same as 2.

26. C. R. Burrows, Radio Propagation Over Plane Earth-Field Strength Curves, B.S.T.J., **16,** pp. 45–75, Jan., 1937.

27. K. A. Norton, The Propagation of Radio Waves Over the Surface of the Earth and in the Upper Atmosphere, Part II, Proc. I.R.E., **25,** pp. 1203–1236, Sept., 1937.

28. Same as 26.

29. National Bureau of Standards Circular 462, Ionospheric Radio Propagation, Superintendent of Documents, U.S. Govt. Printing Office, Washington 25, D.C.

30. National Bureau of Standards, CRPL Series D, Basic Radio Propagation Predictions, issued monthly by U.S. Govt. Printing Office.

31. National Bureau of Standards Circular 465, Instructions for Use of Basic Radio Propagation Predictions, Superintendent of Documents, U.S. Govt. Printing Office, Washington, D.C.

32. E. W. Allen, Very-High Frequency and Ultra-High Frequency Signal Ranges as Limited by Noise and Co-channel Interference, Proc. I.R.E., **35,** pp. 128–136, Feb., 1947.

33. D. K. Bailey, R. Bateman and R. C. Kirby, Radio Transmission at VHF by Scattering and Other Processes in the Lower Ionosphere, Proc. I.R.E., **43,** pp. 1181–1230, Oct., 1955.

34. J. W. Herbstreit, Advances in Electronics, **1,** Academic Press, Inc., pp. 347–380, 1948.

A Reflection Theory for Propagation Beyond the Horizon[*]

By H. T. FRIIS, A. B. CRAWFORD and D. C. HOGG

(Manuscript received January 9, 1957)

Propagation of short radio waves beyond the horizon is discussed in terms of reflection from layers in the atmosphere formed by relatively sharp gradients of refractive index. The atmosphere is assumed to contain many such layers of limited dimensions with random position and orientation. On this basis, the dependence of the propagation on path length, antenna size and wavelength is obtained.

INTRODUCTION

It was pointed out several years ago[1] that power propagated beyond the radio horizon at very short wavelengths greatly exceeds the power calculated for diffraction around the earth. This beyond-the-horizon propagation has stimulated numerous experimental and theoretical investigations.[2] Booker and Gordon,[3] Villars and Weisskopf[4] and others have developed theories based on scattering of the radio waves by turbulent regions in the troposphere. This paper proposes a theory in which uncorrelated reflections from layers in the troposphere are assumed responsible for the power propagated beyond the horizon.

In developing this theory, some arbitrary assumptions of necessity have been made concerning the reflecting layers since, at the present time, our detailed knowledge of the atmosphere is insufficient. However, calculations based on the theory are found to be in good agreement with reported measurements of beyond-the-horizon propagation.

Measurement of the dielectric constant of the atmosphere[5] has shown that relatively sharp variations in the gradients of refractive index exist in both the horizontal and vertical planes. Although the geometrical structure of the boundaries formed by the gradients is not well known, one may postulate an atmosphere of many layers of limited extent and

---

[*] This material was presented at the I.R.E. Canadian Convention, Toronto, Canada, October 3, 1956.

arbitrary aspect.* The number and size of the reflecting layers, as well as the magnitude of the discontinuities in the gradient of dielectric constant which form them, influence the received power.

The reflecting properties of the layers are discussed first. Next, an expression for the received power is obtained by summing the contributions of many layers in the volume common to the idealized patterns chosen to represent the transmitting and receiving antenna beams.† This expression is then used to calculate the effect on received power of changes in such parameters as the orientation of the antennas, wavelength, distance, and antenna size.

The MKS system of units is used throughout.
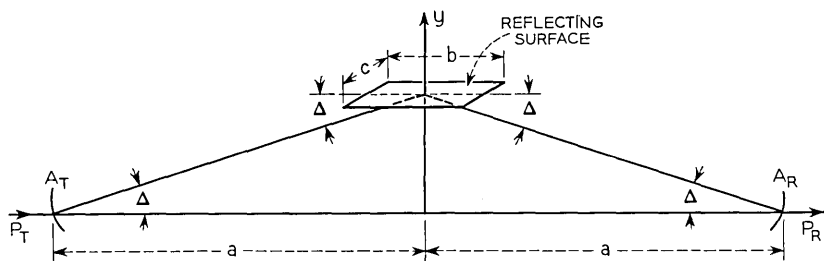
Fig. 1 — Reflection by a layer.

EFFECT OF LAYER SIZE

Propagation from a transmitting antenna of effective area A_T to a receiving antenna of effective area A_R by means of a reflecting layer is illustrated in Fig. 1. The ray from transmitter to receiver grazes the layer at angle Δ. The reflection from the layer depends on the amplitude reflection coefficient, q, which is a function of the grazing angle, and on the dimensions of the layer relative to the dimension of a Fresnel zone.‡ Three cases, depending on the layer dimensions, will be considered.

---

* After this paper was submitted for publication, a report was received giving some measurements of sharp variations in dielectric constant gradient and estimates of the horizontal dimensions of layers in the troposphere. J. R. Bauer, The Suggested Role of Stratified Elevated Layers in Transhorizon Short-Wave Radio Propagation, Technical Report No. 124, Lincoln Laboratory, M.I.T., Sept., 1956.

† Under some conditions, layers outside the volume common to the antenna beams may contribute appreciably to the received power. Phenomena such as multiple reflections and trapping mechanisms are not considered in this study.

‡ The power received by reflection from the layer in Fig. 1 can be calculated approximately by assuming it to be the same as the power that would be received by diffraction through an aperture in an absorbing screen, the dimensions of the aperture being the same as the dimensions of the layer projected normally to the directions of propagation. The field at the receiver is calculated from the distribution of Huygens sources in the aperture. The received power, expressed in

Case 1. Large Layers

If the layer were a plane, perfectly reflecting surface of unlimited extent, the power at the terminals of antenna A_R would be the same as the power received under line-of-sight conditions,[6]

$$P_R = P_T \frac{A_T A_R}{4\lambda^2 a^2}$$

If the layer has an amplitude reflection coefficient, q, the received power is,

$$P_R = P_T \frac{A_T A_R}{4\lambda^2 a^2} q^2$$

This relation applies when the layer dimensions are large in terms of the wavelength and are large compared with the Fresnel zone dimensions; that is, $b > \sqrt{2a\lambda}/\Delta$ and $c > \sqrt{2a\lambda}$.

Case 2. Small Layers

When the dimensions of the layer are small compared with the Fresnel zone, but large compared with the wavelength, the received power is given by the "radar" formula,

$$P_R = P_T \frac{A_T A_R}{\lambda^4 a^4} c^2 (b\Delta)^2 q^2$$

This relation applies when $b < \sqrt{2a\lambda}/\Delta$ and $c < \sqrt{2a\lambda}$.

terms of Fresnel integrals, is

$$P_R = P_T \frac{A_T A_R}{\lambda^2 a^2} [C^2(u) + S^2(u)][C^2(v) + S^2(v)]$$

where $u = \dfrac{c}{\sqrt{\lambda a}}$ and $v = \dfrac{b\Delta}{\sqrt{\lambda a}}$

When u and v are very large, we have, approximately,

$$C(u) = S(u) = C(v) = S(v) = \tfrac{1}{2}$$

and the expression for P_R reduces to that given for Case 1 above, except for the factor q^2.

When both u and v are very small, we have approximately,

$$C(u) = u \qquad C(v) = v$$
$$S(u) = o \qquad S(v) = o$$

and the expression for P_R reduces to that given for Case 2.

When u is large and v is small the expression for P_R given in Case 3 results.

Case 3. Layers of Intermediate Size

If the layer dimensions are such that c is large but $b\Delta$ is small, compared with the Fresnel zone dimension, the received power is given by

$$P_R = P_T \frac{A_T A_R}{2\lambda^3 a^3} (b\Delta)^2 q^2$$

In the atmosphere, c and b are likely to be about equal, on the average, and we have for this case, $\sqrt{2a\lambda} < b < \sqrt{2a\lambda}/\Delta$.

All three of these cases may be present at various times, since the structure of the atmosphere changes from day to day. However, for the purpose of the present study, Case 3 is considered most prevalent and is assumed in all the calculations to follow.

Many of the numerous layers that are assumed to contribute to the received power are not necessarily horizontally disposed, they may be oriented in any direction. Therefore, reflection in the direction of the receiver can take place from layers located both on and off the great circle path. If there are N contributing layers per unit volume in the region V common to the radiation patterns of the transmitting and receiving antennas, then for Case 3,

$$P_R = P_T \frac{A_T A_R N b^2}{2\lambda^3 a^3} \int_V \Delta^2 q^2 \, dV \tag{1}$$

In this relation it has been assumed that the layer size and the number of layers per unit volume remain sensibly constant throughout the common volume.

The integration process requires expressions for the reflection coefficient q and the grazing angle Δ of the layers in the common volume. These quantities are derived in the following sections.

REFLECTION COEFFICIENT OF A LAYER

The reflection coefficient of a plane boundary (Fig. 2) separating two media whose dielectric constants, relative to free space, differ by an increment $d\varepsilon$ is given by Fresnel's laws of reflection. For both polarizations, the plane wave reflection coefficient of the boundary is

$$q = d\varepsilon/4\Delta^2$$
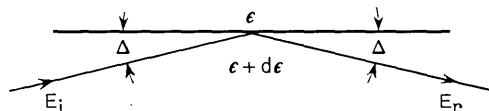
Fig. 2 — Reflection at a boundary between two homogeneous media.

provided $1 \gg \Delta^2 \gg d\varepsilon$. This reflection coefficient for an incremental change in dielectric constant can be used to calculate the reflection from discontinuities in the gradient of the dielectric constant of the atmosphere such as those shown for a stratified medium at $y = 0$ and $y = h$ in Fig. 3(b).

Such variations of dielectric constant are assumed to be representative of discontinuities in gradient as they exist in the physical atmosphere. The variations form the reflecting layers.

The method of calculating the reflection coefficient of such a stratified medium is due to S. A. Schelkunoff[7] and is illustrated schematically in Fig. 3 in which the medium has been subdivided into incremental steps. Consider the reflected wave from a typical incremental layer, dy, situated a distance y above the lower boundary of the layer, 0. From Fig. 3(a) it is clear that the phase of this wave is $4\pi y/\lambda \sin \Delta$ relative to that of a wave reflected from the lower boundary. The incremental reflection coefficient is $d\varepsilon/4\Delta^2 = -K\,dy/4\Delta^2$, where K is the change in gradient of the dielectric constant at the boundaries of the layer. The field reflected by layer dy is therefore,

$$dE_R = -E_i \frac{K}{4\Delta^2} e^{-j(4\pi y/\lambda)\sin \Delta}\, dy$$

One now obtains the complete reflected field by summing the reflections from all increments within the layer of thickness h.

$$E_r = \int_0^h dE_r = jE_i \frac{K\lambda}{16\pi\Delta^2 \sin \Delta} [1 - e^{-j(4\pi h/\lambda)\sin \Delta}]$$

This relation shows that the layer is equivalent to two boundaries at

(a)   (b)

Fig. 3 — Plane-wave reflection at an incremental layer dy within a stratified medium extending from $y = 0$ to $y = h$.

$y = 0$ and $y = h$, each with reflection coefficient

$$q = \frac{K\lambda}{16\pi\Delta^3} \tag{2}$$

If the abrupt change in slope, the solid line in Fig. 3(b), is replaced by a gradual change as indicated by the dotted lines, (2) still holds provided $d < \lambda/4\Delta$. For more gradual changes, $d = n\lambda/4\Delta$ where $n > 1$, the reflection coefficient is

$$q = \frac{K\lambda}{16\pi\Delta^3} \cdot \frac{\sin\frac{\pi n}{2}}{\frac{\pi n}{2}}$$

and q varies with n between $q = 0$ and

$$q = \frac{K\lambda}{16\pi\Delta^3} \cdot \frac{2}{\pi n}$$

Smoothing of the boundaries reduces the value of q.

It will be assumed in all the calculations to follow that reflection from layers in the troposphere is described by (2).

VARIATION OF STRENGTH OF LAYERS WITH HEIGHT

The formula for the reflection coefficient includes the factor K, which represents the change in the gradient of the dielectric constant at the boundaries of the layer. A dielectric constant profile constructed of many randomly positioned gradients is shown schematically in Fig. 4. The variations are shown as departures from the standard linear gradient. Measurements[5] indicate that the fluctuations of the dielectric constant normally decrease with height above ground. The changes in the dielectric constant gradients associated with these fluctuations probably vary in a similar manner so that K is some inverse function of the height above the earth. However, to simplify the computation of received power, to be described later, we have adopted the cylindrical coordinate system shown in Fig. 5, and it is convenient, then, to let K be a function of ρ, the distance from the chord joining the transmitter and receiver to the point in question.

We assume, therefore, that

$$K = \frac{3,200K_1}{\rho} \tag{3}$$

where K_1 is the change in gradient at point A in Fig. 5 which, for a typi-
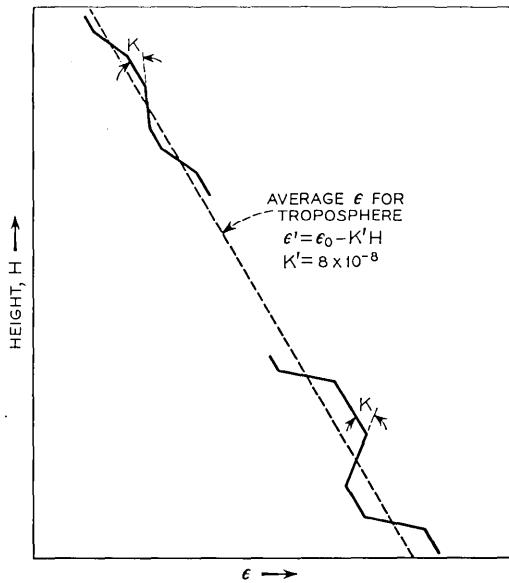
Fig. 4 — Schematic illustration of variation of the dielectric constant in the troposphere.

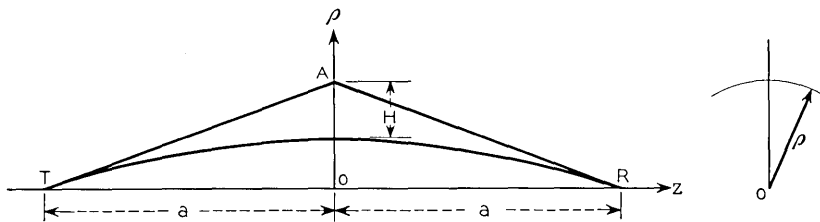Fig. 5 — Coordinate system for a beyond-the-horizon circuit.

cal path length of 200 miles, is about 1,600 meters (1 mile) above the earth or, since $\rho = 2H$, 3,200 meters from the z axis.

Equation 3 is used in all the calculations to follow.

THE GRAZING ANGLE Δ

The grazing angle Δ at the slightly tilted layer shown in Fig. 6 is given by

$$\tan 2\Delta = \frac{2a\rho}{a^2 - z^2 - \rho^2}$$

Throughout the volume common to the antenna patterns, $\Delta \ll 1$, $\rho \ll a$ and $z < a/2$. Then

$$\Delta \approx \frac{\rho}{a} \tag{4}$$

It is evident that Δ is constant and equal to ρ/a when the point (ρ, z) is located on a cylinder with axis TR and radius ρ. It is this feature that
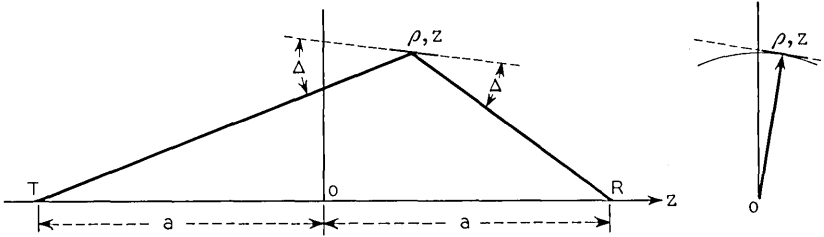
Fig. 6 — Grazing angle Δ at a layer.
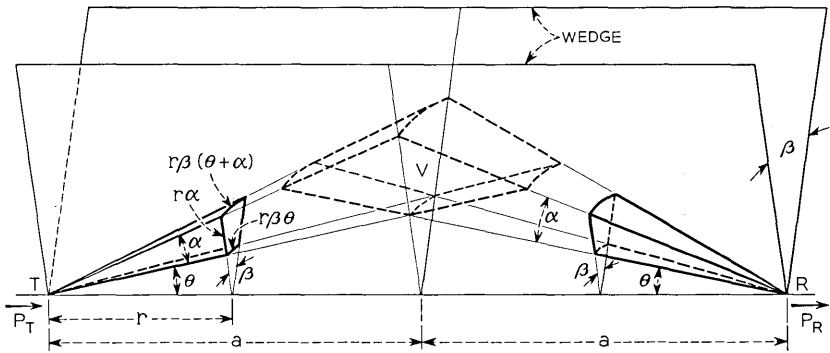
Fig. 7 — Idealized antenna patterns used in this study.

$$dV_1 = 2\left(\frac{\rho_1}{\theta} - a\right)\beta\rho_1 d\rho_1 \qquad dV_2 = 2\left(a - \frac{\rho_2}{\theta + \alpha}\right)\beta\rho_2 d\rho_2$$
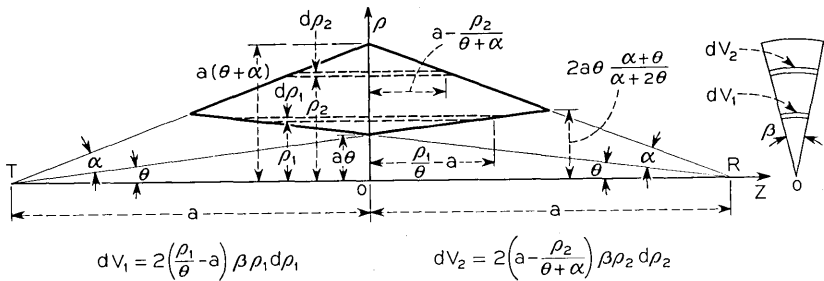
Fig. 8 — Integration over the common volume.

suggested the unusual idealized antenna patterns shown in Fig. 7, which are described in the next section.

CALCULATION OF THE RECEIVED POWER

Substituting (2), (3) and (4) in (1), one obtains for the received power,

$$P_R = P_T M a A_R A_T \lambda^{-1} \int_V \rho^{-6} \, dV \qquad (5)$$

where

$$.M \approx 2000 b^2 K_1^2 N \qquad (6)$$

To integrate over the volume common to actual antenna patterns would be difficult. We have, as mentioned before, replaced the actual patterns with the idealized patterns shown in perspective in Fig. 7 and in plane projection in Fig. 8. The patterns (Fig. 7) are bounded by side planes of the large wedge and by surfaces of cones with axis TR. The common volume is indicated by broken lines and is well defined. Since the grazing angle Δ is constant for the incremental cylindrical volumes dV_1 and dV_2 shown in Fig. 8, it is easy to integrate over the common volume V and we obtain

$$\int_V \rho^{-6} \, dV = \frac{\beta}{6\theta^4 a^3} f\left(\frac{\alpha}{\theta}\right) \qquad (7)$$

$$f\left(\frac{\alpha}{\theta}\right) = 1 + \frac{1}{\left(1 + \frac{\alpha}{\theta}\right)^4} - \frac{1}{8} \left(\frac{2 + \frac{\alpha}{\theta}}{1 + \frac{\alpha}{\theta}}\right)^4 \qquad (8)$$

The function $f(\alpha/\theta)$ is plotted in Fig. 9.

The gain of the idealized antennas is $G = 8\pi/\alpha\beta(\alpha + 2\theta)$ and the effective area is

$$A = \frac{2\lambda^2}{\alpha\beta(\alpha + 2\theta)} \qquad (9)$$

The area of a cross section of the antenna pattern is bounded by two straight sides, $r\alpha$, and two curved sides $r\theta\beta$ and $r(\theta + \alpha)\beta$. The aspect ratio is defined as the ratio of the sum of the lengths of the curved sides to the sum of the lengths of the straight sides. It is equal to one when

$$\beta = \frac{2\alpha}{\alpha + 2\theta} \qquad (10)$$

Substituting (10) in (9) gives the effective area of the idealized antenna
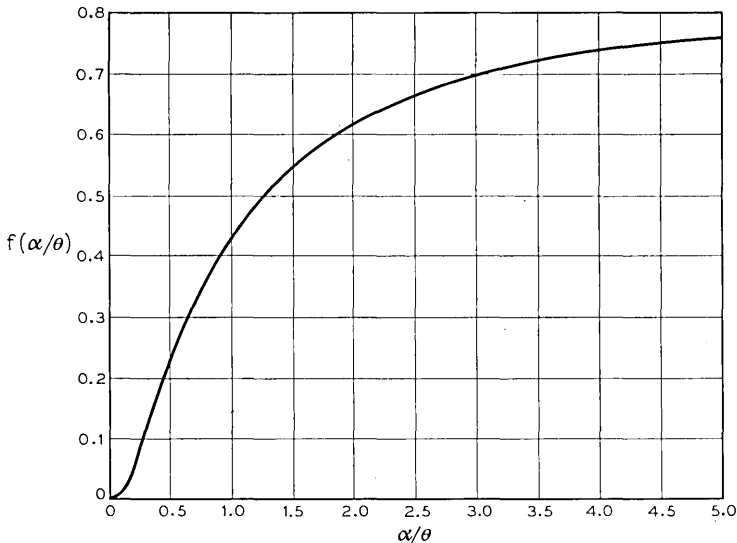
Fig. 9 — The function $f\,(\alpha/\theta)$.

with aspect ratio one,

$$A = \frac{\lambda^2}{\alpha^2} \tag{11}$$

Substituting (7), (10) and (11) in (5) gives for *identical transmitting and receiving antennas* with *aspect ratio one*,

$$P_R = P_T \frac{M}{3} \frac{\lambda^3}{\alpha^3} \frac{1}{\theta^5 a^2} \frac{1}{2 + \dfrac{\alpha}{\theta}} f\left(\frac{\alpha}{\theta}\right)^* \tag{12}$$

For actual antennas, α may be taken to be the half-power beam-width.

In the following sections, (12) will be used to derive some of the general properties of propagation beyond the horizon.

---

* K. Bullington has suggested that a useful form for equation (12) is

$$P_R = \left[\frac{P_T \lambda^2}{4 a^2 \alpha^4}\right]\left[\frac{4 M \lambda}{3 \theta^4}\right]\left[\frac{\dfrac{\alpha}{\theta} f\left(\dfrac{\alpha}{\theta}\right)}{2 + \dfrac{\alpha}{\theta}}\right]$$

where the first term in brackets represents the power that would be received in free space, the second term involves the characteristics of the troposphere, and the third term is a correction factor for narrow beam antennas.

RECEIVED POWER VERSUS ANGLE θ

The angle θ is the angle between the lower edge of the idealized antenna pattern and the straight line joining the terminals (see Fig. 7). The minimum value of θ is determined by the profile of the transmission path. If λ, α and a are constants, (12) can be used to calculate the ratio of the powers, P_{R1} and P_{R2}, received at two different angles, θ_1 and θ_2,

$$\frac{P_{R1}}{P_{R2}} = \left(\frac{\theta_2}{\theta_1}\right)^5 \frac{2 + \dfrac{\alpha}{\theta_2}}{2 + \dfrac{\alpha}{\theta_1}} \frac{f\left(\dfrac{\alpha}{\theta_1}\right)}{f\left(\dfrac{\alpha}{\theta_2}\right)} \tag{13}$$

Equation (13) shows the importance of having the angle θ as small as possible. For example, for $\theta_1 = \alpha$ and $\theta_2/\theta_1 = 1.25$, the power ratio is 3.4 (5 db). Thus in an actual circuit the antenna pattern should be close to the horizon plane.

RECEIVED POWER VERSUS WAVELENGTH

Consider a given path in which a and θ are specified. Equation (12) can be used to calculate the ratio of received powers, P_{R1} and P_{R2}, corresponding to two different wavelengths, λ_1 and λ_2.

$$\frac{P_{R1}}{P_{R2}} = \left(\frac{\lambda_1}{\lambda_2}\right)^3 \left(\frac{\alpha_2}{\alpha_1}\right)^3 \frac{2 + \dfrac{\alpha_2}{\theta}}{2 + \dfrac{\alpha_1}{\theta}} \frac{f\left(\dfrac{\alpha_1}{\theta}\right)}{f\left(\dfrac{\alpha_2}{\theta}\right)} \tag{14}$$

where α_1 and α_2 are the beamwidths of the antenna patterns at wavelengths λ_1 and λ_2 respectively.

Case I. Equal antenna gains at the two wavelengths.

For this case, $\alpha_1 = \alpha_2$ and equation (14) reduces to

$$\frac{P_{R1}}{P_{R2}} = \left(\frac{\lambda_1}{\lambda_2}\right)^3 \tag{15}$$

In free space the power ratio would be

$$\frac{P_{R1}}{P_{R2}} = \left(\frac{\lambda_1}{\lambda_2}\right)^2 \tag{16}$$

or

$$\frac{P_{R1}/P_{R2} \text{ (Beyond-Horizon)}}{P_{R1}/P_{R2} \text{ (Free Space)}} = \frac{\lambda_1}{\lambda_2} \tag{17}$$

Thus if 400 mcs and 4,000 mcs were propagated over the same path, the antenna gains being identical for the two systems, then, on the average, one would expect the received power relative to the free space value at 400 mcs to be 10 db higher than that at 4,000 mcs because of the characteristics of the troposphere.

Case II. Equal antenna apertures for the two wavelengths.

For this case, $\alpha_1/\alpha_2 = \lambda_1/\lambda_2$ and (14) reduces to

$$\frac{P_{R1}}{P_{R2}} = \frac{2 + \dfrac{\alpha_2}{\theta}}{2 + \dfrac{\alpha_1}{\theta}} \frac{f\left(\dfrac{\alpha_1}{\theta}\right)}{f\left(\dfrac{\alpha_2}{\theta}\right)} \tag{18}$$

Experimental data for this case was obtained on the 150 nautical mile test circuit between St. Anthony and Gander in Newfoundland.[8] The antennas for both wavelengths were paraboloids 8.5 meters in diameter. Simultaneous transmission tests at $\lambda_1 = 0.074\ m$ and $\lambda_2 = 0.6\ m$ were conducted for a full year. For this circuit,

$$\theta = 0.94° \ (4/3 \text{ earth radius})$$

$$\alpha_1 = 66\ \frac{0.074}{8.5} = 0.575°$$

$$\alpha_2 = 66\ \frac{0.6}{8.5} = 4.65°$$

Using these values in (18), we get for the ratio of received powers,

$$P_{R1}/P_{R2} = 1.01$$

For antennas of equal aperture in free space,

$$P_{R1}/P_{R2} = (\lambda_2/\lambda_1)^2 = 65.5$$

Therefore,

$$\frac{P_{R1}/P_{R2} \text{ (Beyond Horizon)}}{P_{R1}/P_{R2} \text{ (Free Space)}} = \frac{1}{65} = -18.1 \text{ db}$$

The Summary of Results, Sections 1 and 2 on page 1316 of Reference 8, gives -17 db for this ratio. The agreement between calculated and measured values is very good.

RECEIVED POWER VERSUS DISTANCE

If antenna size and wavelength are specified, (12) gives for two distances, a_1 and a_2 ,

$$\frac{P_{R1}}{P_{R2}} = \left(\frac{a_2}{a_1}\right)^7 \frac{2 + \dfrac{\alpha}{\theta_2}}{2 + \dfrac{\alpha}{\theta_1}} \frac{f\left(\dfrac{\alpha}{\theta_1}\right)}{f\left(\dfrac{\alpha}{\theta_2}\right)} \tag{19}$$

For $a_2 = 2a_1$, (19) gives for different values of α/θ_1

$\alpha/\theta_1 =$	0.5	1	2	4
$P_{R1}/P_{R2} =$	276 (24 db)	197 (23 db)	138 (21.5 db)	104 (20 db)

Fig. 1 in Bullington's paper,[9] which gives the median signal level in decibels below the free space value as a function of distance, shows an 18 db increase in attenuation when the distance is doubled. This corresponds to a ratio of received powers of $18 + 6 = 24$ db. The examples in the table above give an average increase in attenuation of 22 db.

RECEIVED POWER VERSUS ANTENNA SIZE

Equation 14 can be used to calculate the effect on received power of changing simultaneously the size (and, hence, the beamwidths) of the antennas used for transmitting and receiving, the wavelength and distance remaining fixed.

$$\frac{P_{R1}}{P_{R2}} = \left(\frac{\alpha_2}{\alpha_1}\right)^3 \frac{2 + \dfrac{\alpha_2}{\theta}}{2 + \dfrac{\alpha_1}{\theta}} \frac{f\left(\dfrac{\alpha_1}{\theta}\right)}{f\left(\dfrac{\alpha_2}{\theta}\right)} \tag{20}$$

where P_{R1} and P_{R2} are the received powers corresponding to the antenna beamwidths α_1 and α_2 respectively.

As an example, let α_2 be constant and equal to $4°$ and let θ be $1°$, corresponding to a 200-mile circuit. The table below gives the ratio P_{R1}/P_{R2} as α_1 is varied.

α_1	$4°$	$2°$	$1°$	$0.5°$	$0.25°$
P_{R1}/P_{R2} (db)	0	10	18.5	25.7	31.4
Change in db		10	8.5	7.2	5.7

Since α is inversely proportional to the antenna dimensions, the table shows that continued doubling of the antenna dimensions results in less and less increase in output power. The increase varies from 10 to 5.7 db

in the table. This is a characteristic feature of beyond-the-horizon prop-
agation. In free space, doubling the antenna dimensions would result
in a 12-db increase in output power.

Large antennas and high power transmitters are costly, and a proper
balance between their costs requires careful studies which are outside
the scope of this paper. In general, it is not believed worth while from
power considerations to increase the antenna size much beyond the di-
mensions that correspond to a pattern angle, α, equal to angle θ.

Another factor to be considered, however, is the effect of antenna size
on delay distortion in beyond-the-horizon circuits. From simple path
length considerations, one concludes that the delay distortion decreases
when the beamwidths of the antennas are made smaller. Therefore, delay
distortion requirements may dictate antenna sizes that are not justified
by power considerations alone.

SEASONAL DEPENDENCE

Both the effective earth radius, R_e, and the magnitude of the discon-
tinuities in gradient, K_1, are related to the season of the year. During
the summer when the water vapor content of the air is high, the effective
radius and the discontinuities in gradient are larger than in winter. Sub-
stituting a/R_e for θ and assigning summer and winter values for R_e and
K_1, (12) may be used to calculate the ratio of the power received in
summer and in winter.

$$\frac{P_R \text{ (Summer)}}{P_R \text{ (Winter)}} = \left(\frac{K_{1S}}{K_{1W}}\right)^2 \left(\frac{R_{eS}}{R_{eW}}\right)^5 \frac{2 + \dfrac{\alpha R_{eW}}{a}}{2 + \dfrac{\alpha R_{eS}}{a}} \frac{f\left(\dfrac{\alpha R_{eS}}{a}\right)}{f\left(\dfrac{\alpha R_{eW}}{a}\right)} \qquad (21)$$

$$\approx \left(\frac{K_{1S}}{K_{1W}}\right)^2 \left(\frac{R_{eS}}{R_{eW}}\right)^6$$

For example, if we assume $K_{1S} = 2K_{1W}$ and $R_{eS} = 1.2\,R_{eW}$, then $P_{RS}/P_{RW} = 11.9$ (10.75 db). A seasonal variation has been observed.[8, 10]

DEPENDENCE OF RECEIVED POWER ON ANTENNA ORIENTATION

The variation of received power with orientation of the antennas at
the terminals of a beyond-the-horizon circuit differs considerably from
that observed under line-of-sight conditions. Consider, for example, Fig.
10 which shows the beams of the transmitting and receiving antennas
elevated simultaneously. The variation of received power can be calcu-
lated from (13). As an example, consider the 188-mile circuit between

Crawford Hill, N. J., and Round Hill, Mass., for which experimental data is published.[10] For this circuit $\alpha = 0.65°$ (3 db points) and $\theta_1 = 1°$ (4/3 earth radius). The table below gives the calculated variation of received power as angle θ_2 is varied.

$\theta_2 =$	1°	1.1°	1.2°	1.4°	1.6°	1.8°	2°	2.2°
$10 \log_{10} (P_{R1}/P_{R2}) =$	0	2.3	4.5	8.5	12	15	17.9	20.5

The received power versus elevation angle, $\gamma = \theta_2 - \theta_1$, is plotted in Fig. 10. The calculated and experimental curves are in good agreement.

If the beams of the antennas are steered simultaneously in the horizontal plane, Fig. 11, the calculation of the variation of received power is
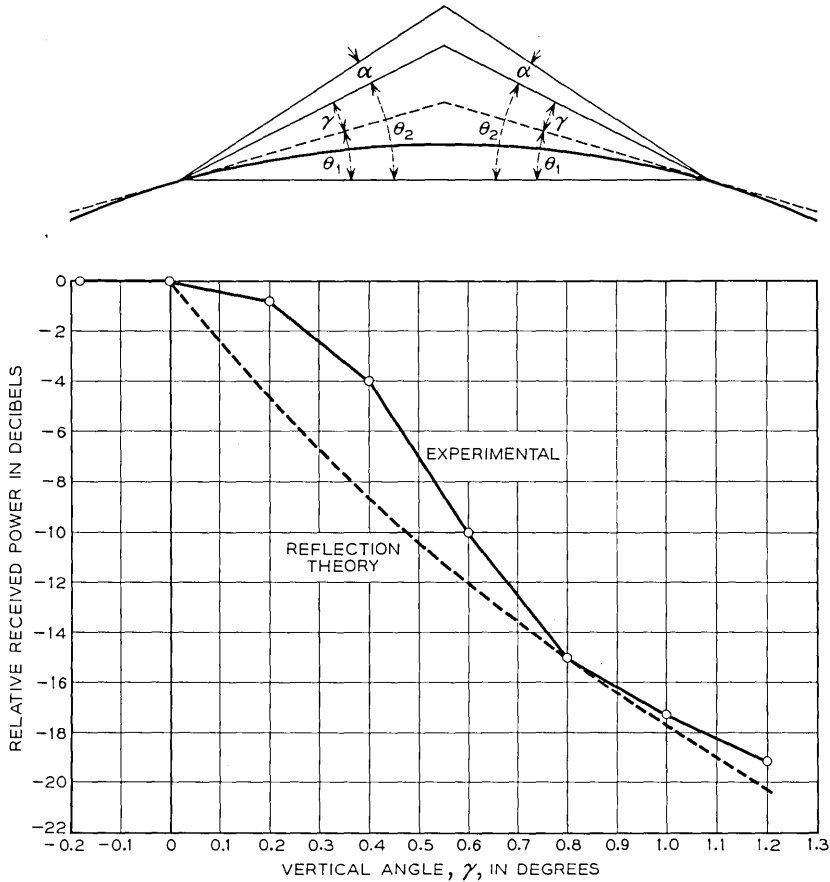

Fig. 10 — Relation between received power and vertical angle γ.

comparatively simple. In horizontal steering, the intersection of the axes of the antenna beams moves along line AB in the figure labelled "Cross section at 0." If the intersection of the beams moved along the circle A-C, the received power would not change. The decrease in power caused by moving the beams from position A to B is given by (13). The calcu-
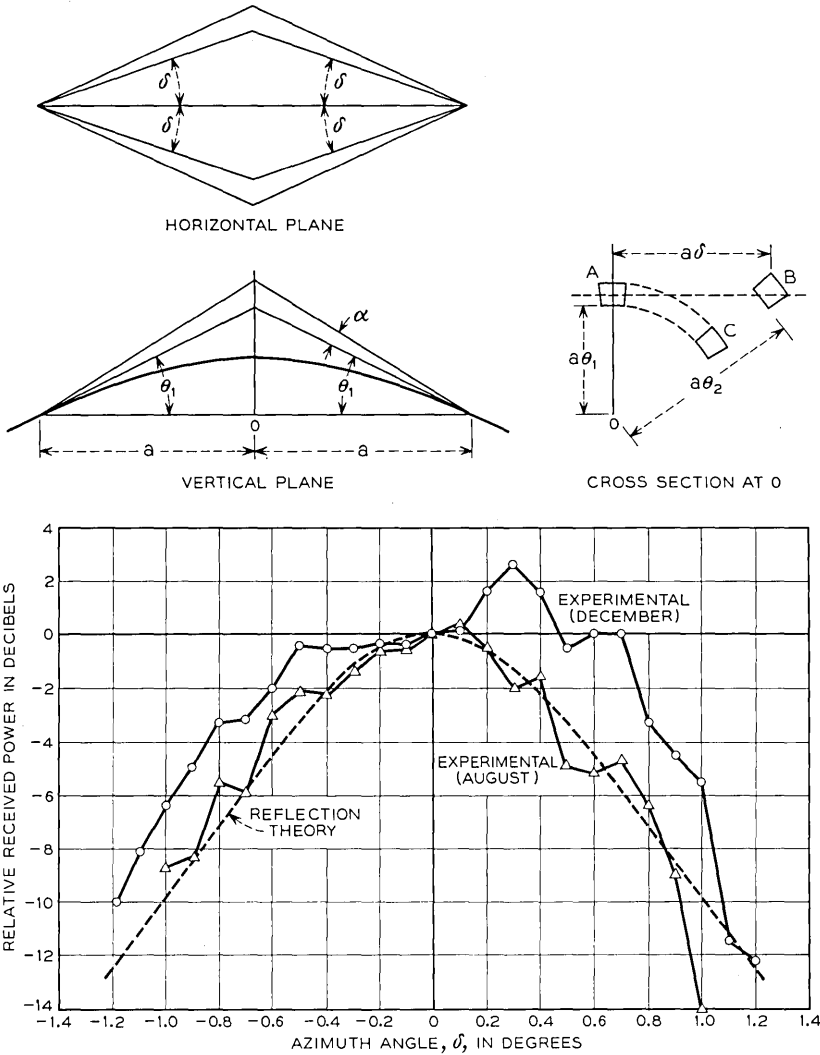

Fig. 11 — Relation between received power and azimuth angle δ.

lations are identical with the calculations for elevation steering; the elevation angle θ_2 is related to the azimuth angle δ and the beamwidth angle α by

$$\delta^2 = (\theta_2 - \theta_1)(\theta_2 + \theta_1 + \alpha)$$

A calculated curve of received power versus azimuth angle is shown in Fig. 11 for the Crawford Hill-Round Hill circuit together with the reported experimental data.[10] The agreement is considered good.

THE VALUE OF FACTOR M IN EQUATION (12)

An average value for the factor M can be obtained from propagation data. Using equation (12), the ratio of received powers corresponding to free space and beyond-horizon transmission is

$$\frac{P_R \text{ (free space)}}{P_R \text{ (beyond-horizon)}} = \frac{0.75\,\theta^5 \left(2 + \dfrac{\alpha}{\theta}\right)}{M\lambda\alpha f\left(\dfrac{\alpha}{\theta}\right)} \tag{22}$$

This ratio was found experimentally to be 5×10^6 (67 db) for the circuit between St. Anthony and Gander in Newfoundland.[8] For this circuit, $\alpha = 0.081$, $\theta = 0.0164$, $\lambda = 0.6$. Substituting these values in (22) we obtain,

$$M = 3 \times 10^{-14} \tag{23}$$

Substituting this value for M in (12) leads to the following equation for a beyond-horizon tropospheric circuit,

$$P_R = P_T \times 10^{-14} \frac{\lambda^3}{\alpha^3} \frac{1}{\theta^5 a^2} \frac{1}{2 + \dfrac{\alpha}{\theta}} f\left(\frac{\alpha}{\theta}\right) \tag{24}$$

Equations (6) and (23) give

$$b^2 K_1^2 N = 1.5 \times 10^{-17} \tag{25}$$

Although values of the layer dimension, b, the change in gradient, K_1, and the number of layers per unit volume, N, are not known, it is interesting to calculate N from (25) assuming reasonable values for b and K_1.

Assuming $K_1 = 4 \times 10^{-8}$, which is half the value of K', the average gradient of the dielectric constant in the troposphere, and $b = 1,000$ (1 km) we find $N = 10^{-8}$ or 10 layers per cubic kilometer.

CONCLUDING REMARKS

The interpretation of propagation beyond the horizon in terms of reflection from layers of limited size formed by variations in the gradient of the dielectric constant of the atmosphere leads to relatively simple results which are in good agreement with reported experimental data. The received power depends on the wavelength, the distance, and the size of the antennas used for the circuit and on the strength and size of the reflecting layers.

As mentioned earlier, the structure of the atmosphere may change markedly from time to time so that large, small and intermediate size layers play their parts at different times. Furthermore, the effective size of a given layer may be different for widely separated wavelengths, depending on the roughness of the layer in terms of the wavelength. All that can be expected of a study such as the present one is that it serve as a guide for estimating the roles of the various parameters involved in beyond-the-horizon propagation.

REFERENCES

1. K. Bullington, Radio Propagation Variations at VHF and UHF, Proc. I.R.E., **38**, p. 27, Jan., 1950.
2. Proc. I.R.E., Oct., 1955.
3. H. G. Booker and W. E. Gordon, A Theory of Radio Scattering in the Troposphere, Proc. I.R.E., **38**, p. 401, April, 1950.
4. F. Villars and V. F. Weisskopf, Scattering of EM Waves by Turbulent Atmospheric Fluctuations, Phys. Rev., **94**, p. 232, April, 1954.
5. C. M. Crain, Survey of Airborne Refractometer Measurements, Proc. I.R.E., **43**, p. 1405, Oct., 1955. H. E. Bussey and G. Birnbaum, Measurement of Variation in Atmospheric Refractive Index with an Airborne Microwave Refractometer, N.B.S. Jour. Res., **51**, pp. 171–178, Oct., 1953.
6. H. T. Friis, A Note on a Simple Transmission Formula, Proc. I.R.E., **34**, pp. 254–56, May, 1946.
7. S. A. Schelkunoff, Applied Mathematics for Engineers and Scientists, D. Van Nostrand Co., Inc., p. 212., 1948, and Remarks Concerning Wave Propagation in Stratified Media, Communication on Pure and Applied Mathematics, **4**, pp. 117–128, June, 1951. See also, H. Bremmer, The W.K.B. Approximation as the First Term of a Geometric-Optical Series, Communication on Pure and Applied Mathematics, **4**, pp. 105–115, June, 1951.
8. K. Bullington, W. J. Inkster and A. L. Durkee, Results of Propagation Tests at 505 mc and 4,090 mc on Beyond-Horizon Paths, Proc. I.R.E., **43**, pp. 1306–1316, Oct., 1955.
9. K. Bullington, Characteristics of Beyond-the-Horizon Radio Transmission, Proc. I.R.E., **43**, pp. 1175–1180, Oct., 1955.
10. J. H. Chisholm, P. A. Portmann, J. T. deBettencourt and J. F. Roche, Investigations of Angular Scattering and Multipath Properties of Tropospheric Propagation of Short Radio Waves Beyond the Horizon, Proc. I.R.E., **43**, pp. 1317–1335, Oct., 1955.

Interchannel Interference Due to Klystron Pulling

By H. E. CURTIS and S. O. RICE

(Manuscript received August 26, 1956)

A source of interchannel interference in certain multichannel FM systems is the so-called "frequency pulling effect." This effect, which occurs in systems using a klystron oscillator, is produced by an impedance mismatch between the antenna and the transmission line feeding it. In this paper expressions are developed for the magnitude of the interference when the speech load is simulated by random noise.

INTRODUCTION

In a recent paper[1] the problem of interchannel interference produced by echoes in an FM system was treated. The mathematical development in that paper can be used to calculate the distortion that arises when a Klystron oscillator is connected to an antenna through a transmission line of appreciable length.

In the system we study, the composite signal wave (the "baseband signal") from a group of carrier telephone channels in frequency division multiplex is applied to the repeller of a Klystron and thereby modulates the frequency of the Klystron output wave. If the antenna does not match the transmission line perfectly, the output frequency is altered slightly by an amount proportional to the mismatch.

This effect, known as "pulling," results in intermodulation between the individual telephone channels. In this study, the composite signal will be simulated by a random noise signal of appropriate bandwidth and power. It is assumed that some particular message channel is idle; i.e., there is no noise energy in the corresponding frequency band (which is relatively narrow in comparison with the bandwidth of the composite signal). If the system were perfect, no power would be received in this idle channel at the output of the FM detector. In the following work, the intermodulation noise falling into this channel because of the "pulling effect" will be computed. This leads to "Lewin's integral," so called, which is tabulated herein.

PULLING EFFECT

In a perfect FM system the carrier wave can be written

$$E_0(t) = A \sin [pt + \varphi(t)] \tag{1}$$

where A is a constant and the signal is $S(t) = d\varphi/dt = \varphi'(t)$, measured in radians/second. As mentioned in the Introduction, we assume that when the FM oscillator is connected directly to a transmission line with a slightly mismatched antenna at the far end, its frequency is changed. The reactive component of the input impedance of the line "pulls" the frequency of the oscillator to its new value. When the antenna is perfectly matched, there is no change in oscillator frequency.

If the characteristic impedance of the line is Z_K and the impedance of the antenna is Z_R, the impedance Z looking into the line is

$$Z = Z_K \frac{Z_R + Z_K \tanh P}{Z_K + Z_R \tanh P}$$

$$= Z_K \frac{1 + \rho e^{-2P}}{1 - \rho e^{-2P}}$$

where ρ is the reflection coefficient

$$\rho = \frac{Z_R - Z_K}{Z_R + Z_K}$$

and P is the propagation constant of the line. If the loss of the line is negligible and the reflection coefficient is small, the input impedance is approximately

$$Z \doteq Z_K[1 + 2\rho(\cos \omega T - i \sin \omega T)] \text{ ohms}$$

where ω is the oscillator frequency in radians per second and T is twice the delay of the line.

It will be observed that the magnitude of the reactive component of Z oscillates as the phase angle ωT increases.

The dependence of the frequency of an oscillator upon the load reactance has been expressed by earlier workers as a "pulling figure." This figure is customarily defined as the difference between the maximum and minimum frequencies observed when the load reactance is varied over one cycle of its oscillation (the variation being accomplished, say, by increasing T). The load is taken to be such that it causes a voltage standing wave ratio of 1.5. This corresponds to a reflection coefficient of 0.20 and 14 db return loss.

In our work, we assume that the change in frequency is directly pro-

portional to the reactive component of the input impedance. More precisely, we assume that the ideal transmitter frequency of $p + \varphi'(t)$ radians/sec is changed by the pulling effect to

$$p + \varphi'(t) + 2\pi r \sin [T(p + \varphi'(t))] \text{ radians/sec} \qquad (2)$$

where r is given by

$$r = 2.5 \mid \rho \mid \times \text{ (Pulling Figure in cycles/sec)}$$

POWER SPECTRUM OF INTERCHANNEL INTERFERENCE

The distortion produced by the pulling effect is given by the third term in (2). This distortion will be denoted by $\theta'(t)$:

$$\theta'(t) = 2\pi r \sin [pT + T\varphi'(t)] \qquad (3)$$

Our problem is to compute the power spectrum of $\theta'(t)$. In particular, we are interested in the case where the signal $\varphi'(t)$ represents the composite signal wave from a group of carrier telephone channels in frequency division multiplex. All of the channels except one are assumed to be busy. Although the power spectrum of $\varphi'(t)$ is zero for frequencies in the idle channel, the same is not true for the power spectrum of $\theta'(t)$. In fact, the interchannel interference (as observed in the idle channel) is given by that portion of the power spectrum of $\theta'(t)$ which lies within the idle channel. We shall denote the corresponding interchannel interference power in the idle channel by $w_c(f) \, df$ where the idle channel is assumed to be of infinitesimal width and to extend from frequency $f - df/2$ to $f + df/2$. The function $w_c(f)$ will now be computed by using the procedure developed in Reference 1.

The first step is to assume the signal $\varphi'(t)$ to be a random noise current. In order to avoid writing φ' a great many times we shall set $\varphi'(t) = S(t)$, where now $S(t)$ stands for the signal. Then the autocorrelation function for the distortion $\theta'(t)$ is

$$
\begin{aligned}
R_{\theta'}(\tau) &= \text{avg } [\theta'(t)\theta'(t + \tau)] \\
&= (2\pi r)^2 \text{ avg } [\sin (Tp + T\varphi'(t)) \sin (Tp + T\varphi'(t + \tau))] \\
&= (2\pi r)^2 \text{ avg } [\sin (Tp + TS(t)) \sin (Tp + TS(t + \tau))] \\
&= \frac{(2\pi r)^2}{2} \text{ avg } [\cos (TS(t) - TS(t + \tau)) \qquad (4) \\
&\qquad\qquad\qquad - \cos (2pT + TS(t) + TS(t + \tau))] \\
&= \tfrac{1}{2}(2\pi r)^2 \{\exp [-T^2 R_s(0) + T^2 R_s(\tau)] \\
&\qquad\qquad - \cos (2pT) \exp [-T^2 R_s(0) - T^2 R_s(\tau)]\}
\end{aligned}
$$

where

$$R_S(\tau) = \int_0^\infty w_S(f) \cos 2\pi f\tau \, df \tag{5}$$

and $w_S(f)$ is the power spectrum of the applied signal $S(t)$. The last expression in (4) follows from the next to the last by analogy with equation (1.14) of Reference 1.

The dc component of the distortion $\theta'(t)$ is its average value $\overline{\theta'}$ which may be computed from

$$\overline{\theta'}^2 = R_{\theta'}(\infty) = \frac{(2\pi r)^2}{2} [e^{-T^2 R_S{}^{(0)}}(1 - \cos 2pT)] \tag{6}$$

This follows from (4) since $R_S(\infty) = 0$.

The auto-correlation function of the distortion, excluding the dc component, is then

$$R_{\theta' - \overline{\theta'}} = \frac{(2\pi r)^2}{2} [e^{-T^2 R_S{}^{(0)}}][(e^{T^2 R_S{}^{(\tau)}} - 1) - (e^{-T^2 R_s(\tau)} - 1) \cos 2pT] \tag{7}$$

The interchannel interference spectrum is

$$w_c(f) = 4 \int_0^\infty R_c(\tau) \cos 2\pi f\tau \, d\tau \tag{8}$$

where, by analogy with equation (1.22) of Reference 1,

$$R_c(\tau) = \frac{(2\pi r)^2}{2} [e^{-T^2 R_S{}^{(0)}}][(e^{T^2 R_s(\tau)} - T^2 R_S(\tau) - 1)$$
$$- (e^{-T^2 R_s(\tau)} + T^2 R_S(\tau) - 1) \cos 2pT] \tag{9}$$

As mentioned before, the function $w_c(f)$ is of interest because

$$P_I = w_c(f) \, df \tag{10}$$

is the average interference power appearing at the receiver in an idle channel of width df centered on frequency f.

RATIO OF INTERCHANNEL INTERFERENCE TO SIGNAL POWER

The average signal power appearing in a busy channel of width df centered on the frequency f is

$$P_S = w_S(f) \, df \tag{11}$$

and hence the ratio of the interchannel interference power to the signal

power is

$$\frac{P_I}{P_S} = \frac{w_c(f)}{w_S(f)} \tag{12}$$

We now obtain an expression for this ratio on the assumption that the random noise signal $S(t)$ (which is used to simulate the multichannel signal) has the power spectrum

$$w_S(f) = \begin{cases} P_0, & 0 < f < f_b \\ 0, & f > f_b \end{cases} \tag{13}$$

where P_0 is a constant. $S(t)$ is measured in radians/sec and $P_0 f_b$ is measured in (radians/sec)^2. $P_0 f_b$ is given by

$$P_0 f_b = \overline{S^2(t)} = \text{avg } [\varphi'(t)]^2 = (2\pi\sigma)^2$$

where σ is the rms frequency deviation of the signal measured in cycles/second. According to (5) this signal has the auto-correlation function

$$R_S(\tau) = \int_0^{f_b} P_0 \cos 2\pi f \tau \, df = P_0 \left[\frac{\sin 2\pi f \tau}{2\pi\tau}\right]_0^{f_b} = (2\pi\sigma)^2 \frac{\sin u}{u} \tag{14}$$

where

$$u = 2\pi f_b \tau$$

The interference power spectrum $w_c(f)$ corresponding to the $w_S(f)$ of (13) may be obtained by substituting (14) in (9) to get $R_c(\tau)$ and then using (8). The result is

$$w_c(f) = 4\frac{(2\pi r)^2}{2} e^{-b} \int_0^\infty [(e^{bu^{-1} \sin u} - bu^{-1} \sin u - 1)$$

$$- (e^{-bu^{-1} \sin u} + bu^{-1} \sin u - 1) \cos 2pT] \frac{\cos au}{2\pi f_b} \, du \tag{15}$$

where u is the same as in (14) and we have set

$$a = f/f_b \qquad b = (2\pi\sigma T)^2$$

This integral may be expressed in terms of Lewin's integral which is studied in Appendix III of Reference 1. Thus

$$w_c(f) = \frac{(2\pi r)^2 e^{-b}}{2\pi f_b} [I(b, a) - I(-b, a) \cos 2pT](\text{radian/sec})^2/\text{cps} \tag{16}$$

where $I(b, a)$ and $I(-b, a)$ are tabulated for various values of a and b. Since we began the problem by dealing directly with $\theta'(t)$ which is a radian frequency, rather than $\theta(t)$ which is a radian phase, $w_c(f)$ has the

TABLE I—VALUES OF $e^{-b}I(b, a)$ FOR $b > 0$

b	e^b	$e^{-b}I(b, a)$					
		$a = 0$	0.25	0.50	0.75	1.00	1.25
0.0	1.000	0.000	0.000	0.000	0.000	0.000	0.000
0.25	1.284	0.082	0.072	0.062	0.052	0.042	0.031
0.5	1.649	0.272	0.241	0.209	0.176	0.142	0.107
1.0	2.718	0.761	0.685	0.602	0.511	0.414	0.314
2.0	7.389	1.560	1.440	1.291	1.117	0.919	0.713
3.0	20.08	1.913	1.801	1.645	1.448	1.215	0.968
4.0	54.60	1.974	1.888	1.751	1.566	1.341	1.098
5.0	148.4	1.905	1.844	1.731	1.571	1.372	1.153
6.0	403.4	1.794	1.751	1.660	1.525	1.356	1.166
7.0	1097.	1.680	1.649	1.575	1.463	1.320	1.157
8.0	2981.	1.576	1.552	1.492	1.398	1.277	1.138

TABLE II—VALUES OF $I(b, a)$ FOR $b < 0$

b	$I(b, a)$					
	$a = 0$	0.25	0.50	0.75	1.0	1.25
0.0	0.000	0.000	0.000	0.000	0.000	0.000
−0.25	0.092	0.080	0.068	0.057	0.045	0.034
−0.5	0.349	0.300	0.254	0.210	0.167	0.125
−1.0	1.25	1.06	0.885	0.723	0.576	0.432
−2.0	4.16	3.41	2.76	2.20	1.76	1.34
−3.0	8.03	6.37	4.97	3.88	3.14	2.46
−4.0	12.6	9.66	7.23	5.49	4.55	3.74
−5.0	17.8	13.2	9.40	6.89	5.93	5.19
−6.0	23.6	16.8	11.4	8.00	7.25	6.85
−7.0	30.0	20.7	13.1	8.71	8.48	8.78
−8.0	37.2	24.8	14.5	8.93	9.59	11.0

dimensions of $(\text{radians/sec})^2/\text{cps}$. The signal in the same dimensions is P_0 or $(2\pi\sigma)^2/f_b$. Therefore the ratio of the interchannel interference power to the signal power is:

$$\frac{P_I}{P_S} = \frac{1}{2\pi} \left(\frac{r}{\sigma}\right)^2 e^{-b}[I(b, a) - I(-b, a) \cos 2pT] \qquad (17)$$

The quantity $e^{-b}I(b, a)$ for $b > 0$ is tabulated in Table I. The quantity $I(b, a)$ for $b < 0$ is given in Table II. These tables, which are also given in Reference 1, are repeated here for the convenience of the reader.

When the rms frequency deviation σ is so small that $b = (2\pi\sigma T)^2$ is small compared to unity, the approximation

$$I(b, a) \approx b^2\pi(2 - a)/4$$

leads to $\qquad \dfrac{P_I}{P_S} \approx (2\pi^2 r\sigma T^2)^2 (2 - a)(1 - \cos 2pT)/2 \qquad (18)$

When σ and T are such that $b \gg 1$, the approximation

$$I(b,\, a) \approx (6\pi/b)^{1/2} \exp\left[b - \frac{3a^2}{2b} \right]$$

leads to $\qquad \dfrac{P_I}{P_s} \approx \left(\dfrac{3}{8\pi^3}\right)^{1/2} \dfrac{r^2}{\sigma^3 T} \exp\left[-\dfrac{3}{2}\left(\dfrac{a}{2\pi\sigma T}\right)^2 \right]$

Equation (17), when converted to decibels, breaks down conveniently into two terms which may be designated D_1 and D_2 :

$$10 \log P_I/P_s = D_1 + D_2$$

$$D_1 = 10 \log (r/\sigma)^2$$

$$D_2 = 10 \log \frac{1}{2\pi} e^{-b}[I(b,\, a) - I(-\, b,\, a) \cos 2pT]$$

(19)
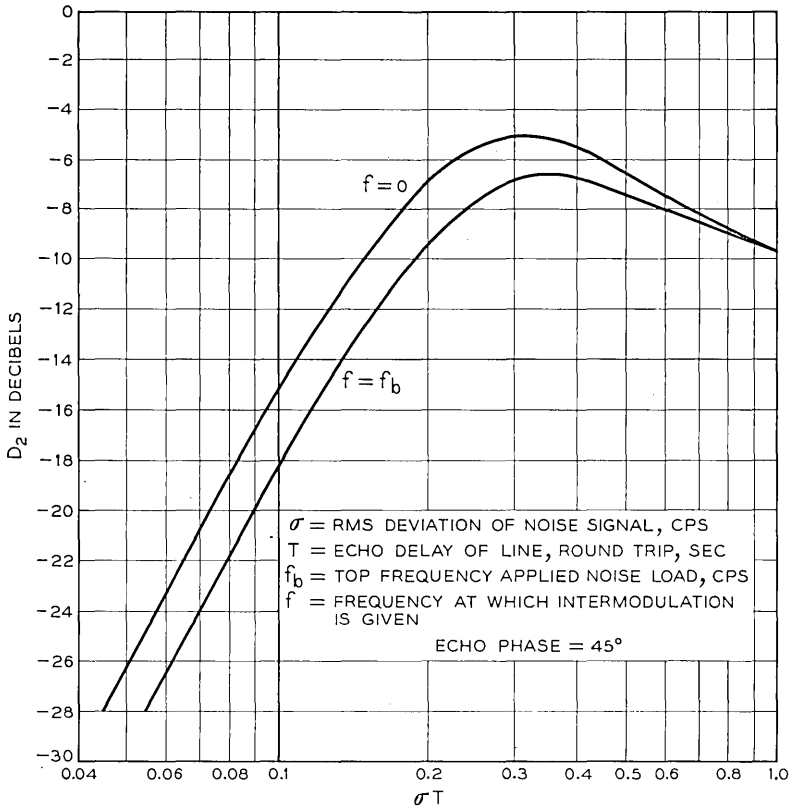
Fig. 1 — Plot of D_2 as a function of σT
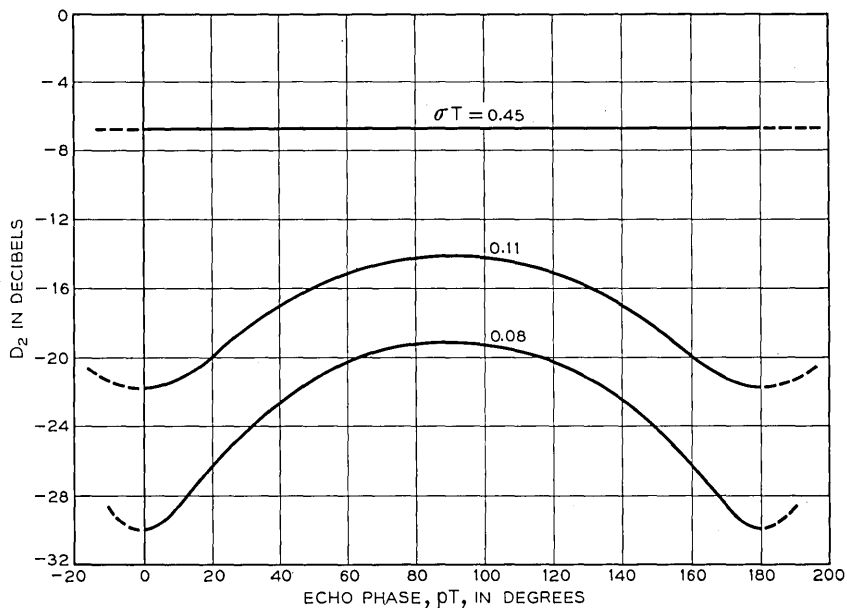
Fig. 2 — Plot of D_2 as a function of echo phase when $f = f_b$

The term D_2 depends only on the rms deviation σ, the round-trip echo delay T of the line, the ratio $a = f/f_b$, and the echo phase pT. The term D_2 is plotted in Fig. 1 as a function of σT for two channels, one at the top and the other at the bottom of the signal band. Since the carrier frequency may be expected to be very high, the carrier phase $2pT$ will be a very large number of radians even with very short wave guide runs. Hence the curves on Fig. 1 are plotted for the average value of $\cos 2pT$ which is zero.

The curves on Fig. 2 show how D_2 depends on pT .and the parameter σT. In this case the channel is taken at the top of the signal band. When pT is an odd multiple of 90 degrees, it turns out that we have even order modulation products only; and when pT is a multiple of 180 degrees, odd order products only. The curves show that the distortion becomes less dependent on the echo phase as the quantity σT increases.

REFERENCE

1. W. R. Bennett, H. E. Curtis and S. O. Rice, Interchannel Interference in FM and PM Systems, B.S.T.J., **34**, pp. 601-636, May, 1955.

Instantaneous Companding of Quantized Signals

By BERNARD SMITH

Instantaneous companding may be used to improve the quantized approximation of a signal by producing effectively nonuniform quantization. A revision, extension, and reinterpretation of the analysis of Panter and Dite permits the calculation of the quantizing error power as a function of the degree of companding, the number of quantizing steps, the signal volume, the size of the "equivalent dc component" in the signal input to the compressor, and the statistical distribution of amplitudes in the signal. It appears, from Bennett's spectral analysis, that the total quantizing error power so calculated may properly be studied without attention to the detailed composition of the error spectrum, provided the signal is complex (such as speech or noise) and is sampled at the minimum information-theoretic rate.

These calculations lead to the formulation of an effective process for choosing the proper combination of the number of digits per code group and companding characteristic for quantized speech communication systems. An illustrative application is made to the planning of a hypothetical PCM system, employing a common channel compandor on a time division multiplex basis. This reveals that the calculated companding improvement, for the weakest signals to be encountered in such a system, is equivalent to the addition of about 4 to 6 digits per code group, i.e., to an increase in the number of uniform quantizing steps by a factor between $2^4 = 16$ and $2^6 = 64$.

Comparison with the results of related theoretical and experimental studies is also provided.

TABLE OF CONTENTS

(Passages marked with an asterisk contain mathematical details which
may be omitted in a first reading without loss of continuity.)

I. INTRODUCTION

Quantized pulse modulation has been the subject of considerable attention in the last decade.[1-17] Proposals for practical application of such modulation usually provide for the transmission, by time division multiplex, of a class of signals covering an extensive power range.[1, 6] Such proposals almost invariably assign a vital role to instantaneous compandors. The present discussion is devoted to the formulation of general quantitative criteria for the choice of a suitable companding characteristic.

A. *Fundamental Properties of Pulse Modulation**

1. *Unquantized Signals*

Unquantized pulse signals are produced when a band-limited signal (such as low-pass filtered speech) is sampled instantaneously at a rate greater than or equal to the minimum acceptable value of slightly more than twice the top signal frequency. The transmission of the continuous range of pulse amplitudes so produced is known as pulse amplitude modulation (PAM). Alternatively one may translate the sampled amplitudes into variations either in the width of periodic pulses of constant amplitude (pulse duration modulation or PDM), or in the spacing of pulses of uniform amplitude and width (pulse position modulation or PPM). Regardless of the mode of transmission, the unquantized signal pulses are sensitive to noise in the transmission medium.

2. *Quantized Signals (PCM)*

Although sampling constitutes temporal quantization, it is convenient to adhere to conventional usage (as codified by Bennett[2] and Black[1]) in restricting the designation "quantized signals" to those which have been quantized in amplitude, as well as sampled in time, in order to permit encoded (i.e., essentially telegraphic) transmission. Thus a finite range of possible signal amplitudes, large enough to accommodate the strongest signal to be encountered in a given application, may be divided into N equal parts or quantizing steps. Each instantaneous pulse amplitude of a PAM signal is then compared with this ladder-like array; amplitude quantization is accomplished by replacing all amplitudes falling in any portion of a quantizing step by a single value uniquely characterizing that interval.

---

* This brief account is intended merely to specify the minimum amount of background information required to avoid confusion in the present discussion. Details may be found in the many excellent and readily accessible references already cited.

Use of a binary number representation permits the encoded transmission of the N possible quantized amplitudes in terms of groups of on-off pulses containing n binary digits per code group (where $N = 2^n$).* These pulses may be considered impervious to noise in the transmission medium in the sense that complete information is conveyed by the mere recognition of the presence or absence of a pulse rather than a determination of a precise magnitude. Consequently such pulses may, in principle, repeatedly be regenerated in the transmission medium, provided that regeneration occurs before the on-off pulses have been rendered indistinguishable from each other by noise.

The designation pulse code modulation (PCM) may therefore be used synonymously with quantized pulse modulation to distinguish the latter from the previously defined varieties of unquantized pulse modulation. In view of the restriction of present interest to the role of quantization *per se*, there is no need to proceed beyond the choice of quantized PAM as the prototype PCM signal in this discussion, in spite of the fact that PDM and PPM may also be quantized to yield PCM.[1]

B. Quantizing Impairment in PCM Systems

From the foregoing it is clear that quantization (i.e., the representation of a bounded continuum of values by a finite number of discrete magnitudes), permits the encoded, and therefore essentially noise-free transmission of approximate, rather than exact values of sampled amplitudes. In fact, *the deliberate error imparted to the signal by quantization is the significant source of PCM signal impairment.*[1-5] Adequate limitation of this quantization error is therefore of prime importance in the application of PCM to communication systems.

A number of methods of reducing quantizing error suggest themselves on a purely qualitative and intuitive basis. For example, one may obtain a finer-grained approximation by providing more, and therefore smaller, quantizing steps for a given range of amplitudes. Alternatively, one may provide a more complete description of the signal by increasing the sampling rate beyond the minimum information-theoretic value already assumed.†

It is also possible to vary the size of the quantizing steps (without adding to their number) so as to provide smaller steps for weaker signals.

---

* Of course, number representations using a base, b, other than two, so that $N = b^n$, are also available. These are presently of academic interest in view of the increased complexity of instrumentation they imply.[3]

† See Fig. 5 of Reference 2 for a quantitative evaluation of the efficacy of this measure.

Whereas the first two techniques result in an increase of bandwidth and system complexity, the third requires only a modest increase in instrumentation without any increase in bandwidth.* This investigation is therefore devoted to the study of nonuniform step size as a means of reducing quantizing impairment.

C. *Physical Implications of Nonuniform Quantization*

1. *Quantizing Error as a Function of Step Size*

Quantizing impairment may profitably be expressed in terms of the total mean square error voltage since the ratio of the mean square signal voltage to this quantity is equal to the signal-to-quantizing error power ratio.

In evaluating the mean square error voltage, we begin by considering a complex signal, such as speech at constant volume, whose pulse samples yield an amplitude distribution corresponding to the appropriate probability density. These pulse samples may be expected to fall within, or "excite", all the steps assigned to the signal's peak-to-peak voltage range. It will be assumed that, for quality telephony, the steps will be sufficiently small, and therefore numerous, to justify the assumption that the probability density is effectively constant within each step, although it may be expected to vary from step to step. Thus the continuous curve representing the probability density as a function of instantaneous amplitude is to be replaced by a suitable histogram.

If the midstep voltage is assigned to all amplitudes falling in a particular quantizing interval, the absolute value of the error in any pulse sample will be limited to values between zero and half the size of the step in question; when combined with the assumed approximation of a uniform probability density within each step, this choice minimizes the mean square error introduced at each level.[5] Summation of the latter quantity over all levels then yields the result that the total mean square quantizing error voltage is equal to one-twelfth the weighted average of the square of the size of the voltage steps traversed (i.e., excited) by the input signal. The direct consideration of the physical meaning of this result (which, as (6) below, will constitute the basis of all subsequent calculations) will now be shown to provide a simple qualitative description of the implications of nonuniform quantization.

---

* We refer to bandwidth in the transmission medium as determined by the pulse repetition rate, which, in the time division multiplex applications envisioned herein, is given by the product: (sampling rate) × (number of digits or pulses per sample) × (number of channels).

2. Properties of the Mean Square Excited Step Size

Fig. 1(a) shows the range of input voltages, between the values $+V$ and $-V$ divided into N equal quantizing steps (i.e., uniformly quantized); Fig. 1(b) depicts the same range divided into N tapered steps, corresponding to nonuniform quantization.

Consider a complex signal, such as speech, whose distribution of instantaneous amplitudes at constant volume results in the excitation (symmetrically about the zero level) of the steps in the moderately large interval $X - X'$. The quantizing error power will be shown to be proportional to the (weighted) average of the square of the excited step size. For uniform quantization, it is clear, from Fig. 1(a), that this average is a constant, independent of the statistical properties of the signal. For a nonuniformly quantized signal, [Fig. 1(b)], the mean square excited step size is reduced by the division of the identical interval $X - X'$ into more steps, most of which are smaller than those shown in Fig. 1(a). Appreciation of the full extent to which the quantizing error power may so be reduced requires the added recognition that the few larger quantizing steps in the range $X - X'$, corresponding to excitation by comparatively rare speech peaks, are far less significant in their contribution to the weighted average than the small steps in the vicinity of the origin, due to the nature of the probability density of speech at constant volume.[18]

It is also clear that weaker signals, corresponding to a contraction of the interval $X - X'$, enjoy the greatest potential tapering advantage since their excitation may be confined to steps which are all appreciably smaller than those in Fig. 1(a). However, if the interval $X - X'$ were to
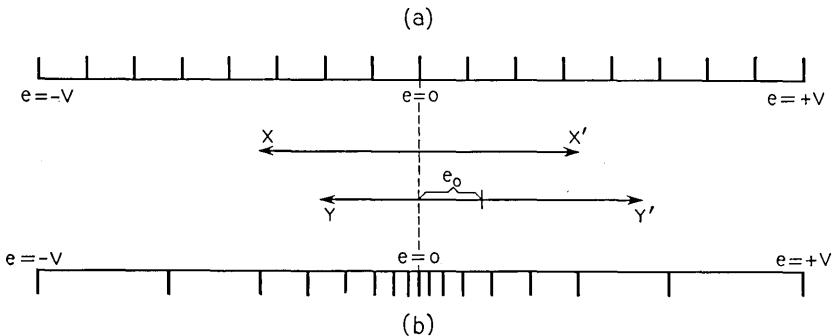

Fig. 1 — (a) Distribution of steps of equal size corresponding to direct, uniform quantization; (b) nonuniform quantization of this range into the same number of steps. The function of the instantaneous compandor is to provide such nonuniform quantization in the manner illustrated in Fig. 2.

increase in size and approach the full range, $+V$ to $-V$, (to accommo-date stronger signals), the excitation of extremely large steps might re-sult in an rms step size exceeding the uniform size shown in Fig. 1(a).

Fig. 1 also indicates that signals (including unwanted noise) too weak to excite even the first quantizing step (and therefore absolutely incapa-ble of transmission) when uniformly quantized, may successfully be transmitted as a result of the excitation of a few steps following non-uniform quantization.

Although the assumption that the average value of the signal is zero is quite proper for speech, subsequent discussion will disclose the possi-bility that the quiescent value of the signal, as it appears at the input to the quantizing equipment, may not always coincide with the exact center of the voltage range depicted in Fig. 1. This effect may formally be described in terms of the addition of an equivalent dc bias to the speech input at the quantizer. As shown in Fig. 1, the addition of such a dc component, e_0, to the signal which previously excited the band of steps labeled $X - X'$, transforms $X - X'$ into an array of equal extent $Y - Y'$, centered about $e = e_0$ instead of $e = 0$. This causes the excitation of some larger steps, in Fig. 1(b), as well as the assignment of greatest weight[18] to the steps in the vicinity of $e = e_0$, which are larger than those near $e = 0$; the net result is an increase in the rms excited step size, and the quantizing error power. This effect will depend on the comparative size of e_0 and the signal as well as on the degree of step size variation. In particular, Fig. 1(a) indicates that the presence of e_0 does not affect the rms excited step size under conditions of uniform quantization.

It is clear from the foregoing that the effect of nonuniform quantiza-tion of PCM signals will vary greatly with the strength of the signal; greatest improvement is to be expected for weak signals, whereas an actual impairment may be experienced by strong signals. The range of signal volumes is therefore of prime importance in the choice of the proper distribution of step sizes.

D. *Nonuniform Quantization Through Uniform Quantization of a Com-pressed Signal*

Nonuniform quantization is logically equivalent to uniform quantiza-tion of a "compressed version" of the original input signal. When applied directly, tapered quantization provides an acceptably high ratio of sam-ple amplitude to sample error for weak pulses, by decreasing the errors (i.e., the step sizes) assigned to small amplitudes. Signal compression achieves the same goal by increasing weak pulse amplitudes without altering the step size.

The instantaneous compressor envisioned herein is, in essence, a non-linear pulse amplifier which modifies the distribution of pulse amplitudes in the input PAM signal by preferential amplification of weak samples. A satisfactory compression characteristic will have the general shape shown in Fig. 2. Thus the amplification factor, (v/e), varies from a large value for small inputs to unity for the largest amplitude (V) to be accommodated, so that the distribution of pulse sizes may be modified without changing the total voltage range. Fig. 2 also illustrates how uniform quantization of the compressor output produces a tapered array of input steps similar to those already considered in connection with Fig. 1(b).

A complementary device, the expandor, employs a characteristic inverse to that of the compressor to restore the proper (quantized) distribution of pulse amplitudes after transmission and decoding. Taken together, the compressor and expandor constitute a compandor.

The resolution of tapered quantization into the sequential application of compression, uniform quantization, and expansion is operationally convenient,[6] as well as logically sound. Since there is a one-to-one correspondence between step size allocations and compression characteristic
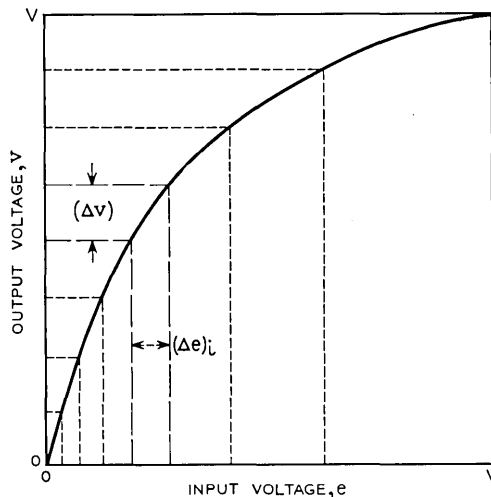
Fig. 2 — Curve illustrating the general shape of a suitable instantaneous compression characteristic. All continuous, single-valued curves connecting the origin to the point (V, V) and rising from the origin with a slope greater than one, i.e., $(dv/de)_{e=0} > 1$, are potential compression characteristics. The symmetrical negative portion $[v(e) = -v(-e)]$ is not shown. The production of a tapered array of input steps $(\Delta e)_i$ by uniform quantization of the output into steps of (equal) size Δv, is also represented.

curves, the central problem of choosing the proper distribution of step sizes will be discussed in terms of the choice of the appropriate compression characteristic; the reduction of quantizing error, corresponding to nonuniform quantization without change in the total number of steps, will be termed companding improvement.

E. *The Mechanism of Companding Improvement in Various Communication Systems*

1. *Syllabic Companding of Continuous Signals*[19, 20]

Originally, the compandor consisted of a compressor and complementary expandor operating at a syllabic rather than instantaneous rate in frequency division systems, since instantaneous companding was found to imply an undesirable increase in bandwidth in such systems.[19]

In spite of the existence of syllabic power variations, a useful understanding of such compandor action may be inferred from the consideration of the long-time average power. Thus, in its simplest form, the compressor might provide amplification varying from a constant value within the range of volumes corresponding to weak speech to little or no amplification for comparatively strong signals prior to transmission. Although it is an amplifying device, the compressor takes its name from the contraction of the transmitted volume range which results from selective amplification of the weakest signals. Since the distortion of the signal by the compressor may virtually be confined to a change in loudness, the compressor output may be expected to be intelligible.

In interpreting a compression characteristic, syllabic application permits the identification of the ordinate and abscissa with $\sqrt{\overline{v^2}}$ and $\sqrt{\overline{e^2}}$, rather than v and e as shown in Fig. 2. This substitution of rms for instantaneous signals not only confines the significance of the compression characteristic to the first quadrant but also removes the need for compandor response to input signals below some small, nonzero, threshold value.

If we designate the mean square noise voltage in the transmission medium by $\overline{v_n^2}$, the amplification of weak signals prior to exposure to this noise provides an increase in the transmitted signal to noise ratio from $(\overline{e^2}/\overline{v_n^2})$ to $(\overline{v^2}/\overline{v_n^2})$, i.e., by a factor of $(\overline{v^2}/\overline{e^2})$. This increase in signal-to-noise ratio may be read directly from the graph of the compression characteristic, and is unaffected by the identical treatment accorded signal and noise at the expandor. Furthermore, noise received during the silent intervals, between speech bursts, is attenuated by the expandor.

Under these circumstances it is appropriate to resolve companding improvement into the separate contributions of an increased signal to noise ratio for weak speech by the compressor, and a quieting of the circuit in the absence of speech by the expandor. The introduction of an independent source of noise in the channel between the compressor and expandor is the key to such behavior.

2. Instantaneous Companding of Unquantized Pulse Signals

Time division systems, employing unquantized pulse modulation (e.g., PAM) are admirably suited to the application of instantaneous companding to the individual pulse samples. Since each pulse is amplified to a degree which varies with its input amplitude, the compressor output is a sampled version of a distorted signal.

As in the syllabic case, the location of the noise source in the channel between the compressor and expandor permits an improvement of the received signal-to-noise ratio for weak signals. Furthermore, the expandor again assumes the separate and distinct task of suppressing channel noise in the absence of speech.

Unfortunately, quantitative expression of the companding improvement is not as simple as in the syllabic case. The response to instantaneous amplitudes much lower than the rms threshold signal (including zero) becomes important and the improvement factor may not (except in the special case of a linear compression characteristic) simply be read from a graph relating instantaneous values of v and e. Instead, one must employ the probability density of the signal in order properly to account for the distinctive treatment accorded individual pulse amplitudes in a complex signal.

3. Instantaneous Companding of Quantized Signals

Although the same physical devices which serve as an instantaneous compressor and expandor in a PAM system may also be used in a PCM system, the functional description of companding improvement is different in the two applications. Whereas the compandor is used to combat channel noise in a PAM system, encoded transmission permits a PCM system to assign this task to the devices which transmit and regenerate code pulses. Thus, assuming that error-free encoded transmission is realized, the quantized signal may be regarded as completely impervious to noise in the transmission medium. Quantization is required to permit such transmission. The sole purpose of the PCM compandor is to reduce the quantizing impairment of the signal by converting uniform to effectively nonuniform quantization.

Although the expandor continues to collaborate with the compressor in improving the quality of weak signals, it is now neither necessary nor possible for it to perform the separate function of quieting the circuit in the absence of speech. Indeed, apart from instrumentational difficulties which might arise, it is conceptually sound to transfer the PCM expandor to the transmitting terminal, with expansion taking place subsequent to quantization but prior to encoding and transmission. Another interesting peculiarity of the PCM expandor is the restriction of its operation, by quantization, to a finite number of discrete operating points on the continuous characteristic.

The use of companding to reduce the quantizing error which owes its very existence to, and is therefore a function of, the signal, is thus significantly different from the use of companding to reduce the effects of an independent source of noise in the transmission medium.

F. *Applicability of the Present Analysis*

Before we proceed to a detailed analysis, it is important to emphasize certain restrictive conditions required for the meaningful application of the results to be derived.

1. *Signal Spectrum*

A signal with a sufficiently complex spectrum, such as speech, is required to justify consideration of the total quantizing error power without regard to the detailed composition of the error spectrum. Although it is known that quantization of simple signals (e.g., sinusoids) results in discrete harmonics and modulation products deserving of individual attention,[8, 9] Bennett has shown that the error spectrum for complex signals is sufficiently noise-like to justify analysis on a total power basis.[2, 12]

2. *Sampling Rate*

The consistent comparison of signal power with the total quantizing error power, rather than with the fraction of the latter quantity appropriate to the signal band, might at first appear to impose serious limitations on the present analysis. Furthermore, the role of sampling has not been discussed explicitly. It is therefore important to note that the justification for this treatment, in the situation of actual interest, has also been given by Bennett.[2] We need only add the standard hypothesis[1-6] that the sampling rate chosen for a practical system would equal the

minimum acceptable rate (slightly in excess of twice the top signal fre-
quency[3]) in order to invoke Bennett's results, which tell us that, for this
sampling rate, the quantizing error power in the signal band and the
total quantizing error power are identical.[2] Thus, sampling at the mini-
mum rate is assumed throughout.

3. Number of Quantizing Steps

As already remarked, the present results are based on the assumption
that N is not small, inasmuch as we assume a probability density which,
although varying from step to step, remains effectively constant within
each quantizing step; indeed the step sizes will be treated as differential
quantities.

Experimental evidence[6, 7, 10] (as well as the analysis to follow) argues
against the consideration of fewer than five digits (i.e., $2^5 = 32$ quantizing
steps) for high quality transmission of speech. Numerical estimates indi-
cate that the present approximation should be reasonable for five or
more digits per code group. These estimates are confirmed by the con-
sistency of actual measurements of quantizing error power with calcula-
tions based on the same approximation (see Fig. 8 of reference 2 for 5, 6,
and 7 digit data obtained with an input signal consisting of thermal
noise instead of speech).

Further indication of the adequacy of this approximation is provided
by the knowledge that Sheppard's corrections (see Section II-B) appear
adequate even when (Δe) is not very small, for a probability density
which (as is the case for speech[18]) approaches zero together with its de-
rivatives at both ends of the (voltage) range under consideration.[24]

Therefore, we are not presently concerned with the limitations imposed
by this approximation.

4. Subjective Effects Beyond the Scope of the Present Analysis

We shall have occasion to study graphs depicting the signal to quan-
tizing error power ratio as a function of signal power. Although these
curves, and the equations they represent, will always be of interest for the
case where even the weakest signal greatly exceeds the corresponding
error power, there exists the possibility of rash extrapolation to the
region where this inequality is reversed. Unfortunately, such extra-
polation may have little or no meaning.* This is particularly clear when
one considers that signals incapable of exciting at least the first quan-
tizing step, in the absence of companding, will be absolutely incapable

---

* This is implicit in the deduction of Equation (6).

of transmission. Under these circumstances, companding may actually *resuscitate* a signal; the mathematical description of resuscitation (as anything short of infinite improvement) is clearly beyond the scope of the present analysis.

At the other extreme, it is probable that there exists a limit of error power suppression beyond which listeners will fail to recognize any further improvement. Our analysis will not be useful in describing this region of subjective saturation. Furthermore, it is possible that the subjective improvement afforded a listener by adding to the number of quantizing steps, or companding, may depend on the initial and final states, even before subjective saturation is reached. For example, it is entirely possible that the change from 5 to 6 digits per code group may provide a degree of improvement which appears different to the listener from that corresponding to the increase from 6 to 7 digits, although the present mathematical treatment does not recognize such a distinction.

II. EVALUATION OF MEAN SQUARE QUANTIZATION ERROR (σ)

A.* *Generalization of the Analysis of Panter and Dite*

The mean square error voltage, σ_j, associated with the quantization of voltages assigned to the jth voltage interval, e_j, is adopted as the significant measure of the error introduced by quantization. If e_j is to represent any voltage, e, in the range

$$Q_j = \left[e_j - \frac{(\Delta e)_j}{2} \right] \leqq e \leqq \left[e_j + \frac{(\Delta e)_j}{2} \right] = R_j \qquad (1)$$

then

$$\sigma_j = \int_{Q_j}^{R_j} (e - e_j)^2 P(e) \, de \qquad (2)$$

where $(e - e_j)$ is the voltage error imparted to the sample amplitude by quantization and $P(e)$ is the probability density of the signal. The location of e_j at the center of the voltage range assigned to this level minimizes σ_j since we shall assume an effectively constant value of $P(e)$ within the confines of a single step.

If the value of $P(e)$ is approximated by the constant value $P(e_j)$ appropriate to e_j in (2), it follows that

$$\sigma_j = (\Delta e)_j^3 P(e_j)/12 \qquad (3)$$

---

* This passage contains mathematical details which may be omitted, in a first reading, without loss of continuity.

The total mean square voltage error, σ, is equal to the sum of the mean square quantizing errors introduced at each level, so that,

$$\sigma = \sum_j \sigma_j = \tfrac{1}{12} \sum_j P(e_j)(\Delta e)_j^{\,3} \tag{4a}$$

$$= \tfrac{1}{12} \sum_j (\Delta e)_j^{\,2}[P(e_j)(\Delta e)_j] \tag{4b}$$

which may be rewritten as

$$\sigma \cong \tfrac{1}{12} \sum_j (\Delta e)_j^{\,2} p_j \tag{4c}$$

since the discrete probability appropriate to the jth step is given by

$$p_j = \int_{Q_j}^{R_j} P(e)\,de \cong [P(e_j)(\Delta e)_j] \tag{5}$$

Hence,

$$\sigma \cong \tfrac{1}{12}[(\Delta e)^2]_{\text{AV}} = \overline{(\Delta e)^2}/12 \tag{6}$$

Thus, the total mean square error voltage is equal to one-twelfth the average of the square of the input voltage step size when the steps are sufficiently small (and therefore numerous) to justify the approximations employed in the deduction of (6). In applying (6), it is important to note that (4) implies that this is a *weighted* average over the steps traversed (or "excited") by the signal.

In the special case of uniform step size, substitution of $(\Delta e)_j = (\Delta e) = $ const. reduces (6) to the simple form

$$\sigma_0 = [\sigma]_{\Delta e = \text{const}} = (\Delta e)^2/12 \tag{7}$$

Equations (6) and (7) provide the basis for the qualitative interpretation of quantizing error power which has already been discussed in connection with Fig. 1.

The deduction of (6) from (4a) is implicit in the work of Panter and Dite.[5] The absence of an explicit formulation of (6) therein* results from the direct application of the equivalent of (4b) to a specific problem involving a particular algebraic expression for $(\Delta e)_j$.

A prior, equivalent derivation of (7), based on a graphical representation of $(e - e_j)$ as a sawtooth error function for uniform quantization has been given by Bennett.[2] Although this derivation bypassed (6), Bennett has also analyzed compressed signals by means of an expression

* The present notation has been chosen to resemble that of Reference 5 in order to facilitate direct comparison by the reader.

[(1.6) of Reference 2] which is equivalent to (6), when the average is expressed as an integral over a continuous probability distribution and (Δe) is replaced by $(de/dv)(\Delta v)$, with $(\Delta v) = $ const. This form of (6) is the point of departure for the calculation in the Appendix.

B. *Operational Significance of σ*

Manipulation of (2) may be shown to result in the expression

$$\sigma = \sum_j \sigma_j = \sum_j e_j^2 p_j - \int e^2 P(e) \, de,$$

which is the difference between the mean square signal voltages following and preceding quantization. Hence σ is proportional to the difference between the quantized and unquantized signal powers. Since σ is intrinsically positive, the quantizing error power is *added* to the signal by quantization and is, in principle, measurable as the difference between two wattmeter readings.

In addition to providing an operational interpretation of the quantizing error power, the rewritten expression for σ reveals the equivalence of σ to the "Sheppard correction" to the grouped second-moment in statistics,[24-27] where calculations are facilitated by grouping (i.e., uniform quantization) of numerical data. The reader who is interested in a more elaborate deduction of (7) from the Euler-Maclaurin summation formula, as well as discussions of the validity of (7), may therefore consult the statistical literature.

III. CHOICE OF COMPRESSION CHARACTERISTIC

A. *Restriction to Logarithmic Compression*

We shall consider the properties of the logarithmic type of compression characteristic,* defined by the equations†

$$v = \frac{V \log [1 + (\mu e/V)]}{\log (1 + \mu)}, \quad \text{for} \quad 0 \leqq e \leqq V \quad (8a)$$

and

$$v = \frac{-V \log [1 - (\mu e/V)]}{\log (1 + \mu)}, \quad \text{for} \quad -V \leqq e \leqq 0 \quad (8b)$$

---

* The author first encountered this characteristic in the work of Panter and Dite[5] and the references thereto cited by C. P. Villars in an unpublished memorandum. He has since learned that such characteristics had been considered by W. R. Bennett as early as 1944 (unpublished), as well as by Holzwarth[16] in 1949.
  † Unless otherwise specified, natural logarithms will be used throughout.

In (8), v represents the output voltage corresponding to an input signal voltage e, and μ is a dimensionless parameter which determines the degree of compression.

Typical compression characteristics, corresponding to various choices of the compression parameter, μ, in (8a), are shown in Fig. 3. The logarithmic replot of Fig. 4 provides an expanded picture of small amplitude behavior, as well as evidence of the probable realizability of such characteristics.

Although restriction of attention to (8) may at first appear to impose serious limitations on the generality of the analysis, this impression is not confirmed by more careful scrutiny of the problem.

Perusal of Fig. 3 indicates that (8) generates a considerable variety of curves which meet the general requirements already enunciated in connection with Fig. 2. Thus, the constant factor, $V/\log (1 + \mu)$, has been chosen to satisfy the condition

$$[v]_{e=V} = V \tag{9}$$

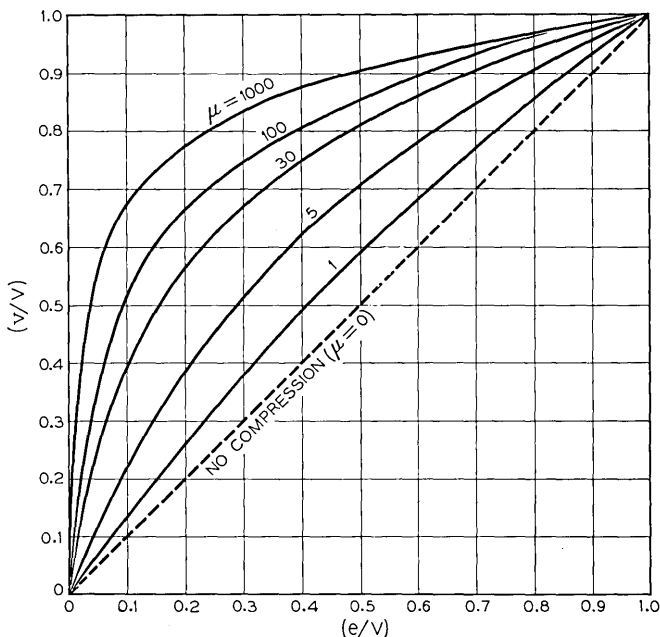Evidence of the significance of the μ-characteristics may be derived

Fig. 3 — Typical logarithmic compression characteristics determined by equation (8a). The symmetrical negative portions, corresponding to equation (8b), are not shown.
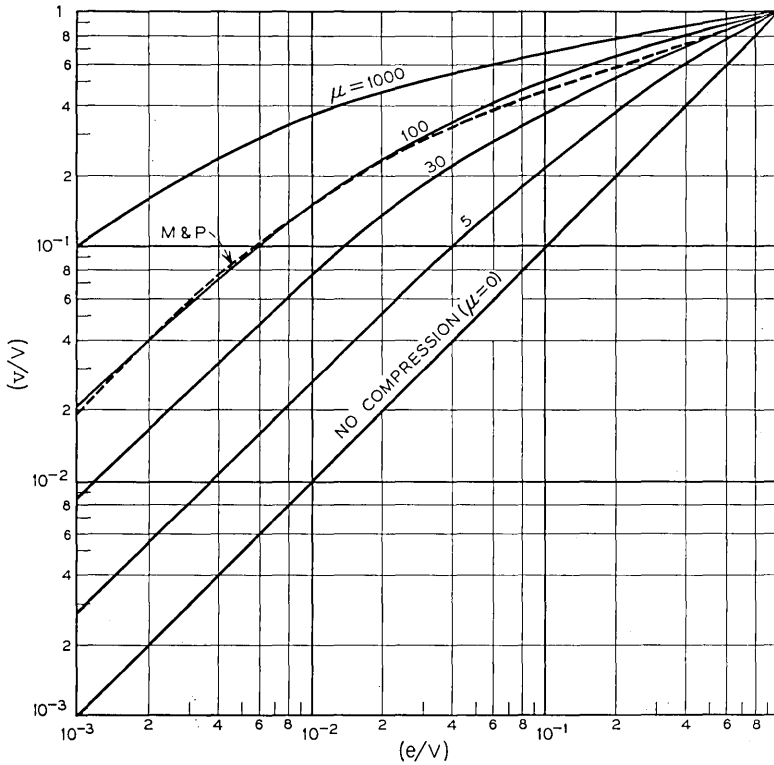
Fig. 4 — Logarithmic replot of compression curves shown in Fig. 3, to indicate detailed behavior for weak samples. The characteristic employed in the experiments of Meacham and Peterson[6] (M & P) is also shown. Similarity between this characteristic and the $\mu = 100$ curve testifies to the probable realizability of these logarithmic characteristics.

from consideration of the ratio of step size to corresponding pulse amplitude, ($\Delta e/e$), since this quantity is a measure of the maximum fractional quantizing error imposed on individual samples. Hence the relation,

$$(e/\Delta e) = [N/2 \log (1 + \mu)](1 + V/\mu e)^{-1}$$

[which follows from (12a)] has been plotted, for $\mu = 10$, 100, and 1000, in Fig. 5. These curves reflect the fact that the sample to step size ratio reduces to the asymptotic forms:

$$(e/\Delta e) \rightarrow N/2 \log (1 + \mu) = \text{const} \qquad \text{for} \qquad (e/V) \gg \mu^{-1}$$

and

$$(e/\Delta e) \rightarrow [N/2 \log (1 + \mu)](\mu e/V) \qquad \text{for} \qquad (e/V) \ll \mu^{-1}$$
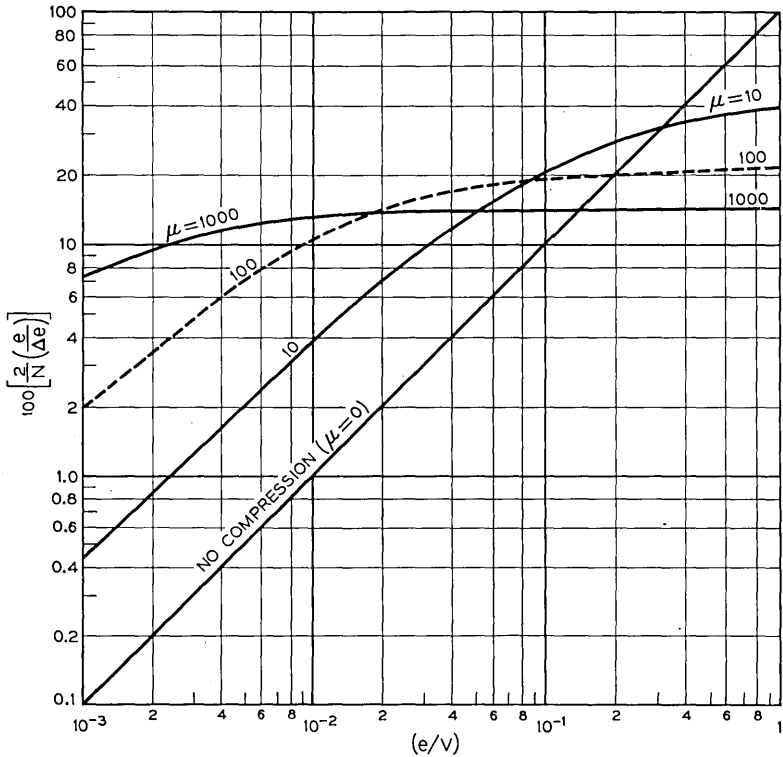
Fig. 5 — Pulse sample to step size ratios, as a function of relative sample amplitude, for various degrees of logarithmic companding (i.e., values of μ). The factor $(2/N)$ in the ordinate permits the curves to be drawn without reference to the total number of quantizing steps (N); the factor (100) is included to permit the ordinates directly to convey the proper order of magnitude for $(e/\Delta e)$, since present interest will be found to center about values of N for which $100(2/N) \sim 1$. As noted in the text, the ordinates, which constitute an index of the precision of quantization, approach constancy for $(e/V) \gg \mu^{-1}$, and vary linearly with abscissa for $(e/V) \ll \mu^{-1}$.

The essentially logarithmic behavior $(e/\Delta e \cong \text{const})$ for large pulse amplitudes is intuitively desirable since it implies an approach to the equitable reproduction of the entire distribution of amplitudes in a specified signal. Although existing experimental evidence indicates that the small amplitudes are not only most numerous,[18] but also most significant for the *intelligibility*[21-23] of speech at constant volume, the absence of comparable evidence on the properties of *naturalness* makes it plausible to consider only those compression characteristics which give promise of providing the same, acceptably small, upper limit on the fractional quantizing error for pulse samples of all sizes.

For sufficiently small input pulses, $(e/\Delta e)$ becomes proportional to e, as a result of the linearity of the logarithmic function in (8) for small arguments. In view of our professed preference for logarithmic behavior, with $(e/\Delta e) \cong$ const., it is important to emphasize that the transition to linearity is not peculiar to (8), but is rather an example of the linearity to be expected of any suitably behaved (i.e., continuous, single-valued, with $(dv/de)_{e=0} > 1$) odd compression function, $v(e)$, capable of power series expansion, in the vicinity of the origin. In (8) this transition to linearity takes place where (e/V) is comparable to μ^{-1}. The extension of the region where $(e/\Delta e) \cong$ const. to lower and lower pulse amplitudes requires an increase in μ, and a concomitant reduction of the $(e/\Delta e)$ ratio for strong pulses.

Further evidence of the significance of the parameter μ may be deduced by evaluating the ratio of the largest to the smallest step size from the asymptotic expressions for $(e/\Delta e)$. Thus we find

$$\frac{(\Delta e)_{e=V}}{(\Delta e)_{e=0}} \rightarrow \mu \qquad \text{for} \qquad \mu \gg 1$$

which is a special form of the more general relation[5]

$$\frac{(\Delta e)_{e=V}}{(\Delta e)_{e=0}} = \frac{(dv/de)_{e=0}}{(dv/de)_{e=V}} = \mu + 1$$

which follows from our standard approximation of

$$(de/dv) \cong (\Delta v/\Delta e)$$

with $\Delta v =$ const.

B. *Comparison with Other Compandors*

An upper bound for companding improvement, which permits the quantitative evaluation of the penalty incurred (if any) through the restriction to logarithmic companding, is established in the Appendix. Comparison of the results to be derived from (8) with this upper bound will reveal that nonlogarithmic characteristics, which provide somewhat more companding improvement at certain volumes, are apt to prove too specialized for the common application to a broad volume range envisioned herein. The μ-characteristics do not suffer from this deficiency since the equitable treatment of large samples, which we have hitherto associated with an "intuitive naturalness conjecture," will be seen to tend to equalize the treatment of all signal volumes.

Finally, it will develop that (8), when applied to (6), has the added merit of calculational simplicity.

IV.* THE CALCULATION OF QUANTIZING ERROR

A. *Logarithmic Companding in the Absence of "DC Bias"*

As previously noted, we consider the effect of *uniformly* quantizing a *compressed* signal. If we designate the uniform output voltage step size by (Δv), then

$$(\Delta v) = \frac{2V}{N} \qquad (10)$$

since the full voltage range between $-V$ and $+V$, of extent $2V$, is to be divided into N equal steps. For a number of levels, N, which is sufficiently large to justify the substitution of the differentials dv and de for the step sizes Δv and Δe, differentiation of (8a) yields

$$\frac{(\Delta v)}{V} = k \left[\frac{1}{1 + (\mu e/V)} \right] \frac{\mu(\Delta e)}{V} \qquad (11)$$

where $k = 1/\log (1 + \mu)$.

Combining (10) with (11) and the counterpart of the latter in the domain of (8b), we find

$$\Delta e = \alpha(V + \mu e) \qquad \text{for} \qquad 0 \leqq e \leqq V \qquad (12a)$$

and

$$\Delta e = \alpha(V - \mu e) \qquad \text{for} \qquad -V \leqq e \leqq 0 \qquad (12b)$$

where

$$\alpha = 2 \log (1 + \mu)/\mu N \qquad (13)$$

Substitution of (12) into (6) yields

$$\sigma = (\alpha^2/12)[V^2 + \mu^2 \overline{e^2} + 2\mu V \overline{|e|}] \qquad (14)$$

where the quantity $\overline{|e|}$ is introduced by the difference in sign in (12a) and (12b). For ordinary compandor applications, we may write

$$\overline{|e|} = 2 \int_0^V eP(e) \, de \qquad (15)$$

since the symmetry of the input signal provides that $P(-e) = P(e)$ and $\bar{e} = 0$.

---

* This passage contains mathematical details which may be omitted, in a first reading, without loss of continuity.

It is convenient to define the quantization error voltage ratio,

$$D = \frac{\text{RMS Error Voltage}}{\text{RMS Input Signal Voltage}} = (\sigma/\overline{e^2})^{\frac{1}{2}} \qquad (16)$$

which takes the form

$$D = \log(1 + \mu)[1 + (C/\mu)^2 + 2AC/\mu]^{\frac{1}{2}}/\sqrt{3}N \qquad (17)$$

when we define the quantities

$$A = \overline{|e|}/\sqrt{\overline{e^2}} = \frac{\text{Average Absolute Input Signal Voltage}}{\text{RMS Input Signal Voltage}} \qquad (18)$$

and

$$C = V/\sqrt{\overline{e^2}} = \frac{\text{Compressor Overload Voltage}}{\text{RMS Input Signal Voltage}} \qquad (19)$$

The simple linear proportionality of Δe to $(V \pm \mu e)$ results from the properties of the logarithmic function in differentiation. Other, seemingly more simple compression equations, when differentiated, yield much more complicated and unwieldy expressions for Δe. The value of this simplicity is evident in the absence, from (14), of moments of e higher than the second.

If we set $A = 0$, (17) reduces to one deduced by Panter and Dite[5]; their analysis erroneously associated A with $\bar{e} = 0$ rather than with $\overline{|e|}$, as a result of their tacit assumption that (12a) and (12b) are identical. They also imposed the restriction of considering only that class of input signals having peak values coincident with the compandor overload voltage, by defining V as the peak value of the signal in specifying C. The definition of C in terms of the independent properties of both signal $(\overline{e^2})$ and compandor (V) is then converted into one based solely on the properties of the signal. This interpretation leads to conclusions quite different from those to be presented here.

B. *Logarithmic Companding in the Presence of "DC Bias"*

It has heretofore been assumed that the input signal is symmetrically disposed about the zero voltage level since it may be expected that $\bar{e} = 0$ for speech. Although this is a standard assumption, subsequent discussion will disclose that it is probable, in actual practice, for the average value of the input signal to be introduced at a point other than the origin of the compression characteristic. In terms of Fig. 1, the signal is

presented to the array of quantizing steps with its quiescent value displaced by an amount e_0 from the center of the voltage interval $(-V$ to $+V)$.

Such an effect, regardless of its origin, may formally be described by considering the composite input voltage

$$E = e + e_0 \tag{20}$$

where e is the previously considered symmetrical speech signal and e_0 is the superimposed constant voltage.

Substitution of E for e in (8) and (12) yields

$$\sigma_E = (\alpha^2/12)[V^2 + \mu^2\overline{E^2} + 2\mu V \,\overline{|E|}\,] \tag{21}$$

where the subscript E is introduced to distinguish this result from (14). Note that the value $[e]_{E=0} = -e_0$ now separates the domain of applicability of (8a) and (12a) from that of (8b) and (12b), so that (15) is replaced by

$$\overline{|E|} = \int_{-V}^{-e_0} (-E)P(e) \, de + \int_{-e_0}^{V} EP(e) \, de \tag{22}$$

which reduces to

$$\overline{|E|} = \overline{|e|} + 2e_0 \int_0^{e_0} P(e) \, de - 2 \int_0^{e_0} eP(e) \, de \tag{23}$$

Since $\bar{e} = 0$, and $e_0 = \text{const.}$, we also find

$$\overline{E^2} = \overline{e^2} + e_0^{\,2} \tag{24}$$

C. *Application to Speech as Represented by a Negative Exponential Distribution of Amplitudes*

It is necessary to assume an explicit function for $P(e)$ in (15) and (23) before applying the general results which have thus far been deduced. We shall assume, as a simple but adequate first approximation, that the distribution of amplitudes in speech at constant volume[18] may be represented by

$$P(e) = G \exp(-\lambda e) \quad \text{for} \quad e \geqq 0 \tag{25}$$

where $P(-e) = P(e)$, $G = \lambda/2$, and $\lambda^2 = 2/\overline{e^2}$. The values of G and λ

follow from the standard relations

$$\int_{-\infty}^{\infty} P(e) \, de = 1$$

and

$$\int_{-\infty}^{\infty} e^2 P(e) \, de = \overline{e^2}$$

When applied to (15) and (18), with the upper limit in (15) replaced by ∞ with negligible error, (25) implies that

$$A = \overline{|e|} / \sqrt{\overline{e^2}} = 1/\sqrt{2} = 0.707 \tag{26}$$

Hence, (17) will be replaced, for numerical calculations, by the relation

$$\sqrt{3}ND = \log(1 + \mu)[1 + (C/\mu)^2 + \sqrt{2}C/\mu]^{\frac{1}{2}} \tag{27}$$

The corresponding substitution of (25) into (23) yields, for the case of $e_0 \neq 0$,

$$\overline{|E|} = e_0 + (\overline{e^2}/2)^{\frac{1}{2}} \exp(-\sqrt{2}C/B) \tag{28}$$

where we have introduced the "bias parameter,"

$$B = V/e_0 \tag{29}$$

When (28) is combined with (13), (21), and (24), we find, after some algebraic manipulation, that

$$\sqrt{3}ND_E = \log(1 + \mu) \\ \cdot [1 + (C/\mu)^2(1 + \mu/B)^2 + (\sqrt{2}C/\mu) \exp(-\sqrt{2}C/B)]^{\frac{1}{2}} \tag{30}$$

where $D_E{}^2 = (\sigma_E/\overline{e^2})$. It is to be noted that D_E has been defined in terms of the ratio of σ_E to $\overline{e^2}$ rather than $\overline{E^2}$, so that

$$D_E{}^2 = \frac{\text{Mean Square Error Voltage}}{\text{Mean Square Speech Voltage}} \tag{31a}$$

$$= \frac{\text{Average Error Power}}{\text{Average Speech Power}} \tag{31b}$$

Examination of (30) reveals that it has the required property of reducing to (27) for $e_0 = 0$, i.e., for $B \to \infty$. Furthermore (27) and (30) indicate that $D_E \geq D$ so that the addition of a dc component increases the quantizing error power when companding is used. The existence of

such an impairment may easily be understood in terms of the physical interpretation of (6), as discussed in connection with Fig. 1.

Equations (27) and (30) also reveal that the penalty inflicted by a finite e_0 is largely determined by the ratio (μ/B). If $(\mu/B) \ll 1$, the presence of e_0 will be unimportant. At the other extreme, if $(\mu/B) \gg 1$, $(1 + \mu/B)^2 \to (\mu/B)^2$ and

$$\sqrt{3}ND_E \to \log(1 + \mu)$$
$$\cdot [1 + (C/B)^2 + (\sqrt{2}C/\mu)\exp(-\sqrt{2}C/B)]^{\frac{1}{2}} \quad (32)$$

which proves to be relatively insensitive to changes in μ for the values of μ, C and B considered herein. In this case B largely usurps the algebraic role previously assigned to μ in (27).

D. *Uniform Quantization*: $\mu = 0$

The mean square quantization voltage error in the absence of companding, corresponding to direct, uniform quantization of the input signal, follows immediately from (7) and (10) since $\Delta v = \Delta e$ under these conditions. Thus

$$\sigma_0 = (\Delta v)^2/12 = V^2/3N^2$$

whence

$$D_0 = (\sigma_0/\overline{e^2})^{\frac{1}{2}} = C/\sqrt{3}N \quad (33)$$

This inverse proportionality of D_0 and N is well known.[2, 3, 5]

Equation (33) may also be deduced by letting μ approach zero in the expressions for D and D_E, since (8) implies that v approaches e as μ approaches zero. The fact that $D_0 = (D_E)_{\mu \to 0}$ reveals that, in the absence of companding, the addition of e_0 does not change the quantizing error power. This conclusion was anticipated in the discussion of Fig. 1.

V. DISCUSSION OF GENERAL RESULTS

Since the nature of a companded signal depends on a rather large number of variables, it is appropriate to consider their respective roles in general terms before discussing detailed system requirements. This general discussion will, however, emphasize those particular modes of operation which are suggested by existing proposals for application of PCM.[1, 3, 6] Thus, we shall consider common channel companding of

speech in time division multiplex systems which employ binary number encoding.

A. *Quantitative Description of Conventional Operation* ($e_0 = 0$)

1. *Number of Quantizing Steps* (N)

The number of steps, N, is related to the choice of code. For a binary code, the relation takes the form, $N = 2^n$, where n is the number of binary digits per code group.

In the present discussion it will usually be convenient to regard n and N as fixed in order to permit comparison of various companding characteristics under the same coding conditions. Since both D and D_0 are inversely proportional to N, the quotient $(D/D_0)^2$, which is equal to the ratio of the quantizing error power in the presence of companding to that in the absence of companding, is independent of N. Consequently, as will be evident in the discussion of (37), the relative diminution of quantizing error (in db) afforded by companding is also independent of N.*

However, the value of N will determine the signal to quantizing error power ratio to which the companding improvement is to be added. Thus the number of digits per code group required for a particular application will ultimately be determined by the value of N which, in combination with suitable companding, will suffice to produce an acceptably low value of quantizing error power in relation to signal power.

2. *Compandor Overload Voltage* (V)

The compandor overload voltage, V, will be determined by the full load power objectives for the proposed system. Specifically, V will be equal to the amplitude of the sinsuoidal voltage corresponding to "full modulation."

3. *Relative Signal Power* (C)

The quantity $C = V/(\overline{e^2})^{\frac{1}{2}}$ will, for a given value of V, be determined by the rms signal voltage $(\overline{e^2})^{\frac{1}{2}}$.

The range of C values appropriate to a given system will therefore reflect the distribution of volumes to be encountered. In fact, the signal

---

* It must of course be understood that this independence requires a value of N sufficiently large to justify the approximations involved in the deduction of (27) and (33).

power in db *below* that corresponding to a full load sine wave is simply

$$10 \log_{10} \left[\frac{V^2/2}{\overline{e^2}} \right] = 10 \log_{10} [C^2/2] = 20 \log_{10} C - 3 \; db \qquad (34)$$

It must be emphasized that C varies *inversely* with the rms signal voltage, so that weak signals are characterized by large values of C and strong signals by small values of C.

4. *Average Absolute Signal Amplitude ($\overline{|e|}$)*

The probability density of the signal manifests itself in the value assigned to the average absolute signal parameter, $A = \overline{|e|}/\sqrt{\overline{e^2}}$. This
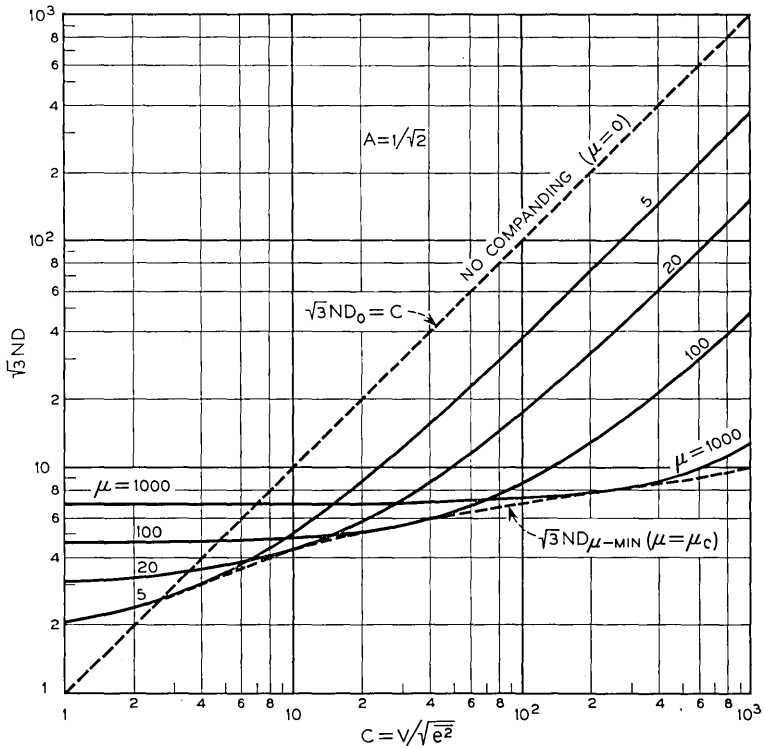

Fig. 6 — Variation of the rms error to signal voltage ratio (D) with relative signal strength, $C = V/\sqrt{\overline{e^2}}$, as given by equation (27) for various degrees of logarithmic companding.

quantity is a constant determined by the statistical properties of the class of signals being studied.

With the present choice of an exponential distribution of amplitudes to represent speech, [see (25)], we have seen that A takes on the value $1/\sqrt{2} = 0.707$. It develops that A is not very sensitive to the choice of $P(e)$, as may be judged by the values $\sqrt{2/\pi} = 0.798$, and $\sqrt{3}/2 = 0.866$ which would replace 0.707 if (25) were replaced by Gaussian and rectangular distributions, respectively. The value $A = 1/\sqrt{2}$ will be used in all numerical calculations; changes in the value of A to describe other classes of signals (e.g., the aforementioned Gaussian or rectangular distributions) will change the plotted results by no more than a fraction of a decibel.

5. Degree of Compression (μ)

From the foregoing it is clear that the essence of the compandor's behavior is embodied in the one remaining variable which appears in (8) and (17): the compression parameter μ.

The significance of μ has already received preliminary attention in connection with Figs. 3 to 5. Fig. 6, where comparison of behavior at constant N is facilitated by the choice of $\sqrt{3}ND$ as ordinate, exhibits the behavior of the ratio D as a function of C at constant μ. It will be observed that the curves in Fig. 6 do not extend below their common tangent which is labeled $\sqrt{3}ND_{\mu-\text{MIN}}$. The significance of this lower bound may be discussed in terms of Fig. 7 and the hypothetical ensemble of compandors to which we now direct our attention.

B. Optimum Compandor Ensemble

Consider the artificial situation in which our communication system includes an ensemble of instantaneous compandors, the members of which correspond to different values of μ in (8). Since companding improvement varies with signal strength, we permit ourselves the luxury of measuring the volume (i.e., C) of the input signal in order to assign the optimum degree of companding compatible with (8), to each individual signal. The compandor assigned to a signal is characterized by that particular value of the compression parameter, $\mu = \mu_c$, which is required to minimize D for a particular value of C. This critical compression parameter may be calculated from the requirement that

$$[\partial D/\partial \mu]_{A,C=\text{const}} = 0 \tag{35}$$

which yields

$$SC^2 + \mu_c A(S - 1)C - \mu_c^2 = 0 \tag{36}*$$

where $S = [(1 + \mu_c) \log (1 + \mu_c)/\mu_c] - 1$, when applied to (17).

The graph of (36) in Fig. 7 may be used to determine numerical values of μ_c without repeated recourse to the equation.

The curve labeled $\sqrt{3}ND_{\mu-\text{MIN}}$ in Fig. 6 was determined by substituting values of μ_c, obtained from Fig. 7, into (27). Each curve in Fig. 6
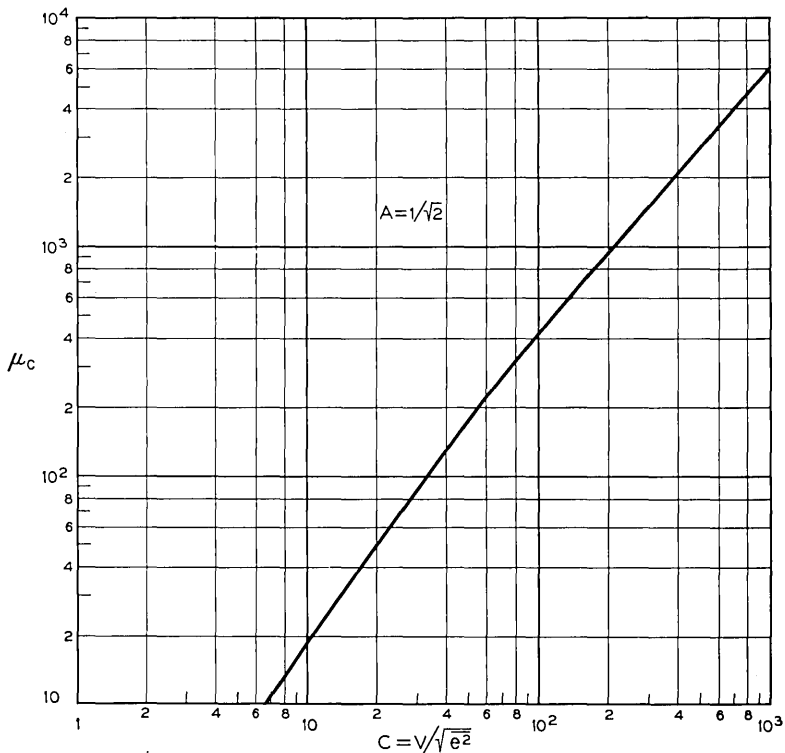

Fig. 7 — Critical compression parameters, μ_c, required to minimize the quantizing error power as a function of relative signal strength, as determined by equation (36). Each point on the curve defines a compandor in the optimum compandor ensemble. It must be understood that such an ensemble provides the best performance consistent with equation (8) rather than the absolute minimum quantizing error discussed in the Appendix.

* A similar equation, with $A = 0$ corresponding to the previously noted erroneous identification of A with $\bar{e}$ rather than $\overline{|e|}$, has been deduced by Panter and Dite.[5] Their definition of C as a "crest factor" changes the significance of what we have called $D_{\mu-\text{MIN}}$ and does not lead to the ensemble interpretation of μ_c.
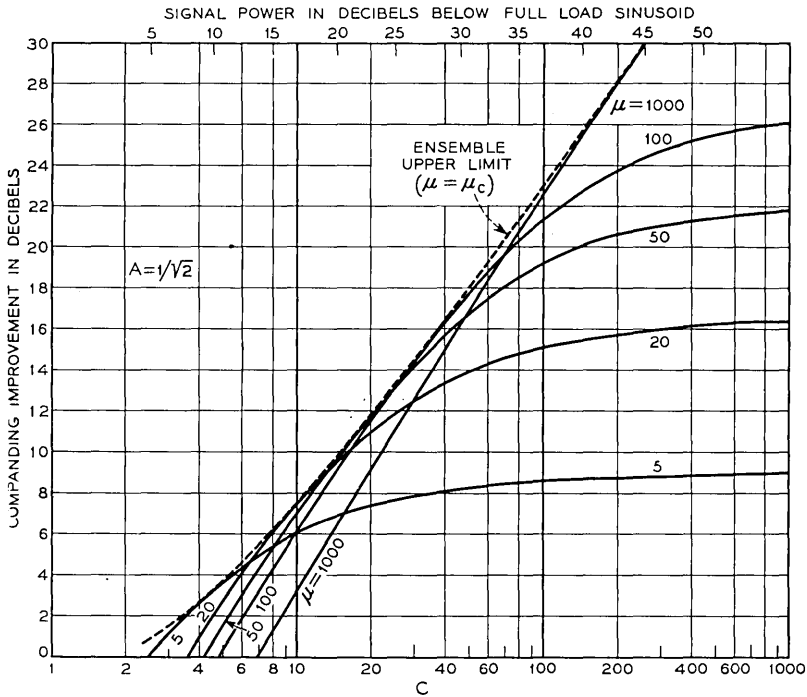
Fig. 8 — Companding improvement (in db), as calculated from equation (37), for various values of μ. The saturated improvement for weak signals (relatively constant ordinate for large C values) is identical with the asymptotic behavior for weak signals which is predicted by Fig. 9.

is tangent to this lower bound at the single value of C which corresponds to $\mu = \mu_c$.

In conventional systems, a single common channel compandor,[6] characterized by a single value of μ, is substituted for the optimum ensemble. Although $D_{\mu-\text{MIN}}$ is then attainable at only one value of C, it is instructive to compare each value of D with the corresponding value of $D_{\mu-\text{MIN}}$. Indeed, consideration of the optimum ensemble has, in one sense, reduced the problem of choosing an appropriate μ for a given application to the choice of that particular value of C at which equality of D and $D_{\mu-\text{MIN}}$ is desired.

In Fig. 6, the line representing performance in the absence of companding corresponds to (33) for D_0 . D_0 and $D_{\mu-\text{MIN}}$ are seen to be similar for strong signals (low values of C). Furthermore, it is important to note that D_0 does not constitute an upper bound for D; thus the companding
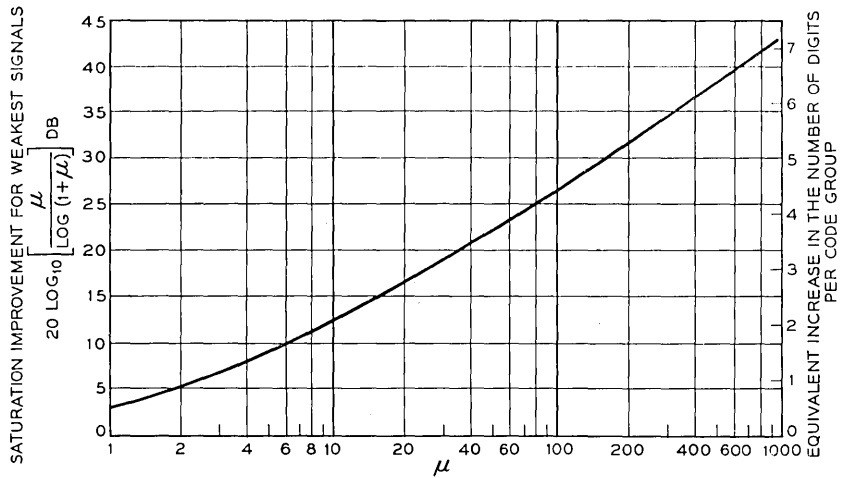
Fig. 9 — Saturated companding improvement for weakest signals as a function of the degree of logarithmic compression (μ). Given a value of μ, the corresponding ordinate represents the reduction of quantizing error power (in db) for signals so weak that their peaks satisfy the relation $(e/V) \ll \mu^{-1}$. Thus weaker and weaker signals are required to exploit the added improvement which follows from an increase in μ. The auxiliary ordinate scale on the right exhibits the increase in the number of digits per code group which may be shown to be equivalent to the linear compression which gives rise to the saturated improvement of weak signals.

improvement of weak signals (large C) is obtained at the price of impairment of strong signals (small C).

C. Companding Improvement for $e_0 = 0$

From the definition of D in (16) it follows that

$$\left[\frac{D_0}{D}\right]^2 = \frac{\text{Mean Square Error Voltage Without Companding}}{\text{Mean Square Error Voltage With Companding}}$$

$$= \frac{\text{Average Quantitizing Error Power Without Companding}}{\text{Average Quantizing Error Power With Companding}}$$

whence, the improvement (in db) due to companding may be evaluated from the expression

$$10 \log_{10} (D_0/D)^2 = 20 \log_{10} (D_0/D) \text{ db} \tag{37}$$

This quantity is plotted against C for various values of μ in Fig. 8. Substitution of $D_{\mu-\text{MIN}}$ for D in (37) yields the optimum ensemble limiting curve. Just as in Fig. 6, each curve is tangent to this limiting curve for a value of C corresponding to coincidence of μ and μ_c .

The abscissa has been furnished with an additional scale, based on (34), showing the signal power in db below that of a full load sine wave. Thus the curves in Fig. 8 embody the information required for the choice of a compandor characteristic in a form which is suitable for practical applications. It is clear that the effect of companding varies considerably with the volume of the signal and that strong signals are actually impaired. For each value of μ, there is a value of C (in the weak signal, or large C range) beyond which the db improvement is essentially independent of C. The threshold value of C corresponding to such saturation increases with increasing μ. This saturated improvement for weak signals reflects the linearity of compression for $(e/V) \ll \mu^{-1}$. In this region, uniform quantization prevails so that the ratio of the uniform step sizes before and after companding (given by the linear amplification factor) may be used to deduce a constant companding improvement for the
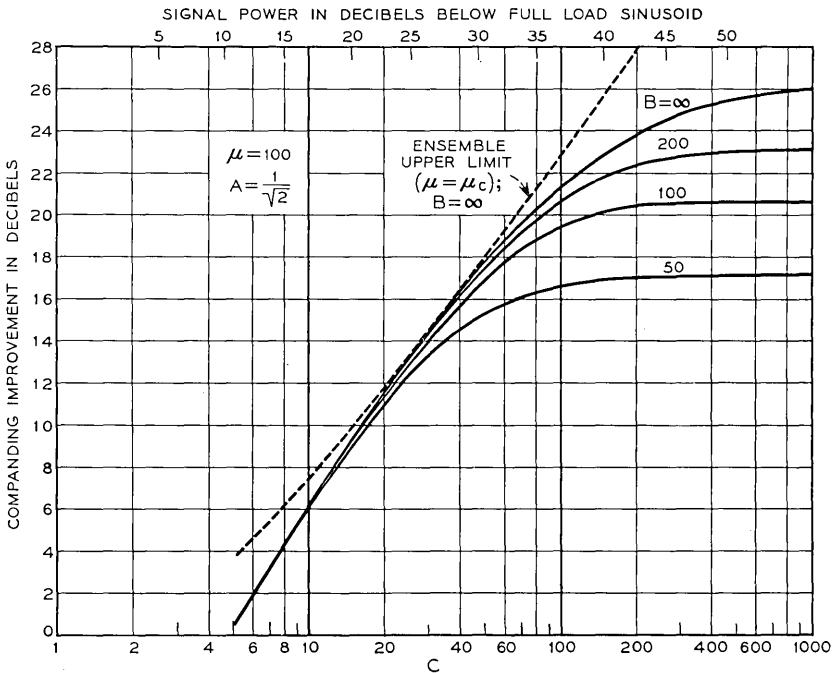

Fig. 10 — Modification of companding improvement, for $\mu = 100$, resulting from the shift of the quiescent value of the signal by an amount e_0 from the center of the quantized voltage range (see Fig. 1). The relative size of the "dc component" is given by the parameter $B = V/e_0$ as defined in equation (29). The algebraic usurpation of the role of μ by B, for $B \ll \mu$, results in the striking similarity of the weak signal behavior of the curves for $B = 50$ and 100 in Figs. 10 to 13.

weakest signals, regardless of the shape of the characteristic in the non-linear region. Equation (8) implies

$$(v/e)_{e\to 0} = (\Delta v/\Delta e)_{e\to 0} = \mu/\log (1 + \mu)$$

so that for each value of μ, the constant companding improvement for the weakest signals is

$$20 \log_{10} [\mu/\log (1 + \mu)] \text{ db}$$

which is plotted in Fig. 9. Fig. 8 supplements Fig. 9 in revealing the actual volumes required for the realization of this weak signal saturation, as well as the detailed behavior for stronger signals.

D. Companding Improvement for $e_0 \neq 0$

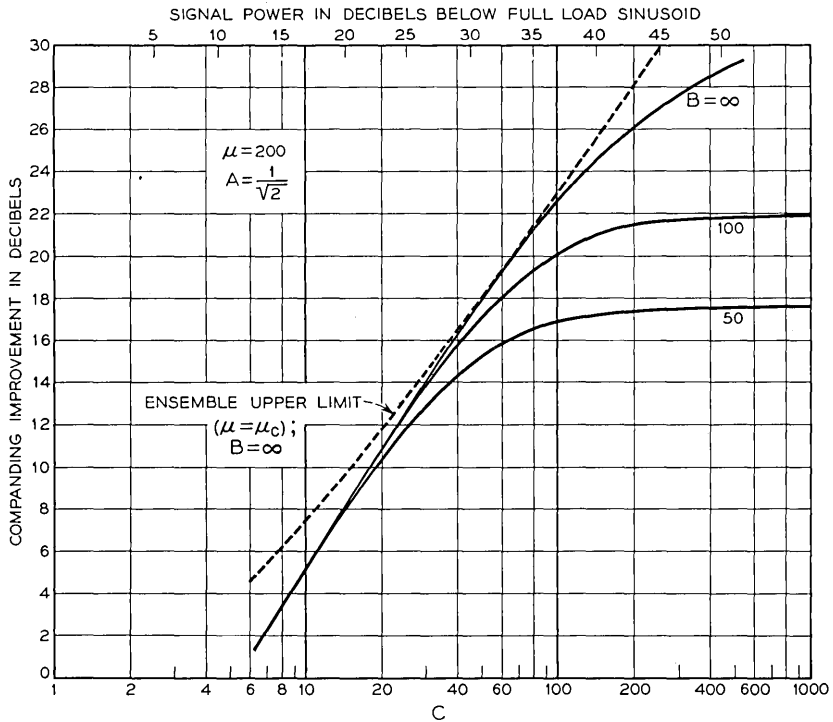Since we will usually regard a nonzero value of e_0 as an undesirable

Fig. 11 — The effect of a "dc component" on companding improvement for $\mu = 200$. For further details, see the caption of Fig. 10.

perturbation, we wish to study the modification of companding improvement produced by the introduction of a finite value of $B = V/e_0$, i.e., substitution of (30) for (27), when N, V, C, A, and μ remain unchanged.

In Figs. 10 to 13 we have replotted the companding improvement curves shown in Fig. 8 for $\mu = 100, 200, 500,$ and $1,000$, respectively. These curves correspond to $B = \infty$. The difference between these curves and those for finite values of B in Figs. 10 to 13 is the impairment (in db) inflicted by the presence of e_0. This impairment may be appreciable for weak signals (large C). As already noted in connection with (32) the impairment is not severe for $(\mu/B) \ll 1$. Furthermore, the appropriation of the algebraic role of μ by B, when $B \ll \mu$, which was previously noted in (32), manifests itself in the striking similarity of the weak signal behavior of all the curves for $B = 50$ and 100 in Figs. 10 to 13.
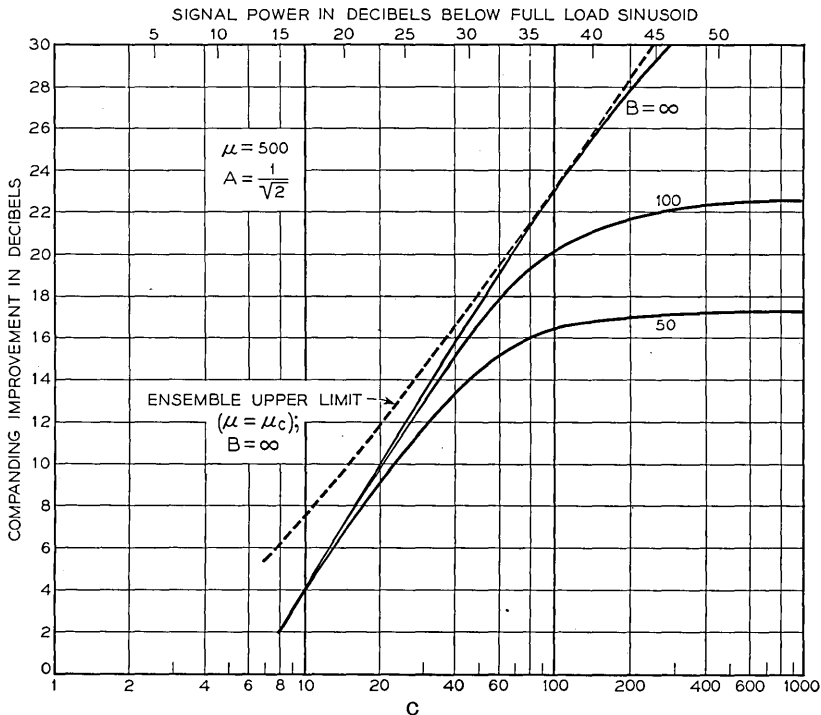

Fig. 12 — The effect of a "dc component" on companding improvement for $\mu = 500$. For further details, see the caption of Fig. 10.
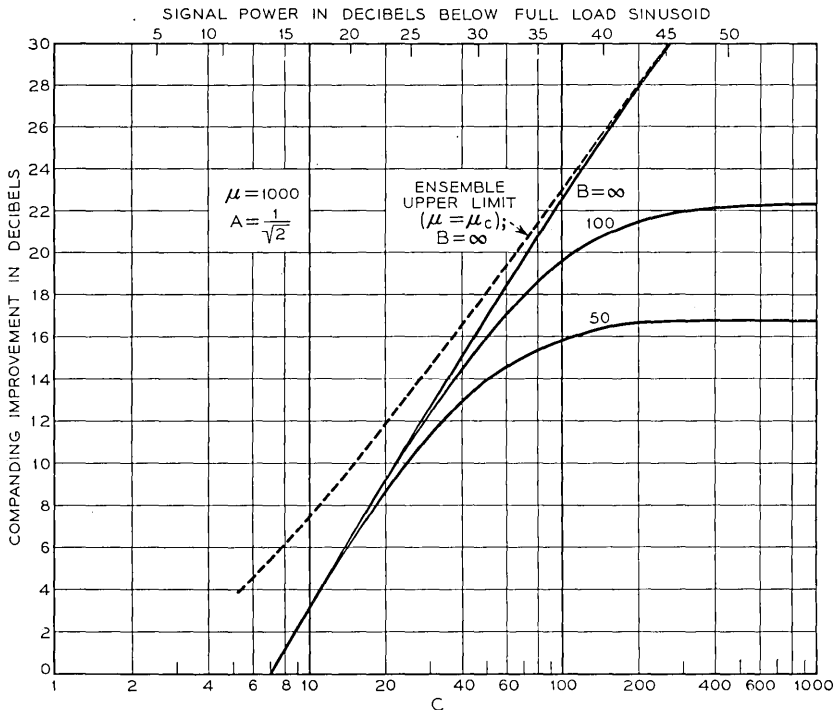
Fig. 13 — The effect of a "dc component" on companding improvement for $\mu = 1,000$. For further details, see the caption of Fig. 10.

VI. APPLICATION OF RESULTS TO A HYPOTHETICAL PCM SYSTEM

Consider the application of these results to the planning of a typical, albeit hypothetical, communication system.

A. *Speech Volumes*

Suppose it is desired to transmit signals covering a 40 db power range, with the strongest and weakest speech volumes each separated by 20 db from the average anticipated signal power at the compressor input.*

The strongest signal power is then used to determine the value of the compandor overload voltage, V. In this case a value of V corresponding to a full load sine wave 10 db above the loudest signal, [see (34)], appears adequate.* Although this choice may at first appear arbitrary,

---

* These values are sufficiently close to those cited as representative by Feldman and Bennett, in connection with Fig. 2 of Reference 11, to be considered quite realistic.

the value of 10 db is probably no more than a few db removed from the value which would be chosen in any efficient application of PCM to quality telephony. It results from the need to balance the requirement of a value of V sufficiently high to avoid intolerable clipping of the peaks of the loudest signals against the obvious advantage of reducing the quantizing step size by minimizing the voltage range to be quantized. We have neglected clipping in our calculations since it was assumed that the significant peaks of the loudest signals should not exceed V for quality telephony. Existing information on clipped speech[21-23] and one digit PCM[10] indicates that the clipping impairment we seek to avoid is largely one of loss of naturalness rather than reduction in intelligibility. The choice of a maximum volume 10 db below a sinusoid of amplitude V implies that speech peaks 13 db, [see (34)], above the maximum rms signal voltage are being ignored, which appears reasonable in the light of available experimental evidence.[18, 22]

It follows from these assumptions that the average and weakest signals are respectively 30 db and 50 db below full sinusoidal modulation.

B. *Choice of Compression Characteristic*

1. *Ideal Behavior for Speech*

If we adopt the aim of achieving the smallest over-all departure from the ensemble limit of improvement, it seems reasonable to choose that compandor in the optimum ensemble which corresponds to average speech ($C \cong 45$). This requirement, in conjunction with Fig. 7, establishes a lower bound of about 150 for μ. The significance of this choice may be clarified by reference to Fig. 14, which depicts departures from the optimum ensemble limit of improvement, resulting from restriction to a single value of μ for all volumes.

The corresponding upper bound will be determined by the alternative of furnishing optimum improvement to the weakest signals ($C \cong 450$) in spite of the concomitant impairment of loud speech. Reference to Fig. 7 then dictates a choice of μ in the vicinity of 2,500. From Fig. 6 it is clear that this value implies that D is essentially constant and independent of C throughout the range of interest. Appreciably larger values of μ would actually lead to the undesirable extreme of $D > D_{\mu\text{-MIN}}$ for all signals under consideration.

We therefore conclude that attention may profitably be confined to the interval $150 \lesssim \mu \lesssim 2,500$, the magnitude of which is adequately conveyed by the simple expression

$$100 \lesssim \mu \lesssim 1,000 \tag{38}$$

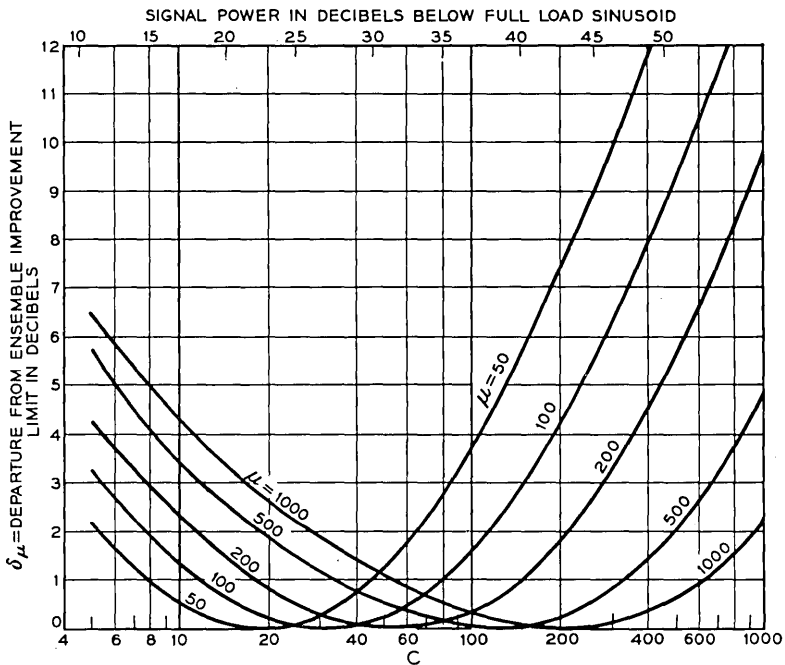SIGNAL POWER IN DECIBELS BELOW FULL LOAD SINUSOID

Fig. 14 — Improvement selectivity, i.e., departures from the ensemble upper limit of improvement due to the use of a single value of μ rather than the ensemble of μ_c values. The minima at $\delta_\mu = 0$ locate the signals (C) for which μ and μ_c coincide. All curves correspond to the case where the "dc component", e_0, is zero.

Lest it appear that this range is so broad as to offer very little practical guidance, it should be noted that (38) defines a rather narrow range of characteristics in Figs. 3 and 4. The assumption that this range may be realized in practice appears reasonable in view of the similarity to the characteristic actually used by Meacham and Peterson, which is shown in Fig. 4.

2. Practical Limitations on Companding Improvement

(a) *Mismatch Between Zero Levels of Signal and Compandor.* Although the present discussion has hitherto been confined to ideal compandor action, it lends itself quite naturally to the analysis of a significant departure from ideal behavior which may be expected to result from the use of an instantaneous compandor on a common channel basis in time division multiplex systems.

It will probably be impractical to balance the channel gating circuits (required to provide sequential connection of individual channels to a

single compressor)[1, 6] sufficiently to guarantee exact coincidence of the average input signal ($\bar{e} = 0$) in each channel and the center of the $-V$ to $+V$ voltage range ($e = 0$) presented by the compressor. Thus the input, e, would appear to the compressor in the form $E = e + e_0$. The consequences of the appearance of the undesirable constant term, e_0, may be inferred from study of Figs. 10 to 13 and (30).

We shall assume that, owing to the present state of gating technology, $B = V/e_0$ may reasonably be expected to assume values in the range $100 \lesssim B \lesssim 1,000$.

For companding corresponding to $100 \lesssim \mu \lesssim 1,000$, Figs. 10 to 13 indicate that, if B can be confined to the vicinity of 1,000, the departure from the ideal behavior corresponding to $B = \infty$ will be virtually negligible.

However, should it prove necessary to work with $B \cong 100$, it is clear from Figs. 10 to 13 that the companding improvement for weak signals would be relatively independent of μ in the interval $100 \lesssim \mu \lesssim 1,000$ (with a saturation value of about 20.5–22.5 db).* In this event, compression to a degree greater than that represented by $\mu = 100$ would provide less improvement for strong and average speech without the compensation of significantly greater improvement for weak signals. Reduction of μ below 100 would not be fruitful since the sensitivity of companding improvement to changes in μ is restored for values satisfying the condition of $(\mu/B) = (\mu/100) < 1$.

The significance of the values $e_0 \sim V/1,000$ and $V/100$ may perhaps better be appreciated in terms of a comparison of e_0 with the weakest signals under consideration. Since $(B/C) = \sqrt{\overline{e^2}}/e_0$, a signal to dc bias power ratio may be calculated, in db, from the expression $20 \log_{10} (B/C)$. For the weakest signals under consideration ($C \sim 400$), the values $B = 1,000$ and 100 correspond respectively to $(\sqrt{\overline{e^2}}/e_0) = 2.5$ and 0.25, or to signal to dc bias power ratios of $+8$ db and -12 db. Thus, for the hypothetical system now under study, the value of e_0 becomes significant (roughly) when it exceeds the weakest rms signal.

Actually e_0 would be expected to vary with time for a given channel and to vary from channel to channel at any instant. On the assumption that $| e_0 | = V/100$ (i.e., $B = 100$) will constitute the upper bound of such variations, the companding improvement corresponding to a particular value of μ must now be specified in terms of the region between the $B = \infty$ and $B = 100$ curves in Figs. 10 to 13, rather than by reference to a single value of B and its corresponding curve. Since the lower

---

* This corresponds to the behavior of D_E for $(\mu/B) \gg 1$ which was noted in the discussion of (30). In this connection, see the discussion of Fig. 19.

bounds of all these regions (see Figs. 10 to 13) are approximately coincident (for $100 \lesssim \mu \lesssim 1{,}000$), the advantage of increasing μ substantially beyond 100 will depend largely on the expectation of encountering values of $e_0 \rightarrow (V/1{,}000)$ with sufficient frequency in the various channels served by the common compressor.

These arguments may of course be applied, with suitable modifications depending on the range of C, μ, and B values requiring attention, to any effect capable of formal description in terms of an effective dc bias superimposed on the signal input to the compressor.

(b) *Background Noise Level.* It does not seem reasonable to strive for an increase of the signal to quantizing error power ratio substantially beyond that value which is subjectively equivalent to the anticipated ratio of signal to background noise from other sources.

Since the quantizing error power depends on the number of digits per code group, the comparison of quantizing error power and noise power is reserved for subsequent discussion of the required number of quantizing steps. It will be noted that the comparison must remain somewhat speculative in the absence of a determination of the subjective equivalence of quantizing error power and noise.

C. *Choice of the Number of Digits Per Code Group*

1. *Ideal Behavior for Speech*

As previously remarked, the number of quantizing steps will determine the ratio of signal to quantizing error power to which the companding improvement is to be added. Since the quantizing error power is inversely proportional to $N^2 = 2^{2n}$, this power will be reduced by 6 db for each additional digit. Comparison of this 6 db per digit improvement with the roughly 24 to 35 db improvement corresponding to weak signals in Fig. 8 (for $100 \lesssim \mu \lesssim 1{,}000$) reveals that, *for such signals, companding is equivalent to the addition of four to six digits per code group, i.e., to an increase in the number of quantizing steps by a factor between $2^4 = 16$ and $2^6 = 64$.* This equivalence is portrayed in Fig. 9. Our failure to realize a companding improvement of about 43 db as predicted for $\mu = 1{,}000$ in Fig. 9 may be traced to the fact that the weakest signals now under consideration are not sufficiently weak to be confined to the linear region $(e/V) \ll \mu^{-1})$ of the $\mu = 1{,}000$ characteristic. This is reflected in the unsaturated improvement exhibited in Fig. 8 for the weakest signals when $\mu = 1{,}000$.

Although it is clearly preferable to suppress quantizing error power by companding rather than by increasing the number of quantizing
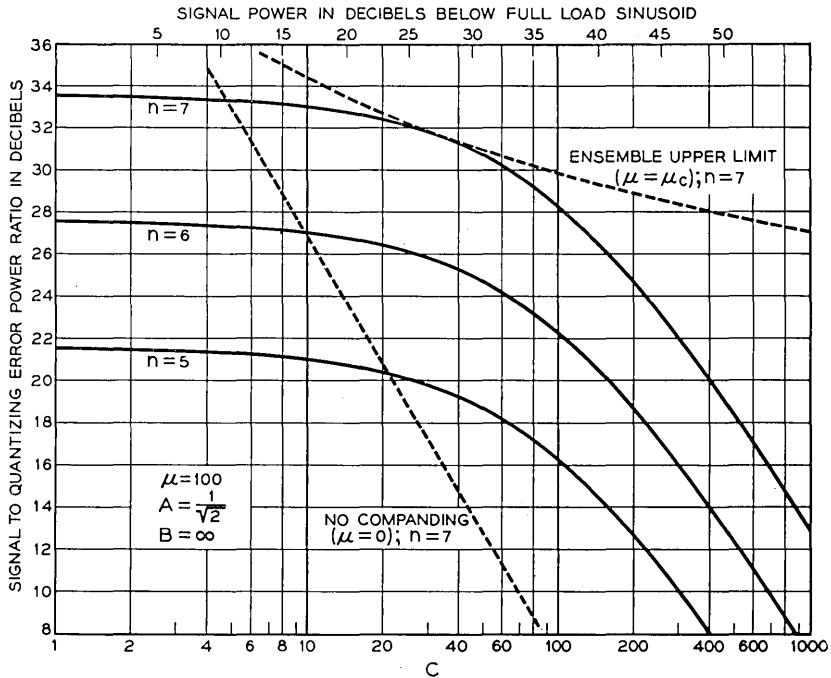
Fig. 15 — Signal to quantizing error power ratios (calculated, in db, from equation (39)) as a function of relative signal power for companding corresponding to $\mu = 100$. Curves are shown for $n = 5, 6$, and 7 digits per code group. For comparison, the results for seven digits in the absence of companding ($\mu = 0$) as well as for the ensemble upper limit ($\mu = \mu_c$) are included. $B = \infty$ throughout.

steps, it is apparent that the upper limit of companding improvement will set a lower limit on the number of digits required for satisfactory operation.

Once again we begin with the consideration of pure speech signals. The expression

$$-10 \log_{10} (D^2) = -20 \log_{10} D$$

$$= \text{Signal to Quantizing Error Power Ratio in db} \tag{39}$$

has been plotted against C in Figs. 15 to 18 for $\mu = 100, 200, 500$, and 1,000 respectively. In each case the behavior for 5, 6, and 7 digits is compared with the extremes of $\mu = 0$ (no companding) and $\mu = \mu_c$ (ensemble upper limit) for 7 digits.

It must be conceded at the outset that experimental work is required to formulate standards for quantizing error power similar to those
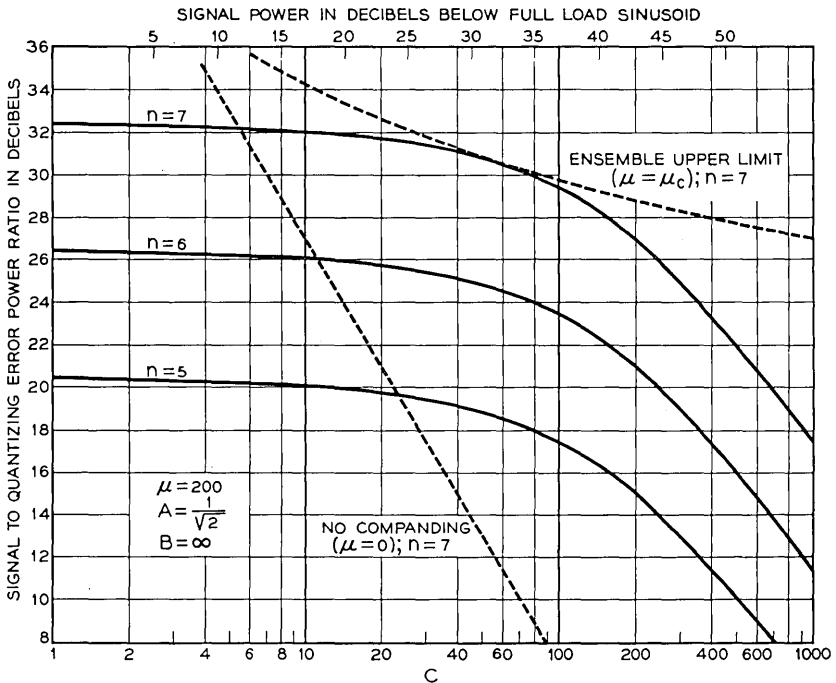
Fig. 16 — Signal to quantizing error power ratios (in db) as a function of relative signal power for companding corresponding to $\mu = 200$. Symbols have the same significance as in Fig. 15. $B = \infty$ throughout.

which have been established for conventional noise and distortion. If these were available, graphs such as those in Figs. 15 to 18 could be used to select the proper number of digits to be used with various degrees of compression. In the absence of such information we shall complete this illustrative study by adopting a signal to quantizing error power ratio of at least 20 db as a tentative standard of adequate performance at all volumes.*

Figs. 15 and 16 show that seven digits (i.e., $2^7 = 128$ tapered quantizing steps) and $\mu \cong 150$ will meet this objective. Furthermore Figs. 17 and 18 indicate that six digits ($2^6 = 64$ tapered steps) would suffice provided (38) is replaced by the more stringent limitation,

$$500 \lesssim \mu \lesssim 1{,}000 \tag{40}$$

---

* This value does not appear unreasonable, as a first approximation, in terms of experience with noise and harmonic distortion.

2. *Practical Limitations*

(a) *Mismatch Between Zero Levels of Signal and Compandor.* From the previous discussion of the effect of e_0 on the choice of μ, it is clear that, if B can be confined to the vicinity of 1,000, the analysis of the required number of digits in the absence of instability ($B = \infty$) may be applied.

On the other hand, behavior for $B = 100$ may be judged from the plot of signal to quantizing error power ratio versus signal power for $\mu = 100$ and 1,000 (with seven digits) shown in Fig. 19. Since this ratio now fails to exceed about 16 db for the weakest signals of interest, we conclude that an increase to eight digits ($2^8 = 256$ tapered steps), with a concomitant 6 db improvement for all signals, is required to meet our 20 db objective. These curves also illustrate the previously noted meager improvement for weak speech which accompanies the increase from $\mu = 100$ to 1,000 when $B = 100$. Actually, an optimum solution is attained for an intermediate value of μ, but the advantage is too small to be of interest (see Figs. 10 to 13).

Fig. 17 — Signal to quantizing error power ratios (in db) as a function of relative signal power for companding corresponding to $\mu = 500$. Symbols have the same significance as in Fig. 15. $B = \infty$ throughout.

The recognition that use of $B = 100$ rather than a value approaching 1,000 may imply a change from six to eight digits per code group (e.g., for $\mu = 1,000$), representing an increase of 33 per cent in the required bandwidth in the transmission medium as well as a significant increase in the complexity of the multiplex terminal equipment, provides the proper perspective for competent appraisal of the cost of improving gate circuitry to the point where B would approach 1,000. These considerations might be of crucial importance in the planning of actual PCM systems.

Finally these results also show that caution is required in attempting to determine an adequate number of digits and/or degree of compression from listening tests employing preliminary experimental equipment. If the conditions of the test do not duplicate exactly the expected behavior of the channel gates to be used in the final system, the transition from the laboratory to practice might lead to an embarrassing disappearance
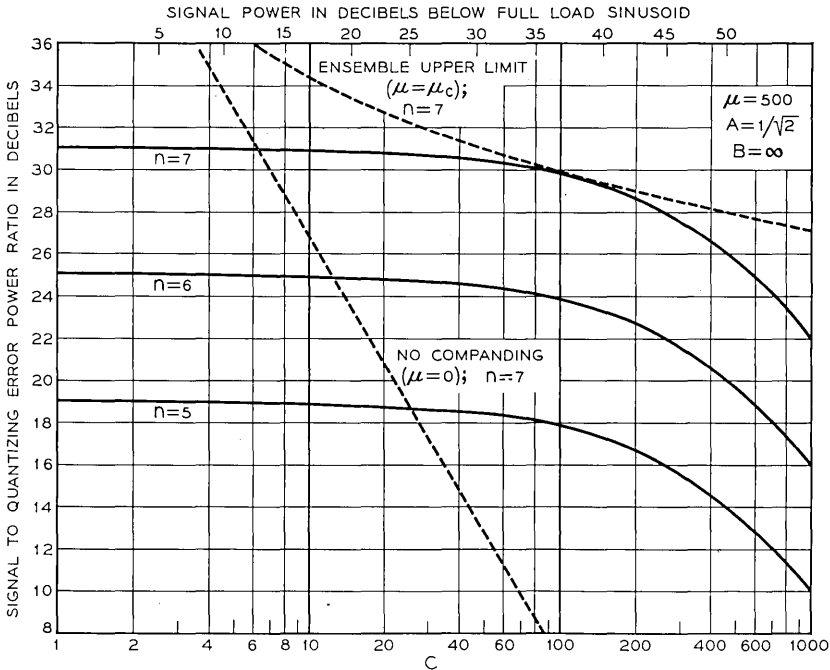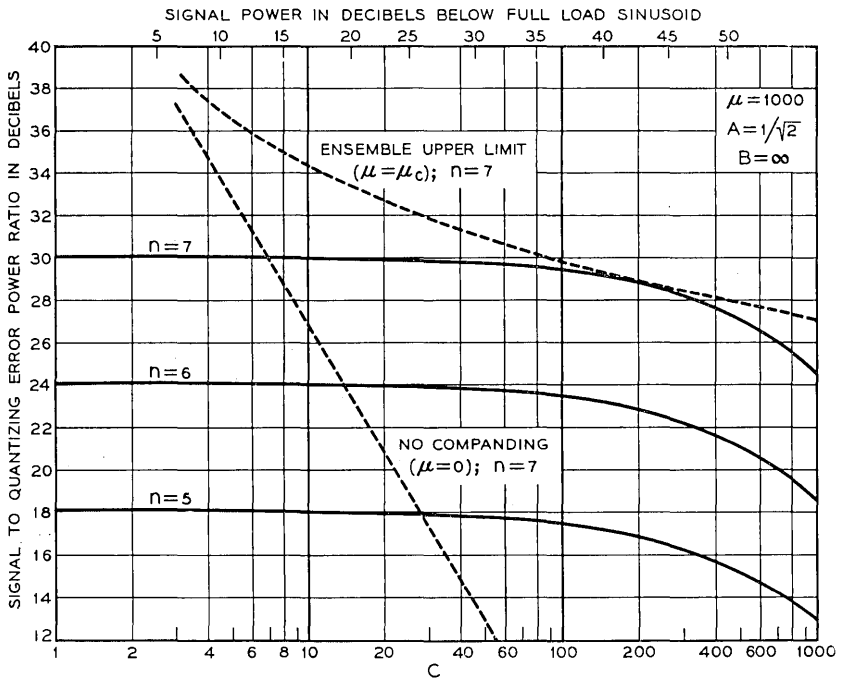

Fig. 18 — Signal to quantizing error power ratios (in db) as a function of relative signal power for companding corresponding to $\mu = 1,000$. Symbols have the same significance as in Fig. 15. $B = \infty$ throughout.
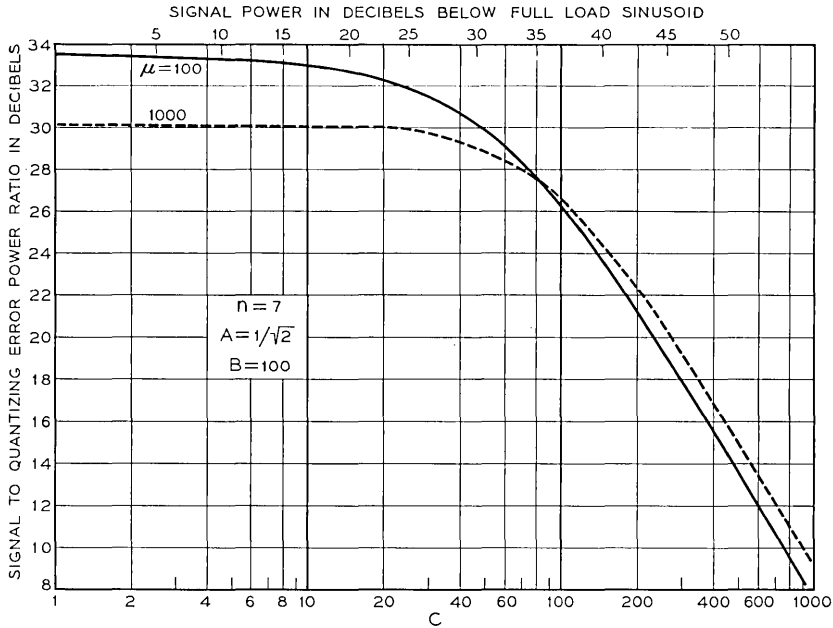
Fig. 19 — Signal to quantizing error power ratios (in db) as a function of relative signal power for companding corresponding to $\mu = 100$ and 1,000 when $n = 7$ digits per code group and a dc component corresponding to $B = 100$ is present in the signal. The influence of the dc component may be judged by comparing these curves with those shown in Figs. 15 and 18 for $n = 7$. Corresponding results for different values of n may be derived by the addition or subtraction of appropriate multiples of 6 db from each ordinate.

of virtually all the anticipated companding improvement for weak signals.

(b) *Background Noise Level.* We have already noted the probable futility of increasing the signal to quantizing error power ratio considerably beyond that value which is subjectively equivalent to the anticipated ratio of signal to background noise from other sources.

If the subjective relation between quantizing error power and noise power were known, the curves in Figs. 15 to 19 could be redrawn for meaningful comparison with ratios of signal to background noise. In the absence of such information, we shall assume as a first approximation, that noise and quantizing error power are directly comparable.*

Suppose that we set an upper limit on the background noise by con-

---

* The similarity between noise and quantizing error power has often been noted. For example, one may consult references 2, 6 and 12 as well as Appendix I on "Noise in PCM Circuits" in Reference 11. The assumption of direct comparability is also to be found in Reference 4.
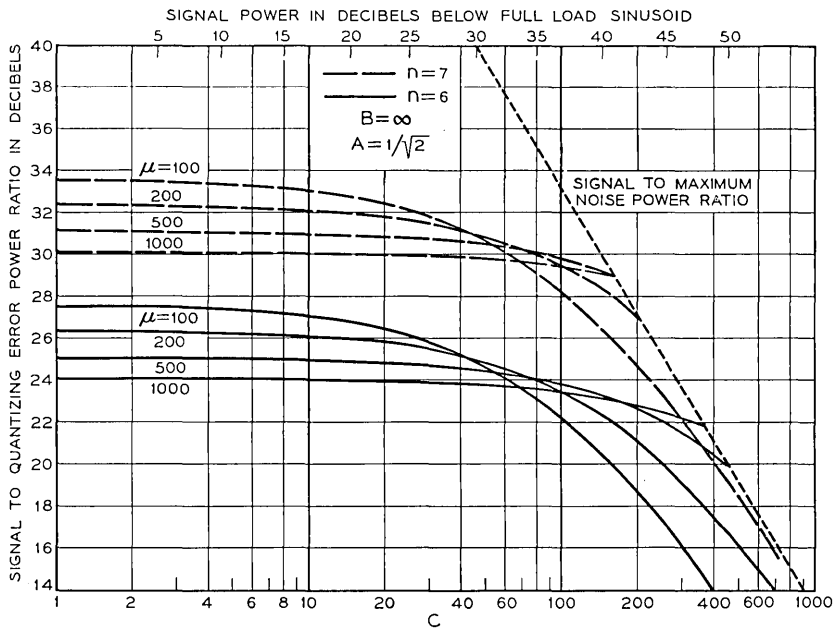
Fig. 20 — Curves illustrating the comparison of signal to quantizing error power ratios with the ratio of signal to background noise. The line representing the signal to maximum noise ratios corresponds to the hypothetical case where the maximum background noise is determined by the requirement that the signal to noise ratio be 20 db for a signal 50 db below full sinusoidal modulation.

sidering a value providing a signal to noise ratio of 20 db for the weakest signals in our hypothetical system. A signal to maximum noise power curve may then be drawn as a function of signal power for this constant value of noise power. Such a graph has been combined, in Fig. 20, with curves such as those which have previously appeared in Figs. 15 to 19. These curves have been terminated at their intersections with the line representing the signal to maximum noise power ratio since we are assuming that little benefit will be derived from a signal to quantizing error power ratio in excess of the signal to maximum noise power ratio.

From Fig. 20 it is apparent that the previous conclusions that six and seven digits are worthy of consideration are unaffected by the stipulation that the signal to quantizing error power ratio should not greatly exceed the signal to maximum noise power ratio. Similarly, the conclusions based on Fig. 19 (for $B = 100$) remain unchanged since the curves therein fall below the maximum noise curve of Fig. 20 for all values of the abscissa.

D. *Possibility of Using Automatic Volume Regulation*

The realization that the quantizing impairment experienced by weak signals in the absence of compression stems from their inability to excite a sufficient number of the quantizing steps which must be provided to accommodate loud signals, leads directly to the suggestion that automatic volume regulation be used to permit all signals to be "loud," i.e., to excite the entire aggregation of quantizing steps. In its simplest form, this would be accomplished by automatic amplification of the long time average speech power in each channel to provide a constant volume input to the common channel equipment.

Study of the present results indicates that if all signals were of constant volume, about 10 to 15 db below full sinusoidal modulation (to provide an adequate peak-clipping margin), satisfactory operation, corresponding to signal to quantizing error power ratios in excess of 20 db, might be achieved *without companding* by using as few as five or six digits per code group. In evaluating this alternative, the advantages of reduction of bandwidth, decreased complexity of quantizing and coding equipment, and elimination of the common channel compandor, must be balanced against the disadvantage of providing separate volume regulators in each channel.

E. *Comparison with Previous Experimental Results*

The literature contains seemingly contradictory statements about whether five,[17] six,[14] or seven[6, 7] digits per code group are required for satisfactory performance in speech listening tests. Evaluation of these conclusions is frequently hampered by the lack of specification of either the degree of companding employed or the range of speech volumes requiring transmission. Different conclusions may therefore be consistent, inasmuch as the systems may differ significantly in the required volume range, degree of companding, size of the "effective dc component" in the signal, and even in the subjective standards used to judge performance.

Fortunately, the description of an experimental toll quality system by Meacham and Peterson[6] is sufficiently detailed to permit some comparison. The range of volumes they considered suggests that direct comparison with our hypothetical system is fairly reasonable. Their empirical choice of seven digits, with a compression characteristic virtually indistinguishable from that corresponding to $\mu = 100$ (see Fig. 4) is in excellent agreement with the present conclusions.

Furthermore, the conclusion that five or six digits, without compand-

ing, might be employed in conjunction with volume regulation is completely consistent with Goodall's experimental results.[10]

VII. CONCLUSIONS

An effective process for choosing the proper combination of the number of digits per code group and companding characteristic for quantized speech communication systems has been formulated. Under typical conditions, the calculated companding improvement *for the weakest signals* proves to be equivalent to the addition of about 4 to 6 digits per code group, i.e., to an increase in the number of quantizing steps by a factor between $2^4 = 16$ and $2^6 = 64$.

Although a precise application of the results requires a more detailed knowledge of the subjective nature of the quantizing impairment of speech than is presently available, the assumption of reasonably typical system requirements yields conclusions in good agreement with existing experimental evidence.

ACKNOWLEDGMENTS

Frequent references in the text attest to the indebtedness of the author to the writings of Bennett and Panter and Dite. It is also a pleasure to acknowledge stimulating conversations on certain aspects of the problem with J. L. Glaser, D. F. Hoth, B. McMillan, and S. O. Rice.

APPENDIX

THE MINIMIZATION OF QUANTIZING ERROR POWER

In spite of the demonstrated utility of the μ-characteristics, one cannot avoid speculating about the possibility of achieving substantially more companding improvement by using a characteristic which differs from (8). We shall therefore outline a study of the actual minimization of quantizing error power without regard to the relative treatment of various amplitudes in the signal. The results will confirm that a significant reduction of the quantizing error power beyond that attainable with logarithmic companding is self-defeating — for it not only imposes the risk of diminished naturalness, but also implies a compandor too "volume-selective" for the applications envisioned herein.

1. The Variational Problem and Its Formal Solution

Equation (6) may be expressed in the form

$$\sigma = \frac{2V^2}{3N^2} \int_0^V (dv/de)^{-2} P(e) \, de \tag{A-1}$$

where $P(e)$ has been assumed to be an even function. The function, $v(e)$, which will minimize $(A\text{-}1)$, subject to the usual boundary conditions at $e = 0$ and $e = V$, may be obtained by solving the Euler differential equation of the variational problem.[28] For $(A\text{-}1)$, this takes the form

$$(dv/de) = KP^{1/3} \qquad\qquad\qquad (A\text{-}2)$$

where the constant K is given by

$$K = V \Big/ \int_0^V P^{1/3}\,de \qquad\qquad (A\text{-}3)$$

Hence the minimum quantizing error is given by

$$\sigma_{\text{MIN}} = 2\left[\int_0^V P^{1/3}\,de\right]^3 \Big/ 3N^2 \qquad (A\text{-}4)^*$$

2. Representation of Speech by an Exponential Distribution of Amplitudes

We shall assume, as in (25), that the distribution of amplitudes in speech at constant volume[18] may be represented by

$$P(e) = G \exp (-\lambda e) \text{ for } e \geqq 0 \qquad (A\text{-}5)$$

where $P(-e) = P(e)$, $G = \lambda/2$, and $\lambda^2 = 2/\overline{e^2}$. With this choice of $P(e)$, the solution of (A-2)† is

$$(v/V) = \frac{1 - \exp\,[(-\sqrt{2}C/3)(e/V)]}{1 - \exp\,(-\sqrt{2}C/3)} \qquad (A\text{-}6)$$

Thus, for any given relative volume (i.e., for each value of $C = V/(\overline{e^2})^{1/2}$), (A-6) specifies the compression characteristic required to minimize the quantizing error power.

We are therefore led to study the properties of the family of characteristics of the form

$$(v/V) = \frac{1 - \exp\,(-me/V)}{1 - \exp\,(-m)} \qquad \text{for} \qquad 0 \leqq e \leqq V \qquad (A\text{-}7)$$

---

* An alternate derivation of (A-2) and (A-4), has been given by Panter and Dite,[5] who also acknowledge a prior and different deduction by P. R. Aigrain. Upon reading a preliminary version of the present manuscript, B. McMillan called my attention to S. P. Lloyd's related, but unpublished work, which proved to contain still another derivation. I am grateful to Dr. Lloyd for access to this material.

† In the vocabulary of analytical dynamics, the direct integrability of the Euler equation may be ascribed to the existence of an "ignorable" or "cyclic" coordinate.[29]

TABLE I—COMPARISON OF THE "μ" AND "m" COMPANDOR ENSEMBLES

Property	μ-Ensemble	m-Ensemble
Defining requirement	Approaches uniform precision in the quantization of all pulse samples outside the unavoidable linear region for small samples	Minimizes quantizing error power for a specific volume, if assume an exponential amplitude distribution for that volume
Compression equation, for $0 \leq e \leq V$, where $v(-e) = -v(e)$	$$\left(\frac{v}{V}\right) = \frac{\log\left(1 + \frac{\mu e}{V}\right)}{\log(1 + \mu)}$$	$$\left(\frac{v}{V}\right) = \frac{1 - \exp(-me/V)}{1 - \exp(-m)}$$
Sample to step size ratio	$\left(\dfrac{e}{\Delta e}\right) = N/2(1 + V/\mu e)\log(1 + \mu)$	$\left(\dfrac{e}{\Delta e}\right) = (N/2M)(me/V)\exp(-me/V)$ where $M = 1 - \exp(-m)$
	$\left(\dfrac{e}{\Delta e}\right) \rightarrow [N/2\log(1 + \mu)](\mu e/V)$ for $(e/V) \ll \mu^{-1}$	$\left(\dfrac{e}{\Delta e}\right) \rightarrow (N/2M)(me/V)$ for $(e/V) \ll m^{-1}$
	$\left(\dfrac{e}{\Delta e}\right) \rightarrow N/2\log(1 + \mu)$ for $(e/V) \gg \mu^{-1}$	$\left(\dfrac{e}{\Delta e}\right) = $ MAX at $(e/V) = m^{-1}$
Ratio of largest to smallest step size = ratio of compression characteristic slopes for zero and overload inputs	$\dfrac{(\Delta e)_{e=V}}{(\Delta e)_{e=0}} = \dfrac{(dv/de)_{e=0}}{(dv/de)_{e=V}} = \mu + 1$	$\dfrac{(\Delta e)_{e=V}}{(\Delta e)_{e=0}} = \dfrac{(dv/de)_{e=0}}{(dv/de)_{e=V}} = \exp(m)$

Saturated companding improvement, corresponding to linear compression of weakest signals	$C \gg \mu: 20 \log_{10} \left[\dfrac{\mu}{\log (1 + \mu)} \right] db$	$C \gg m: 20 \log_{10} \left[\dfrac{m}{1 - \exp(-m)} \right] db$
Relation between relative signal strength and critical compression parameter which provides greatest reduction of quantizing error for a given volume	$C^2 S + \mu_c A C (S - 1) - \mu_c{}^2 = 0$ where $C = V/\sqrt{\overline{e^2}} = $ relative signal strength $S = \left(\dfrac{1 + \mu_c}{\mu_c} \right) \log (1 + \mu_c) - 1$ $A = \overline{|e|}/\sqrt{\overline{e^2}} = $ indep. of volume	$C = 3m_c/\sqrt{2}$
$D^2 = \dfrac{\text{Error Power}}{\text{Signal Power}}$ when $\bar{e} = 0$	$D^2 = \dfrac{[\log (1 + \mu)]^2}{3N^2} \left[1 + \dfrac{C^2}{\mu^2} + \dfrac{2AC}{\mu} \right]$	$D^2 = \dfrac{\sqrt{2} C^3 M^2}{3 N^2 m^2} \left[\dfrac{\exp(2m - \sqrt{2}C) - 1}{2m - \sqrt{2}C} \right]$

with $v(-e) = -v(e)$ as usual. The "m-characteristics" specified by (A-7) are to be compared with the "μ-characteristics" specified by (8).

From the derivation of (A-6) it is known that optimum companding will be produced when m is given by the critical value,

$$m_c = \sqrt{2}C/3 \tag{A-8}$$

This is the analogue of (36) defining μ_c for the μ-ensemble.

3. Properties of the "m-Ensemble"

We shall now interpret the properties of the m-ensemble of compandors, for which the ensemble improvement limit ($m = m_c$) actually
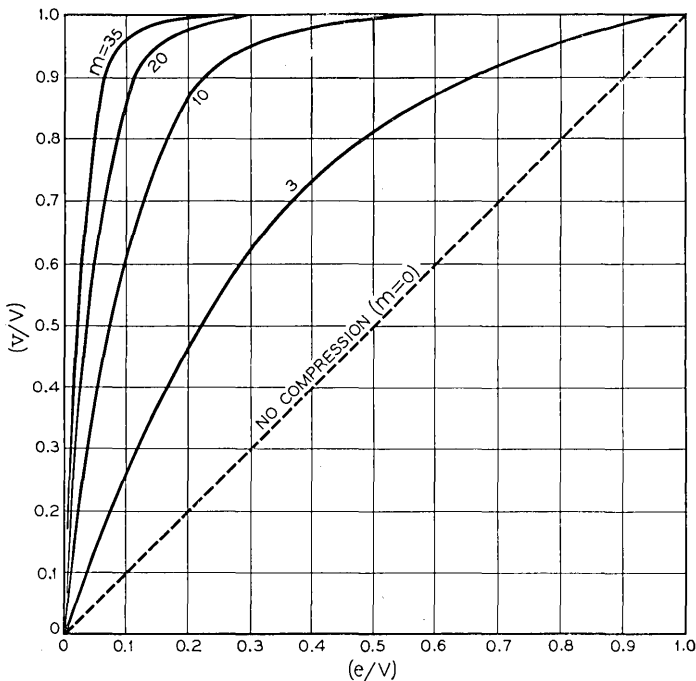

Fig. 21 — Typical m-ensemble compression characteristics determined by equation (A-7). Note the strong emphasis on weak signal amplitudes. These curves may be compared with those for the μ-ensemble in Fig. 3.

minimizes the total quantizing error power, when the probability density is specified by (A-5). Table I summarizes the important properties which may be derived by replacing (8) by (A-7) in the previous detailed analysis of the μ-ensemble.

(a) Compression Characteristics

Compression characteristics, corresponding to various values of m are displayed in Figs. 21 and 22 for direct comparison with the curves in Figs. 3 and 4. The m-characteristics assign very little weight to the larger signal amplitudes in view of the infrequent occurrence of the latter.
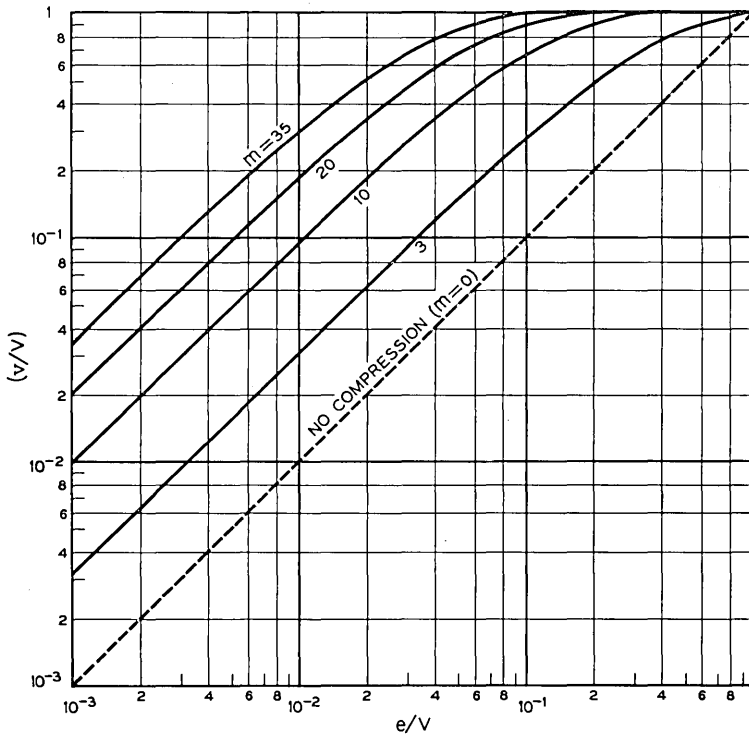

Fig. 22 — Logarithmic replot of compression curves of the type shown in Fig. 21 to indicate detailed behavior for weak samples. These may be compared with the μ-ensemble curves in Fig. 4.

(b) Sample to Step Size Ratio

Fig. 23, where the sample to step size ratio $(e/\Delta e)$ is plotted in the same manner as in Fig. 5, reveals the relative quantizing accuracy accorded various pulse amplitudes.
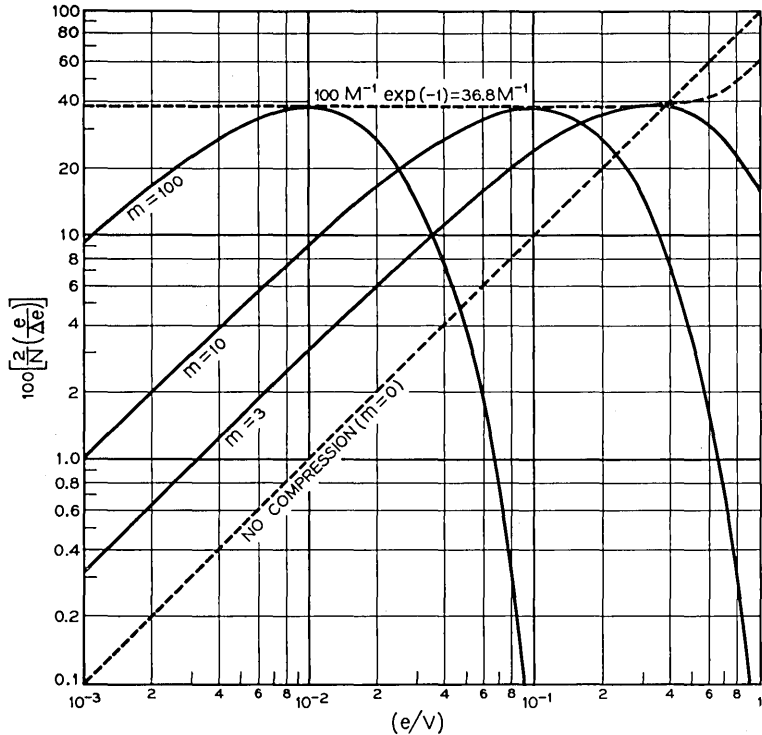

Fig. 23 — Pulse sample to step size ratios as a function of relative sample amplitude, for various compandors in the m-ensemble. The maxima exhibited by these curves occur at $e/V = m^{-1}$; $M = 1 - \exp(-m)$. Compare with Fig. 5.

(c) *Saturated Improvement of Weak Signals*

For signals whose largest samples are confined to the region $(e/V) \ll m^{-1}$, compression is linear, with a saturation improvement noted in Table I and plotted in Fig. 24 for comparison with Fig. 9.
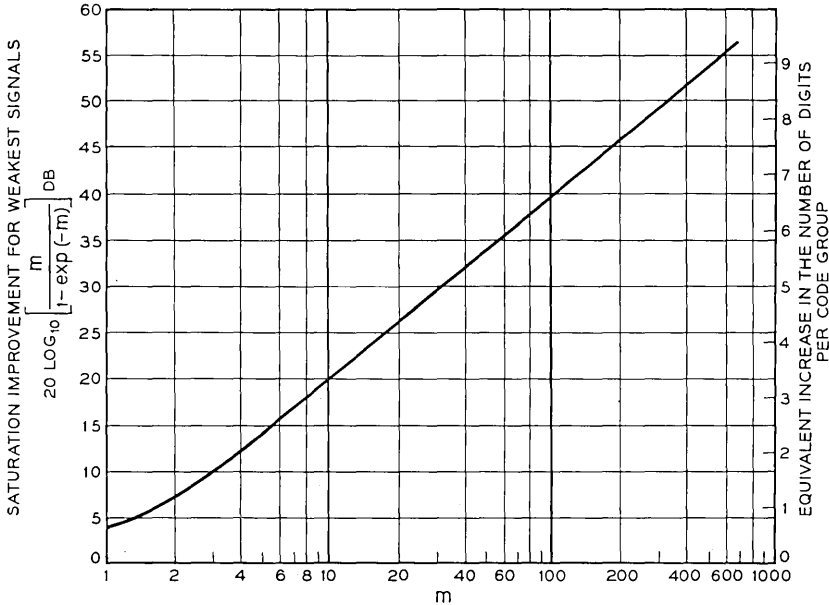
Fig. 24 — Saturated companding improvement for the weakest signals as a function of the degree of "m-type" compression. Given a value of m, the corresponding ordinate represents the reduction of quantizing error power (in db) which results from companding of signals so weak that signal peaks satisfy the relation $(e/V) \ll m^{-1}$. Thus, weaker and weaker signals are required to exploit the added improvement which follows from an increase in m. This curve may be compared with that for the μ-ensemble in Fig. 9.

(d) Variation of Companding Improvement with Volume

Companding improvement curves are shown in Fig. 25 for representative members of the m-ensemble. Each curve is tangent to the ensemble upper limit at the volume for which $m = m_c$. In view of its deduction as the solution of the variational problem, this upper limit actually represents the absolute maximum value of companding improvement for the present choice of $P(e)$.
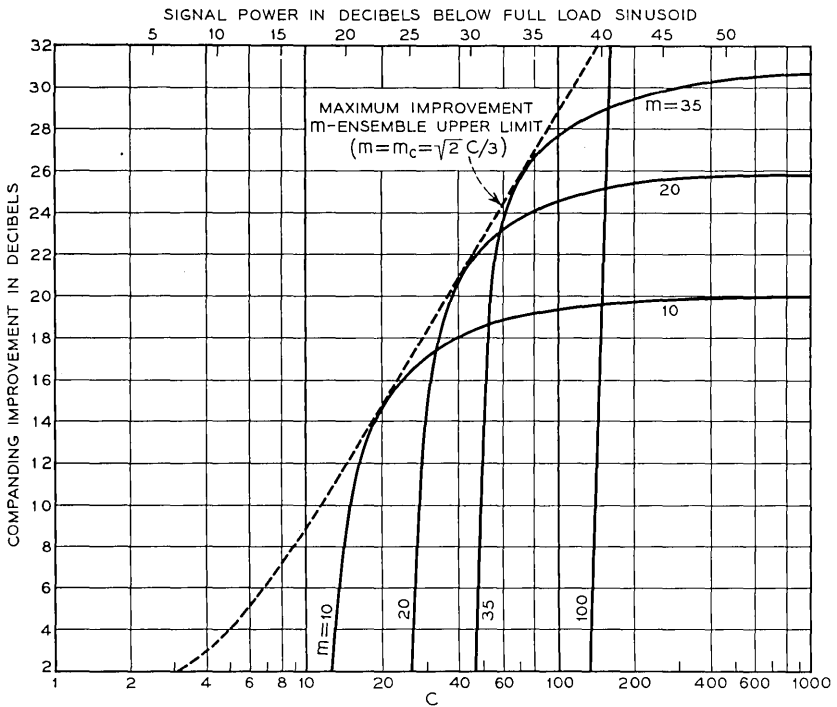

Fig. 25 — Companding improvement curves for representative members of the m-ensemble. These curves are to be compared with those for the μ-ensemble in Fig. 8. Note the important difference between the two ensembles for strong signals (small values of C).

(e) *Signal to Quantizing Error Power Ratios*

The curves in Fig. 26 are drawn for the representative case of $N = 2^7 = 128$ quantizing steps (7 digit PCM). The corresponding ensemble limit is constant, as might be expected from (A-4), except for strong signals where the effects of peak clipping become noticeable.

In the region where this ensemble limit is constant, departures from the improvement limit resulting from the use of a single value of m for all volumes may be read directly from the ordinates shown at the right in Fig. 26. In comparing these departures from maximum improvement with the analogous μ-ensemble curves in Fig. 14, it must always be recalled that, in view of its role in the solution of the variational problem, the m-ensemble limit represents the actual minimum quantizing error power consistent with the probability density specified by (A-5).
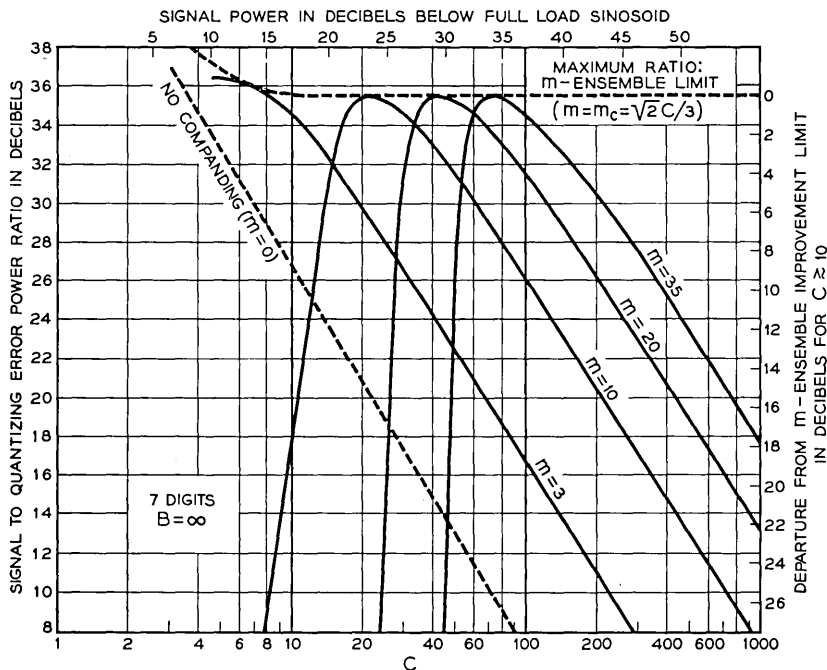
Fig. 26 — Signal to quantizing error power ratios as a function of relative signal power for 7 digits and various m-compandors. The curves may be compared with those for 7 digits in Figs. 15 to 18. The auxiliary ordinates at the right of the present figure apply for $C \gtrsim 10$, where the m-ensemble limit is effectively constant; departures from this limit, resulting from the use of a single value of m for all volumes, may be read directly from this scale, for comparison with Fig. 14. The latter comparison illustrates the narrow volume limitation of the members of the m-ensemble.

(f) Illustrative Application

Consider the possibility of choosing a member of the m-ensemble for application to the hypothetical PCM system already discussed in connection with the μ-ensemble. It will be recalled (see Figs. 15–18) that we were able to choose degrees of logarithmic compression which would yield signal to quantizing error power ratios in excess of about 20 db for all volumes ($4.5 \lesssim C \lesssim 450$) by using as few as six or seven (depending on the choice of μ) digits per code group. In contrast, Fig. 26 reveals that no value of m will meet this requirement since the curves fall so rapidly on either side of the sharp maxima. In short, the members of the m-ensemble are each too specialized for successful application to such a broad volume range.

Further detailed comparison between the numerical results for the two ensembles seems inappropriate, since it is not at all clear that the inequitable treatment of the various samples in a given signal by members of the m-ensemble (see Fig. 23) permits an adequate description of signal quality solely in terms of quantizing error power. Under these circumstances, subjective effects beyond the scope of the present analysis might assume a dominant role.

REFERENCES

1. H. S. Black, Modulation Theory, Van Nostrand, N. Y., 1953.
2. W. R. Bennett, Spectra of Quantized Signals, B.S.T.J., **27**, pp. 446–472, July, 1948.
3. Oliver, Pierce and Shannon, The Philosophy of PCM, Proc. I.R.E., **36**, pp. 1324–1331, Nov., 1948.
4. Clavier, Panter and Dite, Signal-to-Noise-Ratio Improvement in a PCM System, Proc. I.R.E., **37**, pp. 355–359, April, 1949.
5. P. F. Panter and W. Dite, Quantization Distortion in Pulse-Count Modulation with Nonuniform Spacing of Levels, Proc. I.R.E., **39**, pp. 44–48, Jan., 1951.
6. L. A. Meacham and E. Peterson, An Experimental Multichannel Pulse Code Modulation System of Toll Quality, B.S.T.J., **27**, pp. 1–43, Jan., 1948.
7. H. S. Black and J. O. Edson, Pulse Code Modulation, Trans. A.I.E.E., **66**, pp. 895–899, 1947.
8. Clavier, Panter and Grieg, Distortion in a Pulse Count Modulation System, Elec. Eng., **66**, pp. 1110–1122, 1947.
9. J. P. Schouten and H. W. F. Van' T. Groenewout, Analysis of Distortion in Pulse Code Modulation Systems, Applied Scientific Research, **2B**, pp. 277–290, 1952.
10. W. M. Goodall, Telephony by Pulse Code Modulation, B.S.T.J., **26**, pp. 395–409, July, 1947.
11. C. B. Feldman and W. R. Bennett, Bandwidth and Transmission Performance, B.S.T.J., **28**, pp. 490–595, July, 1949.
12. W. R. Bennett, Sources and Properties of Electrical Noise, Elec. Eng., **73**, pp. 1001–1008, Nov., 1954.
13. C. Villars, Étude sur la Modulation par Impulsions Codées, Bulletin Technique PTT, pp. 449–472, 1954.
14. J. Boisvieux, Le Multiplex à 16 Voies à Modulation Codée de la C.F.T.H., L'Onde Electrique, **34**, pp. 363–371, Apr., 1954.

15. E. Kettel, Der Störabstand bei der Nachrichtenübertragung durch Codemodu-
    lation, Archiv der Elektrischen Übertragung, **3,** pp. 161–164, Jan., 1949.
16. H. Holzwarth, Pulsecodemodulation und ihre Verzerrungen bei logarith-
    mischer Amplitudenquantelung, Archiv der Elektrischen Übertragung, **3,**
    pp. 277–285, Jan., 1949.
17. Herreng, Blondé and Dureau, Système de Transmission Téléphonique Multi-
    plex à Modulation par Impulsions Codées, Cables & Transmission, **9,** pp.
    144–160, April, 1955.
18. W. B. Davenport, Jr., An Experimental Study of Speech-Wave Probability
    Distributions, J. Acous. Soc. Amer., **24,** pp. 390–399, July, 1952.
19. S. B. Wright, Amplitude Range Control, B.S.T.J., **17,** pp. 520–538, Oct., 1938.
20. Carter, Dickieson and Mitchell, Application of Compandors to Telephone
    Circuits, Trans. A.I.E.E., **65,** pp. 1079–1086, Dec., 1946.
21. J. C. R. Licklider and I. Pollack, Effects of Differentiation, Integration and
    Infinite Peak Clipping upon the Intelligibility of Speech, J. Acous. Soc.
    Amer., **20,** pp. 42–51, Jan., 1948.
22. D. W. Martin, Uniform Speech-Peak Clipping in a Uniform Signal to Noise
    Spectrum Ratio, J. Acous. Soc. Amer., **22,** pp. 614–621, Sept., 1950.
23. J. C. R. Licklider, The Intelligibility of Amplitude-Dichotomized, Time-
    Quantized Speech Waves, J. Acous. Soc. Amer., **22,** pp. 820–823, Nov., 1950.
24. H. Cramér, Mathematical Methods of Statistics, Princeton Univ. Press,
    Princeton, N. J., 1946, see pp. 359–363.
25. T. C. Fry, Probability and its Engineering Uses, Van Nostrand, N. Y., 1928,
    see pp. 310–312.
26. A. C. Aitken, Statistical Mathematics, Interscience Pub. Inc., N. Y., 3d
    Ed., 1944, see pp. 44–47.
27. W. F. Sheppard, On the Calculation of the Most Probable Values of Frequency-
    Constants for Data Arranged According to Equidistant Divisions of a Scale,
    Proc. London Math. Soc., **29,** pp. 353–380, 1898.
28. R. Courant and D. Hilbert, Methods of Mathematical Physics, Vol. 1, Inter-
    science Pub. Inc., N. Y., English Ed., 1953, see Chapt. IV, especially pp.
    184–187, and p. 206.
29. E. T. Whittaker, A Treatise on the Analytical Dynamics of Particles and
    Rigid Bodies, Cambridge Univ. Press, 4th Ed., 1937, see p. 54.

W. D. Bulloch Appointed Editor of B.S.T.J.

W. D. Bulloch, formerly Editor of the Bell Laboratories Record, has been appointed Editor of the Bell System Technical Journal.

Mr. Bulloch received a bachelor's degree from Dartmouth College and a Master of Science degree in Physics from the University of North Carolina. He taught physics, mathematics and astronomy in the latter institution for several years before joining the staff of Bell Telephone Laboratories.

An Electrically Operated Hydraulic Control Valve

By J. W. SCHAEFER

(Manuscript received August 3, 1956)

The electrohydraulic transducer used in the servos that drive the control surfaces of the NIKE missile is described and its operating characteristics are discussed. Special attention is directed to the secondary dynamic forces that exist in a high-gain device of this type and to the resulting tendency to oscillate. The application of the valve to a servo system is discussed briefly.
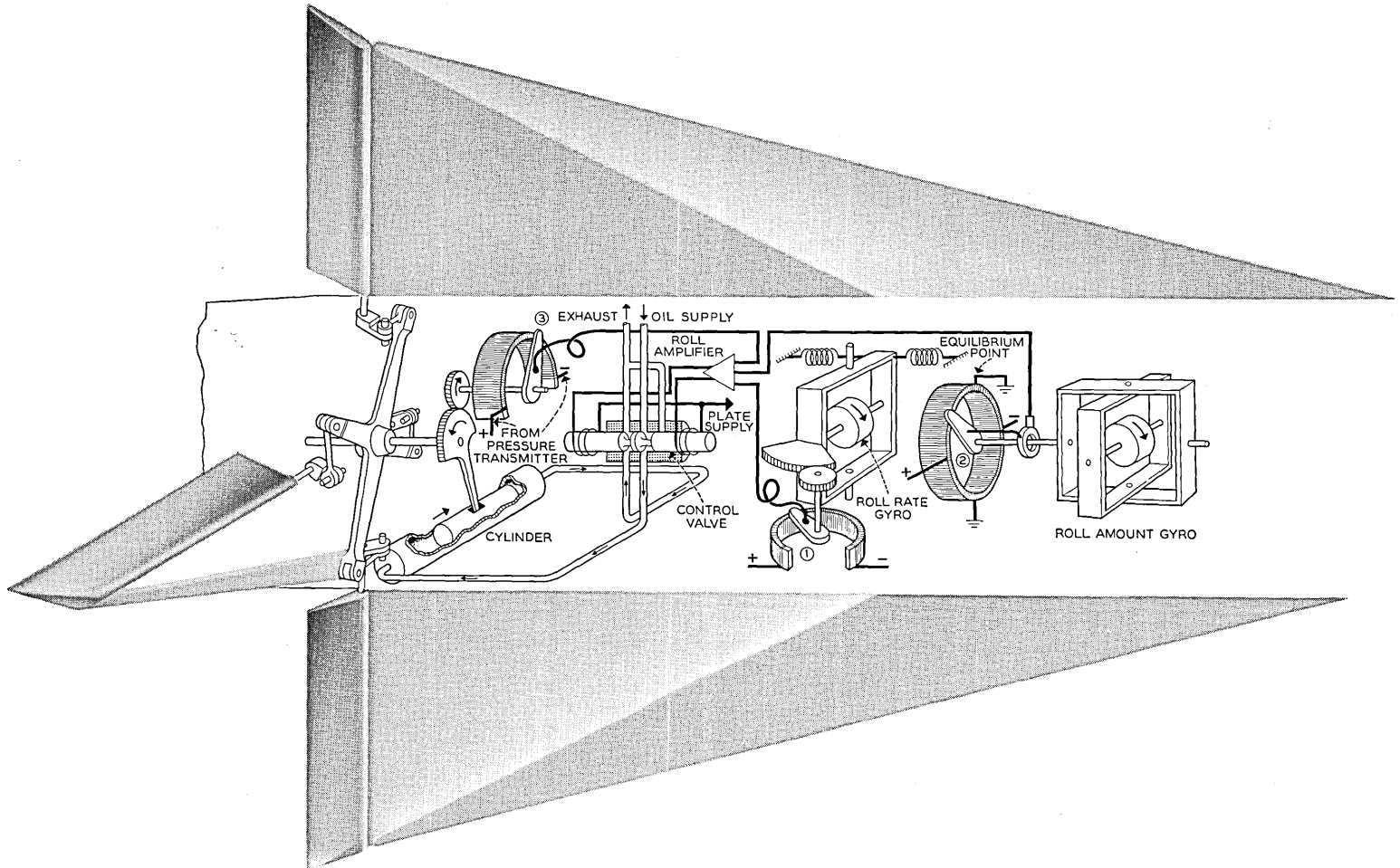
INTRODUCTION

Early in the study of the NIKE guided missile project, it became apparent that the requirements for the fin actuators could not be fulfilled by the servo-mechanisms available at that time (1945). All existing types failed to meet the combined requirements of small size, light weight, high torque, and rapid response. Further investigation showed that the development of a hydraulic servo employing an electrohydraulic transducer appeared to provide a promising solution. A control system of this type, therefore, has been developed for the NIKE missile.

The design of the transducer, or control valve, was one of the principal problems in the development of the missile control systems and is the subject of this article. The specific design of the valve that will be discussed here is known as "Model J-7", and represents the state of the development in 1950. Valves of this type, with varying degrees of modification, are used in missiles of several other projects.

APPLICATION

Fig. 1 is a simplified schematic of the roll positioning system in the NIKE missile. It is the simplest of the three applications of the valve in the missile, but will serve to illustrate the situation in which the valve operates. The purpose of the roll servo is to keep the missile in a predictable roll orientation.

③ EXHAUST ↑ ↓ OIL SUPPLY

ROLL AMPLIFIER

EQUILIBRIUM POINT

+ FROM PRESSURE TRANSMITTER

PLATE SUPPLY

CONTROL VALVE

CYLINDER

ROLL RATE GYRO

②

ROLL AMOUNT GYRO

+ ① −

712

The roll system's reference is an "Amount Gyro," which is a free-free gyro oriented on the ground prior to missile launch. The brush of a four-tap potentiometer (Item 2 in Fig. 1) is connected to the outer gimbal and provides a dc signal whose sign and magnitude indicate the roll position with respect to the stable equilibrium point. This signal is the principal input to the servo amplifier that drives the valve.

A roll-position error exists in the situation illustrated in Fig. 1. The valve is driven in the direction to cause the oil flow to rotate the ailerons, which in turn will roll the missile toward the null position. As the missile rolls, the winding of the roll-amount potentiometer rotates with it. The brush stays fixed in space with the gyro gimbal.

The aerodynamic coupling between the aileron position and the missile's roll position is a complex and variable term in the feedback loop of the servo. The nature of the aerodynamic coupling is such that an otherwise simple servo problem becomes considerably more complicated. During a normal flight the aerodynamic stiffness, and hence the gain in the feedback loop, varies over a 50:1 range. A first order correction for this change is accomplished by a variable gain local loop around the valve, cylinder and amplifier. A potentiometer (Item 3 in Fig. 1) is geared to the fin in such a way that a dc signal is produced, which is proportional to fin position. The gain of this local loop is varied by supplying the potentiometer with voltages that are directly proportional to the measured aerodynamic stiffness. In this way the amount of the deflection of the aileron is made inversely proportional to the aerodynamic stiffness. This effect results in an approximately constant torque about the roll axis of the missile for a given signal. The local loop around the fin position also reduces the effect of any non-linear characteristics of the valve.

A third input to the servo amplifier is provided by a potentiometer that is driven by a spring-restrained gyroscope mounted so that the sensitive axis is aligned with the missile's roll axis. The dc signal produced is proportional to the roll rate. This signal provides some anticipation to the roll position loop. It performs the function of a tachometer in a conventional servo. It also insures that the roll rate is limited to a value that can be handled by the position loop. If very high roll rates were allowed to exist, the roll amount gyro would produce a signal changing in sign at such a rate that the ailerons would be unable to keep up or reduce the rate.

The roll servo insures that the missile's orientation is aligned with the free-free gyro. This enables the yaw and pitch servos to steer about their assigned axes in a consistent manner. The two steering servos are
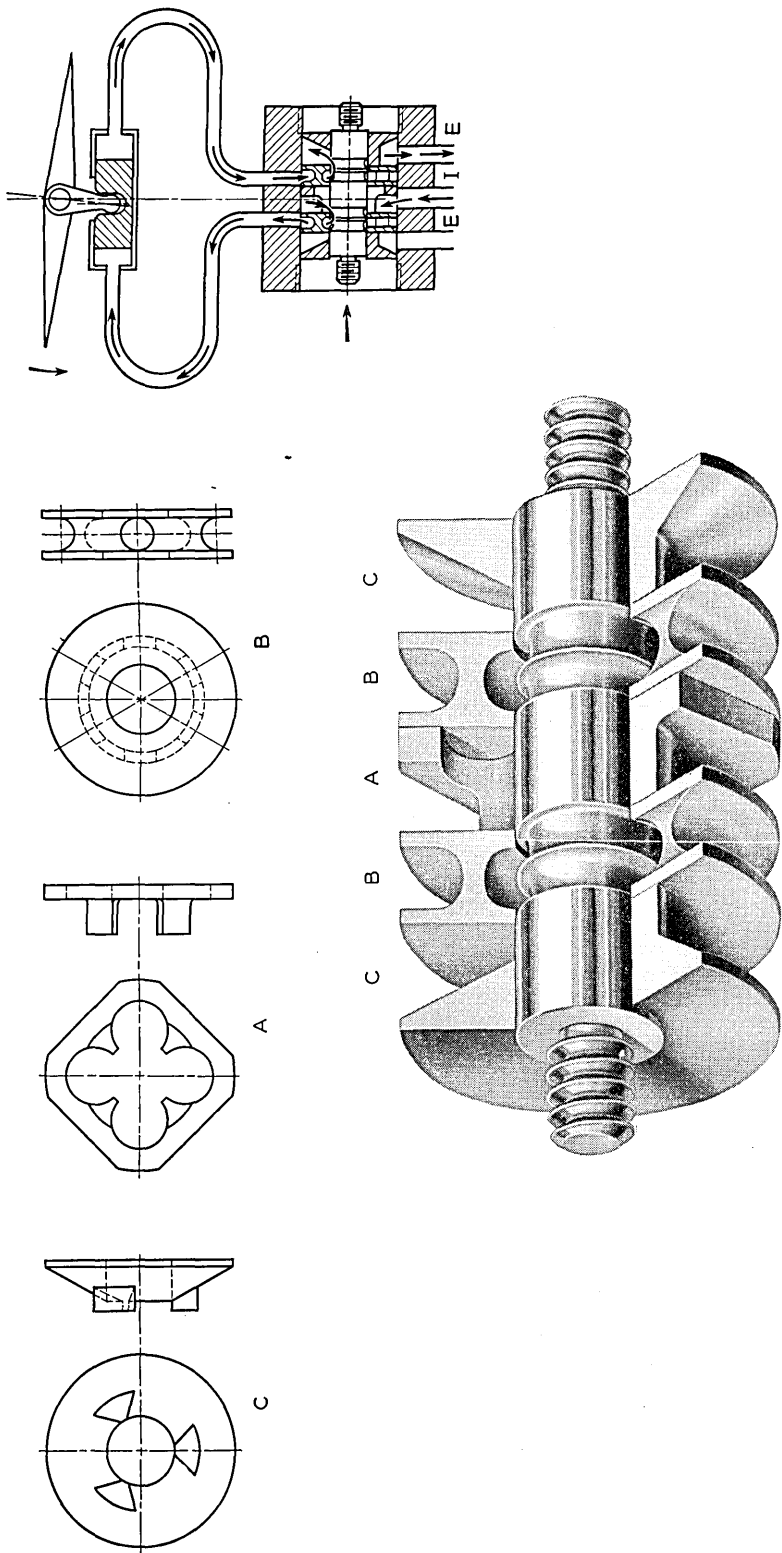
Fig. 2 — Porting arrangement, J-7 solenoid valve.

identical to each other and somewhat similar to the roll system described above. Each of the three systems employs identical valves.

GENERAL DESCRIPTION

Basically, the J-7 valve is a conventional four-way type. Fig. 2 illustrates the porting arrangement. The parts in sections A, B and C are inserts that are shrunk-fit into the valve body. The plunger accurately fits the holes in the inserts, so that oil cannot flow between the plunger and inserts except where the diameter of the plunger is reduced. The annular space around the outside of the center insert is connected to the high pressure oil supply. The radial passages in this insert (part A) carry the oil to its internal cusps. With the plunger centrally located its center land completely covers the port formed by the cusps and no oil flows. With the plunger moved to the right the oil is carried to the cylinder and back to the exhaust in the manner illustrated by the small sketch in the upper right corner. If the motion of the plunger is to the left, a similar performance occurs but the piston and fin are driven in the opposite direction. To illustrate the construction of the inserts, detail sketches are also shown at the top of Fig. 2.

The inserts and the plunger are made of hardened steel. Fig. 3 show- their location in the complete valve. The thickness of the inserts, hence the longitudinal location of the ports, is held to an extremely close tolerance by lapping their parallel faces. Their outside diameter is accurately ground so that a tight seal will occur between the various passages when they are shrunk fit into the internal bore of the body. After assembly, the internal bore formed by the holes in the various inserts is lapped to a straight and accurate cylindrical shape. This process is controlled to provide a diametral clearance of 0.0002 inch on an interchangeable basis. The plunger must slide freely in the bore in spite of the small clearances involved. The longitudinal location of the lands on the plunger must be controlled to a high degree for reasons that will become apparent.

Those parts shown in Fig. 2 are not sectioned in Fig. 3. The valve proper is clamped between two manifolds (O and P); these are moved apart in the picture to better illustrate the internal construction. The brazed laminated manifolds provide the mounting means for the valve and also serve to connect the multiple outlets of the valve body to standard hydraulic fittings for external connections. The manifolds are designed to adapt the valve to a specific application. In this way, different plumbing arrangements can be utilized without changes in the valve proper. The manifold, O, has fittings to connect to the cylinder,
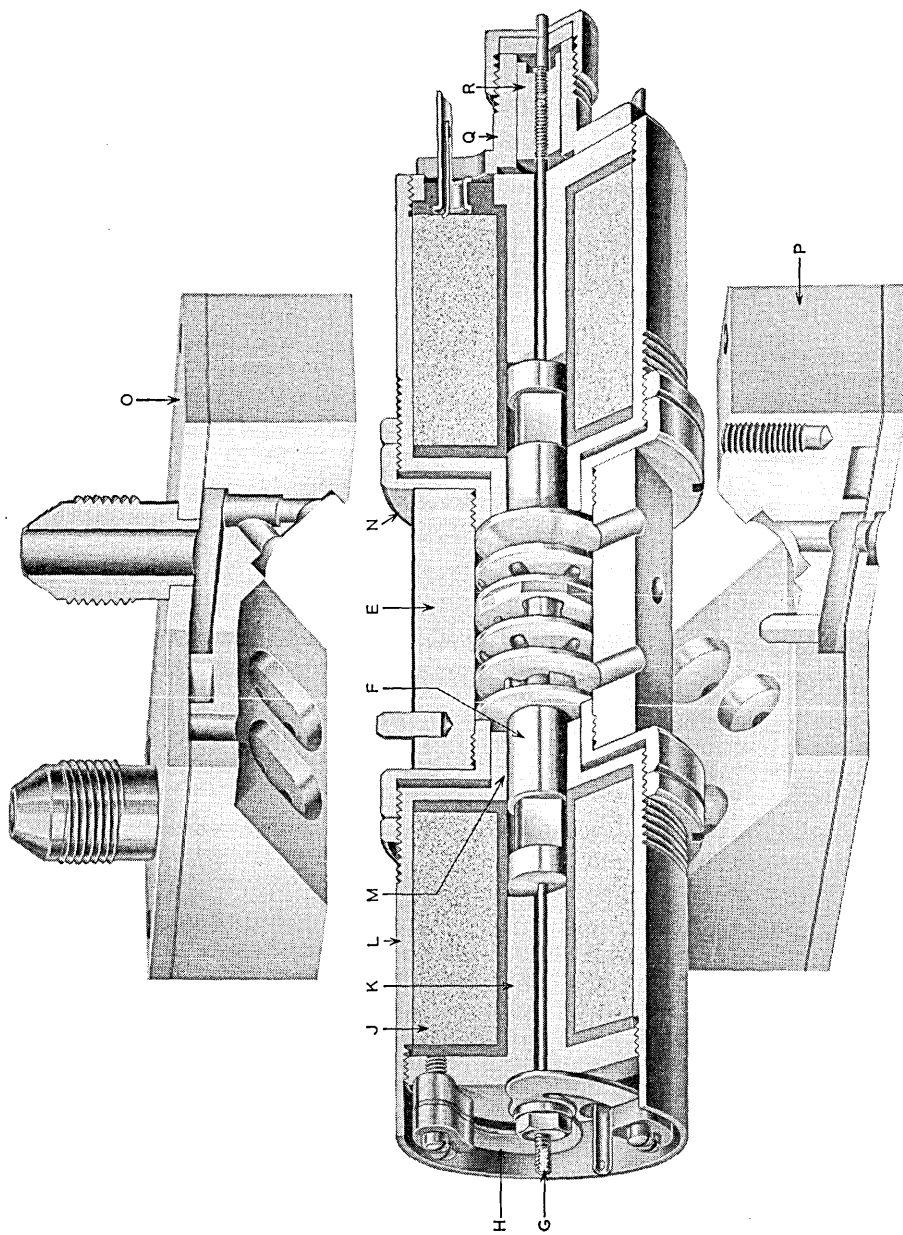
Fig. 3 — Cutaway section, J-7 solenoid valve.
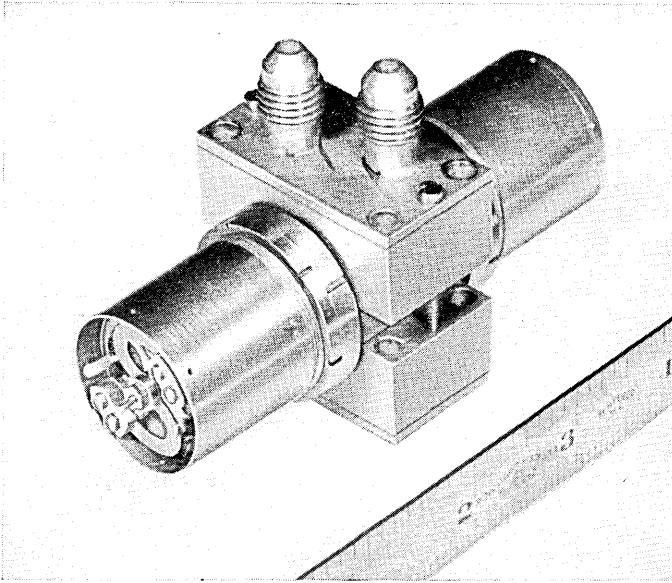
Fig. 4 — J-7 solenoid valve with manifolds.

and the lower manifold, P, serves to connect the pressure and exhaust lines to ports in the structure to which the valve is mounted. The joints between the passages in the manifolds and those in the body are sealed by rubber "O" rings that are inserted in the recesses about the holes on the inner faces of the manifolds. These recesses can be seen in Fig. 3, but the "O" rings are not illustrated. Similarly, "O" rings are used to seal the joints between the manifold, P, and the flat surface to which it mounts.

A pole piece, F, is screwed to each end of the plunger by means of the threads visible in Fig. 2. These parts move as an assembly and form
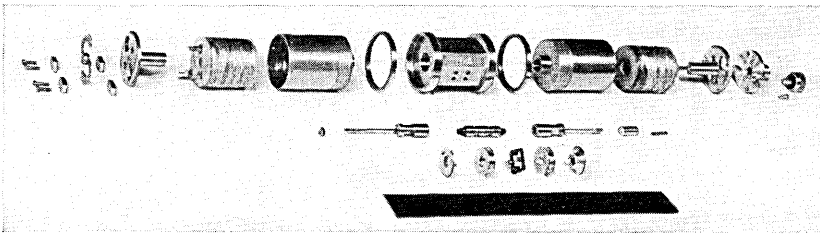
Fig. 5 — Exploded view of J-7 solenoid valve.
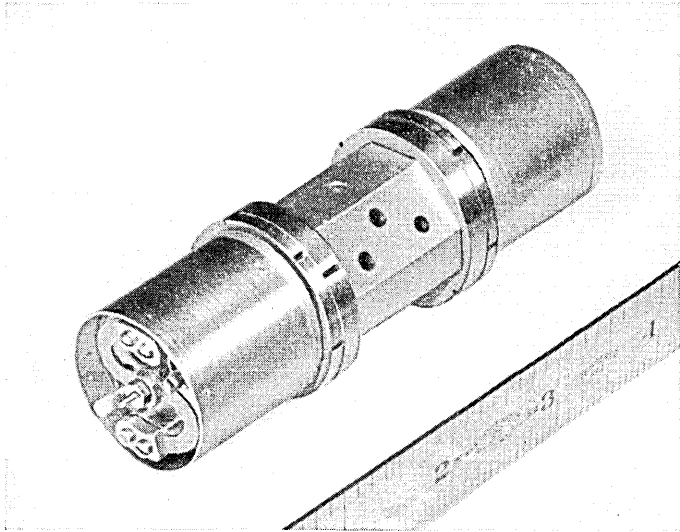
Fig. 6 — J-7 solenoid valve.

the armature of the valve. The push rod, G, attached to the armature, is connected to an S shaped spring, H, which tends to keep the movable assembly centered, or the valve closed.

When a current passes through the coil, J, magnetic flux passes through the fixed pole piece, K, through the coil housing, L, then across the small annular air gap, M, to the moving pole piece, F, and across the air gap between the pole faces near the center of the coil. Flux in the latter gap causes a force on the armature which tends to pull it and the valve
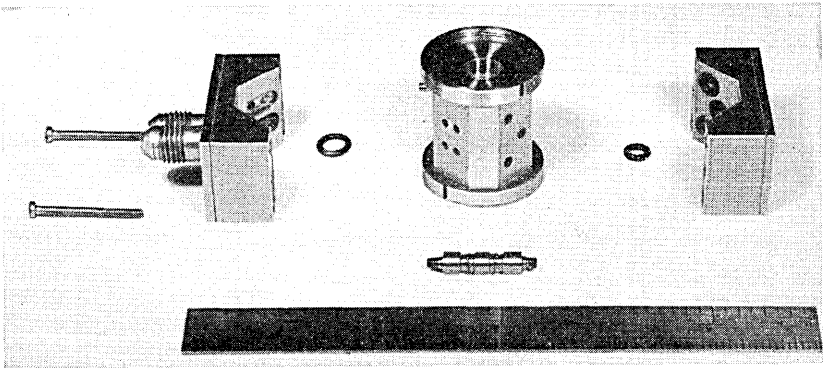
Fig. 7 — Hydraulic parts of the J-7 valve.

plunger toward that coil. If an equal current is flowing in the other coil the forces are balanced and the valve remains centered and closed. If the currents in the two coils are not equal, the valve plunger is moved until the differential magnetic force is balanced by the force in the spring. In this manner the amount of oil flow can be regulated by varying the difference of the currents in the two coils.

The coil housing is attached to the valve body by means of a non-magnetic stainless steel adapter, N. The adapter isolates the steel plunger and inserts from the magnetic flux. Because of the close fit between these parts the presence of flux would cause sticking. A push rod attached to the armature drives an aluminum piston, R, in a cylinder, Q. The small radial clearance between these parts is filled with a viscous fluid so that a damping force is produced that is proportional to armature velocity.

Fig. 4 shows the complete assembly with manifolds attached, while Fig. 5 gives an exploded view of the valve proper with all details in their correct relative positions. Other views of the valve parts are shown in Figs. 6 and 7. Fig. 8 is a view looking into the bore of the hydraulic assembly. This is the hole that is normally occupied by the plunger. The ports formed by the internal shapes of the inserts are clearly visible.

CHARACTERISTICS OF THE ACTUATING MECHANISM

The J-7 valve is designed to be driven by a push-pull dc amplifier. When the amplifier has no input signal, the output current in each side is 10 ma. When a signal is applied, the current in one side is increased and that in the other is decreased; at maximum signal, the current in one coil reaches 19 ma and zero in the other. The dissipation in each coil for quiescent current is about 0.4 watt, and the full signal power is 1.5 watts.

The requirements that the frequency response must extend to dc and that the control power consumption be held to a minimum suggest the use of a dc push-pull output stage. The quiescent dc plate current is used as the magnetizing current for the solenoids instead of providing the field by a permanent magnet or separate coil. In spite of the small output current available from the amplifier, relatively large forces and a high resonant frequency are realized. This is accomplished by an efficient magnetic circuit and low armature mass. The opposing solenoid configuration described makes these features possible.

The magnetic circuit used in the J-7 valve has very low reluctance for a sliding armature type actuator. This low reluctance is accomplished by providing ample thickness in the iron parts and employing
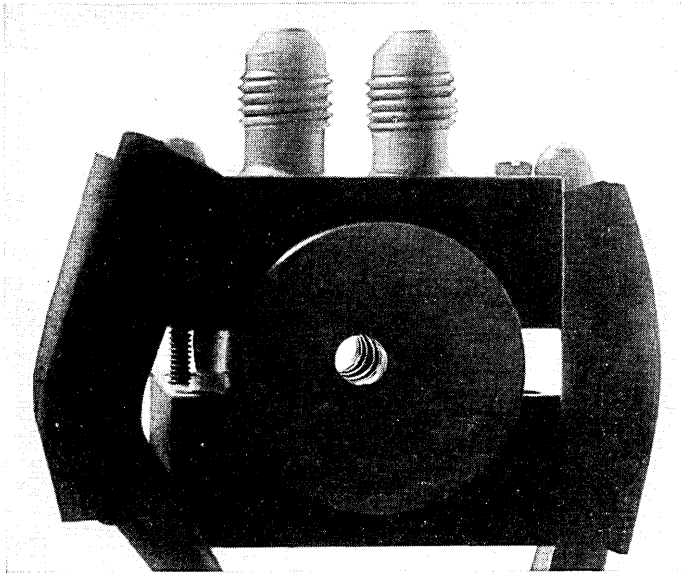
Fig. 8 — Internal view of the J-7 valve body.

very short gaps of considerable cross-sectional areas. It has been shown elsewhere[1, 2] that if the distribution of reluctance of the magnetic structure is symmetrical along its longitudinal axis, minimum leakage flux and hence maximum force would be developed if the working gap were at the exact center of the coil. To a close approximation, the valve solenoids are symmetrical in this manner. The references show that the maximum pull is not sensitive to small changes from the optimum location of the working gap. The gap in the J-7 valve is displaced toward the center of the valve from the location of maximum pull. The slight reduction in magnetic force was accepted as a suitable compromise for the resulting reduction in the mass of the moving pole piece and the corresponding increase in resonant frequency.

The gap between the solenoid pole faces is 0.014 inch when there is no signal and the valve is centered. The two fixed faces have 0.004 inch non-magnetic shims attached so that the maximum motion of the armature is limited to ±0.010 inch. The shims prevent the armature from sticking against the fixed faces by maintaining appreciable gaps. To further compensate for the inverse square law of magnetic attraction, the moving pole pieces have a reduced section that saturates under high flux or large forces. This neck can be seen plainly in Fig. 3. The saturating

sections limit the flux and tend to reduce the pull for short gaps so that the centering spring can be a simple linear member and still not lose control when the armature is near the fixed pole face. The flat surfaces on the neck permit the use of wrenches for assembly. Placing the necks on the moving pole pieces further reduces the mass of the armature assembly.

To illustrate the saturation action, Fig. 9 shows the pull of one of the magnets plotted against gap length for quiescent and maximum current. The shim line and curves from a solenoid without a saturation neck also
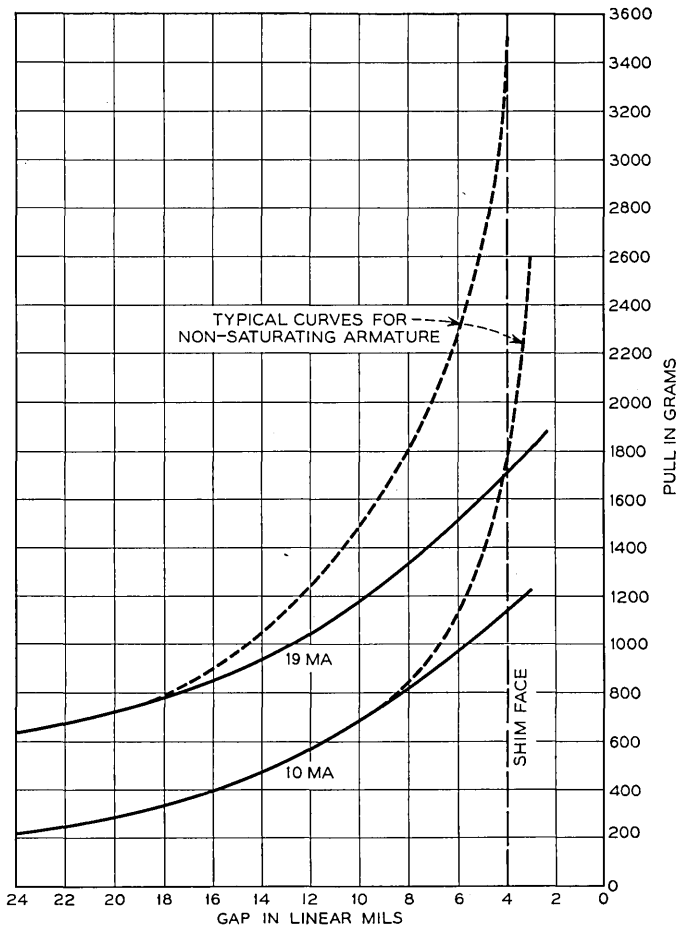
Fig. 9 — Magnetic pull curves for a coil of the J-7 valve.
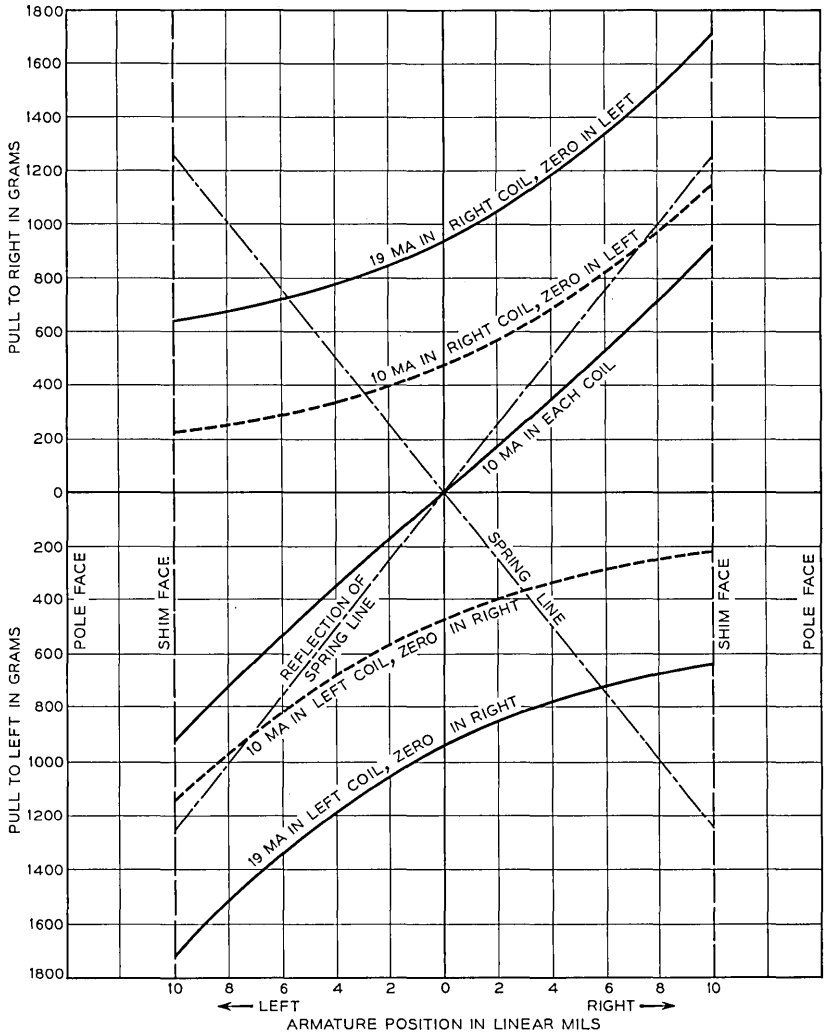
Fig. 10 — Spring and magnetic forces on armature of J-7 valve.

are shown to illustrate the need for these restrictive measures. The need is better appreciated when Fig. 10 is examined. This graph shows the differential pull of the two coils plotted against armature movement for extreme signals and for the balanced condition. There is also a line representing the spring force and one representing its reflection. The latter permits direct comparison of the magnitude of the opposing magnetic and spring forces.

It is important that the spring be able to center the valve when the coil currents are balanced. This means that the stiffness of the spring must be greater in magnitude than the negative stiffness created by the magnetic fields when 10 ma is flowing in each coil. On the other hand, the 19-ma current should be able to pull the armature against the pole piece and therefore must produce more force than the spring. If the shim and saturation limiting were not used it would be impossible to find a straight spring line that would fulfill both these requirements; i.e., its reflection would be between these curves without crossing either of them. The family of curves representing the net magnetic forces for the various intermediate values of current unbalance fall between the extreme cases shown. The intersection of one of these curves and the reflection of the spring line is the position which the armature will assume for that particular coil current. The reason for the relatively large margin of force shown for the 19-ma wide-open condition will be explained later.

Fig. 11 is plotted to show the net forces on the armature. The curves are the difference between the spring line and the two magnetic pull curves of Fig. 10. It can be seen that the forces are such as to cause the armature to move to the center in the balanced condition. In the case of maximum signal, it will move all the way to the shim stop in the direction of the coil which is carrying the current.

When there is no magnetic field present the armature resonance is about 320 cps. When measured statically, or at very low frequencies, with the coils energized, the negative stiffness of the field greatly reduces the effective stiffness of the spring, as seen in Fig. 11. However, when the valve is driven experimentally to find resonance, it occurs near 320 cps. This apparent increase in stiffness with frequency results from eddy currents that retard the change in flux to the extent that the negative stiffness virtually disappears. Eddy currents reduce the effective inductance of the coils from about 40 henries at very low frequency to less than 10 henries at 600 cps.

It is difficult to locate the resonance experimentally because of the large amount of damping provided by the extremely thin oil film between the plunger and the inserts. High resonance frequency of the valve is desired so that it is safely above any frequency encountered in the servo operation, thereby eliminating one consideration in the equalization. Also, a high resonance means that missile acceleration along the valve axis causes little displacement of the unbalanced mass of the armature.

A 250 cps differential dither voltage is superimposed on the push-pull dc signal to overcome the effects of static friction. The resulting 1 ma differential current produces a magnetic force about equal to that re-
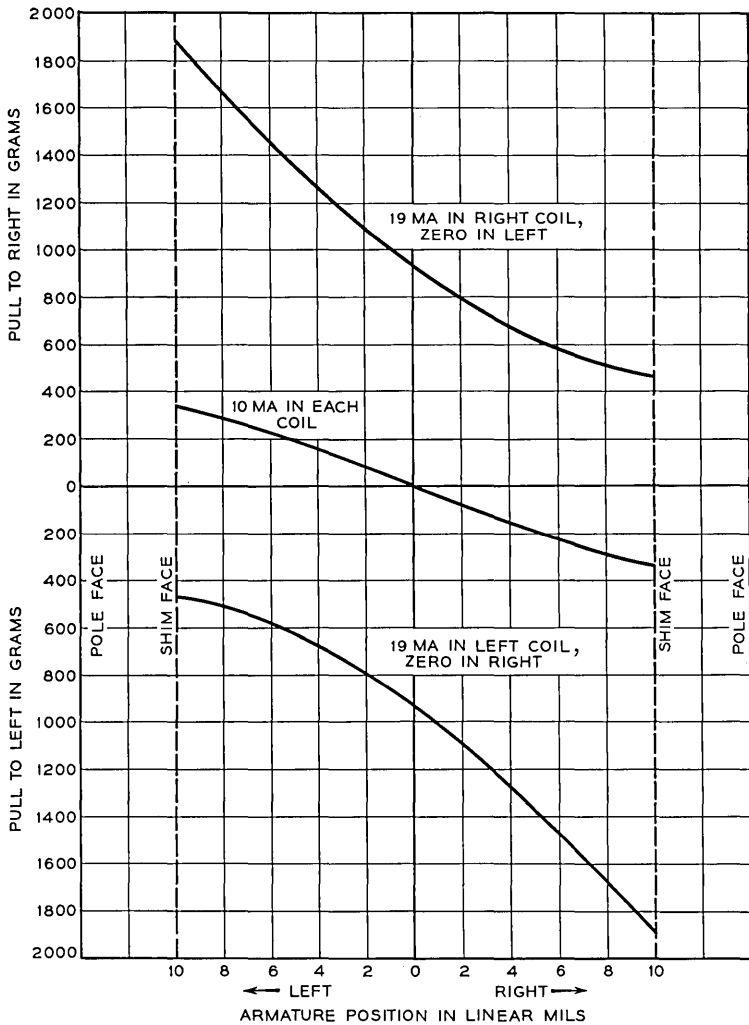
Fig. 11 — Resultant forces on armature of J-7 valve.

quired to move the armature in breaking the friction of the stationary armature assembly. Thus, the signal threshold is reduced by the amount of the dither current and the resulting increase in sensitivity to small signals greatly reduces the phase lags at low amplitude.

STEADY STATE HYDRAULIC CHARACTERISTICS

The J-7 valve is designed to operate from an oil supply having a pressure of 2,000 psi, which is somewhat higher than early valves of this

type. The increase in working pressure is a great advantage for a guided missile application because it results in lower weight, higher gain, and faster response. For example, doubling the pressure permits actuating cylinders of one half the size, an oil reservoir of one half the volume, and an increase in both response and gain by a factor of about three. Such features are sufficiently attractive to be worth a great deal of development effort. However, reliable and stable operation can be achieved under these high-gain conditions only if parasitic forces are kept extremely small.

It was found that the relation between pressure drop and flow is not so simple as one might expect from a sharp-edged, orifice-type control. For large openings of the control orifice, the pressure losses in the fixed orifices and passages of the valve body become an important factor. The following law is an adequate representation of pressure-flow characteristics:

$$p = 10q + \left(2 + \frac{455}{x^2}\right) q^2 \tag{1}$$

where

$$p = \text{pressure drop, psi}$$

$$q = \text{rate of flow, cu in/sec}$$

$$x = \text{valve opening, linear mils}$$

This equation was derived from test data from a model valve. These data confirmed a computational analysis of the hydraulic circuit. Fig. 12 graphically illustrates the equation. It is a plot of flow against valve position for various pressure drops. It will be noted that there is 0.001 inch difference between valve position and valve opening because of this amount of overlap at the ports.

Equation (1) provides the information necessary to compute the maximum output power of the valve. If all the pressure drop were across the control orifices, all the pressure would be utilized to accelerate the oil at this point and only the square term of (1) would exist. If this were the case, the maximum output power would occur when the pressure drop across the valve was one-third of the supply pressure. The other two-thirds of the pressure would be used to produce work in the cylinder. If laminar flow existed throughout the valve the square term would drop out, leaving a linear equation. If this were the case, maximum power would occur with the total pressure equally divided between valve and load. When both the linear the square terms are present, maximum power will occur when the pressure drop across the valve is somewhere
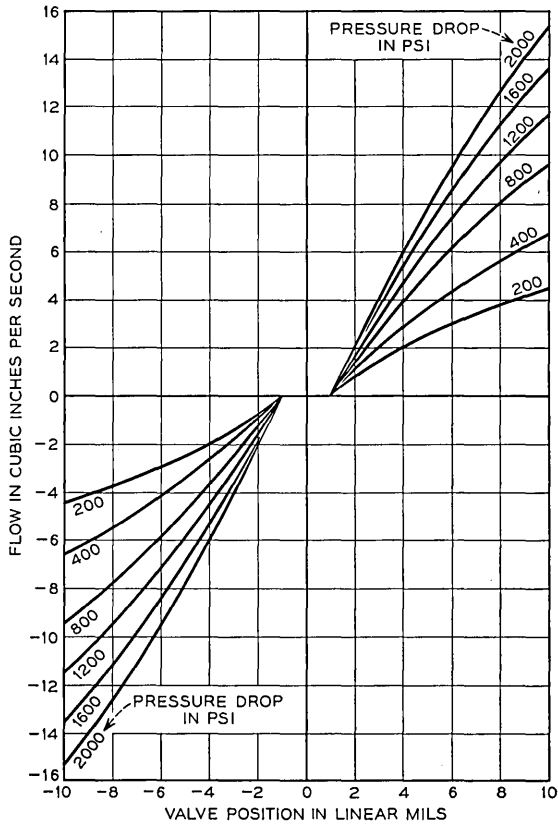
Fig. 12 — Flow characteristics of J-7 valve.

between one-third and one-half the supply pressure. The exact point is dependent on the magnitude of the supply pressure as well as the coefficients in the equation.

The valve will be wide open, an opening of 0.009 inch, when maximum power is produced. In this situation, (1) becomes:

$$p = 10q + 7.6q^2 \tag{2}$$

Useful output power at the load is the product of the flow rate and the pressure exerted on the piston.

$$\dot{W} = (P - p)q \tag{3}$$

where

$$\dot{W} = \text{Output power}$$

$$P = \text{Supply pressure, psi}$$

Therefore

$$\dot{W} = Pq - 10q^2 - 7.6q^3$$

This expression can be differentiated and equated to zero to find the point of maximum power.

$$\frac{d\dot{W}}{dq} = P - 20q - 22.8q^2 = 0 \tag{4}$$

$$q = \sqrt{0.192 + 0.0439P} - 0.439$$

Substituting for q in equation (2) we find that for maximum power

$$p = 0.333\,P + \sqrt{2.15 + 0.49P} - 1.46 \tag{5}$$

The normal supply pressure for the J-7 valve is 2,000 psi. Substituting this value for P in (4) and (5)

$$q = 8.95 \text{ cu in/sec}$$

and

$$p = 696 \text{ psi}$$

When these values are substituted in (3), we find

$$\dot{W} \text{ max} = 11,700 \text{ in lb/sec}$$

$$= 1.77 \text{ horsepower}$$

Examination of the above equations will show that if the valve is used with a very low supply pressure, the linear term in (1) is dominant. In this case the maximum power output occurs when the pressure drop is nearly one-half the supply pressure. In the case of a very high supply pressure, the squared term is dominant and maximum power occurs when the pressure drop across the valve approaches one-third the supply pressure.

The ratio between the electrical quiescent input power to the coils and the maximum hydraulic out power is about 1,600, or a power gain of 32 db. Based on maximum signal the gain is 29 db. All forces must be precisely balanced and tolerances on parts be carefully controlled in order to realize this amount of gain in a single stage mechanical device.

DYNAMIC HYDRAULIC EFFECTS

Examination of the illustrations of the valve will show that it is statically balanced; i.e., pressure on any of the ports does not tend to translate the plunger. However, the flow of oil through a valve of this type produces a force on the plunger which tends to close the ports or

center the armature. This force creates a stiffness that adds to the effect of the mechanical centering spring. The magnitude of the force is quite nonlinear, it varies with pressure drop, and hence, with load as well as with armature displacement. Such variations tend to upset the stability of the servo loop in which the valve is used.

Fig. 13 is a simplified drawing of a valve which can be used to explain the dynamic effect. It will be noted that when the valve plunger is displaced in either direction, the fluid flow is metered by two control orifices in series. The oil flows from oil supply, through the valve body, into a groove in the plunger via the first of the two orifices. The second
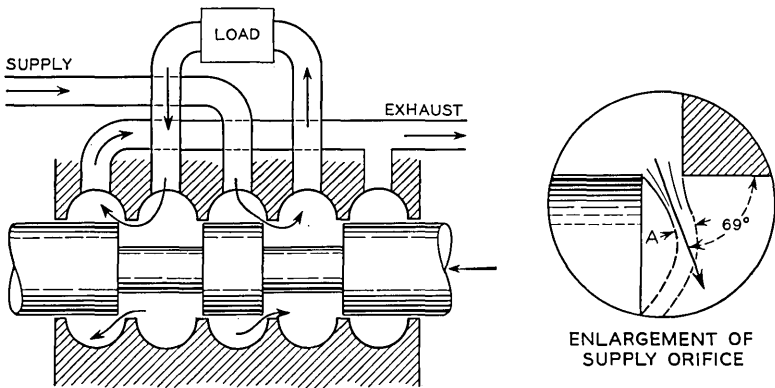
Fig. 13 — Simple valve with rectangular lands.

orifice meters the flow from the other groove in the plunger into the exhaust part of the valve body. Most of the pressure drop in the valve appears across the two orifices and is equally divided between them. The maximum fluid velocity occurs immediately downstream from the orifices at the vena contracta of the jet. This point is labeled "A" in the enlarged insert on Fig. 13. The velocity at this point can be computed by use of Bernoulli's Theorem. In the case of the J-7 valve, where the valve opening is small compared to other passage dimensions, many of the terms of the equation that formulates this theorem can be neglected. In this way the equation becomes

$$h = \frac{V^2}{2g} \tag{6}$$

$$V = \sqrt{2gh} \tag{7}$$

where

V = fluid velocity at the vena contracta, ft/sec

h = pressure drop across orifice, feet

g = acceleration of gravity, ft/sec^2

Von Mises[2] has shown that the departure angle of the jet from a small orifice, such as in the configuration shown in Fig. 13, is 69° from the longitudinal axis. Tests made with an orifice, shaped like those in a simple valve, showed that the jet continues at this angle for a short distance only. Further downstream the jet turns to hug the radial surface on the plunger. This action is depicted by the dotted lines in the insert on Fig. 13. Bernoulli's equation explains that pressure is exchanged for velocity. The low pressure within the jet stream pulls it toward the nearest wall of the cavity. The flow of oil over this surface reduces the pressure on that wall and unbalances the distribution of forces on the surface of the annular grooves in the plunger. The area of reduced pressure causes a net longitudinal force in the direction to center the plunger or close the valve.

Examination of the situation around the exhaust orifice shows that a similar action will occur, but will not result in a comparable force on the plunger. The area of high velocity lies along a surface in the valve body rather than acting on the plunger. The velocity upstream from the orifice is not localized and hence produces forces that are small with respect to those downstream. The fact that the exhaust port forces on the plunger are small compared to those of the intake was confirmed by tests.*

There is a small time lag between the opening of the ports and the dynamic centering force which is proportional to the rate of change of oil flow. This lag results from the fact that finite time is required to change the velocity of the oil mass in the system. At high frequencies, the delay results in a considerable phase lag between the plunger position and the dynamic force. This delay means that fluid velocity, and hence the force, is higher during the quarter cycle in which the valve is closing than it is during the quarter cycle in which the valve is opening.

---

* Considerable work has been conducted on valve theory and design elsewhere since the J-7 valve was developed. Reference 4 is an excellent example of a thorough analysis of valve dynamics with an approach to the problem from a different viewpoint. This reference reports on tests and theories which show the secondary forces from the exhaust and intake orifices to be equal. This is in direct contradiction to the experience with the J-7 valve and remains as an unresolved problem in the mind of the writer.

Therefore, more energy is exerted on accelerating the mass of the plunger during the closing operation than is absorbed in slowing the mass during the opening phase. If the net gain in momentum is larger than can be absorbed by the viscous damping of the oil film in the lapped fit, oscillation[5] will occur. In the case of the J-7 this oscillation tended to occur at slightly over 400 cps.

The Bernoulli force described above was recognized and measured early in the development of this series of valves, but was considered unimportant due to the high stiffness and large damping inherent in the design. The experimental models and the early production models showed no indication of oscillation. Later in the production program, the lapped clearances were increased and high ambient temperatures at the missile test locations were encountered. These two factors combined to reduce the damping, due to the working fluid, to the point where hydraulic oscillation occurred. An external damper was added to alleviate this problem. The damper consisted of an aluminum piston closely fitted to an aluminum cylinder. A viscous fluid (polyisobutylene) between these two parts provided sufficient damping to stabilize operation. This fluid also has the advantage of a relatively small decrease in viscosity with temperature. This type of damper is illustrated on the valve in Fig. 3. (Subsequent improvement in the internal design of the valve reduced the dynamic effect to the point where the need for the external damper has been eliminated.)

Fig. 14 shows a compensated intake orifice configuration corresponding to the insert picture on Fig. 13. It represents the first attempt to balance the dynamic or Bernoulli force. The depth of the annular groove
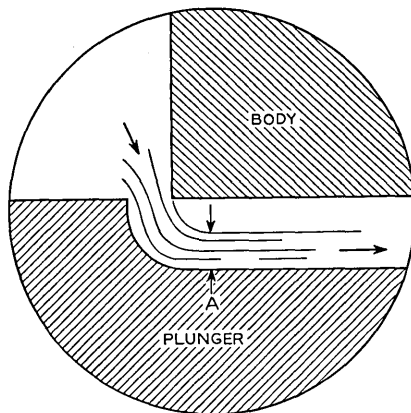

Fig. 14 — A compensated valve orifice.

in the plunger is reduced and a curved surface added to direct the flow parallel to the valve axis. This configuration reduces the dynamic force for two reasons. First, the amount of radial surface exposed to the low pressure is greatly reduced. Second, the curved surface acts much like a turbine blade in deflecting the oil stream and developing a reaction thrust that opposes the Bernoulli force. The reaction thrust increases as the longitudinal component of the high-velocity jet is increased. If the jet can be turned to become parallel with the longitudinal axis without appreciable loss in velocity, the maximum reaction thrust is obtained. In this case, the force is equal to the increase in the longitudinal component of momentum over the conditions of the free jet as shown in Fig. 13.

$$F = \frac{\rho q V}{g} \left(1 - \cos 69°\right) \tag{8}$$

where

F = force, lb

ρ = fluid density, lb/cu in

q = flow rate, cu in/sec

V = fluid velocity, ft/sec

g = acceleration of gravity, ft/sec^2

Calculations of the dynamic forces in accordance with the above reasoning yield only approximate results because the local velocities and their gradients are functions of passage shape as well as pressure drops. The contour of the plunger grooves were computed for use in the first experimental model, whose design was intended to alleviate this problem. Refinements to the initial model were made by cut-and-try methods. Since the forces involved are relatively small, and their magnitude changes so rapidly with plunger position, specialized measuring instruments had to be developed whose sensitivity was high and compliance very low.

A certain amount of contradiction was apparent in the force measurements made. To better understand the action of the oil within the valve, a transparent replica of the cross section of a valve port was used under a microscope. Figs. 15, 16, and 17 are illustrations of typical tests. Fig. 15 is two views of an early type valve with rectangular ports at different openings and pressure drops. The arrows indicate a portion of the cylindrical sliding surface separating the plunger and body. The lower left shadow is the sharp corner at the edge of the annulus in the plunger.
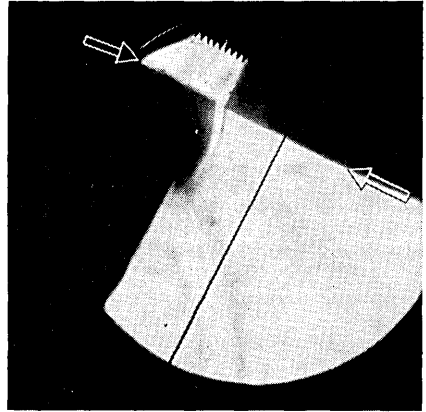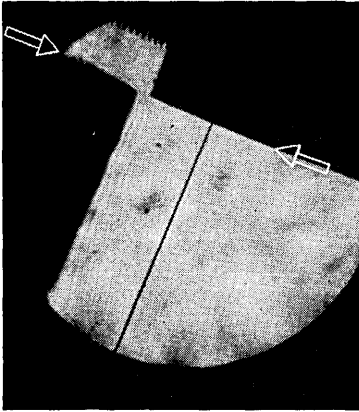
Fig. 15 — Oil flow through simple port.
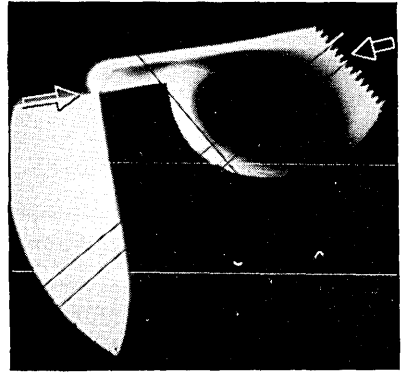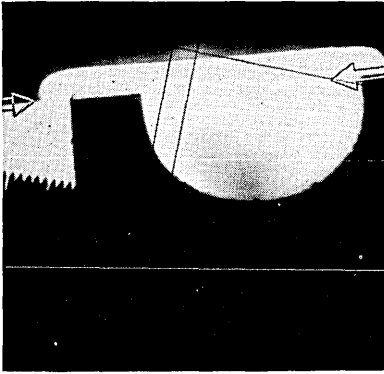
Fig. 16 — Flow through port with decreased Bernoulli effect.
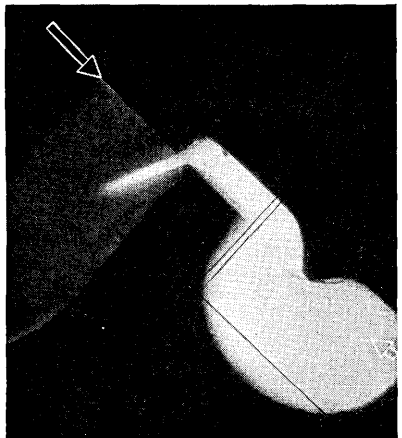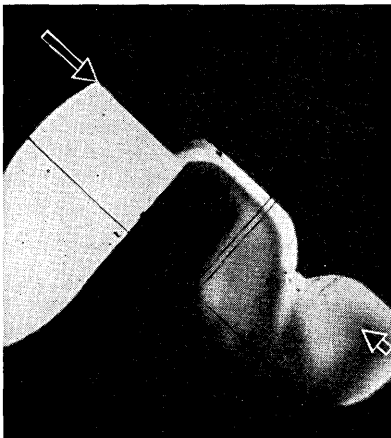
Fig. 17 — Flow through port with decreased Bernoulli effect and increased flow.

The lower light area is oil in the annular groove of the plunger. The oil is flowing from top to bottom. It will be noted that the flow on the downstream side of the orifice hugs the radial surface of the plunger, as discussed above and depicted in Fig. 13. The crosshair and the comb-like scale are a part of the microscope.

Fig. 16 shows two views of a subsequent trial model quite similar to that shown in Fig. 14. Here, the bottom shadow is the insert and the top is the plunger. The flow is from bottom left to top right. This particular design reduced the Bernoulli force but resulted in a serious reduction in flow. This reduction was caused by the large cavitation bubble visible in the right view. This bubble was the result of rapid rotation of oil in the chamber. It prevented the orderly release of the oil through the internal passage to the actuating cylinder (not visible in pictures).

Fig. 17 shows a trial model similar to the J-7. The left illustration
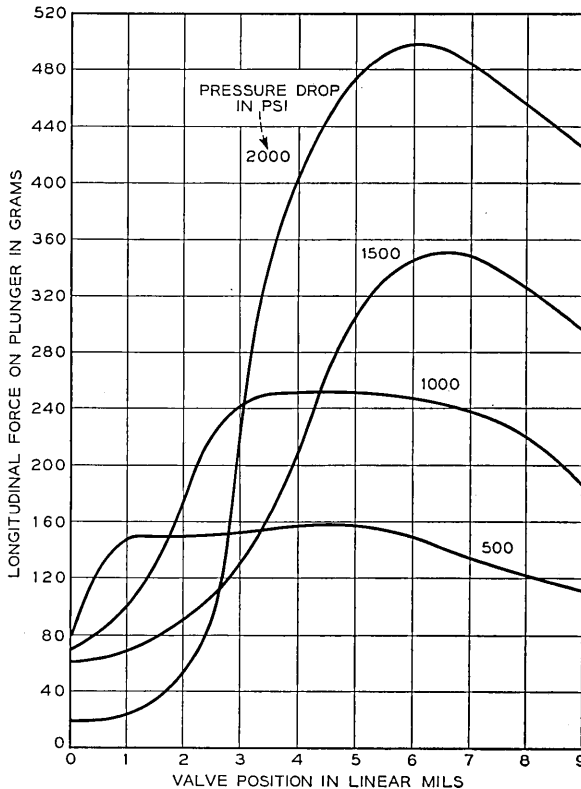
Fig. 18 — Force on plunger of J-7 valve due to Bernoulli effect.

shows the oil flowing from left to right and simulates the intake port of the valve. The extra land on the plunger directs the oil stream toward the escape passage to reduce turbulence and cavitation and increase oil flow. The right illustration illustrates the reverse flow of oil, right to left, and represents the exhaust port of the valve.

Fig. 18 is a plot of the measured Bernoulli force on the J-7 valve. It will be noted that there is little relation between the curves for various pressure drops. No simple equation has been formulated to account for the forces observed. Although Fig. 18 shows the Bernoulli force to be large, Fig. 11 shows that full signal produces enough net force on the armature to overcome this force at any valve position.

A large part of the development effort on the J-7 model was expended on the problem of reducing the forces caused by oil flow. For the same flow conditions, the J-7 has about one-fifth the Bernoulli force of earlier designs with simple rectangular grooves in the plunger.

Subsequent to the initial manufacture of the J-7 valve, the design of the annular grooves and body inserts has been improved continually. Consequently, the Bernoulli force has been further reduced to permit higher operating pressure, and hence more gain, without creating a hydraulic oscillation problem.

THE J-7 VALVE AS A SERVO ELEMENT

For any given set of operating conditions, the transfer function (expressed as cubic inches of oil flow per milliampere of control current unbalance per lb per square inch of pressure drop) can be extracted from the information presented above. However, the resulting family of curves for various load torques would be of little use to the servo designer. The pressure drop available for use by the valve is different for each curve, and they are all quite nonlinear, as is apparent from the data.

The overlap of the valve ports results in another type of nonlinearity that complicates the loop equalization problem. Examination of Fig. 12 will show that the effect of the overlap is a small dead area in the region of zero output of the valve. Small signal levels will cause the valve armature to operate in and around the vicinity of the dead zone, resulting in very little oil flow. Thus, the gain of the valve for very small signals is lower than for signals of greater magnitude.

As mentioned earlier, the effect of the nonlinearities of the valve is greatly reduced by use of the relatively fast-acting local loop which encompasses the valve, actuating cylinder, and amplifier. This inner, or secondary, loop contains sufficient gain to insure that, in spite of the

nonlinearities, the fin position is controlled in strict accordance with the summation of the input signals applied to the amplifier.

The first design of the servo circuits was made by using the slopes and magnitudes of typical and extreme points of operation as obtained from Figs. 11 and 12. The design of the servo equalization networks was obtained by successive refinements made during actual tests of the complete servo systems. These tests were performed with the aid of rather elaborate simulators that subjected the systems to the conditions of actual flight.

The characteristics of the valve and the amplifier which drives it, as applied to a servomechanism, can best be illustrated by plotting gain and phase shift versus frequency in an open loop. Fig. 19 is such a graph. This information was gathered by applying an input signal to the servo amplifier from an oscillator. The valve was driven by the amplifier in the usual manner. The valve controlled the flow of oil to a piston which operated a load that was equivalent to a typical aerodynamic load as seen by the control surface. The voltage from the fin-position potentiometer was compared to the amplifier input. Fig. 19 shows the phase and amplitude comparison of these two voltages. A small amount of feedback was used to prevent the piston from drifting to one end of the cylinder.
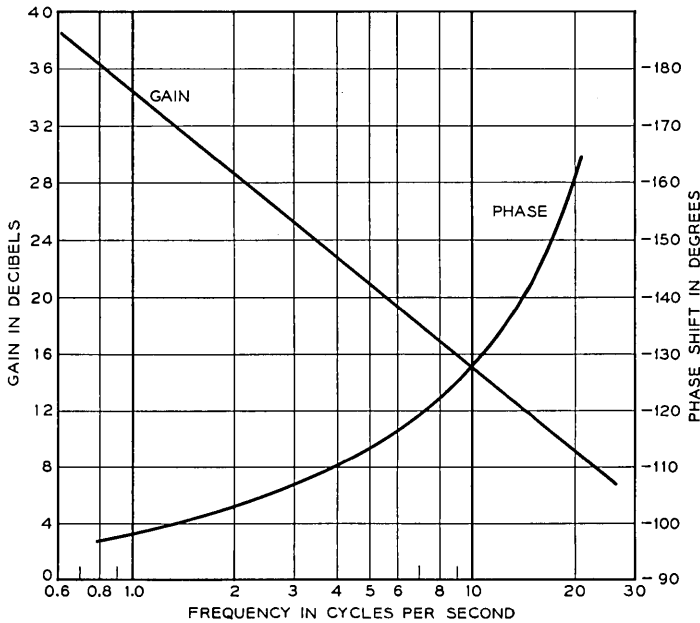
Fig. 19 — Frequency characteristics of J-7 valve.

The data were adjusted to correct for the error introduced in this manner, so that open loop conditions are represented. The equalization networks have compensating leading characteristics to prevent the oscillation suggested by the increasing phase shift at the higher frequencies.

If the servo acted in strict accordance with minimum-phase network theory, the slope of the gain curve would have started to increase at the high frequency end of Fig. 19. The effects of nonlinearities caused by such things as overlap and dither action cause this departure from classical theory. Actually, the slope does start toward 12 db per octave just above the frequency range shown.

Part of the phase shift shown on Fig. 19 is due to the inductance of the coils and the relatively low source impedance of the amplifier used. Later amplifier designs have much higher output impedance, which has greatly reduced this effect.

CONCLUSION

The series of hydraulic valves developed for use in the NIKE missile provide a light-weight, high-performance control element for positioning aerodynamic control surfaces. Although these electrohydraulic transducers provide a high power amplification, they are relatively simple single-stage devices. Their successful application in the NIKE missile has caused hydraulic servos to be considered for many other military control systems, some of which are under active development at this time. The hydraulic servo has many advantages to offer in the high power field that cannot be provided by other conventional types. It is expected that these advantages will foster a great increase in the use of hydraulic servos in high performance applications in the next few years.

ACKNOWLEDGMENT

REFERENCES

1. Peek, R. L. and Wagar, H. N., Magnetic Design of Relays, B.S.T.J., Jan., 1954.
2. Ekelöf, Stig, Magnetic Circuit of Telephone Relays — A Study of Telephone Relays — I, Ericsson Technics, 9, No. 1, pp. 51–82, 1953.
3. Von Mises, R., Berechnung von Ausfluss — und Ueberfallzahlen, Zeitschrift des Vereines Deutscher Ingenieure, 61, pp. 447–452, 469–474, 493–498, May–June, 1917.
4. Lee, Shih-Ying, and Blackburn, John F., Axial Forces on Control-Valve Pistons, Meteor Report No. 65, Mass. Inst. of Tech., June, 1950.
5. Holoubeck, F., Free Oscillations of Valve-Controlled Hydraulic Servos, Royal Aircraft Establishment, Technical Note Mechanical Engineering-100, Nov., 1951.

Strength Requirements for Round Conduit

By G. F. WEISSMANN

Underground conduits are subjected to external loads caused by the weight of the backfill material and by loads applied at the surface of the fill. These external loads will produce circumferential bending moments in the conduit wall. The magnitude and distribution of the bending moments have been determined by measurements of the circumferential fiber strains in thin-walled metal tubes subjected to the external loads. The effects of different backfill materials, different trench width, and trench depth have been investigated. Bending moments caused by static and dynamic loads have been compared. The bending moments are finally expressed in terms of the required crushing strength.

INTRODUCTION

For many years, vitrified clay has been the principal material for underground conduit used as cable duct by the Bell System. Vitrified clay conduit has, in general, given excellent service. It has more than adequate strength and durability for the wide variety of conditions under which it must be used and for the long service life expected of it. For this reason, relatively little attention has been given to the formulation of special strength requirements for this type of conduit during the period in which it has been standard for Bell System use.

For some time other types of conduit, mainly in the form of single duct, have appeared on the market. Many of their properties make them attractive enough to be considered for Bell System use. However, to prevent possible failure or excessive deformation of the conduit under field conditions each type of conduit should meet minimum strength requirements, in order to provide the same reliable service that clay conduit has given. The main purpose of this investigation was to determine the minimum strength requirement for round conduit under various field conditions.

An extensive investigation of the effects of external loads on closed conduits has been conducted at the Iowa Engineering Experiment Sta-

tion.[1,2] However, due to the large diameters of the conduits used and the particular test conditions employed, the test results obtained were not directly applicable for the determination of strength requirements for conduits for the Bell System.

Underground conduits under service conditions are subjected to external loads. These external loads are caused by:

  a. The weight of the backfill material.

  b. The loads applied at the surface of the fill.

The magnitude and distribution of the external loads around the conduit are affected by:

1. The properties of the backfill material.
2. The magnitude of the applied load at the surface of the fill.
3. The height of the backfill over the conduit.
4. The trench width.
5. The bedding condition.
6. The diameter of the conduit.
7. The flexibility of the conduit.
8. Impact.
9. Arrangements of conduits in the trench.
10. Consolidation and compaction of the backfill material.
11. Auxiliary protection of the conduit.
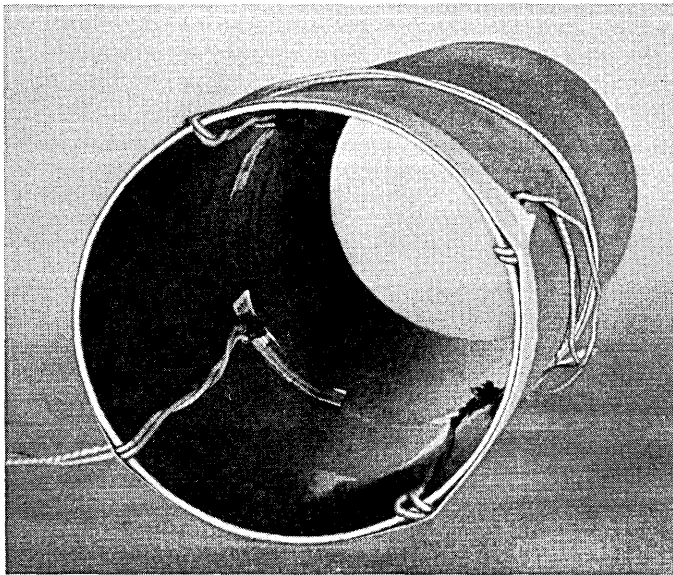
Fig. 1 — Thin-walled tube with SR-4 strain gages.
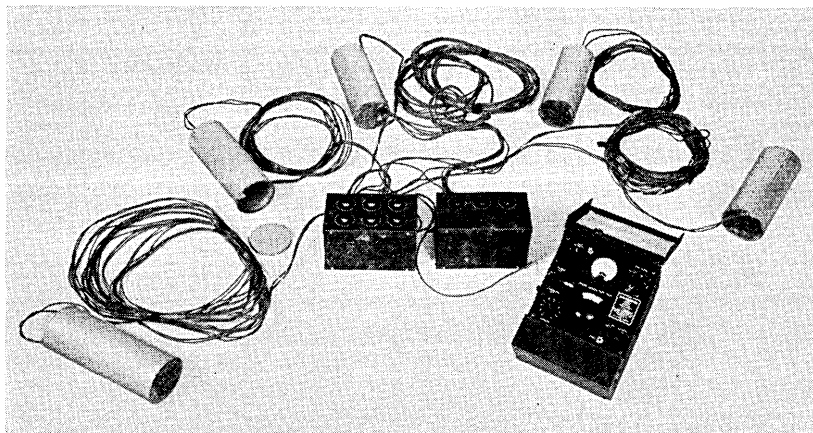
Fig. 2 — Test set.

External loads acting upon the conduit produce circumferential bending moments in the conduit wall. The magnitude and distribution of these bending moments have been determined in tests conducted recently at the Outside Plant Development Laboratory, Chester, New Jersey, and at Atlanta, Georgia. These tests were made with gravel, sand, and clay as backfill, in trenches of various width and depth and under conditions simulating, as nearly as possible, those encountered in the field.

TEST APPARATUS AND PROCEDURE

A test method was developed which permitted the determination of the circumferential bending moments in thin-walled conduits under field conditions.

The test device consisted of thin-walled aluminum or steel tubes of one foot length. The steel tubes used had an outside diameter of 4 inches and a wall thickness of 0.062 inches; the aluminum tubes had an outside diameter of 4.5 inches and a wall thickness of 0.065 inches. SR-4 strain gages were attached to the inside surface of the tube. Each tube was equipped with four equispaced SR-4 strain gages (type A-5), (Fig. 1). One aluminum tube contained, in addition, sixteen SR-4 strain gages (type A-8), which were equally distributed around the internal circumference of the tube. By means of an SR-4 strain indicator and an Edin brush recorder it is possible to measure the strains caused by static, as well as by dynamic loads. The strains could be measured with an accuracy of $\pm 10 \times 10^{-6}$ inch per inch.

TABLE I — LIST OF TESTS AND TEST CONDITIONS

Undisturbed Soil	Backfill Material	Height of Cover	Trench Width	Applied Load	Test Tube
A — Field Tests					
		(inches)	(inches)	(lbs)	
Georgia Clay	Clay	24, 30, 36, 42, 48	18, 22, 30	2250–8500	Aluminum Tube
Georgia Clay	Fine Sand	24, 30, 36, 42, 48	18, 22, 30	2250–8500	Aluminum Tube
Georgia Clay	Clay	24, 30, 36	22	500 lb (dropped 5 and 3 feet)	Aluminum Tube
Georgia Clay	Fine Sand	24, 30, 36	22	500 lb (dropped 5 and 3 feet)	Aluminum Tube
Chester Soil	Clay	18, 24, 30, 36	5	1275–7775	Aluminum Tube
Chester Soil	Fine Sand	18, 24, 30, 36	5	1275–7775	Aluminum Tube
Chester Soil	Fine Sand	24, 30, 36, 40, 48	24	1000–10175	Steel Tube
Chester Soil	$\frac{3}{4}$ in. gravel	24, 30, 36, 40, 48	24	1000–10175	Steel Tube
B — Laboratory Tests					
1. Two-point load 2. Investigation of bedding					

The test equipment used is shown in Fig. 2. Each tube was laid length-wise on the trench bottom between two pieces of plastic conduit of the same outside diameter. The tubes were oriented so that one of the strain gages was at the top of each tube. The trench was then filled with the backfill material. The loads at the surface of the fill were applied by using trucks with various measured wheel loads. The trucks were either moved slowly to a stop in position over each tube, or driven at moderate speed across the trench. Additional impact tests were made with a Hydrahammer, which consists of a 500-pound-weight dropped from different heights onto the surface of the fill. Each tube was subjected,
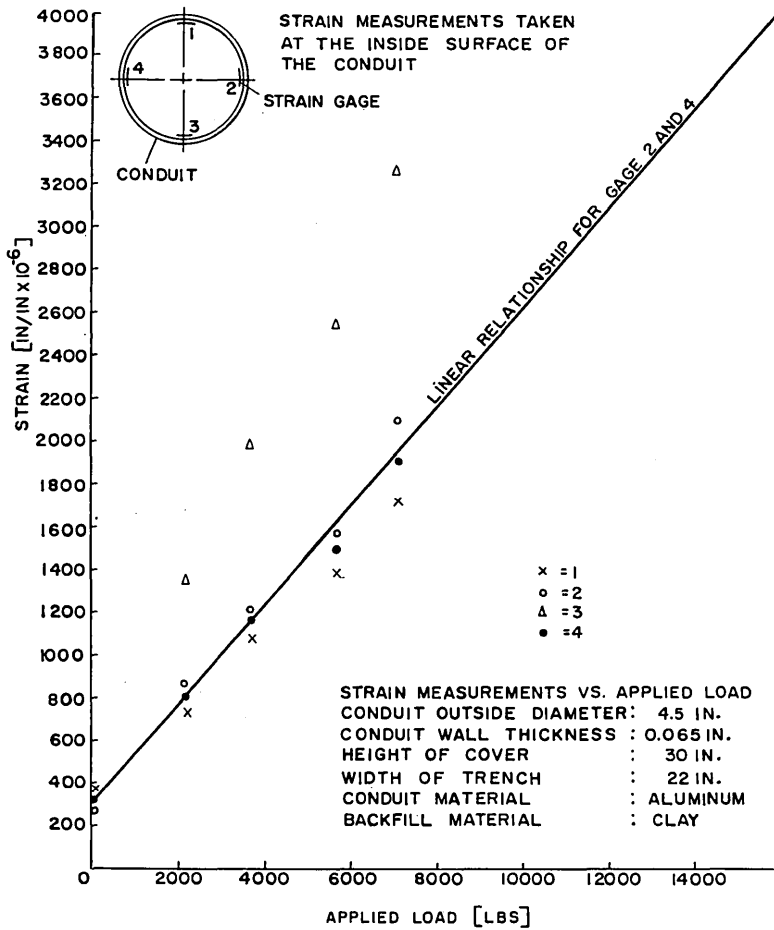
Fig. 3 — Strain measurements versus applied load.

in the laboratory, to various two-point loads (two edge bearing loads). Strain readings were taken during each test.

Table I lists the tests conducted and the test conditions investigated.

TEST RESULTS

Field and laboratory measurements obtained from each strain gage were plotted as a function of the applied load. A typical example for a field measurement is shown in Fig. 3. For this example, as well as for several hundreds of similar measurements, a linear relationship between the measured strains and the applied loads could be observed. For each case this linear relationship was derived from the data using the method of least squares. The straight line in Fig. 3 was plotted by this method and is shown with the data obtained in the test.

MOMENT DISTRIBUTION

Soil pressure acting upon a thin-walled tube will cause circumferential forces and bending moments in the wall of the tube. Furthermore, it is assumed that the strains caused by the compressive forces are small compared with those caused by the circumferential bending moments and are therefore neglected. For pure bending, the following relationship for circumferential bending moments and fibre strains is established.

$$M = \frac{1}{6} h^2 E \epsilon \tag{1}$$

where
M = circumferential bending moment per unit length (in lb/in)
h = wall thickness of tube (in)
E = modulus of elasticity (psi)
ϵ = circumferential fibre strains (in/in)

The circumferential bending moment of a thin-walled tube of unit length subjected to a two-point load is determined analytically:

$$M = \frac{Fr}{2} \left(\frac{2}{\pi} - \sin \theta \right) \tag{2}$$

where
M = circumferential bending moment per unit length (in lb/in)
F = applied two-point load (lb/in)
r = radius of the tube (in)
θ = angle with vertical axis of tube

The calculated circumferential bending moments (2) and those deter-

mined by strain measurements and Equation (1) are compared in Fig. 4. The agreement is very close.

Fig. 5 shows the theoretical moment distribution in a thin-walled tube subjected to a uniformly distributed vertical pressure; Fig. 6 is the theoretical moment distribution in the same tube subjected to a uniformly distributed vertical pressure at the top of the tube and a point load at the bottom of the tube.

Fig. 7 shows the typical experimental moment distribution in a thin-walled tube in an 18-inch wide and 40-inch deep trench with a backfill (36-inch cover) of moist Georgia clay subjected to an applied surface load of 10,000 lb. Fig. 8 shows the moment distribution under the same conditions but with a backfill of moist fine sand.
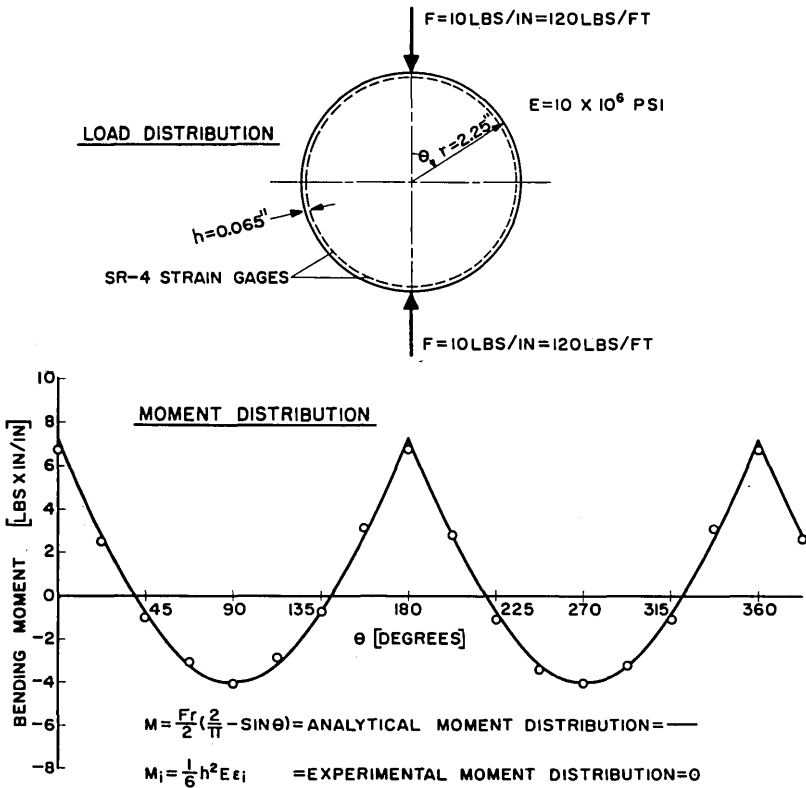
Fig. 4 — Analytical and experimental moment distribution in a thin-walled tube under two-point load.

BEDDING EFFECT

Based on the theoretical considerations illustrated in Figs. 5 and 6, comparison of Figs. 7 and 8 indicates a high load concentration at the bottom of the tube buried in a trench with clay backfill. For a verification of this assumption, a series of additional tests were conducted. The test tube was placed upon (a) a flat steel plate and then covered with moist clay, (b) a flat steel plate and then covered with dry sand, and (c) carefully distributed moist clay and then covered with clay. The external load was then applied. The moment distributions obtained for cases (a), (b), and (c) are shown in Figs. 9, 10 and 11, respectively.

A comparison of the data presented in Figs. 9 and 11 shows the effect of the bedding condition on the moment distribution (steel plate versus clay bedding). These data, as well as theoretical considerations (Figs. 5 and 6), indicate that the bedding condition affects mainly the bending moment at the bottom of the tube and only to a lesser degree the bending moment at right angles to the vertical axis. Due to a change in
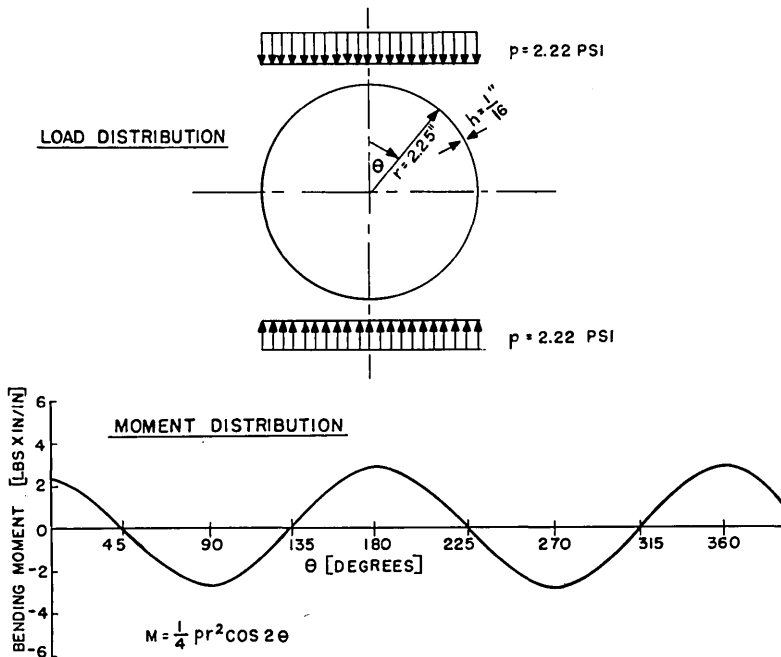
Fig. 5 — Theoretical moment distribution in a thin-walled tube subjected to uniformly distributed vertical pressure.

bedding, the moment at the bottom may vary up to 235 per cent, and the moments at the side points may change a maximum of 12 per cent.[3] The field data indicate that bedding is of particular importance with moist clay backfill, and to a lesser degree for moist fine sand. However, bedding did not appear to affect the moment distribution of the tube for a dry sand or gravel backfill.

TRENCH WIDTH

The effect of the trench width on the magnitude of the bending moments in a conduit has been investigated. The presently available test results indicate the following:

a. No significant difference in the magnitude of the bending moments of the tube (4.5-inch diameter) could be observed for a trench width

$$M = pr^2 \left[\frac{1}{4}\cos 2\theta + \frac{1}{3\pi}\cos\theta + \frac{1}{\pi} - \frac{3}{8} \right] \qquad 0 \le \theta \le 90$$

$$M = pr^2 \left[\frac{1}{3\pi}\cos\theta - \sin\theta + \frac{3}{8} + \frac{1}{\pi} \right] \qquad 90 \le \theta \le 180$$
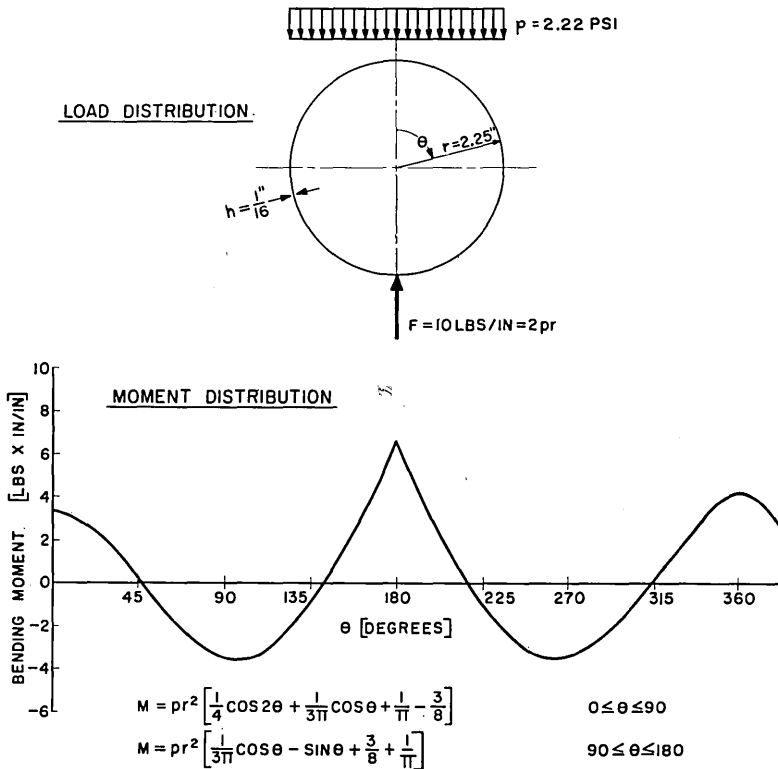
Fig. 6 — Theoretical moment distribution in a thin-walled tube subjected to uniformly distributed vertical pressure at the top and point load at the bottom.

between 18 and 30 inches. The magnitude of the bending moments appeared to be only a function of the backfill material, the applied load, and the height of backfill over the conduit.

b. For a trench width of 5 inches, the bending moments seemed to be independent of the type of backfill material. The same results have been obtained with a backfill of clay, sand, or gravel. This phenomenon indicates that the applied load was carried mainly by the undisturbed soil but deformation of the trench walls together with friction between the backfill material and the trench walls transmitted the load to the conduit. The magnitude of the bending moments in 5-inch wide trenches
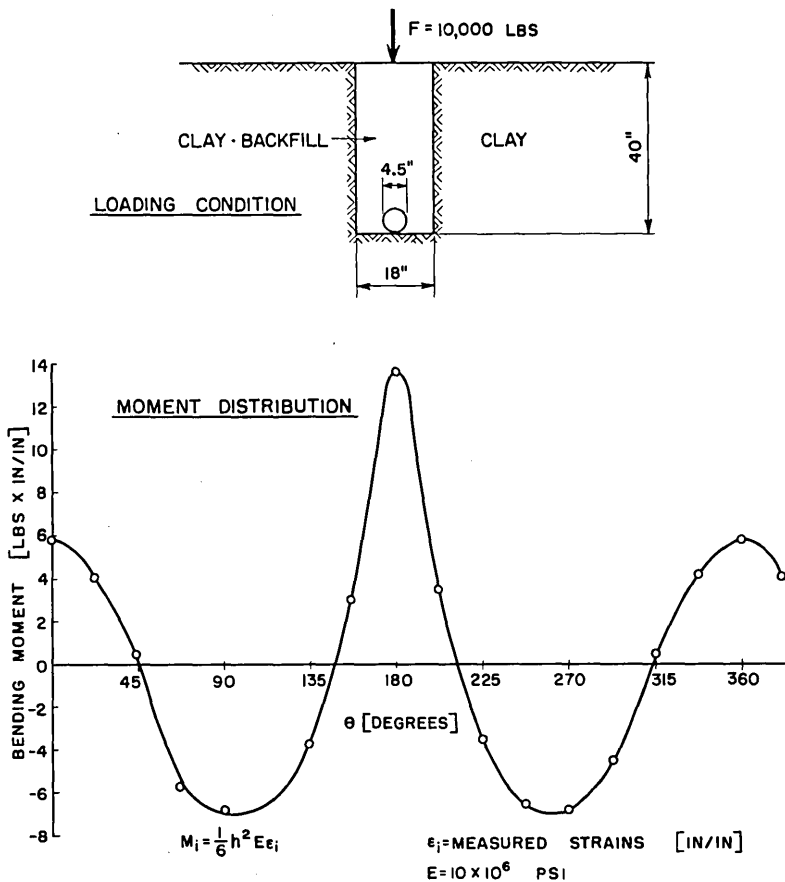
Fig. 7 — Moment distribution in a thin-walled tube, using clay backfill.

depends on the characteristics of the undisturbed soil. A comparison of the values obtained from a 5-inch wide trench dug in sandy clay (typical Chester, N. J. soil) and trenches between 18 and 30 inches wide shows that the values for 5-inch width are greater than for an 18- to 30-inch width when using sand backfill, and less when using clay backfill.
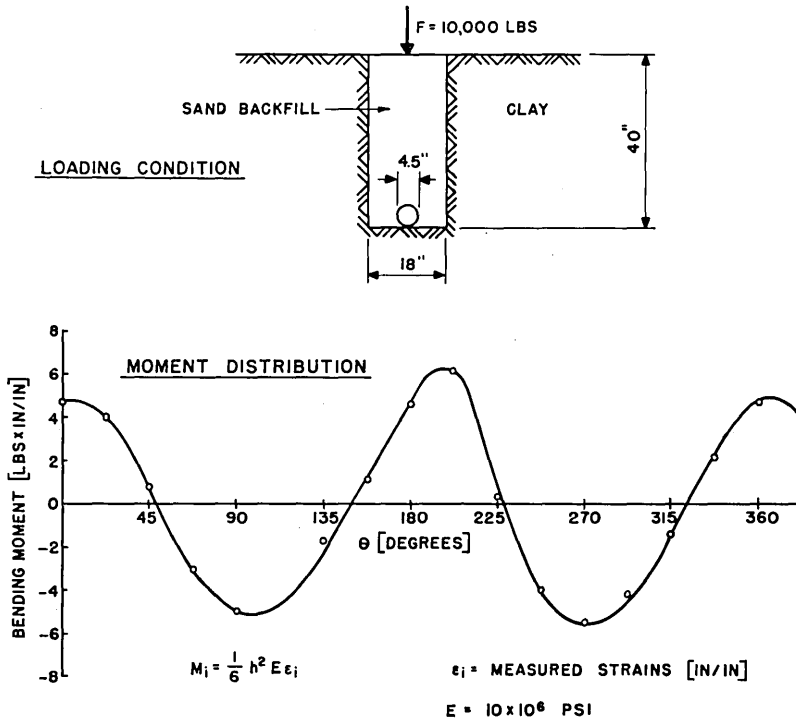
Fig. 8 — Moment distribution in a thin-walled tube, using sand backfill.
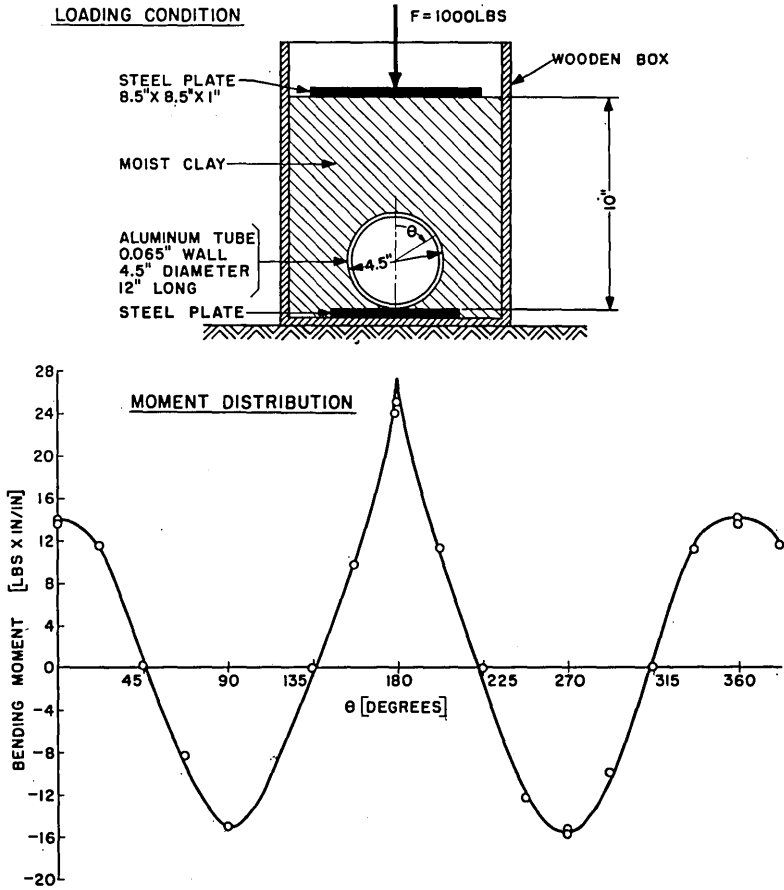
Fig. 9 — Moment distribution in thin- walled tube resting on steel plate and covered with moist clay.
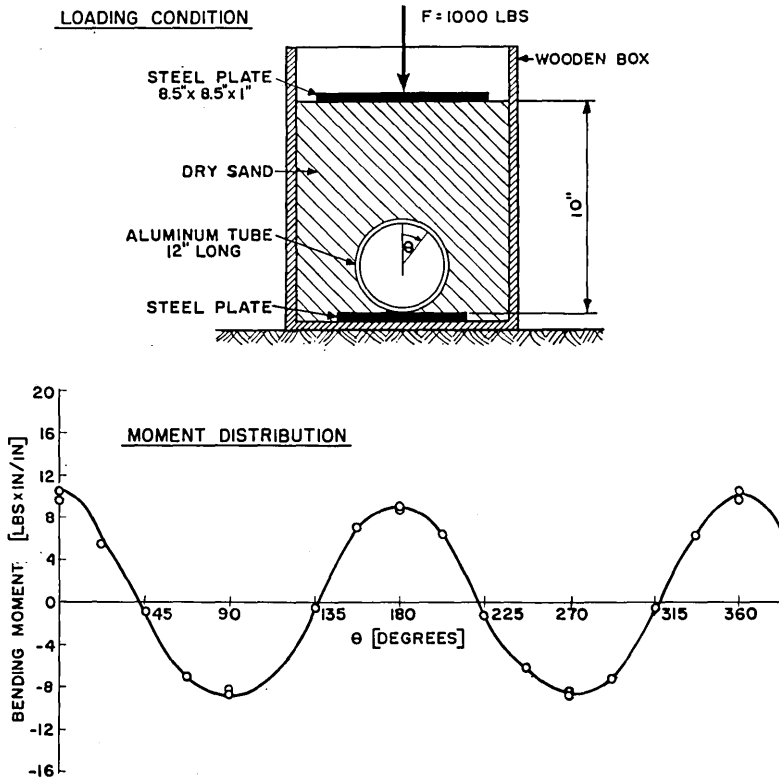
Fig. 10 — Moment distribution in thin-walled tube resting on steel plate and covered with dry sand.
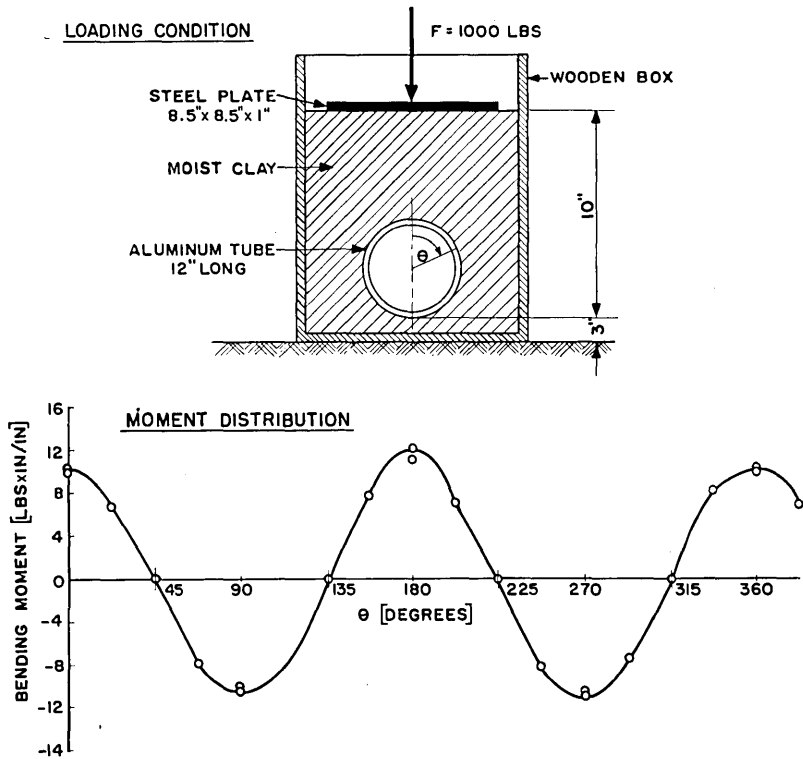
Fig. 11 — Moment distribution in a thin-walled tube in moist clay.

BACKFILL MATERIAL AND HEIGHT OF BACKFILL

Backfill provides the main protection for conduits against loads applied at the surface of the fill. The type of backfill used and the height of the backfill over the conduit are therefore extremely important. Figs. 12, 13, and 14 show the relationship between the bending moments in the conduit and the height of backfill for different applied loads. Fig. 12 shows this relationship for clay as backfill, Fig. 13 for fine sand, and Fig. 14 for gravel. The maximum bending moment is here expressed in terms of the "equivalent two-point load." The equivalent two-point load is the two-point load that will cause the same maximum bending moment in the conduit wall as the maximum bending moments measured in the field. The relationship between the two-point load and the bending moments in the walls of the conduit was given by (2). The equivalent two point load is obtained for $\theta = 0$ and becomes

$$F_{TP} = \frac{12\pi M_{\max}}{r} \tag{3}$$

where

F_{TP} = equivalent two-point load (lb/ft)

$M_{\max}$ = maximum bending moment in conduit (in × lb)

r = radius of conduit (in)
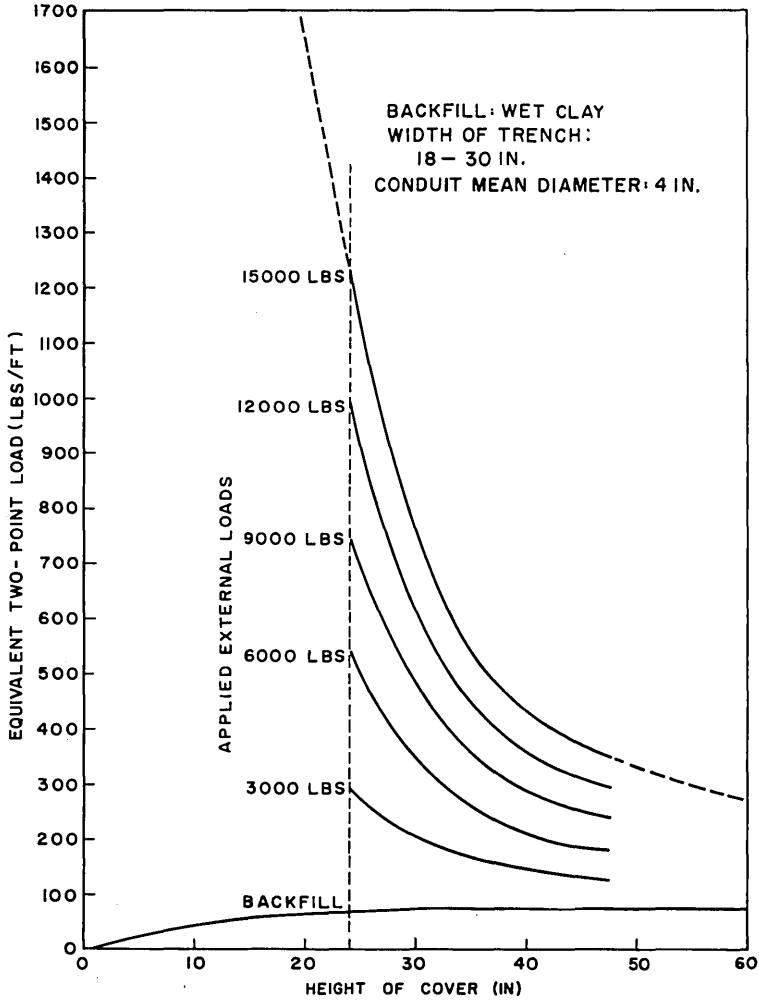
Fig. 12 — Equivalent two-point load versus height of cover for clay backfill.

The two-point load was chosen as a measure of the bending moment for convenience in laboratory testing of new conduits. The two-point load system is undoubtedly the simplest method for testing cylindrical or near-cylindrical shapes in conventional compression testing machines (crushing test). Since most of the supplementary conduit materials are cylindrical in shape, the most obvious requirement would be in terms of minimum two-point loading.

The data in Figs. 12, 13, and 14 were obtained as follows:

The bending moments at points perpendicular to the vertical axis were represented, as a function of the applied load, by a straight line, determined by the method of least squares. This was done for all the investigated depths and backfill materials. The side points were used as a basis of comparison because they were less affected by a change in the bedding conditions. With reference to the considerations of the
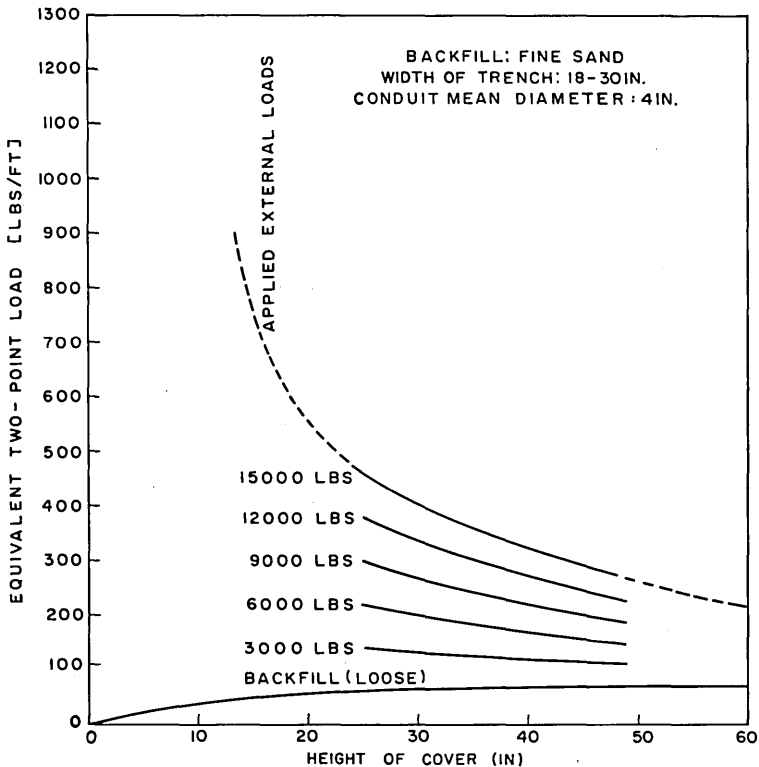
Fig. 13 — Equivalent two-point load versus height of cover for sand backfill.

bedding effect, the possible maximum bending moment at the bottom of the tube was obtained by doubling the values of the side points. Figs. 12 and 14 show clearly that the maximum bending moments occur in wet clay, and also that improvement is obtained by an increase in the height of backfill or a decrease of the applied load. These figures apply to 4-inch diameter tubes. In conversion of results obtained using 4.5-inch diameter tubes, it was assumed that the equivalent two-point load is directly proportional to the tube diameter.

DYNAMIC LOAD

A study was made to determine the effect of moving loads on the maximum bending moment of the conduit. For this purpose trucks were driven over the backfill at a speed of approximately 20 miles per hour, the strains measured and then compared with those obtained by static loads. The results show that for a clay backfill, the bending moments due to dynamic loads were equal to or even smaller than those obtained by static loads. For sand backfill, however, the dynamic loads caused an increase of the maximum bending moments of approximately 10 per cent. These results are in close agreement with dynamic load tests con-
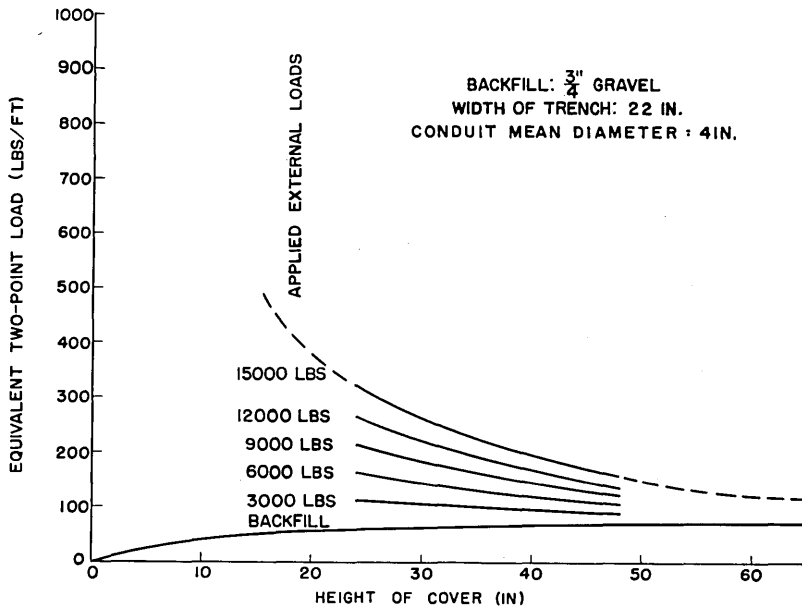
Fig. 14 — Equivalent two-point load versus height of cover for gravel backfill.

ducted by H. Lorenz.[4] Further tests conducted with 500-lb weights dropped from different heights demonstrated that the effect of dynamic loads for clay backfill is of minor importance.

FURTHER INVESTIGATION

The tests previously conducted did not include investigations of the effects of conduit flexibility, various conduit diameters, multiple arrangements of the conduits in the trench, consolidation and compaction of the backfill, and auxiliary protection of the conduit. Studies of these factors are now in progress.

SUMMARY

Strength requirements of underground conduits depend on various factors. The most severe conditions were obtained with wet Georgia clay as backfill for a trench width of 18 to 30 inches. The relationship between the height of backfill, the load applied at the surface of the backfill, and the equivalent two-point load for these conditions is shown in Fig. 12. For example, a round conduit of 4-inch mean diameter under 24 inches of clay cover subjected to an applied load of 15,000 lb should be able to carry a two-point load of 1,250 lb without fracture of excessive deformation. Figs. 12 to 14 can be used to determine the required crushing strength of 4-inch round conduits subjected to different applied loads, buried at different depths with clay, sand, or gravel cover, but only for trench widths of 18 inches or more. Although this investigation is not completed, the results obtained to date may be used, within the indicated limits of application, for the selection of acceptable conduit.

ACKNOWLEDGEMENT

REFERENCES

1. Marston, A., The Theory of External Loads on Closed Conduits in the Light of the Latest Experiments, Bulletin 96, Iowa Engineering Experiment Station.
2. Spangler, M. G., Soil Engineering, International Textbook Company, Scranton, 1951.
3. Marquard, Rohrleitungen und geschlossene Kanäle, Handbuch für Eisenbetonbau, 4, Aufl., Bd. 9, Berlin 1939.
4. Lorenz, H., Der Baugrund als Federung und Dämpfung schwingender Körper, Bauingenieur, p. 11, 1950.

Cold Cathode Gas Tubes for Telephone Switching Systems

By M. A. TOWNSEND

Cold cathode gas tubes perform both switching and memory functions in telephone switching systems. One measure of the performance of a switching diode is the switching voltage gain, defined in terms of the characteristics of the device. Some of this gain must be sacrificed in order to increase the switching speed in a way which is analogous to the gain-bandwidth property of a conventional amplifier. In this paper, methods of achieving a high switching-voltage gain are described in terms of the gas discharge processes. An example is given of an application of these principles to a tube for use as a switch in series with the talking path in an electronic telephone switching system.

INTRODUCTION

Gas discharge tubes have found extensive use in telephone switching and other digital systems. Most of these applications take advantage of the fact that both switching and memory can be provided by a single gas discharge device. The switching characteristics result from the fact that the device is an essentially open circuit when the gas is not ionized and a closed circuit when the gas is ionized. The memory function is possible because the tube can be held in a high current condition, once it is ionized, by a voltage which is too low to initiate this conduction. Thus a triggering signal which ionizes the tube is "remembered" until the holding voltage is removed and the tube is allowed to de-ionize.

In some applications, gas tubes are used as switching devices in series with voice frequency circuits. For this purpose, the tube must offer a low impedance to audio frequency signals in addition to meeting requirements of switching and memory.

This paper first describes some switching characteristics of gas tubes considered as circuit elements. Desirable performance objectives are established in terms of these device characteristics. Following this, physical processes within the tube are described as they relate to circuit per-

formance. Finally, a description is given of a new talking path tube in which improved switching and transmission performance have been achieved.

EXTERNAL SWITCHING PROPERTIES

From the point of view of the external circuit, a gas diode may often be treated as a device which is an open circuit so long as the applied voltage is low, and which becomes a conductor if the applied voltage is raised above a threshold or "breakdown" value for a sufficient length of time. When the tube is conducting currents of the order of a few tens of microamperes or higher, the voltage is relatively independent of current and has a value, referred to as the "sustaining voltage", which is less than the breakdown voltage.

Although the details of actual circuits differ, it is possible to illustrate some important switching principles by the simplified circuit of Fig. 1(a). A gas diode is shown with the cathode connected to a bias voltage E through a load resistor. A signal source, assumed to have zero internal impedance is connected to the anode. The output voltage waveform corresponding to a pulse input is shown in Fig. 1(b). Note that after a time delay, t, the output rises to a voltage that differs from the total applied voltage by an amount equal to the sustaining voltage of the tube. The memory function is illustrated by the fact that the output signal remains after the input signal is removed.

It is often desired to use the output signal resulting from the triggering of one tube to switch one or more additional tubes. Since the input signals can be a few microamperes and the output signal can be tens of milliamperes, a large current gain is available from a gas tube. In many applica-

(a)   (b)
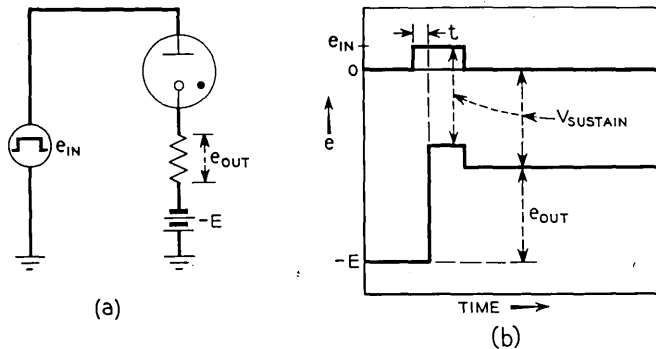
Fig. 1 — Simplified gas diode switching circuit.

tions, however, it is desired to apply the output voltage directly to other tubes without impedance transformation. In this case, voltage gain is of more interest than current gain. The maximum voltage gain per stage, defined as the maximum output voltage divided by the minimum input signal, is limited by variation in tube characteristics as will now be shown.

The bias voltage E of Fig. 1· is expected never to cause breakdown during times when the input voltage is zero. This establishes the upper limit of E as

$$| E | \leqq V_{B\ min} \tag{1}$$

where $V_{B\ min}$ is the minimum breakdown voltage at any point in the life of any tube to be used in the circuit. As the bias voltage E approaches breakdown, the input signal voltage required for triggering approaches zero, and if there were no variation in breakdown voltage or bias voltage, and no noise voltages, the gain could be made to approach infinity.

The input signal, added to the bias, must be made large enough always to cause breakdown. Thus the minimum input signal is determined by $V_{B\ max}$, the maximum breakdown voltage at any point in the life of any tube to be used in the circuit:

$$e_{in} \geqq V_{B\ max} - E \tag{2}$$

Combining (1) and (2)

$$e_{in} \geqq V_{B\ max} - V_{B\ min}$$

or

$$e_{in} \geqq \Delta V_B \tag{3}$$

where ΔV_B is the maximum variation in breakdown voltage among all tubes to be used in the circuit.

The output signal is the difference between the bias voltage and the sustaining voltage of the tube:

$$e_{out} = E - V_{sus} \tag{4}$$

The minimum output voltage corresponds to the maximum sustaining voltage, $V_{sus\ max}$. It is this value that must be used in calculating the maximum gain per stage as limited by the tube characteristics. The gain is then calculated as

$$G = \frac{e_{out}}{e_{in}} = \frac{E - V_{sus\ max}}{\Delta V_B} = \frac{V_{B\ min} - V_{sus\ max}}{\Delta V_B} \tag{5}$$

This gain cannot be realized in practice because additional allowances

must be made for the variation in power supply voltages and protection against noise. In some cases the need for higher speed reduces the gain still further, as will now be shown.

In Fig. 1 a delay, t, is indicated between the application of the triggering signal and the appearance of the output signal. Part of the delay is statistical in nature and part is occasioned by the building up of ionization within the tube. As will be discussed later, the delay can be reduced by tube design techniques. However, for any given tube, the delay is a function of the excess of the tiggering voltage over the breakdown voltage. The larger this overvoltage, V_{ov} , the shorter is the breakdown delay. Since this overvoltage must be added directly to the input signal, the gain is reduced.

Although not shown in Fig. 1, the tube is turned off by applying a signal that reduces the anode-to-cathode voltage below the sustaining value. This turn-off signal must have sufficient duration so that the tube does not again break down at the return to normal bias conditions. If the turn-off pulse duration is less than that needed for complete recovery, the effective breakdown voltage is reduced. Equation (5) can be modified to show the effect of this reduction in turn-off time by defining a quantity V_r , the reduction in breakdown voltage resulting from incomplete recovery of the tube. The combined effects of V_r and V_{ov} are then

$$G = \frac{(V_{B\ min} - V_r) - V_{sus\ max}}{\Delta V_B + V_{ov}} \qquad (6)$$

Equation (6) shows that faster turn-on obtained by increasing the over voltage V_{ov} and faster turn-off obtained by allowing for decrease in breakdown voltage by an amount V_r , both result in a reduction in voltage gain. Thus the familiar trade of speed for gain extends to gas tube switching circuits. Summarizing, it can be seen by (5) that constant breakdown voltage and large difference between breakdown and sustain are desirable switching properties. Also, as shown in (6), the tube should be designed so that the overvoltage needed to cause fast breakdown is small and the recovery of breakdown voltage after the tube is turned off is fast. It is useful to consider now the internal physical processes of a cold-cathode glow-discharge tube in order to see how the desired external properties can be obtained.

PHYSICAL PROCESSES OF A COLD CATHODE GLOW DISCHARGE

Since the gas particles are neutral and the cathode does not spontaneously emit electrons, current flow requires an auxiliary supply of charged particles. A small amount of radioactive material to ionize some
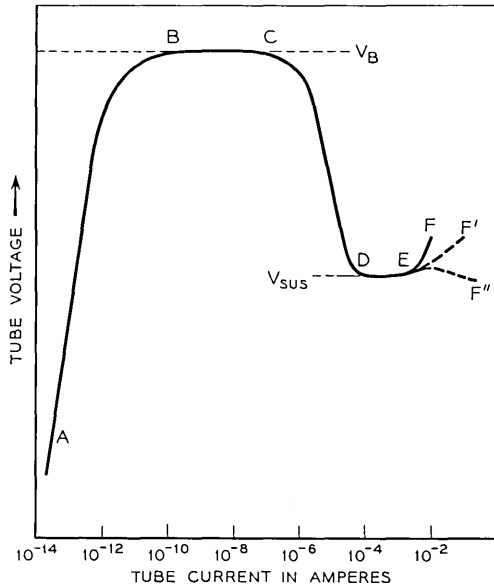
Fig. 2 — Voltage versus current curve of typical gas diodes.

of the gas or very small photoelectric emission of electrons from the cathode are commonly used for this auxiliary supply. A typical voltage-current curve is shown in Fig. 2. At low voltage, the current is very small, often being in the range of 10^{-14} ampere or less. The current increases with the voltage because collisions of electrons with neutral gas atoms produce additional excitation and ionization in the gas. Some of the new ions and excited gas atoms release new electrons by secondary emission when they strike the cathode.

The rate of increase of current with voltage depends on the kind and the pressure of the gas filling, the cathode material, and the tube geometry. An important characteristic of the gas is defined by an ionization coefficient η, which represents the number of new electrons (and ions) produced by a single electron moving through the gas a distance corresponding to one volt of potential difference.[1] This coefficient is a function of the kind of gas and of the quantity E/p_0 where E is the voltage gradient and p_0 is the normalized gas pressure. The fact that there is an optimum E/p_0 at which η is a maximum will be important to later discussion. The electron current at the anode, i_a, produced by gas amplification of a photoelectric current i_0 at the cathode is[1]

$$i_a = i_0 e^{\int_{V_0}^{V} \eta \, dV} \tag{7}$$

where V is the anode voltage and V_0 is the initial voltage through which the electrons must travel before they can ionize.

The ions produced in the space by this process flow back toward the cathode. The ion current i_p resulting from this process is

$$i_p = i_0(e^{\int_{V_0}^{V} \eta dV} - 1) \tag{8}$$

As mentioned above, new electrons are released at the cathode by positive ions, neutral atoms excited to a metastable state, and photons generated in the gas. These secondary processes can be grouped together by defining a coefficient γ as the number of new electrons released at the cathode by all of these processes for each positive ion generated in the cathode-anode space. Thus each electron passing from cathode to anode, on the average, results in the release of M new electrons where

$$M = \gamma(e^{\int_{V_0}^{V} \eta dV} - 1) \tag{9}$$

Each new electron from the cathode is also amplified in the gas so that after n multiplication cycles, the electron current at the anode is[2]

$$i_n = i_0 e^{\int_{V_0}^{V} \eta dV}(1 + M + M^2 + \cdots + M^n) \tag{10}$$

When M is less than unity and $n \to \infty$ (the equilibrium state), (10) reduces to a steady state value of

$$i = \frac{i_0 e^{\int_{V_0}^{V} \eta \, dv}}{1 - M} \tag{11}$$

Since the current is dependent on the initial current i_0, the discharge is said to be non-self-sustaining. This corresponds to the portion AB of the curve of Fig. 2.

If the applied voltage is made high enough, the multiplication factor approaches unity, the current of (11) becomes independent of the initial current, and the tube is said to have broken down. This condition corresponds to the horizontal portion BC of Fig. 2. To control this breakdown voltage, the cathode secondary emission coefficient γ and the gas ionization coefficient η must be controlled.

The secondary emission coefficient is highly sensitive to the surface conditions of the cathode. Pure metals such as molybdenum are often preferred to coated surfaces because they permit highly stable and reproducible emission. With the cathode surface determined, the breakdown voltage can be adjusted by changing the gas filling and tube geometry. Fig. 3 shows the breakdown voltage for a tube having parallel-plane
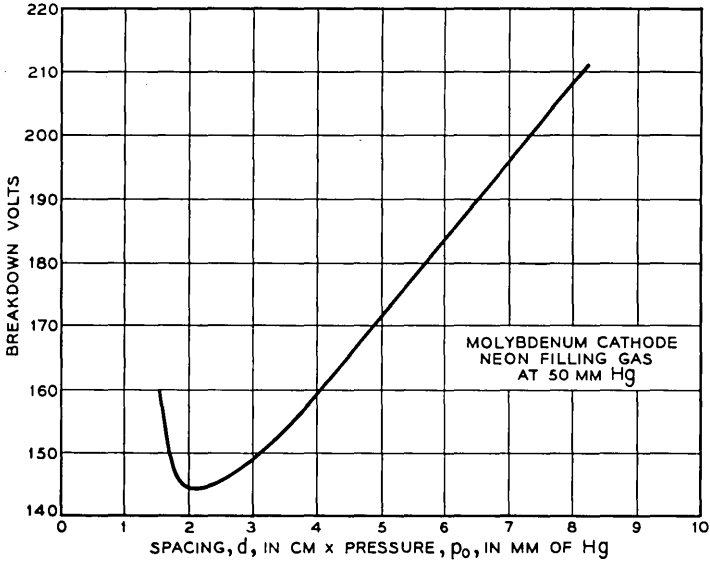
Fig. 3 — Breakdown voltage as a function of spacing and pressure for parallel plane anode and cathode.

anode and cathode geometry, a molybdenum cathode, and neon filling gas. The curve is plotted as a function of the product of pressure p_0 in mm Hg and electrode separation d in cm. Approximately the same plot would obtain for other pressures because both η and γ are functions of (E/p_0) and, for uniform fields, E is simply the voltage divided by the separation

$$\frac{(E)}{(P_0)}_{\text{at breakdown}} = \frac{V_{Bd}}{d} \frac{1}{p_0} \tag{12}$$

Since the variation of γ with E/p_0 is small and may be ignored in this elementary discussion, the minimum breakdown voltage corresponds very nearly to the optimum value of the ionization coefficient η. At spacings or pressures less than optimum, η is reduced because some electrons strike the anode without colliding with gas atoms. At spacings or pressures greater than optimum, η is reduced because electrons do not gain enough energy between collisions to ionize efficiently.

It can be seen that a way of meeting the switching requirement of constant breakdown voltage would be to design the tube to operate at the minimum of Fig. 3. Minor changes in spacing or filling pressure from one tube to another and changes in pressure with tube operation would result in small changes in breakdown voltage. The advantages of op-
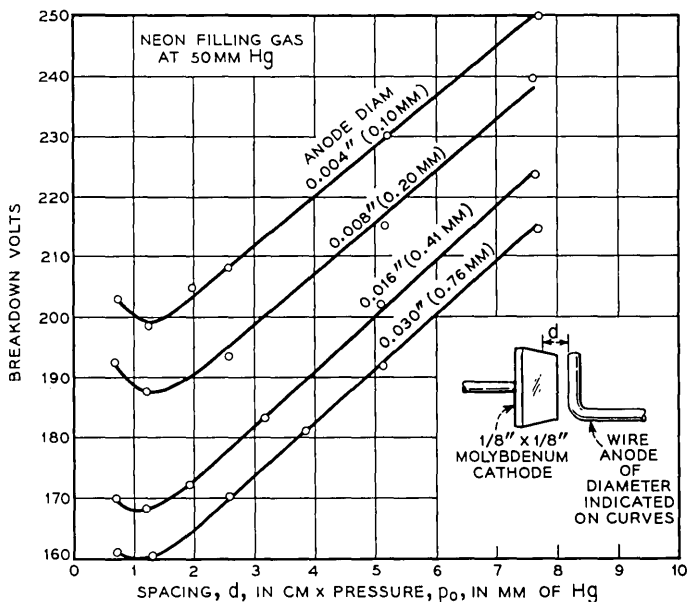
Fig. 4 — Breakdown voltage as a function of spacing and pressure for small wire anodes parallel to cathode surface.

eration at the minimum of the p_0d curve can be retained and the breakdown voltage made higher by resorting to non-uniform geometry. Typical curves are shown in Fig. 4. The cathode was a small rectangular plate and the anode was a wire placed parallel to the cathode surface. It is seen that as the anode diameter is decreased, the minimum of the breakdown curve is increased. The practical limit is set by mechanical stability of the anode and by transmission requirements, as will be discussed later.

The rise in minimum breakdown voltage as the anode size is reduced can be explained on the basis of the distortion of the electric field. Near the cathode, E is lowered, and near the anode, E is increased, as compared to the parallel plane case. If the spacing is adjusted for optimum E/p_0 with parallel planes, then η is necessarily less than optimum for the distorted fields.

Returning now to Fig. 2, we note that, as the current is increased beyond breakdown, the tube voltage falls to a lower sustaining value and again is relatively constant with current. This lower voltage corresponds to the development of a space-charge layer of positive ions near the cathode and an increased voltage gradient at the cathode. This higher

field results in an increase in the ionization coefficient η, and, in some cases,[3] a larger effective value of the secondary emission coefficient γ. This is because electrons released by the secondary emission processes may strike neutral gas atoms and be reflected back to the cathode. A higher gradient increases the probability of escape of such an electron. Thus the multiplication factor M of (9) can equal unity at a lower total applied voltage.

Practical tubes filled with neon or argon gas have sustaining voltages near 100 volts when pure molybdenum or tungsten cathodes are used. Cathodes coated with barium and strontium oxide may sustain at 60 volts. However, since this lower sustain is accompanied by a lower breakdown voltage, the difference between them is not increased. Also, since the coated cathode surface is more variable between tubes and with tube operation, the switching voltage gain may be reduced with such cathodes.

The gas pressure and cathode geometry determine the length of the flat portion DE of Fig. 2. Over this current range, the area covered by the glow discharge increases with current until at E the cathode is completely covered. Increasing the cathode area or gas pressure increases the total current required for coverage. At still larger currents, the sustaining voltage increases rapidly as indicated by the solid curve EF. Broken curve EF′ applies to a special cathode geometry called a hollow cathode.[4] Such a cathode may be formed by the interior of a cylinder or by placing two plane cathodes close together so that the negative glow regions overlap. Under this condition electrons, ions, and excited atoms generated near one cathode can aid in current flow from the other cathode. Dotted curve EF″ applies to a particular form of hollow cathode[5] in which cathode shape and gas pressure have been selected to give a negative slope in the high current region. This negative slope represents a negative resistance and permits audio-frequency signals to be transmitted through the tube without loss.

Anode effects have not been discussed. In general, the anode shape and location do not affect the sustaining voltage or the ability of the discharge to transmit audio frequency unless the anode-cathode spacing is too large. The basic requirement is that the anode should be large enough to intercept enough electrons to carry whatever current is required by the external circuit. Even a small anode placed near the cathode space-charge region can meet this requirement. Thus the sustaining voltage of a tube designed to have a breakdown voltage near the minimum of Fig. 3 or Fig. 4 will not in general be sensitive to the anode size or shape.

The transition from low current to high current in a gas diode can thus be thought of as the process of introducing a space charge of positive ions in the region near the cathode. This is done by raising the voltage temporarily above the breakdown value. To switch back to the low current, it is necessary to decrease the multiplication factor M below unity by temporarily lowering the voltage and allowing the ions and excited atoms to diffuse out of the cathode and anode region. Both the turn-on and the turn-off processes impose time restrictions on the switching characteristics.

The multiplication factor M of (9) applies to an average process. Thus, even though M is greater than unity, it is possible that the ionization and excitation produced in the gas by any individual electron may not release a new electron at the cathode. It is therefore necessary on the average to wait for more than the time between initiating electrons before the discharge starts to build up.

The average statistical delay is then equal to the average time between successful starting events. If N_0 photoelectrons per second are emitted from the cathode and W is the fraction of these which successfully initiate a discharge, the average statistical delay is[6]

$$t_{\text{AV}} = \frac{1}{WN_0} \tag{13}$$

The fraction W would be expected to increase with an increase in the multiplication factor M and hence with the overvoltage above breakdown. It has been shown theoretically and experimentally[7] that this is the case. For voltages only slightly in excess of breakdown, i.e., small overvoltages, V_{ov}, the expression for average statistical delay can be approximated by

$$t_{\text{AV}} \approx \frac{k_s}{V_{\text{ov}}} \tag{14}$$

In practical tubes with overvoltages of 10 volts, the average statistical delay may be of the order of milliseconds with radioactive sources of ionization. Short delays of the order of microseconds are obtained by providing an auxiliary "keep-alive" discharge to a separate electrode or by illumination that provides a photoelectric current in the range of 10^{-12} amperes.

A formative delay in breakdown also occurs because time is required for current to build up to the final value. This time is equal to the product of the number of multiplication cycles and the time per cycle. The number of multiplication cycles required is reduced as multiplica-

tion factor M is increased with increasing overvoltage. The multiplication factor M includes electrons released at the cathode by slow moving metastable gas atoms as well as those released by the faster positive ions. At very low overvoltages, these slow components must be included before the current can build up.[8] At higher overvoltages enough positive ions are produced so that M is greater than unity without waiting for the slow components. Thus the effective time per multiplication cycle is reduced with increasing overvoltage. Since the number of cycles and the time per cycle are both decreased the formative delay decreases rapidly with increasing overvoltage. A typical formative delay for a neon filled, molybdenum cathode switching tube at 5 volts overvoltage might be of the order of 100 microseconds.

APPLICATION TO A TALKING-PATH SWITCHING DIODE

The principles discussed above have been applied in the development of a cold-cathode gas diode for use as a switch in series with the speech path in an electronic switching system. The objectives were a switching voltage gain as high as possible, a breakdown time of less than a few hundred microseconds, and a low transmission impedance for audio-frequency signals.

A sketch of one version of the resulting tube is shown in Fig. 5. The cathode is a molybdenum rod which has a small hollow cathode portion in the upper end. The anode is a small molybdenum wire placed near the minimum breakdown distance and slightly to one side of the opening in the end of the cathode. A barium getter is flashed to one side of the bulb wall and a small tungsten wire spring is arranged to make electrical contact with the getter flash. A neon filling gas at a pressure near 100 mm Hg is used.

The cathode geometry has several interesting properties. It was found that the shape of a cylindrical hollow cathode is unstable at very high current densities and that it will rapidly grow into a spherical cavity with a small orifice.* Typical dimensions are a sphere diameter of 0.030 inch and an orifice diameter of 0.008 inch. At an operating current of 10 milliamperes, the current density in the orifice is of the order of 50 amp/cm². Once the sphere has stabilized it will operate many thousands of hours with relatively small changes in shape. The transmission properties of the stabilized spherical cavity cathode are similar to the earlier negative resistance hollow cathode tubes.[5] Typical im-

---

* This cathode was developed by A. D. White of Bell Telephone Laboratories and will be described more completely by him in a forthcoming publication.

pedance values are 300 ohms negative resistance and 50 ohms inductive reactance at 10 milliamperes operating current, with a superimposed audio-frequency signal of 3,000 cycles per second.

Even though the cathode geometry is stable, some cathode material escapes through the orifice and will rapidly collect on an anode placed directly over the opening. It is therefore necessary to locate the anode to one side of the orifice. The extremely high ionization density near the cathode orifice allows considerable flexibility in anode location without affecting the sustaining voltage or destroying the negative resistance.

High switching-voltage gain is obtained by using a small anode formed by a 0.005-inch diameter molybdenum wire placed perpendicular to the end of the cathode at a spacing of approximately 0.005 inch. Breakdown voltage is nominally 190 volts with a range of ±10 volts over all tubes and over the nominal operating life of 4,000 hours. The sustaining volt-
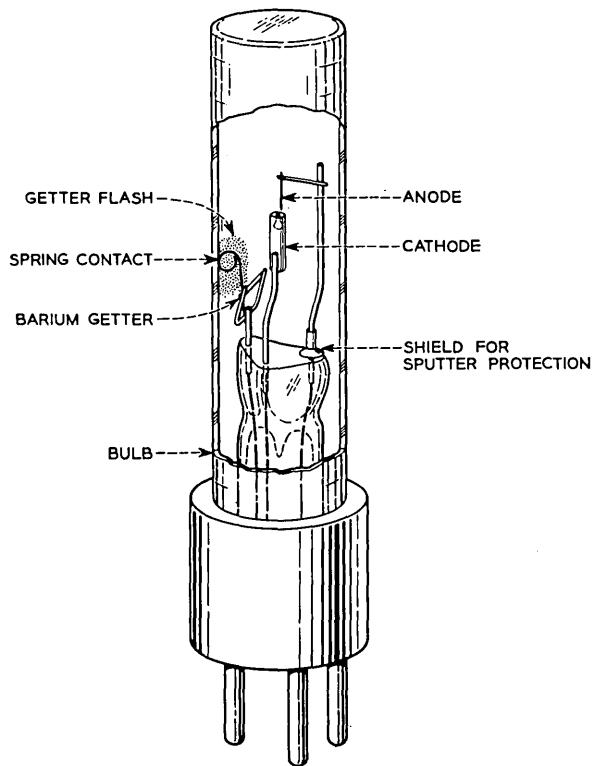
Fig. 5 — A talking-path switching diode.

age at the operating current of 10 ma is 99 $\pm$ 2 volts. Thus the switching gain from (5) is (180–101)/20 or 3.9. In practice, switching is often done without allowing the full 100 milliamperes operating current to flow. Under these conditions, the sustaining voltage may be 10 or 15 volts higher, with a consequent reduction in switching voltage gain.

Short breakdown times were desired for this tube. It was not desirable to use enough radium to obtain the needed initial ionization, since it is expected that large numbers of these tubes will be concentrated in a relatively small space. Also, the molybdenum cathode does not emit photoelectrons unless short wavelength ultraviolet illumination is used. The solution chosen was to use the barium getter flash as an auxiliary photocathode. An electrical contact is made to the getter deposit and this is connected through a high resistance to the main cathode. Visible light or long wave ultraviolet light is readily transmitted through the bulb and produces photoelectric current in the auxiliary gap. This current is amplified by the gas, but remains a non-self-sustaining discharge. Currents of 10^{-10} amperes are readily available with a few foot-candles of illumination. This current is too small to affect the breakdown voltage of the main gap, but produces enough residual ionization to allow breakdown times of the order of 100 microseconds to be obtained with a few volts overvoltage. The high resistance connection to the main cathode may be of the order of 20 to 50 megohms. It protects the photocathode from deterioration which might result from high currents when the main gap is conducting.

Recovery of breakdown voltage following conduction is rapid. Measurements indicate that the breakdown voltage is within the limits of 190 $\pm$ 10 volts in less than 500 microseconds. The relatively high gas pressure and close spacings speed up the deionization process.

The tube described has not been designed for large scale manufacture although several hundred models have been made and tested to establish the feasibility of the design.

SUMMARY

Some useful switching properties of gas diodes can be described by defining the switching-voltage gain. This gain is shown to be equal to the difference between the breakdown and the sustaining voltage divided by the variation in the breakdown voltage. The gain is reduced if faster switching times are required.

The switching-voltage gain is discussed in terms of the physical processes in a gas discharge. It is shown that a high gain can be obtained by using an inefficient anode operating at the minimum of the curve

of breakdown voltage versus the product of gas pressure and anode distance.

A tube is described which uses these principles to achieve a high gain over a useful operating life of 4,000 hours, and which has a negative resistance to audio frequency signals superimposed on the dc operating current. Fast switching is obtained by an auxiliary photoelectric cathode formed by making an electrical connection to a barium getter flash. Satisfactory tube operationg has been obtained for continuous operation for times which are equivalent to 20 to 40 years of intermittent operation in switching systems.

ACKNOWLEDGEMENT

The author is indebted to many members of the gas tube and switching systems development groups at Bell Telephone Laboratories. Among these special mention should be made of A. D. White who originated the cavity hollow cathode and V. L. Holdaway, B. T. McClure, A. M. Wittenberg and C. Depew who made important contributions to the successful development of the tubes.

BIBLIOGRAPHY

1. M. J. Druyvesteyn and F. M. Penning, Rev. Mod. Phys., 12, p. 97–102, 1940.
2. Ibid., page 105.
3. R. N. Varney, Phys. Rev. 93, p. 1156, 1954.
4. Reference 1, p. 139.
5. M. A. Townsend, W. A. Depp, B.S.T.J., 32, pp. 1371–91, 1953.
6. Reference 1, p. 116.
7. F. G. Heymann, Proc. Phys. Soc., 63, Sec. B, 1950.
8. H. L. Von Gugelberg, Helvetica Physica Acta, 20, pp. 307–340, 1947.

Activation of Electrical Contacts
by Organic Vapors

By L. H. GERMER and J. L. SMITH

Unreproducibility of earlier work on the erosion of relay contacts has been traced to the effects of organic vapors in the atmosphere. Carbon from decomposition of these vapors greatly alters the conditions under which an electric arc can be initiated and can be sustained. The importance from the standpoint of erosion comes from the fact that for many circuit conditions contacts activated by this carbon cannot be protected against severe arcing by any conventional capacitance-resistance network. This paper reports investigations which have enabled us to understand the activation of contacts by organic vapors.

TABLE OF CONTENTS

INTRODUCTION

Contamination of surfaces by organic vapors is a subtle factor that influences the electrical erosion of relay contacts. Because of this contamination, contacts in the telephone plant sometimes erode very much more than one would expect from simple laboratory life tests. This caused considerable confusion until about 1945 when the influence of organic vapors was recognized. The term "activation" is used here to describe changes in the surfaces of electrical contacts which give rise to greater arcing when an electrical circuit is completed or broken than would occur if the metal surfaces were clean.* Although its cause is generally carbon from organic vapors, there are occasionally other causes. This paper is an account of recent research[1] on activation produced by organic vapors.†

It has been found that the carbon that causes activation is formed on the electrode surfaces by decomposition of adsorbed organic molecules. Microscopic examination of contacts gives a very sensitive way of detecting incipient activation, since the carbon can easily be seen before any electrical effects are observed. The minimum amount of carbon necessary for activation is of the order of 0.05 microgram.

Activation has been produced on noble metals only, and only by unsaturated ring compounds. When experiments are carried out on clean noble metal surfaces under controlled conditions which do not permit burning of carbon, it is found that the amount of carbon formed by an arc corresponds to approximately a monolayer of organic molecules on the area heated by the arc. After a surface has become active, the amount of carbon formed by each arc is considerably increased and corresponds to the decomposition of several monolayers of molecules. In air, the situ-

---

* The term "activation" has sometimes been used heretofore to signify enhanced erosion resulting from organic vapors. This is a different definition from that used in this paper, due to the fact that in some cases, long sustained arcs produce less erosion than arcs of shorter duration. This is often true for silver surfaces, as described below. In a case of this sort, a surface may have a great deal of carbon on it and be very "active" by our definition, when it would be considered not active at all by the definition that relates activation to rate of erosion.

† Other causes of activation will not be considered here. See Reference 2, page 961.

ation is much complicated by burning of carbon and by the impedance offered by air to diffusion of molecules to the electrode surfaces. Because of these complicating factors, activation will not occur in air if the vapor pressure is too low or if the time between arcs is too short.

Arcs at the making and breaking of clean contacts — clean in the sense that they are free from carbon — produce transfer of metal from one contact to the other with a resulting pit and mound of about equal volumes. The situation is greatly changed by carbon. The presence of carbon causes increased arcing, alters the characteristics of the arcs, and greatly changes the resulting erosion both in character and amount. With carbon present, some or even all of the eroded metal does not stick to the electrodes, and there is often loss of metal from both of them, the missing metal turning up mixed with carbon in a loose black powder. With carbon on the surfaces, successive arcs occur at different places, and the resulting erosion tends to be smooth with the electrodes worn down uniformly all over their surfaces. This is because each arc burns off carbon at its center, while it produces more around its periphery where the metal is cooler, and each new arc strikes on a newly carbonized surface.

Every arc, of either the active sort or of the "inactive" sort which occurs at clean surfaces, is predominantly an arc *in metal vapor*. The active arcs, as well as the arcs at clean surfaces, are of one or the other of two quite distinct types which have been called, respectively, "anode arcs" and "cathode arcs" (Reference 3 and 4 which are concerned with palladium electrodes only). In an anode arc, most of the metal of the arc is vaporized from the anode by electron bombardment, but in a cathode arc the metal is supplied from the cathode by the explosion of small areas due to Joule heating by field emission currents of enormous densities flowing through them. In an anode arc, the erosion is predominantly from the anode, and in a cathode arc from the cathode.

Whether a particular arc is of the anode or of the cathode type is determined by the electrode separation and the contact metal. For palladium electrodes, an arc is an anode arc if the separation is less than about 0.5×10^{-4} cm, but a cathode arc if the separation is greater than this value. The corresponding critical distance for silver is 3 or 4×10^{-4} cm. The carbon particles producing activation permit breakdown at separations for which it would not occur in the absence of carbon, and thus favor cathode arcs. The critical distance of palladium is so small that all active palladium arcs are cathode arcs, with the greater loss of metal from the cathode. For silver, on the other hand, the critical distance is so large that active arcs at silver surfaces are in many cases anode arcs, with the greater loss of metal from the anode as in the case of inactive silver arcs.

PART I — ELECTRICAL EFFECTS

1. OBSERVATIONS ON ACTIVATION

Just how different the behavior of contacts can be in the clean or inactive condition, and in the active condition, is shown strikingly by the oscilloscope traces of Fig. 1. Each trace represents a plot against time of the voltage across a pair of protected relay contacts when the contacts are pulled apart to break a current through an inductive load. The circuits used with the two pairs of palladium contacts were identical, the only difference of any sort being in the conditions of the surfaces of the contacts produced by exposure of the second pair of contacts to organic vapor. In the trace of Fig. 1(a), the potential across the contacts
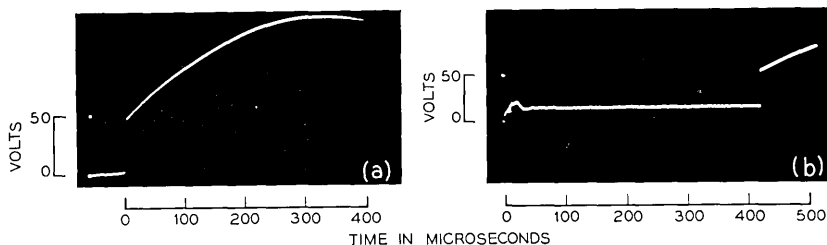
Fig. 1 — Oscilloscope traces of the voltage across relay contacts breaking a current of half an ampere through an inductive relay load. In each case a standard protective network of a 0.5 μf capacitor in series with 100 ohms is in parallel with the contacts. (a) Clean or "inactive" contacts, with no observable arc. (b) Active contacts, with a sustained arc lasting 400 microseconds.

rises abruptly on break from zero to 50 volts, and then continues to increase as the capacitor of the protective network is gradually charged up; there is no arc or other discharge at the contacts. In the trace of Fig. 1(b), the potential rises on break to about 14 volts and remains at this value for 400 microseconds. This represents an electric arc that occurred across the contacts, the 14 volts being the potential characteristic of arcs over short distances at pallaium electrodes (Reference 2, Table II). The energy dissipated at the contacts by this arc was about 25,000 ergs.

A number of worth while experiments upon activation can be carried out with no better method of measuring, or detecting, activation than the observation of oscilloscope traces like those of Fig. 1, or corresponding traces obtained from contacts discharging a small capacitor on closure (Reference 2, Fig. 1). One can find what organic vapors produce activation, and what metals can be activated. This can be extended to discover

what vapor pressure is needed and how the minimum pressure depends upon the conditions of the test; for example, upon the electrical test circuit. Some results of simple tests of this sort will be given before going on to present anything more fundamental about what is happening when contacts become active.

Activation is produced, in general, by repeated operation of a pair of contacts closing or breaking an electric circuit in air containing an organic vapor. At the beginning of a test of this sort, oscilloscope traces look the same as they would look in the absence of the vapor, but with continued operation, arcs may begin to occur when there were initially no arcs, or the durations of arcs may become greater. Activation is not produced by simply allowing contacts to stand idle in an activating vapor even for very long times, and even when the partial pressure of the vapor is extremely high. Nor is activation produced unless currents are made or broken. Operating contacts "dry" in a high pressure of an activating vapor does indeed make them temporarily active,* but this condition is unimportant from the standpoint of erosion. Under conditions that are effective in producing activation, the number of operations required before increased arcing can be detected is usually greater than 100, and often greater than 10^4.

In general, noble metals can be activated by organic vapors and base metals cannot. Vapors of unsaturated ring compounds produce activation and other organic vapors do not. Tests have been made upon the metals Ag, Au, Cu, Pd and Pt which can be activated and upon Co, Cr Fe, Mn, Mo, Ni, Sn, Ta, Ti and W which have not been activated.† The vapors of nearly 50 organic compounds have been tested, about half of them unsaturated ring compounds which produce activation, and about half other compounds which do not. (These are listed, in part only, in Reference 2, Table 1). A very large number of tests have been carried out upon benzene, limonene and styrene. For these three compounds the minimum partial pressures which just produce activation of silver electrodes in air under certain standard conditions, and of platinum electrodes in air, for which the results are the same as for silver, were found to be respectively 0.1, 0.03 and 0.003 mm Hg.

Some insight into activation is obtained by direct examination of active contacts. Black soot can always be seen on active contacts, and if they have been operating for some time in activating vapor, the amount of soot may be great enough to produce a visible deposit under-

---

* See the Section 7.3 on "Brown Deposit."

† Ni and W have been activated in the presence of an organic vapor in a container in which the pressure of air was reduced to 0.01 mm Hg, Reference 5, page 1090.

neath the electrodes. It is clear that the increased arcing of activation is caused by solid carbonaceous material made by decomposition of organic vapor and not by the vapor itself. Clean metal contacts can, in fact, be made to show all of the symptoms of activation by allowing soot from a flame to settle on their surfaces.*† Activation produced in this way is, of course, temporary, lasting only until the deposited soot is burned away.

When one looks for characteristics of arcs between active surfaces to which numerical values can be attached, four features come at once to mind — the electric field at which an arc strikes, the voltage across the arc after it is established, the minimum arc current (which is just the current at which the arc goes out), and finally, after the arc is over, the amount of metal that was gained or lost by each of the electrodes during the arc. All of these quantities have been measured for active arcs as well as for arcs at clean surfaces, and a brief summary of the results of the measurements is given here.

1.1 *Striking Field*

To measure the electrode separation at which an arc strikes between closing electrodes, relay contacts were operated repeatedly, discharging on each closure a capacitor charged to a measured voltage. An arc at each closure was assured by using short leads between the capacitor and the contacts to keep the circuit inductance very low. The time from the initiation of the arc to the touching of the contacts was measured on an oscilloscope.‡

Fig. 2 illustrates the results of measurements made by F. E. Haworth[7] upon palladium electrodes closing at 30 cm/sec to discharge a very small capacitor charged to 50 volts. Before the start of the experiment the electrodes had been cleaned by repeated arcing in air, and the first experimental point represents the closure of these clean electrodes. All of the other measurements were made in air containing a fairly high partial pressure of limonene vapor. Each point plotted on the curve rep-

---

* Unpublished work of P. P. Kisliuk.

† It is interesting to point out that a surface is not made active by rubbing petrolatum upon it, although activation will occur very quickly if an electric current is made or broken at such a greasy surface, so that some of the grease is decomposed.

‡ For inactive arcs, it is necessary to make a correction for the height of the mound of metal thrown up by the arc (Reference 6, page 1136). After the contacts become active, there is no appreciable mound thrown up (at palladium surfaces), and the electrode separation at the initiation of the arc is calculated at once from the closure time and the previously measured electrode velocity. The height of the mound produced before the contacts are active was minimized by using a capacitance of only 40×10^{-12} farad.
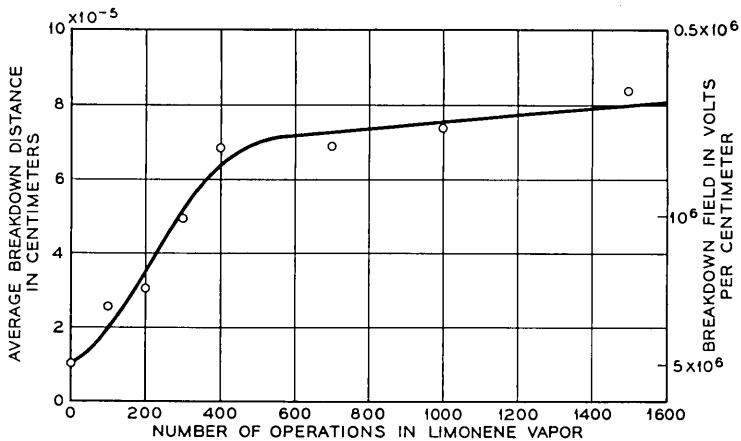
Fig. 2 — Breakdown distance, and apparent striking field, for arcing at relay contacts on closure in the presence of limonene vapor, plotted against number of operations. Each closure discharges a very small capacitor charged to 50 volts. Contacts are clean and inactive at the beginning of the test.

resents the average of 100 separate measurements. During tests of this sort, it was discovered that, with frequent microscopic examination of the electrodes, black sooty material could easily be seen after the first 30 closures, before certain evidence of activation could be obtained in any other known way. In Section 4.1, it is shown that this material is carbon.

The average electrode separation at which an arc struck between clean electrodes at the beginning of the curve of Fig. 2 was about 1×10^{-5} cm and after the electrodes became covered by sooty material, about 8×10^{-5} cm. The apparent striking field was decreased by activation from 5×10^6 to 0.6×10^6 volts/cm. When measurements were made at 250 volts, rather than 50 volts, the striking field in the active condition was only slightly higher, 0.8×10^6 volts/cm. Activation produces a lowering of the apparent striking field, regardless of the value of the applied voltage.*

1.2 *Arc Voltage*

The observed voltage across an arc at active palladium contacts agrees in general with that of palladium cathode arcs, which is about 16 (Reference 4, Fig. 7 and Reference 2, Table II), whereas the arc voltage of

---

* This apparent contradiction of the conclusion of F. E. Haworth[7] is clarified in Section 2.1.
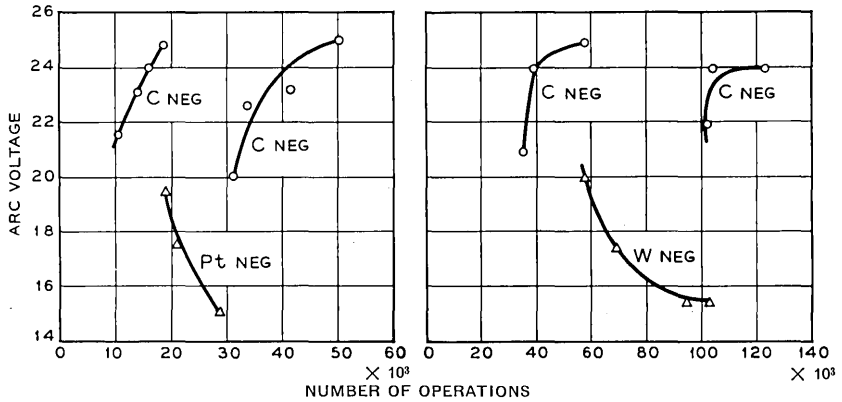
Fig. 3 — Measurements of arc voltage at cathode arcs between a carbon-platinum pair of electrodes, and between a carbon tungsten pair — at successive reversals of striking potential.

carbon is much higher and quite variable in the range from 20 to 30. One is tempted to conclude from this that the vapor in an arc between active palladium contacts is predominantly the metal of the electrodes, not carbon vapor. A more sound conclusion, however, as will be pointed out later, is that the source of electrons on the cathode of an active arc is palladium metal rather than carbon.*

When contact surfaces are very heavily carbonized, an arc voltage substantially higher than that characteristic of the metal of the electrodes is sometimes observed for a short time at the beginning and at the end of an active arc occurring at the discharge of a capacitor into an inductive circuit. An example of this is shown in the oscilloscope trace of Fig. 4. The higher arc voltage at the beginning of this arc, when the current was extremely small, is interpreted as the initiation of the arc between carbon surfaces, and the enhanced voltage at the end is evidence

---

* A very simple experiment has been carried out which proves conclusively that the character of an arc of the type which we call a cathode arc (see below, and Ref. 3 and 4) is determined by the properties of the cathode, and not by those of the anode. This is perhaps self evident, but a direct test is reassuring. The test is simply the observation that, for an arc of the cathode type between electrodes of different materials, the arc voltage is substantially the same as it would be if both electrodes were of the cathode material. The test is made by reversing the potential between the electrodes repeatedly, and after each reversal observing that the arc voltage changes gradually from that characteristic of the anode to that characteristic of the cathode. After each reversal the arc begins to clean from the cathode the anode material that was deposited there before the reversal, when what is now the cathode was the anode. Accompanying this cleaning, the arc voltage goes up or down until it reaches the value characteristic of the cathode itself. Measurements obtained in this way are reproduced in Fig. 3 for a carbon-platinum pair of electrodes and for a carbon-tungsten pair.

that when the current was again small the arc was localized at a new position on a fresh carbon surface so that it was again a carbon arc; during most of the arc time, when the current was larger, the cathode surface was maintained so free from carbon that the source of electrons at the cathode was palladium metal rather than carbon. For lightly carbonized surfaces, which may be just as active as judged by arc duration or any other test that we know of, no such enhanced arc voltage at the beginning or at the end of an arc has been observed. It may well be that for lightly carbonized surfaces the arc voltage is characteristic of carbon for a time too short to be detected by this crude means.

1.3 Minimum Arc Current

The current at which an arc goes out is readily found by observing on an oscilloscope the potential across closing contacts discharging a capacitor through a non-inductive resistor R. At extinction, the potential rises from the arc voltage v to that across the capacitor V_1. The minimum arc current is then $(V_1 - v)/R$. An oscilloscope trace showing such a determination of minimum arc current at the arc initiation potential of 400 volts is reproduced as Fig. 5. (See also Reference 2, Fig. 5 and

Fig. 4 — Oscilloscope trace representing the voltage across an arc at the closure of very heavily carbonized electrodes. Discharge through an inductance of 10^{-4}h of a capacitor of 10^{-8}f charged to 50 volts. Near the beginning and near the end of the arc the source of electrons at the cathode was a carbon surface.

VOLTS

50

0

TIME IN MICROSECONDS
0   3   6
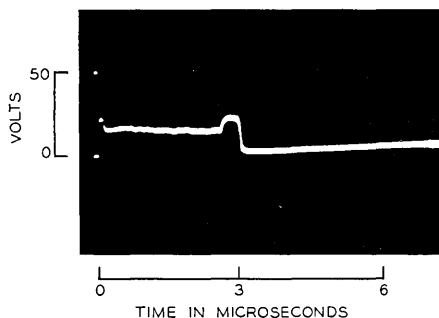
Fig. 5 — Voltage across clean palladium contacts when a capacitor charged to 400 volts is discharged through a resistor of 200 ohms. The closure arc went out at the minimum arc current 0.42 amp.

VOLTS

400

0

TIME IN MICROSECONDS
0   5   10
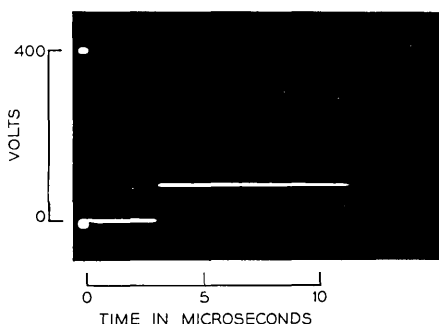
Reference 8, Fig. 1). The minimum arc current is much lower for active contacts than for inactive or clean contacts, and one can perhaps think of the decrease of the minimum arc current for noble metal contacts from a value of the order of 1 ampere for clean surfaces to 0.1 ampere or less for active surfaces as the chief characteristic of activation.

1.4 *Erosion*

Active contacts of palladium and of silver transfer metal in quite different ways. The transfer at active silver contacts is the more complex, and for this reason the transfer that occurs at active palladium contacts
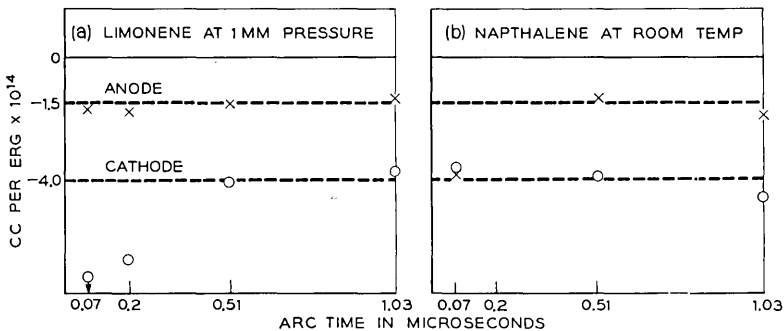
Fig. 6 — Results of measurement by weighing of the erosion of palladium electrodes produced by active arcs in limonene vapor (a) and in napthalene vapor (b).

will be taken up first. The behavior of platinum is in general like that of palladium, and gold is like silver.

1.4 (a) Palladium and Platinum. It is found that arcing on closure at active contacts of palladium or platinum causes loss of metal at the cathode of the order of 4×10^{-14} cc/erg. The anode often loses metal also, but the loss at the anode is considerably less and may be zero in some cases. The results of two sets of measurements upon active palladium contacts are plotted in Fig. 6. These data represent changes in volume (calculated from weighings) per unit of arc energy after repeated arcs in limonene vapor at a vapor pressure of 1 mm Hg, Fig. 6(a), and in the vapor of napthalene saturated at room temperature, Fig. 6(b). Tests were made by closing electrodes to discharge on each closure a properly terminated fixed length of cable charged always to 200 volts, to give in each case a constant arc current of 4 amperes, with the arc lasting for the time determined by the cable length. For the shortest arc time, the energy of

each of the individual arcs was 40 ergs, and for the longest arc time 600 ergs. The results indicate no significant variation of the erosion per unit of energy over this range.

There is some evidence that arcs at the break of active palladium surfaces give significantly lower cathode erosion per unit of energy (1 or 2 $\times$ 10^{-14} cc/erg) than do arcs at closure. The reason for the difference is not clearly understood, but widely different currents and electrode separations may be significant factors.

By examining contacts of palladium or platinum after many active arcs (on either break or closure), it is found that the erosion tends to be uniform over the surface, wearing each electrode down smoothly, with much less loss from the anode than from the cathode. This type of wear is quite different from that produced by arcs at clean surfaces. Erosion by arcs at clean surfaces always gives a mound of metal on one electrode, with a corresponding pit in the other; the loss of metal from one electrode is not appreciably greater than the gain by the other, the entire erosion consisting simply of transfer of metal between the contacts.

Now the inactive arcs at clean surfaces are known to be of two types which have been called "anode arcs" and "cathode arcs."[3, 4] In anode arcs, the transfer of metal is about 4×10^{-14} cc/erg and is from anode to cathode, with a resulting pit in the anode and a matching mound on the cathode (Reference 9, page 1085–1086). In inactive cathode arcs, measurements made in the same way and not yet published have shown that the transfer is smaller — about 1×10^{-14} cc/erg — and is in the opposite direction, from cathode to anode, with a resulting pit in the cathode and a matching mound on the anode.[10] It will be shown later, Section 2.4(a), that arcs at active palladium surfaces are of the cathode type, each individual arc being not readily distinguishable from an inactive cathode arc in the effect it produces on the cathode surface. The reason for the net cathode loss being greater in an active cathode arc than in a cathode arc at clean surfaces is due, at least in part, to some reverse transfer in an arc at clean surfaces.

1.4 (b) Silver and Gold. The erosion of silver surfaces is quite complex, and an adequate description of all of the phenomena encountered is reserved for later publication.[10] A simplified description of the main features of the erosion of silver contacts is given here. Tests upon active gold contacts have been less extensive than upon active silver contacts, but as far as the observations go, gold has been found to behave just like silver.

At active silver surfaces the erosion is, in most cases, from the anode, as it is at inactive surfaces. The arcs are active anode arcs, see Section

2.4(b), which have never been observed at palladium contacts. The metal lost from the anode after a great many active anode arcs tends to be eroded smoothly over the entire surface, like the cathode loss in arcs of the cathode type at palladium contacts. At a moderate pressure of activating vapor, almost all of the metal eroded from a silver anode is transferred to the cathode, but at a high pressure much of it is lost. Whether the metal from the anode is transferred or lost is correlated with the amount of carbon formed by the active arcs; if the production of carbon is small, metal is transferred, but in the presence of much carbon, the metal does not stick to the cathode and is lost. The amount of carbon formed (in air) by active anode type arcs at silver surfaces is very much less than the amount formed by active cathode type arcs at palladium surfaces, and this difference accounts for the fact that a great deal of the eroded metal is transferred at active silver surfaces, although there is always very little transfer at active palladium surfaces.* The erosion of a silver anode by active anode arcs may be as great as 10^{-13} cc/erg, but is lower than this whenever the carbon formation is sufficiently slight to permit much transfer of metal.

Long, sustained break arcs at active silver surfaces become cathode arcs when the electrode separation becomes sufficiently great. Such arcs give cathode erosion resembling that at active palladium surfaces. For a long sustained break arc, the cathode erosion suffered when the electrode separation becomes very large may be greater than the anode erosion occurring when the electrodes are closer together, so that the net loss from the cathode may be the greater. There may even be a small net anode gain.

Measurements of transfer at electrical contacts have sometimes been very confusing in the past, both because of their complexity and because of their apparently erratic character. Now, with well developed insight into the mechanism of short arcs, this complexity of transfer and its varied character have been most useful in improving our understanding of short arcs and of the transfer of metal to which they give rise.

The over-all picture of activation will be given in the following pages.

2. INTERPRETATION OF ACTIVATION

After one has concluded that activation is due to solid carbonaceous material, it is natural that tests should be made upon contacts of solid

---

* At extremely low pressures of activating vapor, active anode arcs at silver surfaces may not only transfer to the cathode practically all of the metal lost from the anode, but the type of erosion may even be changed to the mound and pit type characteristic of inactive arcs.[1]

carbon, and upon metal surfaces on which carbon particles have been dusted. The results of these tests have supplemented measurements upon active noble metal contacts and have led to a great increase in our knowledge of activation. In fact they open the way to a fairly thorough understanding of the subject.

2.1 Striking Field

Five different experiments have been carried out, which were designed to discover the reason for the low striking field at active contacts. Although the results of these experiments do not establish the reason for the low striking field in any definitive fashion, they do lead to an explanation which seems entirely satisfying.

The simplest of these experiments has already been reported at the end of Section 1.1. It is the observation that the striking field at active contacts is much the same at different striking voltages, of course below air breakdown only.

In another experiment, not heretofore published, W. S. Boyle and P. Kisliuk produced active spots at various points along a palladium wire. The wire, which lay on the axis of a glass cylinder, was made active at these selected points by repeated short arcs in an atmosphere containing limonene vapor. The other electrode was operated by an electromagnet outside the cylinder, with the magnet arranged so that the electrode could be placed at any location along the wire or withdrawn completely at any time. After activating a number of points, as determined by continuous oscilloscopic observation, the cylinder was exhausted and field emission currents were drawn from the wire to the cylinder. From observation of a fluorescent coating on the inside of the cylinder, it was found that the positions along the wire, which gave the largest currents, were quite unrelated to the active spots. From this experiment, one can conclude that the work function of active spots along the wire was not lower than the work function of other parts of the wire, and also that there was no significant enhancement of field emission at these spots because of roughness. Thus, the activation of contacts by organic vapors is not due to enhanced field emission currents because of lowering of the work function or because of greater surface roughness.

In a third experiment by F. E. Haworth,[7] measurements were made of the electrode separations at which an arc strikes between a palladium electrode and a smooth palladium surface upon which carbon particles had been deposited. For this experiment, solid carbon particles of fairly uniform size were obtained by blowing air at a low controlled rate

TABLE I — EFFECT OF CARBON PARTICLES UPON
STRIKING DISTANCE

Range of Particle Size (by microscopic measurement)	Average Striking Distance at 50 Volts	Apparent Striking Field
No Particles	0.10×10^{-4} cm	5×10^6 volts/cm
0 to 1×10^{-4} cm	1.4	0.36
0 to 2.5	2.5	0.20
4 to 5	4.3	0.12

through agitated carbon dust and collecting the particles that had been carried upward for a considerable distance in the air stream. The time of deposition of these particles upon the smooth surface was adjusted to give an average distance between particles of about 10 times their diameters. The smooth palladium surface with a fairly uniform, but sparse covering of carbon particles was made the cathode in measurements of striking distance by the oscilloscope method, Section 1.1. For a particular size of particle, 100 measurements were made of striking distance, each measurement at a different point on the surface, so as not to include any measurement of striking distance at a place on the surface where the original particles had already been burned off.* Table I gives the ranges of particle size as found microscopically and the corresponding average measured values of striking distance. The increase of striking distance was just equal to the particle size. At each arc, a particle was destroyed so that the time to closure measured on the oscilloscope corresponded, not to the true striking distance, but to the distance from the anode to the cathode surface upon which the particle rested. The electric field at which the arc struck was very much higher than the calculated values of the third column of Table I, and was not significantly different from the striking field for inactive surfaces.

In the fourth experiment, the striking field was measured between electrodes of solid carbon. One of these was mounted upon a cantilever bar in such a way that it could be moved through extremely small measured distances by pushing on the end of the cantilever bar using a micrometer screw (Reference 4, page 33). The zero point was found by touching the contacts through a high resistance galvanometer circuit; then the contacts were separated and the striking distance found after applying the voltage. Measurements made in this way by M. M. Atalla (Reference 11, Table I) have given, for the striking field for carbon elec-

---

* A correct measure of striking distance is obtained only when the arc energy is sufficient to burn up the carbon particles completely. No appreciable mound of metal is thrown up to falsify the distance measurement, because the arcs are of the cathode type, see Section 2.4(a).

trodes, 2.4×10^6 volts/cm, and our unpublished measurements agree with this. The striking field for carbon surfaces is thus only a little less than that found for cathode arcs at clean metal surfaces (Reference 4, Fig. 8), and very different from the field at which arcs strike between active surfaces.*

In another experiment, tests were carried out upon carbon particles in the 4 to 5×10^{-4} cm range of diameters, deposited sparsely upon a palladium surface as before. A careful comparison was made of the electrode separations at which an arc struck at 50 volts and at 250 volts. At the higher voltage, the distance was greater than at the lower voltage by the factor of only 1.3, offering confirmation that the isolated carbon particles act chiefly as chunks of material, partially closing the electrode gap.

The one way in which the carbon that produces activation differs from other carbon, and in particular from small carbon particles dusted sparsely upon a smooth metal surface, is in the very large number of its particles and in its state of subdivision. This gives an eminently plausible clue to the great electrode separation at which breakdown occurs between active surfaces. According to this model, breakdown occurs at a great separation between active surfaces because, at the electric field corresponding to this separation, electrostatic forces become sufficient to cause motion of small particles which decreases the separa-

---

* In measuring the striking field at carbon surfaces for low voltages by the oscilloscopic method, a value of the order of 0.6×10^6 volts/cm was found earlier (Reference 6, Table I). This result was certainly in error, because of burning of carbon in the arc, so that the separation of the electrodes when the arc ended was greater than it was at the arc initiation.

To check this explanation of the earlier incorrect result, an experiment was carried out in which the time to closure for carbon electrodes was measured as a function of the energy in the arc. In successive tests, a number of different capacitors, each charged to 50 volts, were discharged on the closure of carbon electrodes. The time to closure was found to increase progressively with capacitance for the values 10^2, 10^3, 10^4 and 10^5 $\mu\mu$f. Carrying out the measurements many times and taking average values, it was found that the time to closure increased linearly with the cube root of the capacitance. This suggests strongly that a hole was being burned in one of the electrodes and the increased time to closure was just the time for one electrode to move the depth of the hole. A quantitative value for the volume of the hole can be obtained from the data, on the basis of an assumed hole shape. In earlier work (Reference 9, page 1088), a pit on a metal electrode was assumed to be a spherical segment with the depth equal to one-half of the pit radius. Making the same assumption for the hypothetical hole in the present tests, and assuming an electrode velocity on closure of 30 cm/sec, it turns out that the relationship between volume of the hole and energy of the arc is $V = 4.5 \times 10^{-12}$ cm³/erg. The agreement of this result with that for the erosion of the metal anode in an anode arc (Reference 9, page 1088), is remarkable and must be largely fortuitous. The agreement does, nevertheless, make almost certain that burning of one of the electrodes (the cathode, as we know from other work) is the reason for the oscilloscopic method giving incorrect values for the electrode separation at which an arc strikes between carbon electrodes (Reference 6, Table I).

tion. The experimentally observed field of 0.6×10^6 volts/cm is the field at which this motion becomes appreciable for the very small sooty particles. With the start of motion of this sort the field is increased, and further motion is assured making the situation unstable. The gap is greatly decreased in length before *electrical* breakdown takes place, and the field at electrical breakdown is probably as high as it is at any carbon surface.

2.2 *Arc Voltage*

At the beginning of an active arc, at least one carbon particle is always exploded by the arc current, but only when the surface is very heavily carbonized is an enhanced arc voltage observed, Fig. 4. It must not be thought that the higher arc voltage occasionally found at the beginning of an arc is to be attributed directly to the presence of carbon vapor in the arc during its early stages, because carbon does not have an exceptionally high ionization potential. P. Kisliuk has shown[12] that, in a field emission short arc, the arc voltage should be just slightly larger than the sum of the ionization potential of the metal of the electrodes and of its thermionic work function. Now this result holds quite well for a number of different metal arcs, but does not hold at all for carbon. The short carbon arc is apparently of a different type, and has no well defined arc voltage. On the other hand, although carbon, unlike the noble metals, gives out thermionic electrons copiously long before it is hot enough to vaporize, a true thermionic arc cannot have the enormous current densities that occur in short arcs. (It does not seem impossible that thermionic emission may help to maintain an arc when the current is lower near its end.) The high arc voltage at the beginning and end of an active arc between heavily carbonized surfaces may be due to a dearth of positive ions, requiring a higher applied field to maintain the field emission. In any case, it is like the higher arc voltage of carbon which we do not understand. When the higher arc voltage is not detected, the vaporization of metal must be profuse, and only when vaporization is reduced, as it is when the current is very small near the beginning and end of an arc at the discharge of a capacitor into an inductive circuit, is the higher arc voltage observed. On rare occasions heavily carbonized surfaces show a suddenly enhanced arc voltage for a short interval near the middle of an arc. That this should occur very much less often than at the beginning or end of an arc is understandable.

The observation that the arc voltage sometimes becomes high near the end of an arc suggests strongly that an active arc is moving continually during its life. Only when the current is insufficient to vaporize carbon and underlying metal freely, and thus to maintain the large ion

density necessary for the low voltage field emission arc, does one observe the high and erratic arc voltage characteristic of carbon.

2.3 Minimum Arc Current

Values of minimum arc current for carbon electrodes have already been published. They are of the order of 0.02 to 0.06 ampere and agree fairly well with measurements of minimum arc current for very active metal contacts (Reference 2, Table V). The very low value of the minimum arc current for carbon, either in solid form or dispensed upon the surfaces of active contacts, is related to the low electrical and thermal conductivities of carbon. These low conductivities permit explosion of carbon particles on the cathode by currents too small to vaporize any metal. It has already been pointed out that it is this very low value of minimum arc current which accounts for the greatly enhanced energy that is dissipated at active relay contacts.

From the low value of minimum arc current for active surfaces, one concludes that near its end an active arc is always located at a fresh point on the electrode surfaces, one from which carbon was not burned off earlier in the life of the arc. It had already been concluded from occasional high values of arc voltage near the end of an active arc that this is sometimes true, but the minimum arc current values extend this earlier conclusion to indicate that it is *always* so. An active arc cannot remain in a fixed position as does an inactive anode arc (For example, Reference 4, Fig. 1). The implication is thus suggested that any arc between active palladium contacts is a cathode arc. Further presumptive evidence for this is, of course, furnished by the very much greater electrode separation in the case of active arcs; it is well known[13] that large distances favor cathode arcs, because at great distances the anode cannot be efficiently heated by electron bombardment.

The interpretation of minimum arc current of active cathode arcs to which we have been led can be written down in words, but we have not succeeded in any quantitative formulation. It is well known that every cathode arc is made up of a great number of small arcs moving continually over the electrode surfaces and exploding one point, or one particle after another on the cathode.[3, 4] In the case of an *active* arc, the end comes when the current gets so low that it will no longer explode a carbon particle, or when no suitable particles are available.* The much

* This is a necessary criterion for the end of an active arc only in the case of very short arcs. For electrodes that are being pulled apart to break a current larger than the minimum arc current, an arc will, of course, finally fail because of the great electrode separation, even though the current is above the minimum arc current, as in the final failure of the arc in the oscilloscope trace of Fig. 1(b). For inactive anode arcs the minimum arc current arises in a quite different way and has been interpreted in fairly satisfactory quantitative fashion.[14]

higher minimum arc currents for cathode arcs at clean surfaces is attributed to the higher thermal and electrical conductivities of metals and to the absence of loose material making poor contact with the surface. This picture is supported by the observation that metal contacts are made temporarily active by almost any kind of loose surface particles of very small size (Reference 2, Page 961).

2.4 *Erosion*

2.4(a) Palladium and Platinum. Further evidence that an active arc at palladium or platinum surfaces is always a cathode arc is furnished by the fact that the cathode loses much more metal in an active palladium arc than does the anode. (See also Reference 4, Table I).

The direct way of proving that an active arc at palladium or platinum surfaces is a cathode arc would, of course, be microscopic examination of the contact surfaces after a single arc. This is not practicable because surfaces become active only after repeated arcs, but one can do what is apparently quite equivalent by looking at the damage done by a single arc to surfaces on which small carbon particles have been dusted. Experiments by Haworth do indeed prove that arcs at such surfaces are cathode arcs, even at the low striking potential of 50 volts, and when the maximum diameter of the carbon particle is only 1×10^{-4} cm. Fig. 7(b) is typical of many examinations by Haworth of palladium cathodes after a single arc at surfaces upon which carbon particles had been deposited. The striking potential was 50 volts and the capacitance that was discharged was $C = 10^{-8} f$, so that the energy $C(V_0 - v)v$ was 50 ergs. For comparison, photographs are reproduced in Figs. 7(a) and
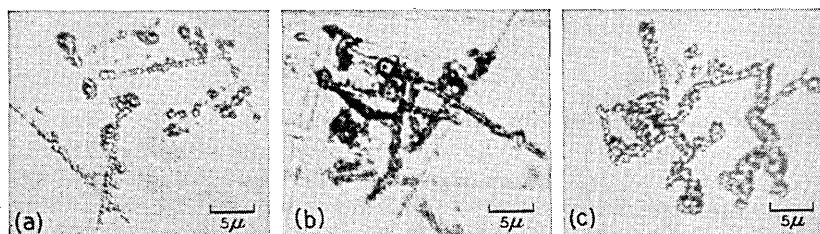
Fig. 7 — Photomicrographs of palladium cathode surfaces after single cathode arcs. The photograph of (b) was obtained after a 50 erg arc with 50 volt striking potential at a surface upon which carbon particles has been deposited. This sort of cathode damage was observed for all of the different sizes of carbon particles which were tested, even for the smallest having diameters of only 10^{-4} cm. The comparison photographs (a) and (c) represent the damage done respectively by 40 erg and 80 erg arcs to palladium surfaces without carbon particles, each arc at the striking potential of 400 volts.

7(c) which show clean palladium cathodes after constant current cathode arcs of 4 amperes lasting, respectively, for 0.072 microsecond and for 0.14 microsecond. The striking potential in each of these arcs was 400 volts, the total arc energy being 40 ergs and 80 ergs. The three photographs of Figs. 7(a), 7(b) and 7(c) represent then the markings made on the cathode by arcs of 40, 50 and 80 ergs respectively. The voltage of 400 was chosen for the two comparison photographs of Figs. 7(a) and 7(c) because this is above the minimum air breakdown potential, and arcs on closure at striking potentials above this value are known to be always cathode arcs (Reference 4, Fig. 4).

Cathode markings such as those of Fig. 7(b) are occasionally produced by arcs at 50 volts on relatively clean palladium surfaces. In general, however, an arc at this low striking potential between clean surfaces is an anode arc, leaving a single well defined pit on the anode, and on the cathode, a single roughened area with considerable metal spattered over from the anode (Reference 9, Fig. 6). While a cathode arc, making on the cathode the type of markings shown in Fig. 7, is rather rare between clean palladium surfaces at a striking voltage as low as 50 (Reference 4, Fig. 4) it is the usual kind of arc between surfaces upon which carbon particles have been dusted, and by implication, it is the sort of arc that occurs between active surfaces. That this arc should cause loss of metal from the cathode is clear from the photographs of Fig. 7, and from the fact that the damage done to the anode sometimes cannot be detected and is always rather slight.*[10] Between clean surfaces, this sort of arc occurs more frequently at higher striking voltages, and invariably on closure when the potential is above the minimum breakdown potential for air. It is the greater striking distance that favors the cathode type of arc, and for active arcs also it is just this enhanced electrode separation, resulting from carbon particles, which can be thought of as the reason for the arc being of this type. There is obviously a critical distance above which arcs are of the cathode type, and for palladium electrodes this critical distance is less than 1×10^{-4} cm. Earlier experiments can be used to define this critical distance better. From the data of Fig. 8 of Reference 4 it appears that this distance for palladium is about 0.5×10^{-4} cm.

Markings made on the cathode by a single arc between active palladium surfaces are doubtless not easily distinguishable from those resulting from a single arc that has been constrained to be of the cathode type only by a high striking potential and the resulting great electrode separation. Nevertheless, when many times repeated, the over-all results

* See the footnote relating to Fig. 3, see page 776.

of cathode arcs between active surfaces, and of cathode arcs between inactive surfaces, are markedly different, as has been pointed out earlier.

The fact that erosion by inactive, or clean-surface, arcs takes the form of a mound on one electrode and a crater in the other means simply that successive arcs tend to occur at the same place on the electrode surfaces. This is because each arc must occur where the electric field between approaching electrodes is highest, and the roughening from one arc will be the site of the highest field before the next discharge occurs.

With carbon particles on the surface, the situation is different. In the case of active cathode arcs, the electric field between approaching electrodes is highest at a point where a group of carbon particles, perhaps pulled up by electrostatic forces, closes a large part of the electrode gap, and an arc must necessarily strike at such carbon particles. In the activating process, carbon is always being formed by an arc, but only at its periphery; at the hottest parts of the arc, carbon which was formed earlier, is completely removed. Not only does each arc move during its lifetime, continually searching out new carbon which was formed earlier, but a later arc will not strike at a point from which carbon was just cleaned by an earlier arc. This restless movement from point to point results finally in erosion that spreads over the surface in a way which is likely to be statistically uniform.

2.4(b) Silver and Gold. Although the character of the erosion at silver (and gold) surfaces, and also its magnitude, are drastically altered by activation, Section 1.4(b), the "direction" of the erosion is still in most cases that characteristic of anode arcs. The predominant loss of metal on closure is usually from the anode for active silver electrodes at voltages too low for air breakdown, just as it is for inactive silver electrodes at low striking voltages. This is in marked contrast to the behavior of palladium surfaces when they become active; for active palladium surfaces, loss of metal is always chiefly from the cathode. The behavior of silver leads naturally to the hypothesis that even when the surfaces are active arcs at low striking voltages are anode arcs, as they are when the surfaces are inactive.

This hypothesis has been subjected to test by F. E. Haworth by the same method used in the case of palladium surfaces. Small carbon particles were dusted on a polished silver surface, and the surface was examined microscopically after it had been subjected to a single arc under the circuit conditions used in similar tests at palladium surfaces. When the maximum particle diameter was 5×10^{-4} cm, it was found from the microscopic examination that all arcs were of the cathode type (see, for example, Fig. 7), but when the maximum diameter was 2.5×10^{-4}

cm all arcs were of the anode type with the characteristic pit on the anode and a roughened spatter of metal on the cathode. It is clear from these tests that active arcs at silver surfaces are of the anode type if the layer of carbonaceous material responsible for activation is not heavy enough to permit an arc to strike at a separation greater than 2.5×10^{-4} cm, but that they are of the cathode type when the layer is sufficiently thick to permit arcs at 5×10^{-4} cm. The electrode separation at which an arc takes place determines the character of the arc.* The critical distance for silver surfaces lies between 2.5 and 5×10^{-4} cm. Erosion at active silver surfaces on closure must be predominantly from the anode unless the layer of activating carbonaceous material is so heavy that arcs strike when the electrode separation is greater than 2.5×10^{-4} cm.

After long continued operation at very high pressures of activating vapor it is sometimes, but not always, found that arcs on closure result in erosion that is chiefly from the cathode. The conclusion drawn from these measurements is that the striking distance at active surfaces on closure at low voltages can sometimes, with considerable difficulty, be made greater than 2.5×10^{-4} cm. Unless great pains are taken to keep surfaces very heavily carbonized, the striking distance on closure at active surfaces at low voltages is of the order of 2.5×10^{-4} cm or less. On closure at voltages that give air breakdown, the erosion of silver is predominantly from the cathode whether the surfaces are active or inactive, because the minimum distance for air breakdown (15×10^{-4} cm) is much above the critical distance for silver.

On breaking active silver contacts in an inductive circuit, erosion is chiefly from the anode unless the arc lasts long enough for the electrode separation to exceed the critical distance of 3 or 4×10^{-4} cm. During the time an arc persists at distances greater than this, the loss is predominantly from the cathode. For velocities typical of a U-type relay, the critical distance may be reached in 10 or 20 microseconds, and equal erosion may be attained in a time of the order of 40 microseconds. If the partial pressure of activating vapor is very high and the surfaces unusually heavily carbonized, much of the eroded metal will be lost. Under more usual conditions of lower vapor pressures, most of the eroded metal is transferred to the opposite electrode. Thus there may be a critical arc duration for which the erosion of each silver electrode is nearly

* Similar tests were carried out upon polished gold surfaces upon which sparse layers of carbon particles had been dusted. For particles of maximum diameter 2.5×10^{-4} cm all arcs were found by microscopic examination of the electrodes to be anode arcs, and for particles in the range of diameters from 4 to 5×10^{-4} cm all arcs were found to be of the cathode type. These results are identical with those found for silver.

zero, and for an arc lasting longer than this time, there may be cathode loss and actual net gain by the anode. No such balancing effect is possible for palladium.

2.4(c) Anode Arcs and Cathode Arcs. The model of an active cathode arc to which we have been led seems fairly clear and rather well established, but the model of an active anode arc is more poorly defined. From electron micrographs of the damage done to the cathode by an arc of the cathode type (Reference 4, Fig. 3), it is known that an arc of this type is intermittent, striking over and over again. In an *active* arc of the cathode type, a carbon particle on the cathode is blown up each time the arc strikes, but always there is metal vaporized from the cathode at the site of the particle and the amount of vaporized cathode metal is greater than the amount of vaporized carbon, so that the arc is an arc in metal vapor.

We know less of an active anode arc, and it may well be that some experiments described above seem to imply a model which is not consistent with other observations. The facts that we know are, that at a lightly carbonized silver surface an arc strikes at an electrode separation much greater than the separation at which it would strike if there were no surface carbon, that the resulting arc produces loss of metal predominantly from the anode, and finally that the minimum arc current is very low. The arc is a true anode arc by our implied definition of such an arc, yet it is certainly an active arc. When the arc current is high, a crater is being produced on the anode as in the case of an inactive anode arc, and also in the case of an active anode arc at a surface on which a few carbon particles of diameters not greater than 2.5×10^{-4} cm have been dusted. When the current becomes too low, or is too long sustained, one presumes that the arc is extinguished as in the case of inactive anode arcs.[14] It may then restrike at another carbon particle. One speculates that an anode arc is intermittent when the arc current is very low, being initiated over and over again as are cathode arcs throughout their lives. A carbon particle is exploded repeatedly on the cathode. Yet, because the separation is less than the critical distance, at each re-ignition of the arc, metal vapor is derived from the anode rather than from the cathode, and possibly the over-all anode erosion results in a single anode pit produced when the current was sufficiently high, plus an array of very small anode pits formed while the current was small and intermittent. This model must be regarded as a plausible speculation without support in direct observation. The existence of the active anode arc is well established although the course of such an arc is speculative.

Some insight into the reason for the existence of a critical electrode

separation, determining whether an arc is of the anode type or of the cathode type, can be obtained from a simplified picture of the evaporation of metal in an arc. One assumes a field emission arc just being established between a cathode point and the anode surface, the initial ions being supplied by oxygen and nitrogen of the air with as yet no metal vaporization. The electrons from the point are assumed to travel in straight lines to the anode and cover uniformly an area $\pi(L \tan \theta)^2$ where L is the electrode separation. If i is the total electron current and v the arc voltage, the power density on the anode is $iv/\pi(L \tan \theta)^2$, decreasing with increasing separation. A lower limit for the power put into the cathode point is $(\rho/d)i^2$ where d is the diameter of the point and ρ the resistivity of the cathode metal. Whether the anode begins to vaporize before the cathode, or vice versa, is determined in some way by the ratio of these quantities $BL^2\rho/d$, where parameters unimportant for the present discussion are grouped together in B. For $L^2\rho/d$ greater than some critical value, we shall have cathode evaporation and an ensuing cathode arc, but for $L^2\rho/d$ less than this value, the anode will begin to evaporate first with a resulting anode arc.

The resistivity that probably counts is the resistivity at the melting point. At the temperature of melting, the resistivity of palladium is nine times greater than that of silver. Thus one can expect from this simple model that the critical distance which determines whether an arc is of the cathode or anode type will be three times greater for silver than for palladium. If a silver point is less sharp than a palladium point, d greater for silver than for palladium, as it may be because of the well known property of silver atoms to migrate at room temperature, the factor will be greater than this value of three. Now we have the experimental estimate of 0.5×10^{-4} cm for the critical distance for palladium. This simple theory predicts that the critical distance for silver shall be greater than this by a factor of three, or perhaps more. The experimental critical distance for silver is between 2.5 and 5×10^{-4} cm.

Quantitative measures of the erosion of contacts of palladium and of silver, which were given in Section 1.4, are collected in Table II for ready reference.

From additional experiments, not reported in Section 1.4, it is known that these values of transfer apply approximately for potentials both above and below the minimum breakdown potential for air. Not all types of arcs occur, however, for both palladium and silver at potentials above and below the minimum breakdown potential. At potentials that give air breakdown, all arcs on closure are of the cathode type for both metals whether active or inactive. At potentials that do not give air

TABLE II— LOSS OR GAIN OF METAL FROM ARCING FOR
PALLADIUM OR SILVER

(in units of 10^{-14} cc per erg)

	Cathode	Anode	
Inactive Arcs			
Anode Type............	4 gain	4 loss	mound and pit
Cathode Type.........	1 loss	1 gain	mound and pit
Active Arcs			
Anode Type............	(loss)	10 loss*	smooth erosion
Cathode Type.........	4 loss†	(loss)	smooth erosion

* This high figure refers to arcs on closure at very heavily carbonized surfaces; for lightly carbonized silver surfaces the anode loss is less and most of the metal is transferred to the cathode.
† This figure refers to arcs at closure of palladium surfaces. The rate of cathode loss at break of palladium surfaces is significantly less, as pointed out in Section 1.4(a); and in cathode arcs at active silver surfaces the rate of loss is still less.

TABLE III— OCCURRENCE OF DIFFERENT TYPES OF ARCS

	Below Air Breakdown	Air Breakdown
Inactive Arcs		
Anode Type..............	Palladium, Silver	No*
Cathode Type............	Palladium Only	Palladium, Silver
Active Arcs		
Anode Type..............	Silver Only	No*
Cathode Type............	Palladium, Silver	Palladium, Silver

* This applies to arcs at closure. Between separating electrodes, air breakdown often occurs when the electrodes are too close together for air breakdown over the shortest path. Under such conditions, arcs between silver surfaces, which are *initiated* by air breakdown, can become anode arcs, and the transfer resulting from such arcs gives dominant anode erosion.

breakdown, all inactive arcs at silver surfaces are of the anode type, and active arcs of the anode type occur for silver only. These facts are tabulated for reference in Table III. All of them are at once predictable from the values of the critical distances for palladium and silver, and from knowledge of the way in which breakdown distance is changed by activation.*

---

* The difference between the transfer behavior of palladium and silver electrodes in the active condition suggested to R. H. Gumley that the damaging effects of activation can be greatly reduced by constructing a relay with negative contacts of silver and positive contacts of palladium. He tried out this idea and found it to be effective. In the absence of activating vapor, a relay in which the negative contacts are silver and the positive contacts palladium has no merit over a relay in which all contacts are palladium, but when vapor is present, the erosion can, under some circumstances, be much reduced by replacing the negative palladium contacts by silver contacts.

The sort of erosion produced by the different types of arcs is shown in the somewhat conventionalized sketches of Fig. 8. These sketches represent cross-sections of the square mating areas (about 1.3 mm on a side) of heavy type U relay palladium contacts. The contact contours are drawn to scale after the metal transfer resulting from repeated arcs with a total energy of 10^8 ergs, using the values of Table II to convert this energy into volumes of metal. The mounds and pits produced by inactive anode arcs and by inactive cathode arcs are assumed to be spherical segments, each having a height equal to half its radius. The smooth erosion resulting from active arcs would have depths which do not show up at all on the scale of this figure. For each electrode in each of the four cases, the erosion is less than 2 per cent of the total volume of the metal of the contact, and represents a fairly early stage in the expected contact life. The electrode separations at which arcs occur correspond respectively to fields of 8×10^6, 4×10^6 and 0.5×10^6 volts/cm. The striking voltage is assumed to be 50 and the separations are drawn
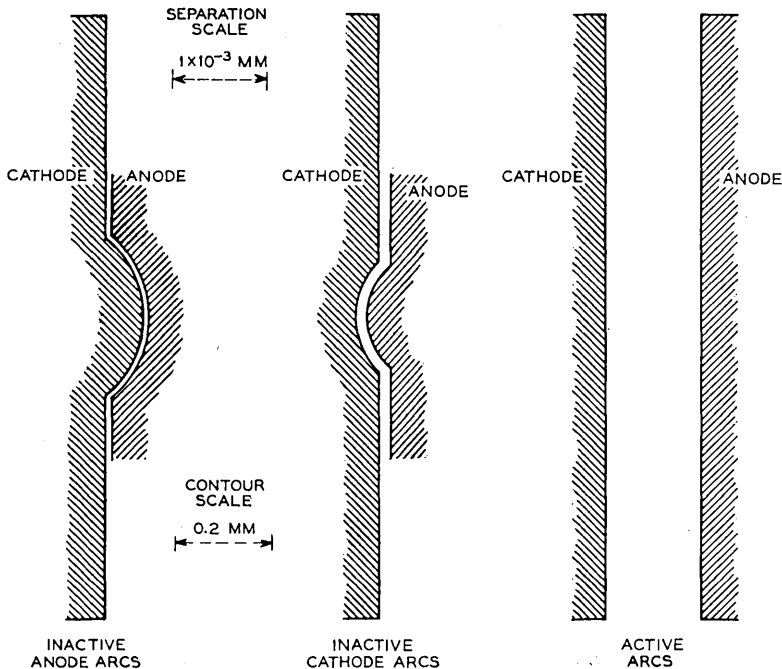
Fig. 8 — Erosion produced by anode arcs at clean surfaces, by inactive cathode arcs and by active arcs of either type, the total energy in each case being 10^8 ergs. The electrode separations at which these arcs strike correspond to 50 volts and are represented here on a greatly expanded scale.

to a scale 200 times greater than the scale of the electrodes. For potentials that give air breakdown, the scale of separation would be changed by large factors.

The sketches of Fig. 8 are of assistance in understanding some of the qualitative erosion differences observed in the four types of arcs (Table II). All of the metal lost from one of the electrodes in an inactive arc of either type comes from the surface of a pit, and from the figure it seems clear that all of it must obviously be intercepted by the other electrode because there is no way for it to escape. This is true even for the case of air breakdown where the electrode separation is much greater ($\sim$15 $\times$ 10^{-4} cm). But for active arcs some of the metal coming from each electrode is permanently lost and not transferred to the other side, even though the separation is much less than it is for the case of air breakdown. The permanent loss of metal in the case of active arcs is due to the presence of carbon. When there is carbon on the surfaces, the metal simply does not stick. Chemical analyses have been made of the black powder produced by active cathode arcs at palladium surfaces, and these analyses show palladium metal as well as carbon. The palladium metal lost from the electrodes turns up in this black powder rather than at new locations on the electrodes.

At palladium surfaces, the net loss amounts to most of the eroded metal, but at silver surfaces, most of the metal is transferred. This difference is related to the amount of carbon left on the surfaces. Carbon is found much more abundantly on palladium than on silver, which accounts for the failure of eroded metal to stick to palladium. The greater net carbon production on palladium is due to the low efficiency of cathode arcs (at active palladium surfaces) in burning carbon; the anode arcs, which occur in general at active silver surfaces, are more effective in burning off carbon. It is to be presumed that the amount of organic vapor decomposed per unit of energy at a silver surface is not so very much less than that decomposed at a palladium surface, even though the net carbon left on the surface is tremendously less in the case of silver.

3. RECAPITULATION

We are ready now to state briefly some of the conclusions about active arcs which have been developed above. All of the observations refer to contacts of palladium or of silver. Less extensive tests upon platinum and upon gold have indicated that platinum behaves the same as palladium, and gold the same as silver.

An active arc is an arc that strikes between one electrode and car-

bonaceous material lying upon the other. If one calculates striking field by dividing the potential by the separation between the metal electrodes, a very low value is obtained, but this is the field at which electrostatic forces cause movement of carbon particles to decrease the separation; the true field at which the arc finally strikes between carbonaceous material and the opposing electrode is not significantly lower than the striking field for arcs at clean surfaces. Some or all of the local carbonaceous material is burned up by the arc, and metal vaporized from one of the electrodes is soon fed into the arc so that for most of its life the ions of the arc are metal ions supplied by atoms from one or the other of the electrodes. This is true for even the most heavily carbonized electrodes.

There is a critical electrode separation, characteristic of the metal of the electrodes, which determines whether the arc is an anode type of arc with metal supplied by the anode or an arc of the cathode type with metal supplied by the cathode. If the separation is greater than this critical value the arc is a cathode arc, and less than this value an anode arc. This critical distance is about 0.5×10^{-4} cm for palladium electrodes and of the order of 3 or 4×10^{-4} cm for electrodes of silver. The ratio of these distances is somewhat greater than the ratio of the square roots of the electrical conductivities of the metals at their melting points. The critical distance for palladium is so small that all arcs at active palladium surfaces are cathode arcs. For silver, on the other hand, the critical distance is so large that most arcs at low voltages at silver surfaces are anode arcs. In any practical application of silver electrodes, the carbonaceous material formed is rarely or never in a sufficiently thick layer to result in cathode arcs for closure at low voltages. In the case of separating silver electrodes, an active arc may last until the electrode separation is beyond the critical distance for silver; the erosion occurring after this distance is reached is predominantly from the cathode, and the larger net loss may, on occasion, be from the cathode.

The erosion resulting from repeated arcing at active surfaces is different in character from that produced by inactive arcs. Inactive arcs give rise to a crater on one electrode and a matching mound on the other, with most of the metal from the crater transferred to the mound. Active arcs, on the other hand, produce smooth erosion without craters and mounds, often with considerable net loss of metal which appears mixed with carbon as a black powder. This smooth erosion is accounted for by the striking of each new arc on carbon formed by preceding arcs, together with the burning off of carbon at the center of each arc and the formation of new carbon around its periphery.

PART II — ACTIVATING CARBON

4. COMPOSITION OF ACTIVATING POWDER AND RATE OF PRODUCTION

Experiments have been carried out designed to discover the chemical composition of the carbonaceous material responsible for activation, how much is made per unit of energy in an arc, and where it is made. Now it has been pointed out above that the reason for the uniform erosion in an active arc is the burning off of this black powder by arcs and the consequent continual wandering of successive arcs always to neighboring spots from which the powder has not been burned. This burning off of black powder makes quantitative measurements in air of its rate of formation quite impractical. Activation in vacuum avoids the destruction by burning, and makes possible direct measures of rate of formation; in these tests, the chemical composition of the powder can be found also. All of the quantitative studies of activation in vacuum were made by P. Kisliuk, but the results have not been previously published.

In Kisliuk's experiments two electrodes, which were of platinum, were mounted in a glass chamber so they could be operated by the magnetic field of a coil placed outside the chamber, in the manner of a dry reed switch. The electric circuit was arranged to discharge on each closure a capacitor charged to a fixed voltage, with no current flowing in the circuit as the platinum contacts are separated. Air was pumped out and the contacts operated in benzene vapor at a constant rate, discharging the capacitor a convenient number of times per minute. Every experiment consisted of measuring the pressure in the system, from which was deduced the rate of disappearance of benzene and the rate of evolution of hydrogen resulting from its decomposition, hydrogen being distinguished from benzene by freezing out the latter in liquid nitrogen. The pressures were measured by an RCA thermocouple gauge (1946) which was shown in control tests not to produce benzene decomposition. The benzene, which had been distilled repeatedly to remove water vapor, was used at initial pressures not to exceed 10^{-2} mm Hg determined by a dry ice-acetone bath. The experimental arrangement is shown in Fig. 9.

4.1 *Composition*

In the first experiments with this system it was found, as had been expected, that with continued operation of the contacts in benzene vapor, the pressure rose steadily, although benzene continued to disappear. The pressure changes corresponded to the evolution of 3.2 $\pm$ 0.6 molecules of H_2 for each vanishing molecule of benzene, agreeing well with

the theoretical value of 3 for complete decomposition of benzene into carbon and hydrogen. The conclusion from this experiment is that the organic material in the black activating powder is just carbon. The precision allows one to say that, if there is any hydrogen at all left in the black powder, it does not exceed 2 hydrogen atoms for every 15 carbon atoms.

4.2 *Rate of Production*

In experiments in which the energy in individual arcs was varied, by using different capacitors in the range from 610 $\mu\mu$f to 40,000 $\mu\mu$f and by using the two potentials 58 volts and 232 volts, it was found that a particular arc energy gives the same carbon formation per erg whether the striking voltage is 232 or 58, from which one deduces that formation of carbon depends upon energy rather than upon capacitance or voltage separately. The amount of carbon formed per individual arc increases with the energy of the arc but not so fast as linearly. The experimental values M of amount of carbon formed can be related to arc energy E by the empirical formula $M = KE^{2/3}$, over the range studied from 5 ergs to 1,250 ergs. A tentative explanation of this $\frac{2}{3}$ power relation is given in the next section.

Starting with clean electrodes and measuring the total amount of carbon formed as a function of number of arcs, it was found that the rate of production of carbon is initially low but increases with time, soon
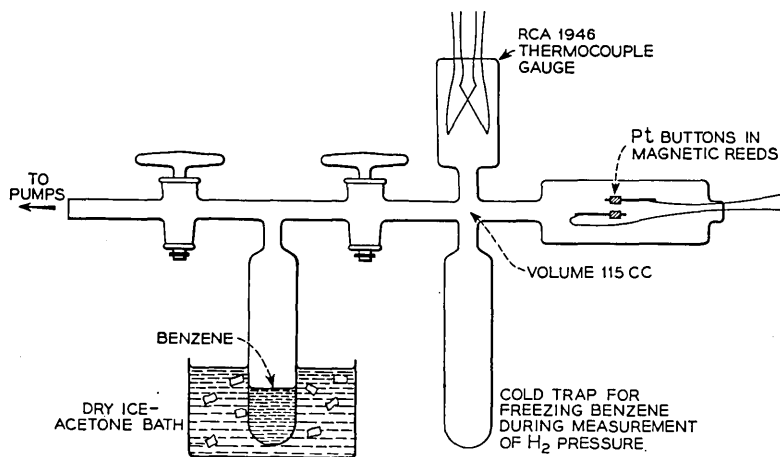

Fig. 9 — Diagram of apparatus used by P. Kisliuk in quantitative measurements of the decomposition of benzene vapor at arcing contacts.

becoming constant. One such set of measurements is plotted as Fig. 10. In this experiment the striking voltage was 232 and the energy in each arc 1,250 ergs. The final slope of the curve of Fig. 10 corresponds to the production of 4.5×10^{-11} gm of carbon per arc — 3.5×10^{-14} gm/erg, 1.8×10^9 atoms/erg — which is 0.04 carbon atom for every electron flowing in the arc, or the decomposition of 3.7×10^{11} benzene molecules per arc, 3×10^8 molecules per erg, or 70×10^{-4} molecule per electron. The lower slope, before the break in the curve, represents the decomposition of 1.1×10^{11} molecules of benzene per arc, or the production of 5×10^8 carbon atoms per erg.

From continuous oscilloscopic observations it was found that the contacts were inactive up to the point where the slope of the curve increased. Here they were slightly active, and beyond this point they were fully active, exhibiting the usual apparent low striking field and low minimum arc current. The amount of carbon required to make the contacts fully active was about 5×10^{-8} gm (2.5×10^{15} atoms) which, if it were in a single spherical speck, would have a diameter of 3.5×10^{-3} cm. Such a speck can be seen quite easily with the naked eye, although an actual deposit of this volume probably could not be seen without a microscope because of its dispersed state.

5. SURFACE ADSORPTION

5.1 *Benzene Molecules on Contact Surfaces*

In an early experiment, the rate of formation of carbon (from measured rate of evolution of H_2) had been found to be independent of benzene pressure down to the lowest pressure tested, which was of the order of 10^{-3} mm Hg. For this reason it was unnecessary to mention absolute pressures in describing the above tests. This lack of dependence on pressure suggests strongly that benzene had been adsorbed on the electrode surfaces and decomposed there, rather than in the space between the electrodes, and that the lowest pressure tested was sufficiently high to keep the surfaces completely covered. This tentative conclusion is confirmed by other considerations given below.

At the pressure of 10^{-2} mm Hg and an electrode separation of 10^{-4} cm, one calculates that only one electron in 3×10^4 can collide with a benzene molecule in the space between the electrodes in the experiment of Fig. 10. The discrepancy between the measured decomposition (70×10^{-4} benzene molecule per electron) and the possible frequency of collision (0.3×10^{-4}) is proof that most of the carbon responsible for activation comes from benzene adsorbed on electrode surfaces rather than from molecules in the space between them.

One gets some insight into the adsorbed films responsible for activation from estimates of the cross-section of an arc and of the amount of benzene adsorbed in a monolayer over an area of this size. A reasonable estimate of the number of molecules in a monolayer of benzene is 7×10^{14} cm^{-2} (Ref. 16), or 14×10^{14} cm^{-2} taking into account the two electrodes. Estimates of cross-sectional size have been published for anode arcs, but for cathode arcs the areas are quite different. Since all of the arcs after a surface has become active are certainly cathode arcs, our first concern is with the cross-sectional areas of cathode arcs. It has been observed that the over-all area of the cathode markings made by inactive cathode arcs increases somewhat less rapidly than linearly with total arc energy, and seems to be independent of arc current and arc duration except as they influence the total energy. In one series of experiments, the areas observed (Ref. 10) for low energy arcs corresponded to somewhat less than 10^7 ergs/cm^2, and to somewhat more than this value for high energy arcs. Assuming for an average value 10^7 ergs/cm^2, we obtain 1.2×10^{-4} cm^2 for the area of the arcs of the curve of Fig. 10.* This area should have adsorbed on it 1.7×10^{11} benzene molecules. The observed rate of decomposition is 3.0×10^8 benzene molecules per erg or 3.7×10^{11} molecules per arc. Looking at photographs such as those of Fig. 7, one does not feel at all confident that all of the surface in the over-all area of the arc ever became hot enough to decompose benzene. If all of it did become hot enough, the surface must, on the average, have been covered by 2 layers of molecules, and if all of the surface did not become sufficiently hot, by more than two layers. For lower energy arcs, when the number of benzene molecules decomposed per erg is appreciably greater, it is natural to assume that the surface must, on the average, be covered by a still deeper layer of benzene. At least part of the difference between the estimated thicknesses of the layers of benzene molecules for high energy arcs and for low energy arcs can, however, be attributed to the fact that the energy per square centimeter increases with increasing energy, 10^7 ergs/cm^2 being only an average value. The data indicate only that the adsorbed benzene layer is several (greater than 2) molecules thick.

The observed expression $M = KE^{2/3}$ of the above section, relating amount of carbon formed M to total arc energy E, can be accounted for if, in the particular experiment in which this relation was found, the over-all arc area increased with the $\frac{2}{3}$ power of the energy. In various tests

* One should note that the energy density measurements were made upon clean surface or *inactive* cathode arcs, but are being applied here to *active* cathode arcs. Some justification for this is afforded by the fact that the active 50 erg cathode arc of Fig. 7(b) had an over-all area of about 3×10^{-6} cm^2 giving for the energy density 1.5×10^7 ergs/cm^2.

it has been noted that area increases less rapidly than linearly with energy, but it is certain that no universal rule applies in all cases; for example, by restricting the total electrode area, the over-all arc area can be forced to be constant independent of energy.[10] One can conclude only that all of the facts are accounted for by a benzene layer several molecules thick on the electrode surfaces with decomposition by each arc of all of the benzene within its over-all area.

We are now in a position to consider the much lower rate of decomposition of benzene during the initial period before the electrodes became active. In Fig. 10, this lower initial rate is 1.1×10^{11} molecules per arc. This is somewhat less than the number of molecules calculated to lie in a monolayer on the surface covered by an arc. The area used in this calculation was that of a cathode arc, but it is well known that before contacts become active a large proportion of the arcs are anode arcs which have smaller areas (Reference 9, page 1088). The estimated area may, however, be about correct because in the case of an anode arc, carbon is decomposed by heat over an area larger than that of the arc itself.

Within the precision of the estimates we are able to make, it can be said that for inactive contacts operating in benzene vapor each arc decomposes a single layer of adsorbed molecules of benzene. After the contacts become active, the amount decomposed by each arc is greater and is the equivalent of several layers of molecules. It was surmised long ago that much of the vapor adsorbed on active contacts is held by carbon already on the surface rather than by the surface metal. The increased
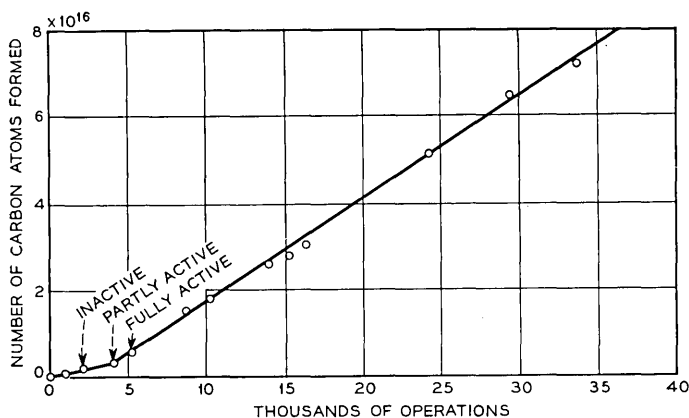

Fig. 10 — Measurements by P. Kisliuk of the amount of carbon formed at arcing platinum contacts, each arc 1,250 ergs. The final slope represents the production of 3.5×10^{-14} gm of carbon per erg of arc energy, or one benzene molecule decomposed for every 150 electrons flowing in the arc.

TABLE IV — BENZENE DECOMPOSITION IN ACTIVE AND
INACTIVE ARCS

Measurements		1250 erg arcs (232 volts)	15 erg arcs (58 volts)
Carbon required for full activity	1	2.5×10^{15} atoms	No data
Carbon formed in active arcs	2	1.8×10^9 atoms/erg	7×10^9 atoms/erg
Carbon formed in inactive arcs	3	5×10^8 atoms/erg	No data
Benzene decomposed in active arcs	4	3.0×10^8 molecules/ erg	13×10^8 molecules/ erg
	5	70×10^{-4} molecule per electron	300×10^{-4} molecule per electron
Calculations			
Absorbed benzene in a mono- layer (Ref. 16)	6	14×10^{14} molecules per cm^2	14×10^{14} molecules per cm^2
Benzene molecules struck in space (Compare lines 5 & 7)	7	0.3×10^{-4} molecule per electron at 10^{-2} mm Hg	0.03×10^{-4} molecule per electron at 10^{-3} mm Hg
Active Arcs			
Arc area at 10^7 ergs/cm^2	8	1.2×10^{-4} cm^2	0.015×10^{-4} cm^2
Number of molecules in one monolayer on arc area	9	1.7×10^{11} molecules	0.02×10^{11} molecules
Decomposed per arc (from line 4)	10	3.7×10^{11} molecules of benzene	0.2×10^{11} molecules of benzene
Effective* thickness of adsorbed layer on basis of 10^7 ergs/cm^2	11	2.2 molecules	10 molecules
Inactive Arcs			
Arc area	12	$<1.2 \times 10^{-4}$ cm^2	
Number of molecules in one monolayer on arc area	13	$<1.7 \times 10^{11}$ mole- cules	
Decomposed per arc (from line 3)	14	1.1×10^{11} molecules	No data
Thickness of adsorbed layer	15	1 molecule	No data

* The benzene is probably adsorbed on spongy carbon of much greater true area.

adsorption for contacts already active is doubtless due to the greater surface area resulting from the presence of this carbon.

Many of the numerical values considered here are collected in Table IV for ready reference. These data refer to arcs at platinum surfaces. It is our present opinion that the amount of carbon formed at silver surfaces in similar experiments would be found to be only slightly smaller per unit of energy, although unfortunately no experiments were carried out upon silver.

5.2 *Inhibiting Surface Films*

One concludes from the above experiments that activation by benzene vapor is the result of firm adsorption of benzene molecules on the elec-

trode surfaces, with heat producing decomposition into carbon and hydrogen rather than evaporation of undamaged molecules. Surface films prevent such strong adsorption, and metals with surfaces that are normally covered by oxide films cannot be activated.

In some very recent experiments in extremely high vacuum, P. Kisliuk has found[17] that benzene molecules are strongly adsorbed upon a tungsten surface that is perfectly clean, but if there is on the surface just one single layer of oxygen molecules, benzene molecules are not adsorbed. M. M. Atalla has reported (Reference 5, page 1090), on the other hand, that tungsten (and nickel also) can be activated if the pressure of air is as low as 10^{-3} mm Hg. It seems probable that arcs at operating contacts remove adsorbed oxygen temporarily, and at sufficiently low air pressures this may be replaced in part by organic molecules rather than by oxygen.

Even at palladium surfaces, some cleaning by arcs seems to be necessary before benzene molecules can be adsorbed. This conclusion is reached in unpublished adsorption experiments carried out by W. S. Boyle upon palladium surfaces in air containing benzene vapor. In this work, two optically flat palladium surfaces are separated by an exceedingly small distance to make an electrical capacitor. With a very sensitive capacitance bridge, one can detect the change in capacity that would be produced by the adsorption on the palladium surfaces of even a small fraction of a monolayer of benzene molecules. In experiments carried out with this equipment it was found that benzene molecules are not adsorbed upon a palladium surface in air at atmospheric pressure. To reconcile this conclusion with the well known facts of activation, it seems necessary to conclude that even a palladium surface can adsorb benzene molecules only after it has been partly cleaned by arcing.

5.3 *Alloys*

When a base metal is mixed with a noble metal, the result can be an alloy which is activated less readily by organic vapors than would be the noble metal constituent alone. In the curve of Fig. 11 is plotted the number of operations required under a particular set of standard conditions to activate a series of alloys of palladium and nickel. In air, nickel itself cannot be activated at all. The amount of carbon formed from benzene decomposition on the surface of a palladium-nickel alloy is always less than the amount which would be formed under the same conditions upon pure palladium. One does not know whether benzene is held less firmly on the alloy surface so that there is more likelihood
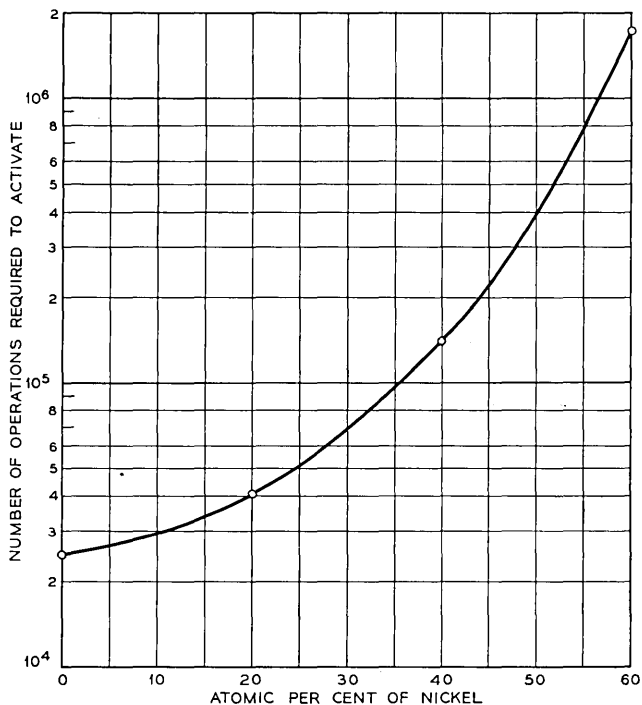
Fig. 11 — Resistance to activation of various alloys of nickel and palladium.

that a heated molecule will evaporate rather than decompose, or whether there are just fewer sites on the surface which can take molecules.

6. ACTIVATION IN AIR

Electrical contacts are not so readily activated by organic vapors in the presence of air as they are when air is absent. Air inhibits the activating process in at least three different ways, and sometimes in a fourth way. These are:

1. Covering up the metal surface so that activating molecules cannot be adsorbed upon it until some of it has been cleaned temporarily by arcing.

2. Offering obstruction in the path of organic molecules on their way to an adsorption site on the metal, so that the molecules diffuse slowly through air up to the surface, whereas in the absence of air, an adsorbed film is formed much more quickly at the same pressure of the organic vapor.

3. Burning off in each arc some of the carbon formed on the surface in preceding arcs.

4. Sputtering and burning off carbon from the cathode in a glow discharge, when such a discharge occurs.

The first of these effects of air has made itself evident in the experiments of Kisliuk, Atalla and Boyle described above. It will not be discussed further. Observations and experiments have been made upon the other three effects of air, and these will be described below. Burning off of carbon in an arc is mentioned first because it can be most nearly separated from other effects and studied individually.

6.1 *Burning of Carbon*

On a surface uniformly covered by organic molecules, carbon must be burned off on the area covered by an arc, but new carbon can be formed on an annular ring surrounding the arc where the metal temperature is lower. As a consequence of this, whereas in the absence of air contacts are activated very much more promptly by high energy arcs than by low energy arcs, in air the situation is less simple. The general result of many experiments is that in air high energy arcs are less efficient in producing activation than are low energy arcs. On the other hand, arcs of extremely low energy are also quite ineffective. There seems to be an optimum arc energy at which contacts can be activated most promptly, which may be of the order of 100 ergs. Activation can be expected to be most prompt when the difference between the area of the arc and the area of the annular ring around the arc is a maximum.

The outer edge of this annular ring is the position on the metal surface at which the maximum temperature just reaches the decomposition temperature of adsorbed organic molecules, about 600°C for the case of benzene. If the width of the ring is Δ and its inner radius R, each arc can be assumed to burn carbon from an area πR^2, and to form new carbon on an area $\pi[(R + \Delta)^2 - R^2]$. Now Δ certainly increases with increasing energy (being zero for zero energy), but on the simplifying assumption that it is independent of energy, the difference area, which is

$$A = \pi[(R + \Delta)^2 - 2R^2] \tag{1}$$

will be a maximum for that energy that makes R equal to Δ. It is interesting to find the value $R = R_1$ for a 100 erg arc, which is known to be very efficient in producing activation, and then to estimate the maximum temperature reached at the outer edge of the annular ring for $\Delta = R_1$. The simple model predicts that this maximum temperature should be 600°C. When the calculation is carried out in rough fashion, the

temperature is found to be of the order of 300°C, rather than 600°C. The correct order of magnitude gives support to the general ideas behind the theory.

According to this very simple model, activation takes place most promptly for arcs of 100 ergs energy, and for such arcs the *net* carbon formed per arc corresponds to the benzene molecules adsorbed on the area $2\pi R_1^2$, which is obtained from Eq. (1) by setting $R = \Delta = R_1$. In vacuum at the same energy, the carbon formed per arc would come from benzene on the area $4\pi R_1^2$. Thus for 100 erg arcs activation will occur almost as quickly in air as in vacuum, but for arcs of greater energy, much more slowly than in vacuum. Qualitative observation has confirmed this general conclusion.

That this picture is, however, over simplified in a fundamental manner is clear from the effect of electrode contours upon ease of activation. For flat electrodes, activation is very much more prompt when the surfaces make good contact over a large area than when misalignment results in contact on a rather small area. Furthermore, flat contacts can often be activated very promptly under conditions for which crossed wires cannot be activated at all. (Reference 8, page 335). In a qualitative way this is understood, but the inhibiting effect of restricted areas is not amenable to quantitative consideration. This effect makes quite clear that the model of an annular ring about an arc is too idealized to be of much quantitative value.

One might expect that the burning off of carbon would be greatly influenced by atmospheric conditions, and thus the ease of activation would depend upon such conditions. This is indeed found to be the case in experiments in which the air contains water as well as the activating vapor. In unpublished experiments F. E. Haworth determined the number of operations required to activate contacts under a particular set of standard conditions for a wide range of relative humidity. In the range from 10 to 88 per cent relative humidity, the number of operations to make contacts fully active increased exponentially from 1.4×10^3 to 1.0×10^6, and at relative humidities of 95, 98 and 100 per cent, activation was not attained at all. Furthermore the process of activation could be reversed by water vapor, and contacts that had been made fully active in dry air containing an organic vapor were made completely inactive by continued operation in the same vapor after the addition of water. The effect of water in these experiments may have been due to covering the surfaces so thoroughly with water molecules that the activating vapor could not be adsorbed, or to burning carbon by the water gas reaction, $C + H_2O \rightarrow CO + H_2$. The exponential relationship between num-

ber of operations required to make contacts active and relative humidity has no clear interpretation in our present state of knowledge.

6.2 *Diffusion of Activating Vapor*

In Kisliuk's vacuum experiments the amount of carbon formed and the degree of activation attained was independent of benzene vapor pressure. This is not at all the case when activation is produced by operating contacts in air. In fact, one of the earliest observations was a minimum vapor pressure below which contacts could not be activated (Reference 2, Table I). In more careful later tests it was found that the minimum vapor pressure is a function of rate of operation of the contacts, the minimum pressure being actually proportional to the rate of operation over a factor of 100 which was the range tested (Reference 8, Fig. 2). Obstruction offered by air supplies the explanation of this rate effect. Activation cannot occur if electrodes are separated between one arc and the next for a time which is short in comparison with the time required to cover the surface with one monolayer of organic molecules. A rough order of magnitude calculation confirms this conclusion.

As an approximation, one assumes one dimensional diffusion to an electrode surface from the space in front of it, with all molecules reaching the surface sticking to it. Boundary conditions for the solution of the diffusion equation, $\partial C/\partial t = D\partial^2 C/\partial x^2$, are then:

$$C = C_0 \text{ at } t = 0 \text{ for } x > 0$$

$$C = 0 \text{ at } x = 0 \text{ for all values of } t$$

The concentration of activating molecules in the space in front of the electrode is then $C = C_0 \, \mathrm{erf} \, [x/2 \, (Dt)^{1/2}]$. The total number of molecules to have reached the surface at any time t_1 is,

$$m = \int_0^{t_1} D \left. \frac{\partial C}{\partial x} \right\}_{x=0} dt = 2C_0(D/\pi)^{1/2} t_1^{1/2}$$

expressed in molecules/cm², when C_0 is given in molecules/cm³. We are interested in the value of t_1 for which m is the number of molecules in a monolayer, and the maximum rate of operation of contacts for activation to occur can be expected to be comparable with

$$n = \tfrac{1}{2} t_1 = 2C_0{}^2 \, D/\pi m^2 = 8.1 \times 10^{22} \, D(p/m)^2, \tag{2}$$

where p is the partial pressure of activating vapor in mm Hg. The factor $\tfrac{1}{2}$ in $n = \tfrac{1}{2} t_1$ appears because diffusion to the surface can occur only when the electrodes are separated, and it is assumed that they are separated for half of the time.

The best data we have for testing this relation are represented by ex-

periments upon activation in vapor of the organic compound fluorene.[8] According to the observations, the critical rate of operation was found to be proportional to the partial pressure of fluorene rather than to its square as in (2). This is a discrepancy which must be overlooked in our present state of knowledge. To test (2) for fluorene at 20°C, we require values of D, the diffusion coefficient of fluorene in air, p, the partial pressure of fluorene at 20°C, and m, the number of adsorbed fluorene molecules per cm^2 of surface. The value of $D = 0.067$ cm^2/sec. was obtained from a linear relation between $1/D$ and (molecular weight)$^{1/2}$, which holds quite well for a number of organic compounds. The value $p = 0.04$ mm Hg is the geometrical mean between 0.23 and 0.007 mm Hg, respectively the vapor pressures of napthalene and anthracene at 20°C. We have estimated $m = 3.3 \times 10^{14}$ molecules/cm^2, which is related to the corresponding number for benzene, 7×10^{14} in the inverse ratio of the molecular weights.[16] These numerical values give from (2)

$$n = 0.75 \text{ operation/second}$$

as the critical rate that will just permit one monolayer in the time the contacts are separated. The observed critical rate for activation at 20°C from Fig. 2 of Reference 8 is 3. The agreement is pretty good when the crudeness of the model is considered.

6.3 *Sputtering and Burning in a Glow Discharge*

If both arcs and glow discharges occur when electrical contacts are operated in an atmosphere containing an activating organic vapor, the activation of the contacts resulting from the arcs is inhibited by the occurrence of the glow discharges.* This effect is sometimes very beneficial in extending the life of telephone relay contacts. In fact a very simple protective network, consisting only of an inductance of the order of 10^{-4} henry placed very close to one of the contacts, has been devised which, under some conditions, will increase the contact life by a factor of about 10.

Quantitative measurements have been made of this inhibiting action of a glow discharge, and from them it has been concluded that the effect is attributable to sputtering and burning of carbon in the discharge. In making these measurements, a pair of contacts was operated in an atmosphere containing limonene vapor in such a way that arcs and glow discharges occurred alternately in controlled fashion. A charged capacitor was discharged in an arc at each closure. By the use of an auxiliary synchronized relay in series with one of the contacts, the circuit was

* It should be pointed out incidentally that a glow discharge in air can also activate silver electrodes. It produces silver nitrite on their surfaces,[18] and silver electrodes with a layer of nitrite are fully active until the layer is burned off.

changed periodically so that a glow discharge could be made to occur at each contact break, or at every 6th, 60th, or 600th break. The glow current was always 0.04 ampere lasting for a time that could be accurately set by means of a synchronized shunt tube.

In all of the tests, the energy in each closure arc was 190 ergs. Measurements were made at partial pressures of limonene of 0.05 and 1 mm Hg. At the lower pressure it was found that the contacts remained inactive indefinitely whenever the time of glow discharge on break was on the average more than 0.25 microsecond for each closure arc, and activation would ultimately take place if the average glow time per closure arc was less than this value. (At the limonene pressure of 1 mm Hg there was a corresponding critical glow time of about 1 microsecond). The obvious interpretation of these tests is that a glow discharge of 0.04 ampere lasting for 0.25 microsecond sputters and burns off as much carbon as is made by an arc of 190 ergs under the conditions of the experiment. To test this conclusion, one needs to know how much carbon is produced by an arc of 190 ergs, and one needs to know the sputtering rate of carbon in a normal glow in air at atmospheric pressure.

Measurements of the sputtering of carbon in a normal glow discharge were undertaken by F. E. Haworth, since such data are not available in published literature. Carbon and graphite electrodes were weighed before and after a normal glow discharge of 0.006 ampere lasting for various lengths of time. The loss of the carbon or graphite negative electrode in nitrogen was found to amount to about 0.15 atom per ion of the discharge. In air the loss was much greater, four times larger for graphite and 15 times larger for carbon (2.3 carbon atoms/ion for carbon in air). The increase in air was attributed to burning, and the difference between carbon and graphite losses in air was believed to be due to smaller crystal size and looser bonding in the carbon case.*

If we use the highest loss figure of 2.3 carbon atoms/ion we find that a glow discharge of 0.04 ampere for 0.25 microsecond should remove 14×10^{10} carbon atoms. From Table IV, one finds that a 190 erg inactive arc in activating benzene vapor produces 9.5×10^{10} carbon atoms in the absence of air (line 3), and an active arc produces 34×10^{10} carbon atoms (line 2).† The net carbon which is left after each arc in air is, of course, considerably less than it would be in the absence of air (Section 6.1), but the order of magnitude agreement between these numerical

---

* The sputtering rate of 0.15 atom/ion for carbon in nitrogen in the normal glow is about what is reported by Güntherschulze[19] for silver in the *abnormal* glow but is greater by a factor of about 400 than that found for silver in the *normal* glow in experiments by Haworth.[18] Obviously sputtering rates for carbon are exceptionally high.

† It is believed that these figures are substantially the same for limonene and for benzene.

values leaves little doubt that we have correctly interpreted the inhibiting effect of glow discharges upon activation.

6.4 *"Hysteresis" Effects*

Sometimes a pair of completely inactive electrical contacts of a noble metal can be activated very quickly, and an apparently identical pair of contacts cannot be activated at all under exactly the same experimental conditions. In the first case a great amount of carbon may be formed, and in the second case no detectable carbon at all. In order to clear up this confusion, some controlled experiments were carried out upon the activation and deactivation of silver and palladium electrodes in air containing benzene vapor at various partial pressures. From these experiments, it has been possible to relate the variability of earlier results to previous history of the contacts, and the entire behavior is now quite well understood.

In these tests adjustable benzene vapor pressure was obtained by first bubbling air at a controlled rate through benzene maintained at constant temperature by a bath of acetone and dry ice, and then mixing the saturated air with clean air in the proper proportions. In certain tests silver contacts were operated in air flowing from this apparatus, discharging a capacitor on each closure. The number of operations required to produce complete activation was measured for many different values of the benzene vapor pressure. With contacts that had been cleaned in a standard way before each test, it was found that the number of closures required for activation rose extremely rapidly with decreasing vapor pressure over a narrow range of pressures. There was always a lower pressure limit below which it seemed impossible to activate the contacts at all. All of the tests were made at the high operating rate of 60 closures per second.

When the contacts had been cleaned by abrasion before each individual test, the minimum pressure below which activation could not be attained was of the order of 2 mm Hg. (This pressure was exceptionally high because of the high operating rate, see Section 6.2.) A different result was found for contacts that had been previously activated and then cleaned only by repeated arcing; for these contacts the minimum pressure for activation was about 0.7 mm Hg. The factor of 3 between these minimum pressures is doubtless related to the fact that, for those electrodes which had been cleaned by arcing only, there existed neighboring carbonized areas which were never cleaned. Each such area can be expected to hold about three times as much adsorbed benzene on the average as does the same area of clean metal, see Section 5.1, and especially lines 2 and 3 of Table IV. Thus for such surfaces more carbon can

be expected to be formed by each arc. The model is not sufficiently well defined to permit any more exact conclusions.

In another experiment, silver electrodes, which had first been completely activated, were operated for a long period at a greatly reduced benzene vapor pressure. It was found that they remained completely active unless the pressure was very much less than the minimum of 0.7 mm Hg at which activation could be produced. In repeated tests at a variety of low benzene vapor pressures, the number of operations required for the contacts to become inactive was recorded. This number was found to increase very abruptly with increasing vapor pressure, and above about 0.02 mm Hg the contacts remained active indefinitely. This result must again be related to the capacity of a mass of spongy carbon to hold a great amount of adsorbed benzene. Very probably the upper limit of pressure below which contacts cannot be deactivated, depends upon the thickness of the carbon layer produced before the benzene pressure is lowered.

Similar but less extensive experiments were carried out with palladium electrodes.

These hysteresis effects observed in the activation and deactivation of contacts seem capable of explaining the erratic observations that had been made previously. If the immediate history of contacts is sufficiently well known, behavior can perhaps be predicted fairly well for various experimental conditions.

7. BROWN DEPOSIT

Closely related to the activation of relay contacts is the formation of polymerized layers of organic material upon contact surfaces as a result of friction. This material, which is commonly known as "brown deposit", is produced at contacts which do not make or break current. Its mode of formation is thus entirely different from that of the carbon which is the cause of activation. Both have, however, a common origin in layers of organic molecules adsorbed upon surfaces. Discovery of brown deposit and most of the investigation of it were carried out elsewhere (Ref. 20), but some discussion of brown deposit is appropriate here because of its relation to the carbon of activation and because of a study of its formation by P. Kisliuk.

7.1 *Composition*

The composition of brown deposit was determined by Kisliuk in an apparatus similar to that used to investigate the carbonaceous material responsible for activation, Fig. 9, and by the same analytical procedure. The apparatus was modified so that a palladium or platinum electrode

could be rubbed back and forth upon another electrode of the same mate-
rial. The driving force was a magnet outside the glass apparatus.

In tests carried out in benzene vapor in the absence of air, it was found
that the deposit formed on the electrodes contained 65 per cent as much
hydrogen as was in the original benzene, about 2 atoms of hydrogen for
every 3 carbon atoms, this figure having a possible experimental error of
as much as 20 per cent. The brown deposit formed by friction thus differs
significantly from the pure carbon produced by arcing which is responsi-
ble for activation.* The experimentally determined composition of the
brown deposit does not, of course, distinguish between hydrogen or
benzene simply adsorbed in the deposit and hydrogen existing in it in
some combined form.

7.2 Rate of Production

In Kisliuk's experiments, which were carried out in the absence of
air, the rate of production of brown deposit was found to be independent
of benzene vapor pressure down to 3×10^{-3} mm Hg, which was the
lowest pressure tested, just as was the case in the formation of carbon
by arcs.

When air is present, the rate of formation of brown deposit may de-
pend upon vapor pressure of the organic molecules. Unpublished experi-
ments have indicated, furthermore, that there may be a limiting vapor
pressure below which the deposit does not form, with this pressure de-
pendent upon the idle period between operations.[20]

In some of Kisliuk's vacuum tests a palladium electrode was rubbed
back and forth over an area determined microscopically to be about
4×10^{-3} cm^2, and produced the polymerization on each rub of $2.1 \times
10^{10}$ molecules of benzene, or 5×10^{12} molecules per cm^2 of rub. This is
smaller than the number of molecules in a monolayer (7×10^{14} per cm^2,
Reference 16) by a factor of 140. Part of the discrepancy is certainly due
to the fact that the true area of contact of the electrodes is less than the
apparent area as seen under the microscope. From more careful estimates
of area it has been found by other observers that the amount of benzene
that is polymerized by friction is, in general, comparable with that ad-
sorbed as a monolayer on the rubbing surfaces.

7.3 Brown Deposit and the Carbon of Activation

Although both brown deposit and the carbon of activation are pro-
duced from the decomposition of adsorbed organic molecules, there are

---

* In this connection, it is interesting to point out, however, that any metal
surface, upon which brown deposit has been produced by friction in an appro-
priate atmosphere, is found to be fully active when tested in a suitable circuit.
This activity naturally does not last after the brown deposit has been burned off.
In this characteristic, the brown deposit behaves like any foreign more or less
insulating layer upon a contact surface.

several differences in the conditions necessary for formation. The carbon is produced on a noble metal but not on a base metal (in air); brown deposit, on the other hand, has been formed on vanadium, molybdenum and tantalum, but it has never been produced on silver and only sparingly on gold.[20] The failure of electrodes of silver and of gold to form brown deposit has been associated with the high thermal conductivities of these metals, with the idea in mind that polymerization of organic molecules to brown deposit requires frictional heat. Whether this is true has not been established.

Both brown deposit and the carbon of activation can be formed from any of a great variety of unsaturated ring compounds. Various unsaturated aliphatic compounds which have been tested, and some saturated aliphatic compounds (for example, pentane), can be made to produce brown deposit to a limited extent, but activation has never been attained with any aliphatic compound. It seems probable that some activating carbon is produced from these compounds but the burning off in the arc makes activation impossible.

ACKNOWLEDGMENT

The work reported here is the joint effort of a number of persons whose contributions are acknowledged in the appropriate places. The authors coordinated the investigation and are responsible for its general plan. The authors are indebted furthermore to R. H. Gumley for many helpful criticisms.

REFERENCES

 1. R. H. Gumley, Bell Lab. Record, **32**, p. 226, 1954.
 2. L. H. Germer, J. Appl. Phys., **22**, p. 955, 1951.
 3. L. H. Germer and W. S. Boyle, Nature, **176**, p. 1019, 1955.
 4. L. H. Germer and W. S. Boyle, J. Appl. Phys. **27**, p. 32, 1956.
 5. M. M. Atalla, B.S.T.J., **34**, p. 1081, Sept., 1955.
 6. L. H. Germer, J. Appl. Phys. **22**, p. 1133, 1951.
 7. F. E. Haworth, J. Appl. Phys., **28**, p. 381, 1957.
 8. L. H. Germer, J. Appl. Phys. **25**, p. 332, 1954.
 9. L. H. Germer and F. E. Haworth, J. Appl. Phys., **20**, p. 1085, 1949.
10. L. H. Germer, to be published.
11. M. M. Atalla, B.S.T.J., **32**, p. 1493, Nov., 1953.
12. P. Kisliuk, J. Appl. Phys., **25**, p. 897, 1954.
13. L. H. Germer, Electrical Breakdown between Close Electrodes in Air, to be published.
14. W. S. Boyle and L. H. Germer, J. Appl. Phys., **26**, p. 571, 1955.
15. J. J. Lander and L. H. Germer, J. Appl. Phys., **19**, p. 910, 1948.
16. B. M. W. Trapnell, Advances in Catalysis, Vol. III, Academic Press, New York, 1951, pp. 1-24.
17. P. Kisliuk, to be published.
18. F. E. Haworth, J. Appl. Phys., **22**, p. 606, 1951.
19. A. Güntherschulze, Z. Physik, **36**, p. 563, 1926.
20. H. W. Hermance and T. F. Egan, 1956 Electronics Symposium, Electrical Engineering, to be published.

Bell System Technical Papers Not Published in this Journal

AARON, M. R.[1]

The Use of Least Squares in Network Design, Trans. I.R.E., **PGCT, CT-3,** pp. 224–231, Dec., 1956.

ANDERSON, J. R.[1]

A New Type of Ferroelectric Shift Register, Trans. I.R.E., **PGEC, EC-5,** pp. 184–191, Dec., 1956.

ANDERSON, P. W., see Clogston, A. M.

ANDREATCH, P., JR.,[1] and THURSTON, R. N.[1]

Disk-Loaded Torsional Wave Delay Line. I — Construction and Test, J. Acous. Soc. Am., **29,** pp. 16–19, Jan., 1957.

AUGUSTYNIAK, W. M., see Wertheim, G. K.

BALA, V. B., see Matthias, B. T.

BASHKOW, T. R.,[1] and DESOER, C. A.[1]

A Network Proof of a Theorem on Hurwitz Polynomials and its Generalization, Quarterly Appl. Math., **14,** pp. 423–426, Jan., 1957.

BOND, W. L., see McSkimin, H. J.

BOZORTH, R. M.[1]

Magnetic Properties of Materials, Am. Inst. Phys. Handbook, Chapter 5, pp. 206–244, Feb., 1957.

BREIDT, P., JR.,[1] GREINER, E. S., and ELLIS, W. C.[1]

Dislocations in Plastically Indented Germanium, Acta Met., Letter to the Editor, 5, p. **60,** Jan., 1957.

---

[1] Bell Telephone Laboratories.

BRIDGERS, H. E., see tabulation at the end.

BRIDGERS, H. E., see tabulation at the end.

BURKE, P. J.

The Output of a Queueing System, Operations Research, **4,** pp. 699–704, Dec., 1956.

CLEMENCY, W. F.,[1] ROMANOW, F. F.,[1] and ROSE, A. F.[2]

The Bell System Speakerphone, Elec. Engg., **76,** pp. 189–194, March, 1957.

CLOGSTON, A. M.,[1] SUHL, H.,[1] WALKER, L. R.,[1] and ANDERSON, P. W.[1]

Ferromagnetic Resonance Line Width in Insulating Materials, J. Phys. Chem. Solids, **1,** pp. 129–136, Nov., 1956.

CORENZWIT, E., see Matthias, B. T.

D'AMICO, C.,[1] and HAGSTRUM, H. D.[1]

An Improvement in the Use of the Porcelain Rod Gas Leak, Rev. Sci. Instr., **28,** p. 60, Jan., 1957.

DESOER, C. A., see Bashkow, T. R.

DILLON, J. F., JR.[1]

Ferrimagnetic Resonance in Yttrium Iron Garnet, Phys. Rev., Letter to the Editor, **105,** pp. 759–760, Jan. 15, 1957.

DITZENBERGER, J. A., see Fuller, C. S.

DOBA, S., JR.[1]

The Measurement and Specification of Nonlinear Amplitude Response Characteristics in Television, Proc. I.R.E., **45,** pp. 161–165, Feb., 1957.

EDELSON, D., see tabulation at the end.

---

[1] Bell Telephone Laboratories.
[2] American Telephone and Telegraph Company.

ELLIS, W. C., see Breidt, P., Jr.

EVANS, D. H.[1]

A Positioning Servomechanism With A Finite Time Delay and A Signal Limiter, Trans. I.R.E., **PGAC, AC-2,** pp. 17–28, Feb., 1957.

FLASCHEN, S. S., see tabulation at the end.

FLASCHEN, S. S., see Garn, P. D.

FRY, T. C.[1]

Automatic Computer in Industry, Am. Stat. Assoc. J., **51,** pp. 565–575, Dec., 1956.

FULLER, C. S.,[1] and DITZENBERGER, J. A.[1]

Effect of Structural Defects in Germanium on the Diffusion and Acceptor Behavior of Copper, J. Appl. Phys., **28,** pp. 40–48, Jan., 1957.

FULLER, C. S.,[1] and MORIN, F. J.[1]

Diffusion and Electrical Behavior of Zinc in Silicon, Phys. Rev., **105,** pp. 379–384, Jan. 15, 1957.

FULLER, C. S., see Reiss, H.

GALT, J. K.,[1] AND KITTEL, C.[4]

Ferromagnetic Domain Theory, Solid State Physics: Advances in Research and Applications (book), 3, pp. 437–564, 1956, Academic Press, Inc., New York.

GARN, P. D.,[1] and FLASCHEN, S. S.[1]

Analytical Applications of Differential Thermal Analysis Apparatus, Anal. Chem., **29,** pp. 271–275, Feb., 1957.

GARN, P. D., and FLASCHEN, S. S.

Detection of Polymorphic Phase Transformations by Continuous Measurement of Electrical Resistance, Anal. Chem., **29,** pp. 268–271, Feb., 1957.

---

[1] Bell Telephone Laboratories.
[4] University of California, Berkeley.

GARN, P. D., see tabulation at the end.

GAST, R. W.[5]

Field Experience with the A2A Video System, Elec. Engg., **76,** pp. 44–49, Jan., 1957.

GEBALLE, T. H., see Kunzler, J. E.

GIBBONS, J. F.[1]

A Simplified Procedure for Finding Fourier Coefficients, Proc. I.R.E., Letter to the Editor, **45,** p. 243, Feb., 1957.

GREINER, E. S., see Breidt, P., Jr.

GROSS, W. A.[1]

The Second Fundamental Problem of Elasticity Applied to a Plane Circular Ring, J. Appl. Math. and Phys., **8,** pp. 71–73, 1957.

GOULD, H. L. B., and WENNY, D. H.[1]

Supermendur — A New Rectangular-Loop Magnetic Material, Elec. Engg., **76,** pp. 208–211, March, 1957.

HAGSTRUM, H. D.[1]

Effect of Monolayer Adsorption on the Ejection of Electrons from Metals by Ions, Phys. Rev., **104,** pp. 1516–1527, Dec. 15, 1956.

HAGSTRUM, H. D., see D'Amico, C.

HAMMING, R. W.[1]

Harnessing the Digital Computers, Columbia Engg. Quarterly, **10,** pp. 16–19, 54, March, 1957.

HANSON, R. L.,[1] and KOCK, W. E.[1]

Interesting Effect Produced by Two Loudspeakers Under Free Space Conditions, J. Acous. Soc. Am. Letter to the Editor, **29,** p. 145, Jan., 1957.

---

[1] Bell Telephone Laboratories.
[5] New York Telephone Company.

HAWKINS, W. L., see tabulation at the end.

HERRING, C.[1]

Theoretical Ideas Pertaining to Traps or Centers, Photoconductivity Conference (book), pp. 81–110, 1956. John Wiley & Sons, New York.

HULL, G. W., see Kunzler, J. E.

KARP, A[1].

Japanese Technical Captions, Proc. I.R.E., Letter to the Editor, 45, p. **93**, Jan., 1957.

KING, B. G.[1]

Discussion on "An Investigation into Some Fundamental Properties of Strip Transmission Lines with the Aid of an Electrolytic Tank", Proc. I.R.E., **104,** p. 72, Jan., 1957.

KITTEL, C., see Galt, J. K.

KOCK, W. E., see Hanson, R. L.

KOWALCHIK, M., see Thurmond, C. D.

KUNZLER, J. E.,[1] GEBALLE, T. H.,[1] and HULL, G. W.[1]

Germanium Resistance Thermometers Suitable for Low-Temperature Calorimetry, Rev. Sci. Instr., **28,** pp. 96–98, Feb., 1957.

KULKE, B.,[1] and MILLER, S. L.[1]

Accurate Measurement of Emitter and Collector Series Resistances in Transistors, Proc. I.R.E., Letter to the Editor, **45,** p. 90, Jan., 1957.

KUNZLER, J. E., see tabulation at the end.

LANDER, J. J., see Thomas, D. G.

LAW, J. T., see tabulation at the end.

[1] Bell Telephone Laboratories.

LUNDBERG, C. V., see tabulation at the end.

LUNDBERG, J. L., see tabulation at the end.

MATTHIAS, B. T.,[1] WOOD, E. A.,[1] CORENZWIT, E.,[1] and BALA, V. B.[1]

  Superconductivity and Electron Concentration, J. Phys. Chem. Solids, **1,** pp. 188–190, Nov., 1956.

McMILLAN, B.[1]

  Two Inequalities Implied by Unique Decipherability, Trans. I.R.E., **PGIT, IT-2,** pp. 115–116, Dec., 1956.

McSKIMIN, J. H.,[1] and BOND, W. L.[1]

  Elastic Moduli of Diamond, Phys. Rev., **105,** pp. 116–121, Jan. 1, 1957.

MENDIZZA, A.[1]

  The Standard Salt Spray Test — Is It A Valid Acceptance Test?, Plating, **44,** pp. 166–175, Feb., 1957.

MENDIZZA, A.[1]

  The Standard Salt Spray Test — Is It A Valid Acceptance Test?, Symposium on Properties, Tests and Performance of Electrodeposited Metallic Coatings, A.S.T.M. Special Tech. Publication 197, pp. 107–117, 1957.

MILLER, R. C., see Smits, F. M.

MILLER, S. L., see Kulke, B.

MORIN, F. J., see Fuller, C. S.

NELSON, L. S., see Tabulation at the end.

PALMQUIST, T. F.[6]

  Multiunit Neutralizing Transformers, Elec. Engg., **76,** p. 201, March, 1957.

---
[1] Bell Telephone Laboratories.
[6] Bell Telephone Company of Canada, Montreal.

PATERSON, E. G. D.[1]

Some Observations on Quality Assurance and Reliability, Proc. Third National Symp. on Reliability and Quality Control in Electronics, pp. 129–132, Jan., 1957.

PIETRUSZKIEWICZ, A. J., see Reiss, H.

POTTER, J. F., see tabulation at the end.

PRINCE, E.,[1] and TREUTING, R. G.[1]

The Structure of Tetragnal Copper Ferrite, Acta Crys., 9, pp. 1025–1028, Dec., 1956.

READ, M. H., see Van Uitert, L. G.

READ, W. T., JR.[1]

Dislocation Theory of Plastic Bending, Acta Met., 5, pp. 83–88, Feb., 1957.

REISS, H.[1]

Theory of the Ionization of Hydrogen and Lithium in Silicon and Germanium, J. Chem. Phys., 25, pp. 681–686, Oct., 1956.

REISS, H., see tabulation at the end.

REISS, H.,[1] FULLER, C. S.,[1] and PIETRUSZKIEWICZ, A. J.[1]

Solubility of Lithium in Doped and Undoped Silicon, Evidence for Compound Formation, J. Chem. Phys., 25, pp. 650–655, Oct., 1956.

ROMANOW, F. F., see Clemency, W. F.

ROSE, A. F., see Clemency, W. F.

ROSE, D. J.[1]

Microplasmas in Silicon, Phys. Rev., 105, pp. 413–418, Jan. 15, 1957.

SCHLABACH, T. D., see tabulations at the end.

[1] Bell Telephone Laboratories.

SCHNETTLER, F. J., see Van Uitert, L. G.

SEIDEL, H.[1]

  Ferrite Slabs in Transverse Electric Mode Wave Guide, J. Appl. Phys., **28,** pp. 218–226, Feb., 1957.

SLICHTER, W. P., see tabulation at the end.

SMITS, F. M.,[1] and MILLER, R. C.[1]

  Rate Limitation at the Surface for Impurity Diffusion in Semiconductors, Phys. Rev., **104,** pp. 1242–1245, Dec. 1, 1956.

SUHL, H.[1]

  The Theory of Ferromagnetic Resonance at High Signal Powers, J. Chem. and Phys. of Solids, **1,** pp. 209–227, Jan., 1957.

SUHL, H., see Clogston, A. M.

TIEN, P. K.[1]

  The Backward-Traveling Power in the High Power Traveling-Wave Amplifiers, Proc. I.R.E., Letter to the Editor, **45,** p. 87, Jan., 1957.

THOMAS, D. G.,[1] and LANDER, J. J.[1]

  Hydrogen as a Donor in Zinc Oxide, J. Chem. Phys., **25,** pp. 1136–1142, Dec., 1956.

THURMOND, C. D.,[1] TRUMBORE, F. A.,[1] and KOWALCHIK, M.[1]

  Germanium Solidus Curves, J. Chem. Phys., Letter to the Editor, 25, pp. 799–800, Oct., 1956.

THURSTON, R. N.[1]

  Disk-Loaded Torsional Wave Delay Line. II — Theoretical Interpretation of Results and Design Information, J. Acous. Soc. Am., **29,** pp. 20–25, Jan., 1957.

THURSTON, R. N., see Andreatch, P., Jr.

  [1] Bell Telephone Laboratories.

TREUTING, R. G., see Prince, E.

TRUMBORE, F. A., see Thurmond, C. D.

VAN UITERT, L. G.,[1] READ, M. H.,[1] and SCHNETTLER, F. J.[1]

  Permanent Magnet Oxides Containing Divalent Metal Ions—I, J.
  Appl. Phys., Letter to the Editor, **28,** pp. 280–281, Feb., 1957.

VAN UITERT, L. G.,[1] see tabulation at the end.

WALKER, L. R., see Clogston, A. M.

WENNY, D. H., see Gould, H. L.

WERNICK, J. H., see tabulation at the end.

WERTHEIM, G. K.,[1] and AUGUSTYNIAK, W. M.[1]

  Measurement of Short Carrier Lifetimes, Rev. Sci. Instr., **27,** pp.
  1062–1064, Dec., 1956.

WOOD, E. A., see Matthias, B. T.

YERKES, E. P.[7]

  Comfort A. Adams 1956 Edison Medalist — Medal History, Elec.
  Engg., **76,** p. 224, March, 1957.

THE ENCYCLOPEDIA OF CHEMISTRY — BOOK PUBLISHED BY REINHOLD
  PRESS, NEW YORK, JANUARY, 1957.

  BRIDGERS, H. E., **Germanium and Its Compounds,** p. 445, and
  Semiconductors, pp. 852–583.

  EDELSON, D., **Polar Molecules,** pp. 767–769.

  FLASCHEN, S. S., **Calcination,** pp. 161–162.

  GARN, P. D., **Electrolysis,** pp. 341–342.

  HAWKINS, W. L., **Autoxidation,** p. 116.

---

[1] Bell Telephone Laboratories.
[7] Bell Telephone Company of Pennsylvania, Philadelphia.

KUNZLER, J. E., **Calorimetry,** pp. 163–165.

LAW, J. T., **Vacuum Techniques,** pp. 964–965.

LUNDBERG, C. C., **Antiozonants,** pp. 97–98, and **Solutions,** pp. 873–874.

NELSON, L. S., **Olefin Compounds,** pp. 661–663.

POTTER, J. F., **Porosity,** pp. 775–776.

REISS, H., **Thermodynamics,** pp. 930–933.

SCHLABACH, T. D., **Photometric Analysis,** pp. 735–736.

SLICHTER, W. P., **Paramagnetism,** p. 700.

VAN UITERT, L. G., **Equilibrium,** pp. 363–364.

WERNICK, J. H., **Carbonates,** pp. 173–174.

Recent Monographs of Bell System Technical Papers Not Published in This Journal*

ALLISON, H. W., see Moore, G. E.

ARNOLD, S. M.

Growth and Properties of Metal Whiskers, Monograph 2635.

AUGUSTYNIAK, W. M., see Wertheim, G. K.

BASHKOW, T. R.

Effect of Nonlinear Collector Capacitance on Rise Time, Monograph 2742.

BÖMMEL, H. E., see Mason W. P.

BOZORTH, R. M.

Ferromagnetism, Monograph 2679.

BRATTAIN, W. H.

Development of Concepts in Semiconductor Research, Monograph 2743.

BRIDGERS, H. E., and KOLB, E. D.

Distribution Coefficient of Boron in Germanium, Monograph 2684.

CHEN, W. H., see Lee, C. Y.

COMPTON, K. G.

Potential Criteria for Cathodic Protection of Lead Cable Sheath, Monograph 2655.

DAVID, E. E., and McDONALD, H. S.

Note on Pitch-Synchronous Processing of Speech, Monograph 2744.

DEHN, J. W., and HERSEY, R. E.

Recent New Features for No. 5 Crossbar Switching System, Monograph 2745.

FAY, C. E.

Ferrite-Tuned Resonant Cavities, Monograph 2713.

FRY, T. C.

The Automatic Computer in Industry, Monograph 2755.

GILBERT, E. N.

Enumeration of Labelled Graphs, Monograph 2680.

GOLDEY, J. M., see Moll, J. L.

HAGSTRUM, H. D.

Auger Ejection of Electrons from Molybdenum by Noble Gas Ions, Monograph 2716.

HAGSTRUM, H. D.

Metastable Ions of the Noble Gases, Monograph 2714.

HERSEY, R. E., see Dehn, J. W.

HOLONYAK, N., see Moll, J. L.

JAYCOX, E. K., and PRESCOTT, B. E.

Spectrochemical Analysis of Thermionic Cathode Nickel Alloys, Monograph 2756.

KOLB, E. D., see Bridgers, H. E.

KRUSEMEYER, H. J., and PURSLEY, M. V.

Donor Changes in Oxide-Coated Cathodes, Monograph 2717.

LANDER, J. J., see Thomas, D. G.

LEE, C. Y., and CHEN, W. H.

Several-Valued Combinational Switching Circuits, Monograph 2746.

LOVELL, L. C., see Vogel, F. L., Jr.

MASON, W. P.

Internal Friction and Fatigue in Metals at Large Strain Amplitudes, Monograph 2758.

MASON, W. P.

Physical Acoustics and Properties of Solids, Monograph 2761.

MASON, W. P., and BÖMMEL, H. E.

Ultrasonic Attenuation at Low Temperatures for Metals, Normal and Superconducting, Monograph 2748.

MATLACK, R. C.

Role of Communications Networks in Digital Data Systems, Monograph 2678.

METREYEK, W., see Winslow, F. H.

McDONALD, H. S., see David, E. E.

McSKIMIN, H. J.

Wave Propagation and Measurement of Elasticity of Liquids and Solids, Monograph 2749.

MERZ, W. J.

Switching Time in Ferroelectric $BaTiO_3$ and Crystal Thickness, Monograph 2721.

MILLER, R. C., and SAVAGE, A.

Diffusion of Aluminum in Single-Crystal Silicon, Monograph 2722.

MOLL, J. L., TANENBAUM, M., GOLDEY, J. M., and HOLONYAK, N.

P-N-P-N Transistor Switches, Monograph 2723.

MOORE, G. E., and ALLISON, H. W.

Emission of Oxide Cathodes Supported on a Ceramic, Monograph 2724.

MOSHMAN, J., see Tien, P. K.

OHM, E. A.

A Broad-Band Microwave Circulator, Monograph 2726.

OWENS, C. D.

Modern Magnetic Ferrites and Their Engineering Applications, Monograph 2709.

OWENS, C. D.

Properties and Applications of Ferrites Below Microwave Frequencies, Monograph 2727.

PATERSON, E. G. D.

Nike Quality Assurance, Monograph 2728.

PIERCE, J. R., and WALKER, L. R.

Growing Electric Space-Charge Waves, Monograph 2729.

PIERCE, J. R.

Instability of Hollow Beams, Monograph 2751.

PRESCOTT, B. E., see Jaycox, E. K.

PURSLEY, M. V., see Krusemeyer, H. J.

ROSE, D. J.

Townsend Ionization Coefficient for Hydrogen and Deuterium, Monograph 2731.

SAVAGE, A., see Miller, R. C.

SLEPIAN, D.

Note on Two Binary Signaling Alphabets, Monograph 2733.

SPROUL, P. T.

A Video Visual Measuring Set with Sync Pulses, Monograph 2752.

TANENBAUM, M., see Moll, J. L.

THOMAS, D. G., and LANDER, J. J.

Hydrogen as a Donor in Zinc Oxide, Monograph 2753.

TIEN, P. K., and MOSHMAN, J.

Noise in a High-Frequency Diode, Monograph 2735.

TORREY, M. N.

Quality Control in Electronics, Monograph 2736.

VAN UITERT, L. G.

Dielectric Properties of and Conductivity in Ferrites, Monograph 2737.

VOGEL, F. L., JR., and LOVELL, L. C.

Dislocation Etch Pits in Silicon Crystals, Monograph 2738.

WALKER, L. R., see Pierce, J. R.

WEINREICH, G.

Acoustodynamic Effects in Semiconductors, Monograph 2764.

WEISS, M. T.

Improved Rectangular Waveguide Resonance Isolators, Monograph 2739.

WERTHEIM, G. K.

Carrier Lifetime in Indium Antimonide, Monograph 2740.

WERTHEIM, G. K., and AUGUSTYNIAK

Measurement of Short Carrier Lifetimes, Monograph 2754.

WINSLOW, F. H., and MATREYEK, W.

Pyrolysis of Crosslinked Styrene Polymers, Monograph 2741.

Contributors to This Issue

KENNETH BULLINGTON, B.S., University of New Mexico, 1936; M.S., Massachusetts Institute of Technology, 1937; Bell Telephone Laboratories, 1937–. Mr. Bullington's first work with the Laboratories was on systems engineering on wire transmission circuits, and since 1942 he has been concerned with transmission engineering on radio systems, particularly over-the-horizon radio propagation. In 1956, he was awarded the Morris Liebmann Memorial Prize of the I.R.E. and the Stuart Ballentine Medal from the Franklin Institute for contributions in tropospheric transmission and the application of those contributions to practical communication systems. He is a Fellow of the I.R.E., and a member of Phi Kappa Phi, Sigma Tau and Kappa Mu Epsilon.

ARTHUR B. CRAWFORD, B.S.E.E. 1928, Ohio State University; Bell Telephone Laboratories 1928–. Mr. Crawford has been engaged in radio research since he joined the Laboratories. He has worked on ultra short wave apparatus, measuring techniques and propagation; microwave apparatus, measuring techniques and radar; microwave propagation studies and microwave antenna research. He is author or co-author of articles which appeared in the Bell System Technical Journal, Proceedings of the I.R.E., Nature and Bulletin of the American Meteorological Society. He is a Fellow of the I.R.E. and a member of Sigma Xi, Tau Beta Pi, Eta Kappa Nu, and Pi Mu Epsilon.

HAROLD E. CURTIS, B.S. and M.S., Massachusetts Institute of Technology, 1929; Department of Development and Research of the American Telephone and Telegraph Company, 1929; Bell Telephone Laboratories, 1934–. Mr. Curtis has been concerned with transmission problems related to multi-channel carrier telephony. He has also been engaged in studies of transmission engineering aspects of the microwave radio relay system. His work at the Laboratories has also included pioneering transmission studies of the coaxial cable, the shielded pair and quad, and the waveguide. Mr. Curtis holds ten patents relating to carrier telephony.

HARALD T. FRIIS, E.E., 1916, D.Sc., 1938, Royal Technical College (Copenhagen); Western Electric Company, 1919; Bell Telephone Lab-

oratories, 1930–. Dr. Friis, Director of Research in High Frequency and Electronics, has made important contributions on ship-to-shore radio reception, short-wave studies, radio transmission (including methods of measuring signals and noise), a receiving system for reducing selective fading and noise interference, microwave receivers and measuring equipment, and radar equipment. He has published numerous technical papers and is co-author of a book on the theory and practice of antennas. The I.R.E.'s Morris Liebmann Memorial Prize, 1939, and Medal of Honor, 1954. Valdemar Poulson Gold Medal by Danish Academy of Technical Sciences, 1954. Danish "Knight of the Order of Dannebrog," 1954. Fellow of I.R.E. and A.I.E.E. Member of American Association for the Advancement of Science, Danish Engineering Society and Danish Academy of Technical Sciences. Served on Panel for Basic Research of Research and Development Board, 1947–49, and Scientific Advisory Board of Army Air Force, 1946–47.

LESTER H. GERMER, B.A., Cornell, 1917; M.A., Columbia, 1922; Ph.D., Columbia, 1927; Western Electric Co., 1917–24; Bell Telephone Laboratories, 1925–. With the Research Department, Dr. Germer has been concerned with studies in electron diffraction, structure of surface films, thermionics, contact physics, order-disorder phenomena, and physics of arc formation. He has published about seventy papers and has three patents. In 1931 he received the Elliott Cresson medal of the Franklin Institute. He is a member of the American Physical Society, Sigma Xi, the New York Academy of Sciences, the A.A.A.S., and the American Crystallographic Society of which he served as president in 1944.

DAVID C. HOGG, B.S., University of Western Ontario, 1949; M.S. and Ph.D., McGill University, 1950 and 1953; Bell Telephone Laboratories, 1953–. Mr. Hogg has been engaged in studies of artificial dielectrics for microwaves, antenna problems, and over-the-horizon and millimeter wave propagation as a member of the Radio Research Dept. During World War II, Mr. Hogg served with the Canadian Army in Europe and from 1950–51 did research for the Defense Research Board of Canada. He is a member of Sigma Xi, and a senior member of the I.R.E.

STEPHEN O. RICE, B.S., Oregon State College, 1929; California Institute of Technology, Graduate Studies, 1929–30 and 1934–35; Bell Telephone Laboratories, 1930–. In his first years at the Laboratories, Mr. Rice was concerned with the non-linear circuit theory, with special

emphasis on methods of computing modulation products. Since 1935 he has served as a consultant on mathematical problems and in investigations of the telephone transmission theory, including noise theory, and applications of electromagnetic theory. Fellow of the I.R.E.

J. W. SCHAEFER, B.M.E., Ohio State University, 1941; Bell Telephone Laboratories, 1940–. Mr. Schaefer has worked on dial design and dial test equipment, and during the war years contributed to the design and development of anti-aircraft fire control equipment and guided missiles. After the war, Mr. Schaefer proposed a means of steering missiles from which evolved NIKE. He is now working on anti-aircraft guided missile systems. He is a member of A.S.M.E., the Army Ordnance Association, Tau Beta Pi and Sigma Xi.

BERNARD SMITH, B.S., City College of New York, 1948; A.M., 1951, and Ph.D., 1954, Columbia University; Lecturer, City College of New York, 1948–1954; Bell Telephone Laboratories, 1954–. In addition to the transmission studies in which he has been engaged since joining the Laboratories, his present duties include teaching information theory in the Communications Development Training Program. He is a member of the American Physical Society, Phi Beta Kappa, Sigma Xi and Kappa Delta Pi.

JAMES L. SMITH, B.S., Newark College of Engineering, 1956; Bell Telephone Laboratories, 1941–. Mr. Smith worked on problems concerned with relay contact erosion as a technical aide, and in 1956 began his work on solid state switching networks. He is a member of the A.I.E.E. and Tau Beta Pi.

MARK A. TOWNSEND, B.S., Texas Technological College, 1936; M.S., Mass. Institute of Technology, 1937; Bell Telephone Laboratories, 1945–. Mr. Townsend's early work with the Laboratories was on the development of gas discharge tubes for use in telephone switching systems. More recently, his work has been in the exploratory development of systems for digital data transmission and of a small electronic switching system. He is a member of the A.I.E.E., and senior member of the I.R.E.

GERD F. WEISSMANN. Dipl.–Ing. Technical University of Berlin, 1950; M.S. Pennsylvania State University, 1953; Bell Telephone Laboratories, 1953–. Mr. Weissmann's work at the Laboratories has been in stress analysis, engineering mechanics, strain measurements, soil mechanics and metals properties and testing. He also has worked with outside plant problems and metallurgical engineering.